Joint impacts of climate and land use change on the terrestrial biosphere

Dissertation

zur Erlangung des akademischen Grades

doctor rerum naturalium

(Dr. rer. nat.)

im Fach Geographie

eingereicht an der

Mathematisch-Naturwissenschaftlichen Fakultät

der Humboldt-Universität zu Berlin

von

Diplom-Geoökologe Sebastian Ostberg

Präsidentin der Humboldt-Universität zu Berlin

Prof. Dr.-Ing. Dr. Sabine Kunst

Dekan der Mathematisch-Naturwissenschaftlichen Fakultät

Prof. Dr. Elmar Kulke

Gutachter:

1. Prof. Dr. Wolfgang Lucht
2. Prof. Dr. Wolfgang Cramer
3. Prof. Dr. Patrick Hostert

Tag der mündlichen Prüfung: 9. Mai 2018

Abstract

Humans have a long history of shaping their environment to better suit their needs that dates back at least to the development of agriculture in the early Holocene. However, human-induced environmental change has accelerated dramatically with industrialisation and has now reached a magnitude that rivals that of geological forces. In light of the scope of anthropogenic changes it has been suggested that humanity is pushing the Earth System out of the Holocene into a new geological epoch: the Anthropocene.
The two major pathways of human interference with the terrestrial biosphere are

1. directly through land use change (LUC), primarily for agriculture,
2. indirectly through anthropogenic climate change (CC) which in turn drives ecosystem change.

This dissertation presents an attempt to assess human-induced biosphere change through both these pathways in a consistent and quantitative way. Its main objectives are

1. to quantify how much anthropogenic forcing has already shifted the biosphere from its potential natural state over the course of the last ∼300 years,
2. to systematically explore the space of plausible future scenarios for the terrestrial biosphere until the end of the 21st century.

The analysis is based on an integrated indicator of macro-scale changes in biogeochemical characteristics and ecosystem structure: the Γ metric. Large shifts in these basic building blocks of the biosphere are taken to indicate a risk to more complex ecosystem properties as they potentially disrupt long-standing biotic interactions such as predator-prey relations, complementarity and competition regarding resource use, or mutual interactions like pollination.
This dissertation relies on simulations with the dynamic global vegetation, agriculture and hydrology model LPJmL to quantify how biogeochemical characteristics and ecosystem structure have responded to historical LUC and CC. For future projections LPJmL

is driven by a large number of CC and LUC scenarios, using the same indicator to measure the impact on the biosphere.

Simulation results show that major impacts on the biosphere from CC and LUC — defined by Γ exceeding a threshold of 0.3 — have expanded from merely 0.5% of the land surface in 1700 to 25–31% of the land surface today. Land use has been the main anthropogenic driver causing major ecosystem change in the past and is currently responsible for major ecosystem change on 16–19% of the land surface. CC has caused major ecosystem change on 5–10% of the land surface since the beginning of the 20th century.
Assuming that the ultimate goal of the Paris Agreement can be reached and global warming can be limited to below 2 °C above pre-industrial levels major CC impacts on the biosphere are still projected to expand to 16–27% of the land surface by the end of the 21st century. Concurrent expansion of land use could result in major human-induced ecosystem changes from both CC and LUC on 40–53% of the land surface by century's end. If greenhouse gas emissions cannot be reduced and global warming exceeds 4 or even 5 °C humans may profoundly transform ecosystems covering 67–80% of the land surface. In this worst-case scenario analysed here, another roughly 20% of the land surface are projected to experience moderate ecosystem change, leaving only 3–8% of terrestrial ecosystems with only minor human alteration.

Overall, results show that CC is expected to take over as the main anthropogenic driver of major ecosystem change during this century in all but the most ambitious climate mitigation scenarios. Despite a growing world population, some land use scenarios project that future efficiency improvements in the agricultural system will allow for a reduction of agricultural land and hence a reduction of the impact of LUC on the terrestrial biosphere compared to today. Yet, results also show that reduced LUC impacts will likely not be able to compensate for the increase in CC impacts, and human-induced transformation of the biosphere is likely to grow during this century regardless of the considered scenario.

Zusammenfassung

Schon seit langem haben Menschen ihre Umwelt gestaltet, um sie ihren Bedürfnissen anzupassen, eine Geschichte, die mindestens bis zur Entwicklung landwirtschaftlicher Praktiken im frühen Holozän zurückreicht. Mit der Industrialisierung hat die vom Menschen verursachte Umweltveränderung jedoch enorm zugenommen und nimmt nun eine Größenordnung an, die sonst nur von geologischen Prozessen erreicht wird. In Anbetracht des Ausmaßes anthropogener Veränderungen wird vermutet, dass die Menschheit das Erdsystem aus dem Holozän in eine neue geologische Epoche drängt: das Anthropozän.
Die zwei Hauptpfade, über die der Mensch die terrestrische Biosphäre verändert, sind

1. direkt durch Landnutzungswandel (LNW), in erster Linie für die Landwirtschaft,
2. indirekt durch Klimawandel (KW), welcher seinerseits zu Ökosystemveränderungen führt.

Die vorliegende Dissertation unternimmt den Versuch, die vom Menschen über beide diese Pfade verursachten Veränderungen der Biosphäre konsistent und quantitativ zu bestimmen. Ihre Hauptziele sind

1. zu quantifizieren, wie stark die Biosphäre im Verlauf der letzten ca. 300 Jahre bereits durch anthropogene Triebkräfte verändert wurde,
2. den Raum plausibler Zukunftsszenarien für die terrestrische Biosphäre bis zum Ende des 21. Jahrhunderts systematisch zu erforschen.

Die Analyse basiert auf einem integrierten Indikator für makro-skalige Veränderungen der biogeochemikalischen Eigenschaften und der Ökosystemstruktur: der Γ-Metrik. Große Verschiebungen bei diesen grundlegenden Bausteinen der Biosphäre bedeuten ein Risiko für komplexere Ökosystemeigenschaften, da sie möglicherweise lange bestehende biotische Interaktionen wie Räuber-Beute-Beziehungen, Komplementarität und Konkurrenz bei der Ressourcennutzung oder symbiotische Beziehungen wie z.B. Bestäubung unterbrechen.
Die vorliegende Dissertation stützt sich auf Simulationen mit dem dynamischen globalen Vegetations-, Agrar- und Hydrologiemodell LPJmL, um zu quantifizieren, wie biogeochemische Eigenschaften und die Ökosystemstruktur auf historischen LNW und KW

reagiert haben. Für die Zukunftsprojektionen wird LPJmL mit einer großen Anzahl an Klima- und Landnutzungsszenarien angetrieben, wobei derselbe Indikator verwendet wird, um die Auswirkungen auf die Biosphäre zu bestimmen.

Die Simulationsergebnisse zeigen, dass sich schwerwiegende Auswirkungen von LNW und KW auf die Biosphäre — definiert als eine Überschreitung des Grenzwertes von 0,3 durch Γ — von lediglich 0,5% der Landoberfläche um 1700 auf 25–31% der Landoberfläche heute ausgedehnt haben. Landnutzung war in der Vergangenheit der wichtigste anthropogene Treiber für schwerwiegende Ökosystemveränderungen, mit einem derzeitigen Ausmaß von 16–19% der Landoberfläche. KW hat seit Anfang des 20. Jahrhunderts schwerwiegende Ökosystemveränderungen auf 5–10% der Landoberfläche verursacht. Unter der Annahme, dass das Hauptziel des Pariser Klimaabkommens, die globale Erwärmung auf weniger als 2 °C über vorindustriellem Niveau zu begrenzen, erreicht werden kann, werden sich schwerwiegende Klimafolgen für die Biosphäre trotzdem bis zum Ende des 21. Jahrhunderts auf 16–27% der Landoberfläche ausdehnen. Die gleichzeitige Ausweitung der Landwirtschaft könnte dazu führen, dass der Anteil der Landoberfläche mit schwerwiegenden Ökosystemveränderungen durch LNW und KW bis zum Ende des Jahrhunderts auf 40–53% ansteigt. Sollten die Treibhausgasemissionen nicht reduziert werden können und die globale Erwärmung 4 oder sogar 5 °C übersteigen, könnte die Menschheit Ökosysteme auf 67–80% der Landoberfläche grundlegend verändern. In diesem Worst-Case-Szenario werden für weitere etwa 20% der Landoberfläche mittelschwere Ökosystemveränderungen prognostiziert, so dass in nur 3–8% der terrestrischen Ökosysteme maximal geringe menschliche Veränderungen zu erwarten sind.

Insgesamt zeigen die Ergebnisse, dass KW in diesem Jahrhundert voraussichtlich in allen außer den ambitioniertesten Klimaschutzszenarien den Platz als Haupttreiber für schwerwiegende Ökosystemveränderungen übernehmen wird. Trotz einer wachsenden Weltbevölkerung gehen einige Landnutzungsszenarien davon aus, dass zukünftige Effizienzsteigerungen in der Landwirtschaft eine Verringerung der landwirtschaftlichen Fläche und damit eine Verringerung der Auswirkungen von LNW auf die terrestrische Biosphäre im Vergleich zu heute ermöglichen werden. Die Ergebnisse zeigen jedoch auch, dass verminderte Landnutzungsauswirkungen wahrscheinlich nicht in der Lage sein werden, die Zunahme von Klimafolgen zu kompensieren, so dass die vom Menschen verursachte Transformation der Biosphäre in diesem Jahrhundert wahrscheinlich unabhängig vom Szenario wachsen wird.

Contents

List of Figures

List of Tables

List of Tables

Part I.

General Introduction

Sebastian Ostberg

1. Setting the scene

It is a basic concept in ecology that organisms interact with their environment to create, modify and maintain habitats, a process referred to as 'ecosystem engineering' (Jones et al. 1994). While beavers or elephants are often named as examples (e.g. Jones et al. 1994; Chapin et al. 2011; Haynes 2012), humans are probably the biggest ecosystem engineer of all (Smith 2007). Even before the development of early agriculture, humans were actively changing their environment through predation and the modification of landscapes, often through the use of fire (Kirch 2005; Smith 2007; Steffen et al. 2007). Over the course of the Holocene, the geological epoch that started after the last Ice Age $\approx 11\,700$ years ago (Walker et al. 2009), humans have 'extended their geographic reach to the most remote places on Earth, domesticated hundreds of species of plants and animals, developed agriculturally based societies and urbanism, and saw their own numbers increase dramatically' (Kirch 2005). However, it has been argued that anthropogenic modification of the Earth system as a whole really picked up pace with the industrialisation, giving birth to the 'Anthropocene' as a proposed new geological era (e.g. Crutzen 2002; Steffen et al. 2007, 2011). The reasoning behind this new era is that, collectively, humankind has become a global geophysical force, in some respects 'overwhelming the great forces of nature' (Steffen et al. 2007). A simple, global indicator of the progression of the Anthropocene is the rise in atmospheric carbon dioxide (CO_2) concentrations (Steffen et al. 2007), but signs of this new era manifest, among others, in the oceans (Tyrrell 2011), sediment fluxes (Syvitski and Kettner 2011), stratigraphic records (Zalasiewicz et al. 2011), and the terrestrial biosphere (Ellis 2011).

This dissertation explores quantitatively the transformation of the terrestrial biosphere in the Anthropocene from an Earth system perspective. On the one hand, it presents an attempt to assess quantitatively how much anthropogenic forcing has already shifted the biosphere from its potential natural state over the course of the last ≈ 300 years, a kind of stocktaking. The second objective of this dissertation is to systematically quantify

the space of plausible future scenarios for the terrestrial biosphere until the end of the 21st century.

1.1. The terrestrial biosphere in the Earth system

The biosphere represents the 'part of the Earth system comprising all ecosystems and living organisms, in the atmosphere, on land (terrestrial biosphere) or in the oceans (marine biosphere), including derived dead organic matter, such as litter, soil organic matter and oceanic detritus' (IPCC 2013a). While oceans cover $\approx 71\%$ of the Earth's surface, the focus of this dissertation is on the remaining $\approx 29\%$ lying above sea level. Terrestrial ecosystems cover the overwhelming majority of land surfaces on all continents except Antarctica. It is estimated that they are home to three to 25 times as many eukaryotic species as marine ecosystems (Mora et al. 2011; Benton 2001), but estimates of the total number of species on Earth vary widely and only a minority of species have actually been documented up to this point (e.g. May 2010; Costello et al. 2013; Roskov et al. 2016).

Within the Earth system, the terrestrial biosphere constitutes a crucial part of the global carbon (C) cycle. Terrestrial plants capture $\approx 123 \pm 8\,\mathrm{PgC}$ ($1\,\mathrm{Pg} = 10^{15}\,\mathrm{g}$) each year from the atmosphere through the process of photosynthesis (values for 1998–2005, Beer et al. 2010), which is almost 14 times the estimated amount of anthropogenic emissions into the atmosphere ($9.0 \pm 0.5\,\mathrm{PgC/yr}$, values for 2000–2009, Le Quéré et al. 2016). Roughly half of that terrestrial gross primary production (GPP) is used by plants themselves and returned to the atmosphere by autotrophic respiration, while the other half is converted into living biomass—a process referred to as net primary production (NPP)—and forms the basis for maintenance, growth, and reproduction of all heterotrophs, essentially the base of terrestrial food chains (Vitousek et al. 1986; Prentice et al. 2001; Chapin et al. 2011). Overall, the terrestrial biosphere stores about 450–650 PgC in living biomass, 1500–2400 PgC of dead organic matter in litters and soils and another estimated 1700 PgC in permafrost. In comparision, 829 PgC are stored in the atmosphere (Ciais et al. 2013).

Terrestrial ecosystems also play an important role in regulating the global freshwater cycle. Roughly 60% of all precipitation over land leaves the biosphere and returns to the

atmosphere by way of evapotranspiration (ET) while the rest runs off and flows into the oceans through rivers and streams (Oki and Kanae 2006). Vegetation characteristics such as leaf area and rooting depth influence all three components of ET: transpiration, evaporation of intercepted precipitation from vegetation canopies, and evaporation from non-vegetated surfaces, as well as the overall partitioning into ET and runoff (Gerten et al. 2004; Donohue et al. 2007; Chapin et al. 2011). Transpiration through plant stomata is believed to constitute the largest single component of ET, with estimates of global transpiration/ET ratios varying between 0.38–0.48 in a land surface model (Alton et al. 2009), 0.63 in a dynamic global vegetation model (DGVM) (Rost et al. 2008a) and 0.8–0.9 based on isotope measurements from lake catchments (Jasechko et al. 2013). By modulating the ET/runoff ratio the terrestrial biosphere may also influence precipitation itself because local ET is a significant source of local precipitation in many regions, a process called 'moisture recycling' (Trenberth 1999). Since most freshwater in rivers and streams has its origin in runoff (either directly as surface runoff or after filtration through soils) processes in the terrestrial biosphere modulate water quality as well, most prominantly nutrient loads, but also pathogens, pesticides and other toxic compounds (e.g. Vitousek et al. 1997; NRC 2000; Erisman et al. 2013).

1.2. Land use and climate change as global drivers of biospheric change

From a systems analytical perspective, land use and climate both represent external drivers or forcings acting upon the terrestrial biosphere (Stone et al. 2013). Ecosystems, communities and species are often impacted by a number of confounding factors all at once, posing a challenge for the attribution of observed changes to a specific driver (Stone et al. 2013; Cramer et al. 2014). For instance, significant range shifts have been observed in some indigenous South African bird species for several decades, of which range extensions towards the south have been attributed to climate change whereas range extensions towards the west are consistent with land use drivers (Hockey et al. 2011).

Humans use the biosphere to supply them with a number of ecosystem services, i.e. 'benefits people obtain from ecosystems' (MEA 2005). These include: (1) provisioning

services, e.g. food, fresh water, wood, fiber, fuel; (2) regulating services, e.g. regulation of climate, floods, soil fertility, or water purification; (3) cultural services, e.g. aesthetic, spiritual, educational or recreational value, sense of identity; (4) supporting services, i.e. fundamental processes that permit the delivery of the other categories of services, e.g. primary production, nutrient cycling (MEA 2005; Balvanera et al. 2017). Over the last three centuries, human population has increased by more than one order of magnitude from roughly 600 million in 1700 to 7.4 billion today (Klein Goldewijk et al. 2010; UNPD 2015). This growth in numbers has been accompanied by an increase in the use of ecosystem services. So far, humans have been particularly successful at enhancing the delivery of one provisioning service: food production. From an Earth system perspective, however, this expansion of food production has resulted in a profound transformation of the biosphere—the terrestrial biosphere in particular—with crops and livestock contributing 90% of total food production and 70% of food production coming from specific 'cultivated systems' (Wood et al. 2005).

Climate is the dominant control of the distribution of major vegetation types at regional to global scales (Woodward and Williams 1987). Because of the close link between climate and vegetation, climate classification systems such as the Köppen scheme commonly correlate climate classes with biome categories (Köppen 1936; Belda et al. 2014). Climate envelopes describe the range of conditions within which species can maintain viable populations (Woodward et al. 2004; Williams and Jackson 2007). Human activities act as both biogeochemical and biogeophysical drivers of changes in the climate system. The former refers mostly to the emission of greenhouse gases (GHG), which have a warming effect, and the emission of particulate air pollutants, which may have a cooling or warming effect. The latter includes changes in surface albedo, surface roughness and latent heat flux induced by anthropogenic land cover change, but also geophysical effects of aerosols (Myhre et al. 2013).

The following subsections provide a short overview of the extent of anthropogenic land use and climate forcing and list a few examples of changes in the terrestrial biosphere linked to these two drivers. For climate change, the Intergovernmental Panel on Climate Change (IPCC) provides a comprehensive global review of the existing scientific literature on climate forcing (IPCC 2013b) and climate impacts on a number of human and natural systems (IPCC 2014a, 2014b) in its 5th Assessment Report (AR5). No singular assessment of comparable detail exists for land use.

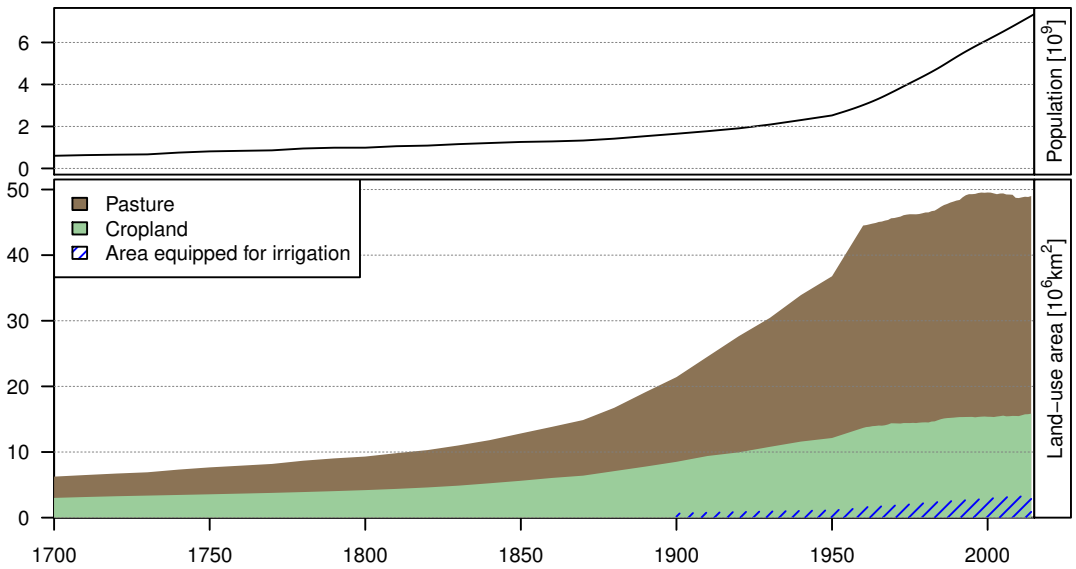

Figure I.1.: Indicators of historical land use forcing. Population data based on Klein Goldewijk et al. (2010) for 1700–1949 and UNPD (2015) for 1950–2015. Cropland and pasture area based on Klein Goldewijk et al. (2011) for 1700–1960 and FAO (2016) for 1961–2014; area equipped for irrigation based on Siebert et al. (2015) for 1900–1960 and FAO (2016) for 1961–2014.

1.2.1. Current extent of anthropogenic land use forcing

According to data by the Food and Agriculture Organization of the United Nations (FAO), croplands have grown to a global extent of 15.8 million km^2, while permanent meadows and pastures account for another 33.2 million km^2, bringing the total agricultural area to 49 million km^2 (values for 2014, FAO 2016, Figure I.1). While agricultural expansion roughly followed population trends during the 18th, 19th and early 20th century (Klein Goldewijk et al. 2010; Klein Goldewijk et al. 2011, Figure I.1), technological advances from the 'Green Revolution' allowed food production to increase mostly through intensification during the second half of the 20th century. These advances include adoption of high-yielding crop cultivars, increased use of fertilisers and pesticides, and mechanisation and irrigation (e.g. Cassman et al. 2005; Foley et al. 2005; Burney et al. 2010; Foley et al. 2011). For example, fertiliser application has increased by 500% since 1960 (Tilman et al. 2001; Foley et al. 2011). Irrigation extent has almost tripled since 1950, with roughly 20% of global croplands presently equipped for irrigation (Siebert et al. 2015, Figure I.1). Irrigated crops account for 33% of total crop production. The importance of irrigation is even bigger for cereal crops where average irrigated yields are

66% above rainfed yields (Siebert and Döll 2010). Overall, production of food and feed crops has increased by 235% since 1961 (from 1.8 to 6.2 billion tonnes), while global cropland has only increased by 15% during the same time (FAO 2016). Trends in agricultural area vary by region (Cassman et al. 2005): Cropland area has been decreasing in Europe and China since 1950. The majority of cropland expansion since 1980 took place in Southeast Asia, parts of Asia, the Great Lakes region of eastern Africa, and in the Amazon Basin. On the other hand, the southeastern US, eastern China, and parts of Brazil experienced major cropland abandonment (Cassman et al. 2005). While food production has generally kept up with the growing demand, almost 800 million people are still undernourished globally today, most of them living in developing countries (FAO et al. 2015).

1.2.2. Impacts of anthropogenic land use

Out of the 24 ecosystem services evaluated in the Millennium Ecosystem Assessment, 15 were found to be degraded or being used unsustainably (MEA 2005). To measure the impact of human land use at the global scale Vitousek et al. (1986) introduced the concept of human appropriation of net primary production (HANPP). Using a variety of methodologies and definitions, HANPP has been estimated to range anywhere between 4% and 55% globally (e.g. Vitousek et al. 1986; Rojstaczer et al. 2001; Imhoff et al. 2004; Haberl et al. 2007; Krausmann et al. 2013). Regardless of the exact definition, HANPP essentially represents a reduction in the amount of energy available to other species in the terrestrial biosphere 'which must use the leftovers' (Vitousek et al. 1986). This reduction may happen either directly through harvest, by changing the productivity of ecosystems or by human-induced fires (Haberl et al. 2007). The latter study estimated HANPP to account for roughly 24% of potential terrestrial NPP. While population has increased fourfold over the course of the 20th century, HANPP has roughly doubled (Krausmann et al. 2013). Despite these apparent gains in efficiency, which slowed down agricultural expansion and were achieved mostly through agricultural intensification, roughly 30% of potential forests and 70% of savannas, shrublands and grasslands had been converted to agricultural areas by the end of the 20th century (Pongratz et al. 2008). During the 1980s and 1990s, more than 80% of new agricultural areas in the tropics came at the expense of forests (Gibbs et al. 2010). Changes in land use and management led to cumulative emissions of 190 ± 65 PgC for the period 1750–2015, which correspond to

32% of total anthropogenic carbon emissions since 1750 (600 ± 70 PgC, Le Quéré et al. 2016). While vegetation modelling indicates that land use is responsible for a $\approx 24\%$ reduction in global vegetation carbon compared to potential natural vegetation, carbon losses due to land use change have been partially offset by increases in biomass caused by climate change and rising CO_2 concentrations, leading to a net loss of 30 ± 45 PgC since 1750 (Bondeau et al. 2007; Ciais et al. 2013).

Besides impacts on the global carbon cycle, irrigation in agriculture represents the largest human freshwater use, accounting for 60–70% of total water withdrawals and 80–90% of total freshwater water consumption (Frenken and Gillet 2012; Döll et al. 2012; Döll et al. 2014; Wada et al. 2014; Hoogeveen et al. 2015; Jägermeyr et al. 2015). Irrigation is particularly important in semiarid and arid regions where it may account for more than 95% of withdrawals (Döll et al. 2012). In many regions of the world, water withdrawals exceed local renewable supplies, but there is high uncertainty regarding the share of nonrenewable sources (Vörösmarty et al. 2005; Döll et al. 2009; Döll et al. 2014).

Agricultural activity is the main source (besides fuel combustion) of reactive nitrogen (N_r) in the environment, and N_r creation has increased from 15 Tg in 1860 to 187 Tg in 2005 (1 Tg = 10^{12} g) (Galloway et al. 2008). Only a fraction of the nitrogen applied as fertiliser is retained in food products (Wood et al. 2005; Erisman et al. 2013). Leaching and atmospheric emissions of N_r (leading to deposition in other areas) impact air quality and human health and cause acidification and eutrophication in aquatic ecosystems (Erisman et al. 2013). High N_r deposition may induce species composition changes towards more nitrophilic plants, enhance susceptibility to stress, cause direct foliar damage, and as a whole is linked to reduced plant species richness in many terrestrial ecosystems (Bobbink et al. 2010; Dise et al. 2011; Erisman et al. 2013). Biodiversity is also affected directly by the conversion of species-rich habitats such as tropical and subtropical dry and monsoon forests or temperate broadleaved and mixed forests into croplands, where only 30 different crops provide about 90% of the world population's calorific requirements (Wood et al. 2005).

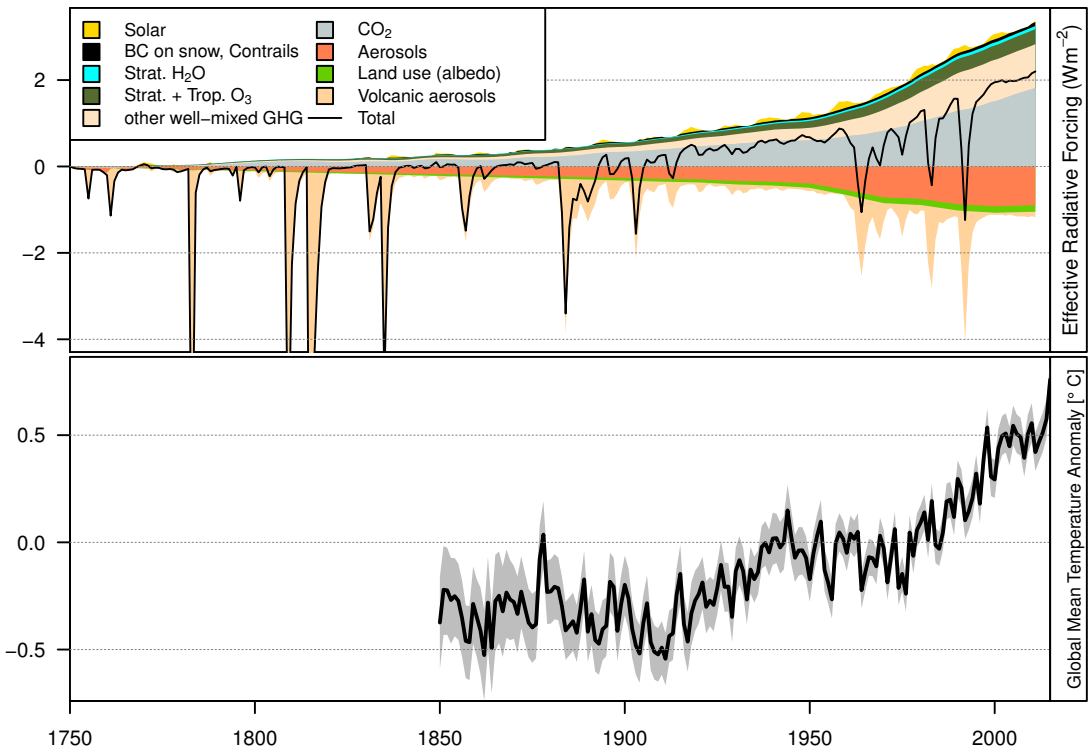

Figure I.2.: Indicators of historical climate forcing. Effective radiative forcing modified after Myhre et al. (2013); BC, black carbon; strat., stratospheric; trop., tropospheric. Global mean surface temperature anomaly relative to 1961–1990 based on HadCRUT version 4.5 provided by the Met Office Hadley Centre and the Climatic Research Unit at the University of East Anglia (`http://www.metoffice.gov.uk/hadobs/hadcrut4/`, accessed January 25, 2017; Morice et al. 2012). Grey shading shows the 95% confidence interval of all the uncertainties described in the HadCRUT4 error model.

1.2.3. Current extent of climate change forcing

Atmospheric CO_2 concentration has risen by more than 40% from a pre-industrial value of 278 ± 5 parts per million (ppm) in 1750 to 402.85 ± 0.10 ppm in 2016 (Joos and Spahni 2008; Hartmann et al. 2013; Dlugokencky and Tans 2017). The concentration of other greenhouse gases (GHG) has also increased because of human activities: atmospheric methane (CH_4) has increased by a factor of 2.5 from 722 ± 25 parts per billion (ppb) to 1803 ± 2 ppb in 2011, while nitrous oxide (N_2O) concentration has increased by $\approx 20\%$ from 270 ± 7 ppb to 324.2 ± 0.1 ppb (MacFarling Meure et al. 2006; Myhre et al. 2013). To compare different biogeochemical or biogeophysical drivers of climate change they

are commonly expressed as radiative forcing (RF, Figure I.2), i.e. 'the change in the net, downward minus upward, radiative flux (expressed in Wm^{-2}) at the tropopause or top of atmosphere' (IPCC 2013a). RF from additional well-mixed GHG, which include CO_2, CH_4, N_2O as well as a number of halocarbons, between 1750 and 2011 has been estimated at $2.83 \pm 0.29\,\mathrm{Wm}^{-2}$ (Myhre et al. 2013, Figure I.2). RF from changes in ozone (O_3) and stratospheric water vapour adds 0.35 ± 0.20 and $0.07 \pm 0.05\,\mathrm{Wm}^{-2}$, respectively, with significant latitudinal variations (Myhre et al. 2013). On the other hand, aerosol-cloud and aerosol-radiation interactions have a cooling effect estimated at $-0.9\,\mathrm{Wm}^{-2}$ (likely range -1.5–$-0.4\,\mathrm{Wm}^{-2}$, Boucher et al. 2013, Figure I.2). Besides its contribution to GHG and aerosol emissions, the biogeophysical impact of land use on climate is complex because radiative processes such as albedo changes (cooling effect of $-0.15 \pm 0.10\,\mathrm{Wm}^{-2}$) may be counterbalanced by non-radiative processes such as ET and surface roughness changes (warming effect), likely leading to an overall biogeophysical cooling of deforestation in high latitudes versus a warming effect in the tropics (Myhre et al. 2013). Irrigation induces local cooling which is opposite in sign and may exceed GHG-induced warming in magnitude in regions with large irrigated areas (Kueppers et al. 2007; Lobell et al. 2009).
Changes in solar irradiance and aerosol emissions from volcanic eruptions represent the largest natural forcings of climate change since 1750: The best estimate of the former is $0.05 \pm 0.05\,\mathrm{Wm}^{-2}$ compared to 1750, whereas volcanic eruptions can cause significant negative RF, but effects last only for a short period of time (Myhre et al. 2013, Figure I.2).

Temperature records show that global mean surface temperature has increased by 0.78 (0.72–0.85) K between the average 1850–1900 period and the average 2003–2012 period, but they also show substantial decadal and interannual variability (Hartmann et al. 2013). Warming occurred primarily during two periods lasting from $\approx$ 1900–1940 and from $\approx$ 1970 onwards (Figure I.2). Because of insufficient observations, there is only low confidence in changes of precipitation averaged over global land areas before 1950 and medium confidence afterwards, although there has likely been an overall increase in precipitation over the mid-latitudes of the northern hemisphere since 1901, while tropical land areas experienced a drying trend from the mid-1970s to mid-1990s followed by an increase in precipitation over the last decade (Hartmann et al. 2013).

1.2.4. Recent impacts of climate change

There is comprehensive evidence that changes in climate have caused impacts on natural systems on all continents and across the oceans in recent decades (IPCC 2014c). Impact observations vary by the degree of confidence in detection and confidence in attribution to climate change (Settele et al. 2014). Changes in phenology such as spring advancement of bud burst or arrival of migratory birds and delay of biological autumn or winter, e.g. leaf fall, are some of the most prominent changes of plants and animals to climate change, associated with a high confidence in both detection and attribution (e.g. Parmesan 2007; Jones et al. 2009a; Peñuelas et al. 2013). Changes in phenology differ between species which may affect inter-species relations such as the synchrony of life cycles between predator and prey or the competition among different species for resources (e.g. Parmesan 2006; Peñuelas et al. 2013). Besides changes in phenology, the ranges of many species are shifting in latitude at speeds averaging between 6 and 17 km, or in elevation at 6 to 11 m per decade (e.g. Parmesan and Yohe 2003; Chen et al. 2011). Range shifts are often inferred from small-scale observations along a range boundary or from changes in species' abundances in local communities (Parmesan 2006). Range shifts are also often driven by other factors (see for example Hockey et al. 2011 mentioned above), resulting in only medium confidence in both detection and attribution to climate change (Settele et al. 2014).

Besides its role in driving climate change, the rise in atmospheric CO_2 concentration has a strong direct effect on plant productivity, referred to as the CO_2 fertilisation effect (e.g. Hickler et al. 2008; Donohue et al. 2013). Increased CO_2 concentration directly stimulates photosynthesis in C3 plants, while both C3 and C4 plants benefit from increased water use efficiency under water-limited conditions because of a reduction in stomatal conductance (Long et al. 2006; Ainsworth et al. 2008). Long-term satellite records of leaf area index (LAI) show a persistent greening trend of large parts of the globe over recent decades which has been attributed predominantly to CO_2 fertilisation (70%), followed by nitrogen deposition (9%), climate change (8%) and land cover change (4%) (Zhu et al. 2016). For warm, arid environments, Donohue et al. (2013) report an 11% increase of vegetation cover between 1982 and 2010 driven by CO_2 changes, adding to a 14% greening driven by precipitation changes. There is high confidence that terrestrial and freshwater ecosystems have sequestered $\sim 1/4$ of the anthropogenic CO_2 emissions in the past three decades, driven by positive effects of CO_2 fertilisation,

warming climate, nitrogen deposition and recovery from past disturbances such as land use (Settele et al. 2014). While boreal forests as a whole have been a relatively constant net sink of $0.5 \pm 0.1\,\mathrm{PgC/yr}$ between 1990 and 2007 there are concerns that at least the sink in Canadian forests has been decreasing in recent years due mostly to increased wildfires and bark beetle outbreaks (Kurz et al. 2008; Pan et al. 2011; Stinson et al. 2011). Beck and Goetz (2011) also note a contrast of increasing tundra and decreasing boreal forest productivity in North America. *Larix* species common to northern Eurasia were significantly less likely to exhibit negative trends in productivity than *Picea* species which dominate North America (Goetz et al. 2007). Deforestation has more than offset the carbon sink in intact and regrowing tropical forests (Pan et al. 2011). In addition, there is evidence that intense drought may reverse the long-term trend of biomass accumulation, and that feedbacks between fires — facilitated by forest fragmentation and anthropogenic ignition sources — and drought are already causing wide-spread forest degradation over large areas such as the southeastern Amazon region (Phillips et al. 2009; Brando et al. 2014).

1.3. Prospects for the terrestrial biosphere until 2100

Since the future cannot be known, scenario analysis is a common method to study alternative possible futures. Scenarios are 'plausible description[s] of how the future may develop based on a coherent and internally consistent set of assumptions about key driving forces [...] that [...] are neither predictions nor forecasts, but are useful to provide a view of the implications of developments and actions' (IPCC 2013a). Human population is expected to grow in numbers for the next decades, as is humanity's hunger for food, energy and other resources—the main anthropogenic drivers that have pushed the Earth system out of the Holocene into the Anthropocene. The United Nations Population Division (UNPD) projects total population to reach 9.75 billion by 2050 and 11.2 billion by 2100 in a median fertility scenario, but has also explored a number of alternative scenarios leading to 7.3 to 26 billion people in 2100 (UNPD 2015). Population projections in the four Representative Concentration Pathways (RCPs) and the five Shared Socioeconomic Pathways (SSPs) are in a similar range as the low and median variants by UNPD reaching 8.7 to 12 billion and 6.9 to 12.6 billion people in 2100, respectively (van Vuuren et al. 2011a; KC and Lutz 2017). Scenarios of future land

use forcing depend chiefly on future demand, which is a function of population, but also affluence, dietary choices and non-food demand such as bioenergy production. Secondly, land use forcing is determined by the question whether an increase in demand is fulfilled by extensification, i.e. an increase in land use area, or intensification, i.e. an increase in production per area unit (e.g. Tilman et al. 2011; Johnson et al. 2014). For example, the four scenarios underlying the RCPs project global cropland—which includes bioenergy plantations in the majority of cases—to reach 11.3–21 million km^2 in 2100, while pastures cover 17.9–37.1 million km^2 (Hurtt et al. 2011). Cropland increases in three of the scenarios while pastures decrease in three out of four cases.

Scenarios of future anthropogenic climate forcing are determined by a wide range of variables including socioeconomic change, technological change, energy and land use, and emissions of greenhouse gases and air pollutants (van Vuuren et al. 2011a). Working group III (WGIII) of the IPCC assessed roughly 300 baseline and 900 mitigation scenarios for AR5 (IPCC 2014d). Baseline scenarios, i.e. those without additional mitigation, reach atmospheric GHG concentration levels between 750 and more than 1300 ppm CO_2eq (CO_2 equivalent) in 2100, with a projected global warming between 2.5 and 7.8 K above pre-industrial levels, while mitigation scenarios span a range between 430 and roughly 720 ppm CO_2eq (IPCC 2014d). Taking into account the uncertainties in the climate system, only scenarios that do not exceed—even for a limited overshoot period—530 ppm CO_2eq are more likely than not to keep global warming below 2 K above pre-industrial levels (Clarke et al. 2014).
Spatially resolved climate projections from general circulation models (GCMs) and Earth system models (ESMs) are only available for a small subset of emissions scenarios. Scenario uncertainty combined with climate model uncertainty, i.e. different models simulating a different response to the same forcing, limits the ability to assess impacts of climate change systematically and consistently as a function of global mean temperature change (Hawkins and Sutton 2009, 2011).

2. Main research questions

In the previous sections I have outlined the global role of human land use and climate change as major drivers of ecosystem change in the Anthropocene. I have given some examples of the multitude of observed and simulated impacts resulting from the two drivers that have been reported in the scientific literature. The overarching question of this dissertation is:

- What are the individual and joint impacts of human interference with the biosphere through climate and land use change during the Anthropocene?

In the context of this dissertation 'land use' refers to the use of land for crop production or the use as pastures and rangelands. Built-up area, while locally important in cities, only covers ≈ 0.5 million km^2 globally and is not included as a global driver of biome change in this analysis (Klein Goldewijk et al. 2010). 'Climate change' refers to changes in temperature, precipitation and cloud cover (radiation) beyond interannual variability. Direct effects of changes in atmospheric CO_2 concentration on vegetation are also included in climate change impacts.

Using these definitions, I will explore the following questions:

1. **Given that the climate policy debate is focussed very much on temperature targets, what are the risks of different levels of global warming for ecosystems? Is there a 'safe' level of warming where impacts remain low?**
   For this question, I will explore eight emissions scenarios for the 21st century spanning the range from strong mitigation to business as usual with a high reliance on fossil fuels. These scenarios are constructed specifically to lead to global warming of 1.5 to 5 K compared to the pre-industrial level in 2100. Each scenario will be assessed for a number of climate models in order to account for GCM uncertainty.

2. **What has been the magnitude of human interference with the biosphere through land use and climate change over the course of the Anthropocene? When did human activities start to become a force of major ecosystem change? Which of the two forcings, land use or climate change, has been the dominant one?**
   For this question, I will trace the expansion of agriculture from 1700 to today, as well as the rise in CO_2 concentrations following the Industrial Revolution and the resulting climate change during the 20th and early 21st century.

3. **How do projected population growth (with the associated demand for land) and climate change interact in pushing the biosphere further out of its Holocene state? Given that climate mitigation may entail a sizeable contribution of biofuels to the global energy mix, are there trade-offs between land use change and climate change?**
   For this question, I will explore a number of integrated assessment scenarios that provide projections of both future emissions and land use until 2100.

3. Methodology

3.1. Metric of biosphere change

In this dissertation I will focus on the impacts of land use and climate change on the carbon and water cycle of the terrestrial biosphere as well as vegetation composition in terms of major functional types. While these aspects represent only a subset of the full impact of human actions they are crucial to the functioning of the biosphere within the Earth system as a whole. Vegetation productivity and structure determine to a large extent the ability of ecosystems to provide habitats, food and other resources to consumers such as animals and, ultimately, humans as well.

I will use an aggregated metric of joint changes in macroscopic ecosystem features, including carbon and water fluxes and stores as well as vegetation structure, to evaluate

ecosystem changes caused by climate and land use change ('Γ' metric, Heyder et al. 2011). The metric operates under the assumption that substantial changes in these basic characteristics 'imply far-reaching, potentially self-amplifying transformations in the underlying system characteristics, food chains and species composition' and a risk that 'adaptation fails on short time scales and the system restructures or collapses' (Heyder et al. 2011). It allows for a spatially explicit, globally consistent quantification of ecosystem change over time under both historical and future scenario conditions. Γ values range between 0 and 1. Values below 0.1 are interpreted to indicate a risk of minor, values between 0.1 and 0.3 a risk of moderate, and values above 0.3 a risk of major ecosystem changes. To illustrate the magnitude of change corresponding to a certain Γ value, Figure B.2 in Appendix B presents the difference between present-day biomes, assuming each biome was transformed completely into the others. As shown, moderate changes ($0.1 < \Gamma < 0.3$) may already correspond to the difference between similar, yet distinct biomes — such as a temperate broadleaved and a temperate coniferous forest — while major changes ($\Gamma > 0.3$) indicate a transformation to a completely different biome. While the original Γ metric was developed to assess climate-driven changes in natural ecosystems, I will expand it here to apply it to both climate-driven and land-use-driven changes. Details about the calculation of the different components of Γ are provided in section E.1 and section E.2 of Appendix E.

3.2. Biosphere model

I will use the well-established dynamic global vegetation model (DGVM) LPJmL (Sitch et al. 2003; Bondeau et al. 2007) to quantify shifts in the carbon and water cycle as well as dynamic vegetation composition of the terrestrial biosphere in response to climate and land use change. LPJmL is capable of simulating key physiological and ecological processes such as phenology, photosynthesis, respiration, carbon allocation and turnover between tissue pools, and evapotranspiration for natural vegetation, represented by 9 plant-functional types (PFTs, Sitch et al. 2003), agricultural ecosystems represented by 12 crop-functional types (CFTs) and managed grasslands (Bondeau et al. 2007), and herbaceous and woody plants grown as dedicated 2nd-generation biomass plantations (Beringer et al. 2011). PFTs of the natural vegetation compete for light, space and water, and their composition in a grid cell is determined dynamically based on climatic

suitability, growth efficiency, climatic stress and fire disturbance (Thonicke et al. 2001; Sitch et al. 2003). Crops, managed grasslands and biomass plantations grow on prescribed areas and may be irrigated or rainfed (Bondeau et al. 2007; Beringer et al. 2011). Since the model is being developed continuously, the different parts of this dissertation use different versions of LPJmL. A more in-depth description of relevant model processes is provided in each part.

3.3. Scenarios

I will explore the first research question outlined above using a new set of climate change scenarios created specifically for this analysis. The generation of the 'PanClim' climate dataset is described in Part II of this thesis. The 'PanClim' scenarios are based on 8 stylised emissions trajectories chosen from a large ensemble of emissions scenarios to specifically reach a global warming of 1.5, 2, 2.5, 3, 3.5, 4, 4.5 and 5 K above pre-industrial level around the year 2100. The scenarios contain no further socioeconomic information.

The second research question comprises a historical analysis. I will use a historical land use reconstruction based on the HYDE database and enriched with additional topical detail on crop types and irrigated areas to assess the impact of historical land use change on the biosphere (Klein Goldewijk and van Drecht 2006; Portmann et al. 2010). Observed climate data and a reconstruction of historical atmospheric CO_2 concentrations will be used to assess the impact of historical climate change on the biosphere (Keeling et al. 2001; Schneider et al. 2011; Becker et al. 2013; University of East Anglia Climatic Research Unit (CRU) et al. 2013; Harris et al. 2014).

The third research question expands upon the historical analysis conducted for research question 2. I will use the Representative Concentration Pathways (RCPs) which were developed by integrated assessment models (IAMs) (van Vuuren et al. 2011a). The RCPs include both emissions scenarios and land use scenarios for the 21st century based on a set of socioeconomic assumptions. Climate change projections based on the RCPs were produced by a large number of climate models as part of the Coupled Model Intercomparison Project Phase 5 (CMIP5, Taylor et al. 2012). The RCP land use

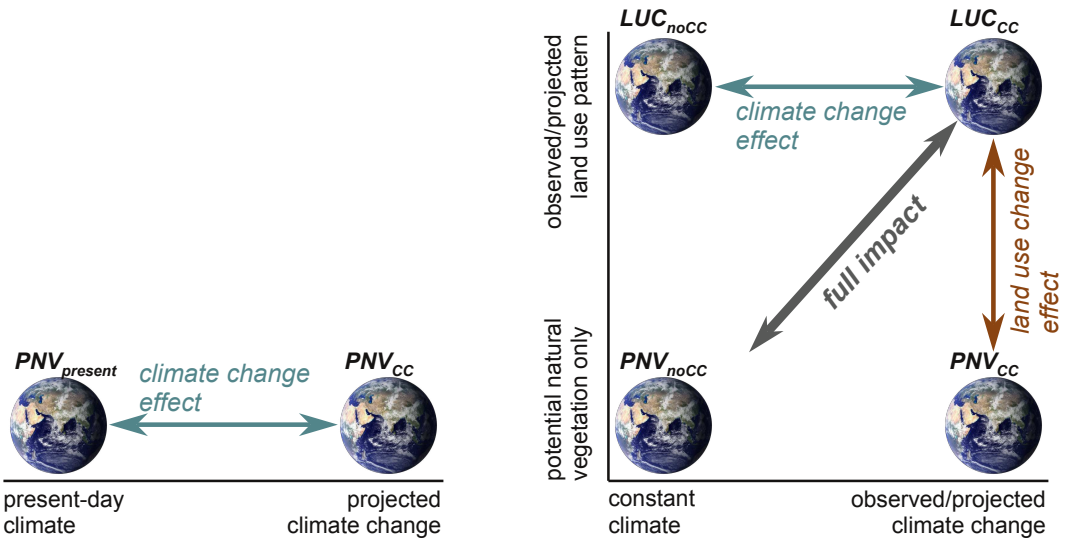

Figure I.3.: Illustration of reference conditions. Left: Setup for research question 1: Climate change impact is calculated as the difference between natural vegetation under climate change (PNV_{CC}) and natural vegetation under present-day climate ($PNV_{present}$). Right: Setup for research question 2 and 3: LUC_{CC} refers to a simulation with climate change and land use change. PNV_{CC} refers to a simulation with climate change, but without any land use. LUC_{noCC} refers to a simulation with land use change, but with a constant reference climate. PNV_{noCC} refers to a simulation using a constant reference climate and without any land use. Earth image by NASA Goddard Space Flight Center.

scenarios have been harmonised to provide a common spatial and temporal resolution and a smooth transition from historical land use patterns (Hurtt et al. 2011).

To assess the changes driven by climate and land use change, it is necessary to define suitable sets of reference conditions for each of the research questions. For question 1, I will use natural vegetation under present-day climate as the reference for the changes to natural ecosystems caused by climate change ($PNV_{present}$, left panel in Figure I.3). Future climate change impacts are commonly assessed in comparison to a baseline representative of present-day conditions (Carter et al. 1994).
For research questions 2 and 3, I will use potential natural vegetation as a reference for the impact of human land use on the biosphere (PNV_{CC}, right panel in Figure I.3). In order to be comparable, the reference for climate change impacts should ideally be 'a world without anthropogenic climate change' which, however, is not easily defined. Based on attribution studies, human activities are extremely likely the cause for the majority

of observed warming since 1951 (Bindoff et al. 2013). While GHG-induced warming may be detectable as early as the mid-19th century (Abram et al. 2016), the contribution from internal variability, natural and anthropogenic forcing to early observed warming is difficult to quantify (Bindoff et al. 2013). Also taking into account the availability of observation-based gridded climate data, which are used to drive the LPJmL model, climate conditions representative of the first 30 years of the 20th century will be used as the climatic baseline, referred to as 'noCC' in Figure I.3. LUC_{noCC} provides the reference conditions for the impacts of climate change, i.e. a world without climate change, but with land use. Finally, PNV_{noCC} provides the reference for the combined impact of climate and land use change (right panel in Figure I.3).

4. Structure of the thesis

This thesis presents the results of a cumulative dissertation. As such, the thesis contains several self-contained parts which have already been published as peer-reviewed research articles (Part II, Part III, Part IV, Part V) or are currently under revision for publication as a peer-reviewed article (Part VI). Each part focuses on different aspects, time periods and methodologies. All the parts contribute to the overall research questions of the thesis (Figure I.4).

- Part I provides a general introduction to the dissertation subject and outlines the main research questions.
- Part II describes the methodology used to create the 'PanClim' climate dataset which forms the basis of climate impact simulations in Part III and Part IV.
- Part III and Part IV both explore climate change impacts on the biosphere as a function of the level of global warming. Part III provides an in-depth analysis of the areas at risk of major climate change impacts. Part IV expands upon this analysis and explores indications of these changes for (plant) biodiversity and also adds an analysis of changes in freshwater availability which may bear special societal relevance in regions prone to water scarcity.

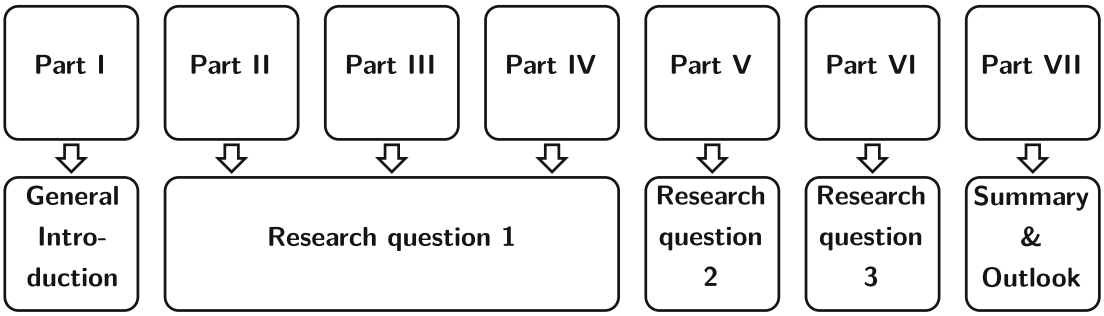

Figure I.4.: Thesis structure. The diagram illustrates how the different parts contribute to the main research questions.

- Part V explores the temporal evolution of human interference with the biosphere through both land use and climate change over the course of the last three centuries.
- Part VI extends the historical analysis of joint impacts of climate and land use change conducted in Part V to assess how humanity's impact on the biosphere may develop during the 21st century under a range of scenarios.
- Part VII provides a summary and synthesis of the different parts of the thesis and an outlook.

4.1. Author contributions

Part I and Part VII have been written by myself alone while the other parts have been prepared in collaboration with co-authors listed at the beginning of each part. My contribution to each part was as follows:

- For Part II, I partly contributed to designing the study, jointly developed the methodology with Jens Heinke, predominantly conducted programming and data processing for the pattern extraction and pattern application, and partly contributed to preparing the manuscript. I did not contribute to the evaluation of the patterns and the effect of the application method or the creation of the emissions scenarios.
- For Part III, I predominantly designed the study, completely performed the simulations and completely conducted the analysis of results. I mostly prepared the manuscript.

- For Part IV, I partly contributed to designing the study, completely performed the simulations, predominantly conducted the analysis of results for terrestrial ecosystems and biodiversity, partly conducted the analysis of results for water scarcity, and partly contributed to writing the manuscript.
- For Part V, I predominantly designed the study, completely performed the simulations, completely conducted the analysis of results, and predominantly prepared the manuscript.
- For Part VI, I predominantly designed the study, partly contributed to the collection and preparation of the scenario data, completely performed the simulations, completely conducted the analysis of results, and predominantly prepared the manuscript.

Part II.

A new climate dataset for systematic assessments of climate change impacts as a function of global warming[1]

Jens Heinke, Sebastian Ostberg, Sibyll Schaphoff, Katja Frieler, Christoph Müller, Dieter Gerten, Malte Meinshausen, and Wolfgang Lucht

[1] An edited version of this part has been published under the Creative Commons Attribution 3.0 License as: J. Heinke et al. 2013. 'A new climate dataset for systematic assessments of climate change impacts as a function of global warming.' *Geoscientific Model Development* 6 (5): 1689–1703. doi:10.5194/gmd-6-1689-2013

Abstract

In the ongoing political debate on climate change, global mean temperature change (ΔT_{glob}) has become the yardstick by which mitigation costs, impacts from unavoided climate change, and adaptation requirements are discussed. For a scientifically informed discourse along these lines, systematic assessments of climate change impacts as a function of ΔT_{glob} are required. The current availability of climate change scenarios constrains this type of assessment to a narrow range of temperature change and/or a reduced ensemble of climate models. Here, a newly composed dataset of climate change scenarios is presented that addresses the specific requirements for global assessments of climate change impacts as a function of ΔT_{glob}. A pattern-scaling approach is applied to extract generalised patterns of spatially explicit change in temperature, precipitation and cloudiness from 19 Atmosphere-Ocean General Circulation Models (AOGCMs). The patterns are combined with scenarios of global mean temperature increase obtained from the reduced-complexity climate model MAGICC6 to create climate scenarios covering warming levels from 1.5 to 5 degrees above pre-industrial levels around the year 2100. The patterns are shown to sufficiently maintain the original AOGCMs' climate change properties, even though they, necessarily, utilise a simplified relationships between ΔT_{glob} and changes in local climate properties. The dataset (made available online upon final publication of this paper) facilitates systematic analyses of climate change impacts as it covers a wider and finer-spaced range of climate change scenarios than the original AOGCM simulations.

5. Introduction

Impacts of anticipated future climate change on ecosystems and human societies are reason for major concern. Projections of such impacts are, however, characterised by uncertainties in greenhouse gas (GHG) emissions scenarios, their implementation in climate models (involving *inter alia*structural uncertainties of climate models) and their subsequent use in impact models. Despite intense research summarised, for example, by the Intergovernmental Panel on Climate Change's Working Group II report (IPCC 2007a), assessments commonly lack systematic quantification of impacts as a function of global warming, as only a small and often opportunistic selection of available climate change scenarios is employed. This hampers direct comparisons between studies (e.g. Müller et al. 2011) and also our understanding of how impacts and their likelihood change over time or as a function of global mean temperature (T_{glob}). The magnitude of impacts to be expected given specific degrees of T_{glob} rise has gained increasing attention in recent years due to the United Nations Framework Convention on Climate Change's stipulation to prevent 'dangerous climate change' and the ensuing discussion on whether this would be met by a 2-degree mitigation target (rather than, for example, a 1.5 or 3 degree target). Besides requiring an understanding of how impacts individually and collectively accumulate with increasing T_{glob}, an understanding of the consequences of missing a given target is important for this discussion (e.g. Mann 2009). Compilations of individual impact studies have helped to illustrate the underlying 'reasons for concern' (Smith et al. 2009) but do not provide the consistent quantitative information needed.

In view of the importance of mitigation targets for the debate on climate change mitigation and the substantial investments required to meet them, the number of studies that scrutinise systematically and consistently the worldwide impacts to be expected as a function of ΔT_{glob}, let alone their uncertainties, is surprisingly small. Examples for global assessments of impacts ordered along ΔT_{glob} and derived with single impact modelling frameworks are those by Arnell et al. (2011); Gosling et al. (2010), and Murray et al. (2012) for freshwater availability, and those by Gerber et al. (2004); Scholze et al. (2006); Sitch et al. (2008), and Heyder et al. (2011) for ecosystems and the carbon cycle. Other assessments have focused on diverse impacts given a ΔT_{glob} of 4 degrees (see New et al. 2011).

While much of the uncertainty in T_{glob} is attributable to the fact that the exact development of future GHG emissions cannot be known — requiring a scenario approach (Hawkins and Sutton 2009) — the parameterisation of Atmosphere-Ocean General Circulation Models (AOGCMs) additionally contributes to uncertainty in regional temperature and precipitation changes associated with a given ΔT_{glob} (Hawkins and Sutton 2011). Most of above-mentioned studies could account only partly for the latter, as they either relied on a small selection of AOGCMs or grouped larger ensembles according to the ΔT_{glob} reached by the individual AOGCMs by the end of their simulation period (e.g. Scholze et al. 2006). More rigorous assessments of impacts as a function of global warming are generally limited by the availability of AOGCM simulations in the CMIP3 archive. The range of warming levels covered by the different AOGCMs differs widely and the increase in T_{glob} over the twenty-first century for the highest emission scenario A2 is only 3.4 in the multi-model mean (Meehl et al. 2007).

Overall, systematic assessments of climate change impacts as a function of global warming require that a large ΔT_{glob} range be covered (from, for example, 1.5 to 5 degrees), and that the respective ΔT_{glob} levels are reached at around the same time. Furthermore, for every ΔT_{glob} level, information on local changes in key climate variables (such as temperature, precipitation, radiation or cloudiness) should consider an AOGCM multi-model ensemble as large as possible, in order to account for the substantial climate model-structural uncertainty. Such consistent information is not directly available in the existing CMIP3 and CMIP5 climate databases — it requires fusion of comprehensive datasets on climate change patterns from different AOGCMs with different ΔT_{glob} trajectories (and underlying emissions trajectories), information on observed climate (without AOGCM biases), and reduced-complexity models able to overcome the high computation requirements of AOGCMs.

To address some of these features, a number of studies (e.g. Gosling et al. 2010; Murray et al. 2012) have used emulated rather than original AOGCM output, calculated with the so-called 'pattern-scaling' technique (Mitchell 2003) that makes use of the correlation between local long-term mean changes of climate variables and ΔT_{glob}. Scaling coefficients were found to differ spatially and seasonally, but particularly for temperature they are nearly independent of the GHG emission scenarios considered and sufficiently accurate over a wide range of ΔT_{glob} (Solomon et al. 2009; Mitchell 2003; Huntingford and Cox 2000). Hence, pattern-scaling is an efficient method to generate climate scenarios for

systematic analyses of climate impacts as a function of ΔT_{glob}.

Using a comprehensive pattern-scaling approach covering monthly mean surface temperature, cloudiness and precipitation, we here present a newly collated global dataset of climate change scenarios that overcomes most of the above problems and is suited for systematic, macro-scale impact assessments with empirical or process-based impact models. It is based on GCM-specific scaling patterns that are combined with time series of ΔT_{glob} generated by a reduced-complexity climate model, MAGICC6 (Meinshausen et al. 2011a). The emissions scenarios are designed such that each of eight ΔT_{glob} levels (1.5 to 5 degrees above pre-industrial levels in 0.5 degree steps) is reached by 2100. Monthly climate anomaly patterns are derived for each of 19 AOGCMs available from the World Climate Research Programme's (WCRP's) Coupled Model Intercomparison Project phase 3 (CMIP3) multi-model dataset. Scaling the derived generic change patterns per degree of global mean warming with the ΔT_{glob} trajectories generates transient time series of climate anomalies up to 2100. This dataset enables consistent analyses of impacts as a function of ΔT_{glob} at the end of the century, and improved comparability of climate patterns and resulting impacts for given T_{glob} levels. The dataset is referred to as 'PanClim' (PAtterN scaling CLIMate dataset) to indicate its methodological background and its wide-spanning coverage of the scenario space (pan, Greek for 'all', 'involving all members'). The complete PanClim dataset is available for download from `http://www.panclim.org`.

6. Methods

Figure II.1 sketches the steps of data processing and combination involved in the creation of the climate scenarios, described in detail in the following sections. Section 6.1 describes the extraction of scaling patterns — i.e. the spatial fields of local (monthly) climate change per one degree of ΔT_{glob} — from AOGCM simulations. Section 6.2 covers the generation of T_{glob} trajectories by the MAGICC6 model, and their combination with the derived scaling patterns to generate time series of mean local climate anomalies for the given warming scenarios. Section 6.3 focuses on the combination of these local anomalies

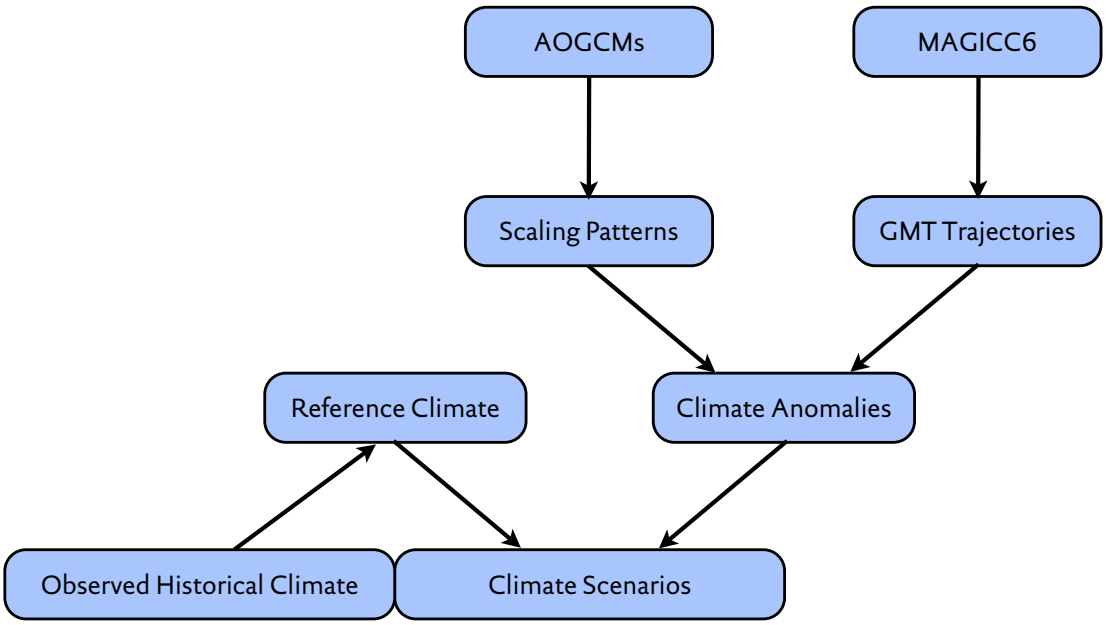

Figure II.1.: Flow chart of data processing for the generation of climate scenarios.

with data on observed variability and climatological means to generate climate scenarios harmonised with historical observations, covering the entire global land area.

6.1. Derivation of scaling patterns from AOGCM simulations

The basic concept behind the methodology described in this paper is that any simulated or observed monthly time series $V(x, m, y)$ of a climate variable V (e.g. air temperature) in location x, month m, and year y can be decomposed as follows:

$$V(x, m, y) = \overline{V}(x, m) + \Delta\overline{V}(x, m, y) + e(x, m, y) \tag{II.1}$$

where $\overline{V}(x, m)$ denotes the long-term mean and $\Delta\overline{V}(x, m, y)$ the long-term mean change of variable V; the term $e(x, m, y)$ describes the natural interannual variability around the long-term mean.

The general idea of the pattern scaling approach is to relate the local anomalies in the long-term mean $\Delta\overline{V}(x, m, y)$ in Equation II.1 to a global scaler for which scenario trajectories can be easily obtained (Mitchell 2003). In agreement with previous studies

(e.g. Huntingford and Cox 2000; Mitchell 2003), we here use global mean temperature ΔT_{glob} as scaler and assume a linear relationship between local monthly climate anomalies $\Delta\overline{V}(x,m,y)$ and $\Delta T_{\text{glob}}(y)$:

$$\Delta\overline{V}(x,m,y) = V^*(x,m) \cdot \Delta T_{\text{glob}}(y) \tag{II.2}$$

where $V^*(x,m)$ is the *scaling coefficient*, i.e. the change in $\overline{V}(x,m)$ per degree of ΔT_{glob} for each location and month but independent of time (y). The entirety of all scaling coefficients $V^*(x,m)$ for a particular variable and AOGCM is referred to as *scaling pattern*.

Substitution of Equation II.2 in Equation II.1 and subtraction of $\overline{V}(x,m)$ from both sides of the equation gives:

$$V(x,m,y) - \overline{V}(x,m) = V^*(x,m) \cdot \Delta T_{\text{glob}}(y) + e(x,m,y) \tag{II.3}$$

Equation II.3 describes all deviations of V from the long-term mean $\overline{V}(x,m)$ as sum of changes in the long-term mean (expressed by the linear relationship to $\Delta T_{\text{glob}}(y)$) and interannual variation around the long term mean. This equation has the form of a simple linear regression model that provides the basis for estimating scaling coefficients from AOGCM simulations. For the estimation of $V^*(x,m)$ from AOGCM simulations, the monthly data were linearly interpolated from their original spatial resolution to the target resolution used here, a regular 0.5×0.5 arc-degree grid. Estimates of $\overline{V}(x,m)$ are obtained from the pre-industrial control run (equilibrium simulation without any anthropogenic forcing) available for all AOGCMs with lengths between 100 and 990 simulation years. Subtraction of $\overline{V}(x,m)$ from simulations with climate forcing yields deviations from the long-term climatological mean that are taken as a dependent variable in the estimation of $V^*(x,m)$ by linear regression. The corresponding independent variable $\Delta T_{\text{glob}}(y)$ is obtained from estimates of $T_{\text{glob}}(y)$ that are calculated as annual area-weighted global averages (including oceans) of $T(x,m,y)$. Since the extraction of patterns of $V^*(x,m)$ is based on linear regression, the residual errors $e(x,m,y)$ in Equation II.3 are in fact a mixture of interannual variability and the imperfection of the regression model. The quality of the fit obtained can thus be evaluated by comparison of residual errors and respective interannual variability estimated from the control simulation (see section 7.2). We applied the above methodology to estimate scaling patterns for near-surface air temperature, cloudiness and precipitation. Additionally, we studied logarithmic precipitation to reflect an alternate assumption of exponential rather

than linear precipitation change. In the logarithmic precipitation regression model, exclusion of dry months alters the estimated trend of precipitation amounts under climate change. This problem is not purely of numerical nature but highlights that the change in frequency of rain months and the change in the rainfall amounts for rain months represent qualitatively different information that should be addressed separately. Hence, we removed dry months (<1 mm per month) from the linear fit (Equation II.3) of both precipitation and logarithmic precipitation so that both regression models capture the change in rainfall amounts for rain months only.

Building on the basic principle of the pattern-scaling approach, the change in frequency of rain months (p) was considered separately by applying a logistic regression model, in which probabilities are logit-transformed and related to a linear predictor term, which gives a generalised linear regression model:

$$\begin{aligned} \text{logit}\left(p(x,m,y)\right) &= \ln\left(\frac{p(x,m,y)}{1-p(x,m,y)}\right) \\ &= \beta_0(x,m) + \beta^*(x,m)\cdot\Delta T_{\text{glob}}(y) \end{aligned} \tag{II.4}$$

where $\beta_0(x,m)$ and $\beta^*(x,m)$ denote the pre-industrial value and the scaling coefficient, respectively, for logit-transformed probability of rain month occurrence in location x and month m. For the estimation of both model coefficients from time series of dry/rain month occurrence we used the glm () function (Generalised Linear Model) from the core package 'stats' of the statistical software R (R Development Core Team 2011).

6.2. Construction of climate scenarios from derived patterns

6.2.1. Construction of scenarios of global mean temperature increase

The derived scaling patterns $V^*(x,m)$ for the different climate variables are the basis for constructing time series of local anomalies of climate variables consistent with prescribed T_{glob} trajectories. We ran the MAGICC6 model to obtain physically and systemically plausible ΔT_{glob} trajectories and corresponding trajectories of atmospheric CO_2 concentration ($[CO_2]$) (required for some impact models). MAGICC6 is a highly efficient reduced-complexity carbon cycle climate model (Meinshausen et al. 2011a) that has been shown to closely emulate mean results of complex AOGCMs from the

CMIP3 data base (Meinshausen et al. 2011b). Here, MAGICC6 was used to calculate ΔT_{glob} and $[CO_2]$ for a large number of artificial emissions pathways, constructed as described by Meinshausen et al. (2009). For that purpose MAGICC's carbon cycle parameters were adjusted to reproduce the Bern carbon cycle model and the climate model parameters were chosen to reproduce the median responses of the CMIP3 AOGCM ensemble. Climate sensitivity, for example, was set to 3.0 K.

From the generated large ensemble of pathways we selected those pairs of ΔT_{glob} and $[CO_2]$ trajectories where average ΔT_{glob} in the period 2086–2115 reached 1.5, 2.0, 2.5, 3.0, 3.5, 4.0, 4.5, and 5.0 degrees above the pre-industrial level (see Figure II.2). The definition of the temperature target for a period rather than for a single year (e.g. 2100) was chosen because the analysis of time periods is common practice in impact assessments to avoid spurious effects from interannual variability. 30 yr is a typical length used in impact studies in hydrology, agriculture, and ecosystems, for which our new data set is designed.

An outstanding feature in Figure II.2 that illustrates the above-mentioned physical and systemic plausibility is the initially stronger increase in T_{glob} in the lower than in the high temperature scenarios. Stronger mitigation scenarios tend to show a much faster decrease in aerosol emissions than in CO_2 emissions, as a rapid decrease of CO_2 emissions is accompanied by a switch to 'cleaner' sources of energy. This correlation between CO_2 and aerosol emissions results from our use of the Equal Quantile Walk method (Meinshausen et al. 2006) to create the different emission profiles that led to the various warming levels. The drop in aerosol emissions in combination with the much shorter residence time of aerosols in the atmosphere results in a rapid reduction of the aerosol cooling effect (see Ramanathan and Feng 2008). As a consequence, the committed warming from current $[CO_2]$ can unfold before a further reduction of CO_2 emissions eventually results in an overall decrease in radiative forcing and temperature. Conversely, the CO_2 emissions in the high temperature scenarios are accompanied by high aerosol emissions that maintain the cooling effect. Besides the possibility to produce T_{glob} scenarios together with consistent $[CO_2]$ trajectories, the consideration of such effects is the major advantage of applying MAGICC6 in this study.

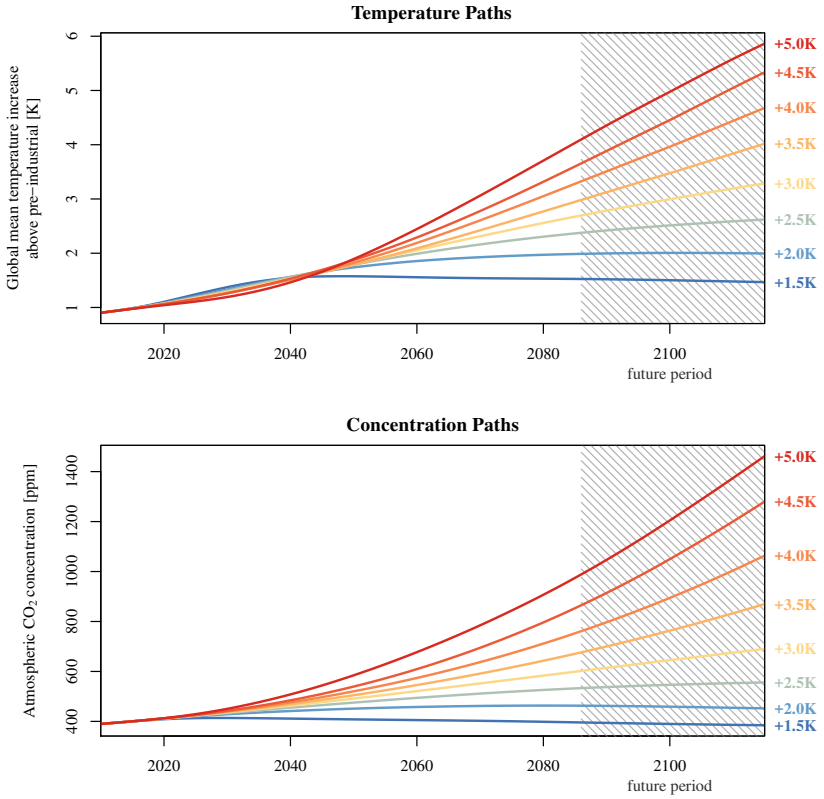

Figure II.2.: Trajectories of global mean temperature increase used in this study and corresponding atmospheric CO_2 concentrations from the MAGICC6 model. The shaded area indicates the time period for which the temperature targets are calculated.

6.2.2. Construction of local time series of climate anomalies

Local time series of climate anomalies $\Delta\overline{V}_{\text{scen}}(x, m, y)$ for the four climate variables were obtained by multiplying the scaling coefficients $V^*(x, m)$ with the $\Delta T_{\text{glob}}(y)$ trajectories for each scenario (Equation II.2). Because the obtained time series of anomalies are combined with climate observations in the next step (see section 6.3), it is necessary to account for the climate change signal already present in these observations. Anomalies are therefore calculated relative to the last year of observations, 2009. This is achieved by subtracting the T_{glob} increase above pre-industrial level for the year 2009 ($\sim 0.9\,\text{K}$) from the T_{glob} trajectories of the MAGICC6 scenarios before multiplying them with the anomaly patterns. In all cases, anomalies were only calculated if the significance level of

the slope of the regression model is >0.9; otherwise they were set to zero.

For temperature, the obtained local anomalies can be used without any restriction. In the case of cloudiness and precipitation, however, the obtained anomalies may result in an exceedance of the lower and, in the case of cloudiness, also the upper limit of possible values for these variables. For cloudiness this problem is less critical as it is not used directly in impact models but serves, among other parameters, as a proxy for atmospheric transmissivity and emissivity in the estimation of radiation budgets. We therefore consider a simple capping of anomalies to prevent the exceedance of upper and lower limits, a sufficiently accurate solution. In contrast to cloudiness, precipitation is an essential variable and calculation of anomalies that would result in physically implausible negative precipitation rates should be avoided from the beginning. Anomalies for decreasing precipitation are therefore estimated from the regression models for logarithmic precipitation, which is equivalent to the assumption of exponential precipitation decrease. As there is no indication that precipitation would increase exponentially with T_{glob}, precipitation increases are estimated from the linear regression models for untransformed precipitation. For small change rates, the linear and the exponential approach yield very similar anomalies, while for large change rates the linear approach avoids unrealistically augmented increases and the exponential approach avoids negative precipitation rates (see also Watterson 2008). For estimating rain month frequency anomalies, changes in the linear predictor term of Equation II.4, i.e. anomalies of logit probabilities, were calculated. These obtained anomalies can be used without restrictions, as the range of logit probabilities is unconstrained. For the transformation into actual frequency anomalies see section 6.3.4.

6.3. Creation of climate scenarios from observed climate and derived climate anomalies

In order to obtain complete scenario time series of climate variables $V_{\mathrm{scen}}(x,m,y)$ that can be used for transient impact model simulations, the local scenario time series of climate anomalies $\Delta\overline{V}_{\mathrm{scen}}(x,m,y)$ are combined with time series — here referred to as 'reference time series' $V_{\mathrm{ref}}(x,m,y)$ — that provide the long-term climatological mean $\overline{V}(x,m)$ and interannual variability $e(x,m,y)$ (Equation II.1). Reference time series

for temperature and cloudiness are constructed from and are consistent with the CRU TS3.1 global climate dataset (Harris et al. 2014); reference time series for precipitation are based the GPCC full reanalysis dataset version 5 (Rudolf et al. 2010).

Because GPCC and CRU datasets have a slightly different land mask, the GPCC dataset was adjusted to the CRU land mask (67 420 grid cells) by filling up missing cells by interpolation. For this, the five neighbouring cells with the highest weight — calculated from distance and angular separation (New et al. 2000) — within a 450 km radius were used. If < 5 values were available, the interpolation was performed on this reduced data basis; if < 2, the precipitation from the CRU TS3.1 dataset was used. Grid cells only present in the GPCC land mask but not in the CRU land mask were excluded. Altogether, 767 grid cells were introduced by interpolation, 298 grid cells were directly taken from CRU TS3.1, and 1013 grid cells were omitted from the GPCC dataset.

106-yr reference time series covering the scenario period (2010–2115) were composed as a random sequence of years from historical observations of the period 1961–2009. To preserve interannual autocorrelation, spatial coherence, and correlation among climate variables, all months and grid cells for all climate variables were taken from the same year. Prior to resampling, the trend in temperature was removed in a way that the detrended time series of temperature are representative for the climatologic mean of year 2009 obtained from the trend analysis. In the process of data preparation, observations of precipitation and cloudiness were found to exhibit strong interannual/interdecadal variability, which negatively affects the robustness of estimated trends. In order to avoid spurious effects from removing these trends, the original data were used directly for generating the reference time series for cloudiness and precipitation. The time series of resampled observations obtained are assumed to represent variability and climatology for the reference year 2009, to be consistent with the reference year for the derived anomalies. This consistency between the constructed reference time series, derived anomaly time series, and observations allows for seamless combination of historic observations with future climate projections and thus for transient impact model runs.

The combination of the anomalies with the reference time series is a crucial step and related to the general problem of whether to apply climate anomalies as an absolute change:

$$V_{\mathrm{scen}}(x,m,y) = V_{\mathrm{ref}}(x,m,y) + \Delta\overline{V}_{\mathrm{scen}}(x,m,y) \tag{II.5}$$

or a relative change:

$$V_{\text{scen}}(x,m,y) = V_{\text{ref}}(x,m,y) \cdot \frac{\overline{V}_{\text{base}}(x,m) + \Delta\overline{V}_{\text{scen}}(x,m,y)}{\overline{V}_{\text{base}}(x,m)} \tag{II.6}$$

where $\overline{V}_{\text{base}}(x,m)$ is the basis for the anomalies in the AOGCM, i.e. the long-term climatological mean of the AOGCM's representation of present-day climate. Where biases in the AOGCM's representation of present-day climate are small, the application of anomalies as relative change imposes a similar mean change to the scenario time series than the application as absolute change. That is, the difference between the mean of the scenario time series and the reference time series is similar to the original anomaly. As biases increase, climate anomalies are progressively altered with the relative approach. This alteration is an expression of the adjustment of the absolute anomaly derived from a biased base level in the AOGCM to the observed level, which is the actual motivation for using the relative approach. The relevance of this adjustment is particularly apparent where decreases from overestimated levels in the AOGCM are applied to lower observed levels. Without the attenuation of the anomaly by the relative approach the application of a negative change might well lead to negative values. However, for the reverse case — increases from underestimated levels — this approach is less favourable as it may lead to an unrealistic augmentation of the absolute anomaly.

Another difference between the two approaches is that with the absolute application of anomalies interannual variability remains unchanged, while with the relative application interannual variability is altered in a way that the coefficient of variation remains constant. The relevance of this variability adjustment is most apparent for cases where negative anomalies bring the mean of the scenario time series close to zero. In these cases a corresponding decrease of variability is required to prevent the occurrence of negative values.

The procedures used to apply the anomaly time series to the reference time series for different climate variables are described in the remaining part of this section. In order to improve readability, the parameters x and m are omitted; only the parameter y is used to differentiate terms that vary over time from time-invariant terms. Thus, Equations II.7–II.14 can be seen to describe the processes for a particular location x and month m but apply to all locations and months.

6.3.1. Temperature

Since temperature biases in AOGCMs are very small compared to absolute temperature levels, the application as absolute or relative change would give very similar results. However, temperature anomalies are commonly treated as absolute changes in the literature and are thus applied as absolute change here:

$$T_{\mathrm{scen}}(y) = T_{\mathrm{ref}}(y) + \Delta\overline{T}_{\mathrm{scen}}(y) \tag{II.7}$$

where $T_{\mathrm{scen}}(y)$, $T_{\mathrm{ref}}(y)$, and $\Delta\overline{T}_{\mathrm{scen}}(y)$ are the temperature time series of the scenario, the reference time series, and the time series of anomalies, respectively.

6.3.2. Cloudiness

For cloudiness, anomalies were applied as relative changes. Due to the problem of augmentation of anomalies when applied as relative change to higher observed levels, there is a risk of exceeding the upper 100% limit in these cases. Increases in cloudiness are therefore applied as relative decreases of cloudlessness, i.e. 100% – cloudiness:

$$\mathrm{Cld}_{\mathrm{scen}}(y) = \begin{cases} \mathrm{Cld}_{\mathrm{ref}}(y) \cdot \frac{\overline{\mathrm{Cld}}_{\mathrm{base}} + \Delta\overline{\mathrm{Cld}}_{\mathrm{scen}}(y)}{\overline{\mathrm{Cld}}_{\mathrm{base}}} & \text{for } \Delta\overline{\mathrm{Cld}}_{\mathrm{scen}}(y) < 0 \\ 100 - (100 - \mathrm{Cld}_{\mathrm{ref}}(y)) \cdot \frac{100 - \left(\overline{\mathrm{Cld}}_{\mathrm{base}} + \Delta\overline{\mathrm{Cld}}_{\mathrm{scen}}(y)\right)}{100 - \overline{\mathrm{Cld}}_{\mathrm{base}}} & \text{for } \Delta\overline{\mathrm{Cld}}_{\mathrm{scen}}(y) > 0 \end{cases} \tag{II.8}$$

with $\mathrm{Cld}_{\mathrm{scen}}(y)$, $\mathrm{Cld}_{\mathrm{ref}}(y)$, $\Delta\overline{\mathrm{Cld}}_{\mathrm{scen}}(y)$, and $\overline{\mathrm{Cld}}_{\mathrm{base}}$ denoting the cloudiness time series of the scenario, the reference time series, the time series of anomalies, and the present-day climatological mean cloudiness in the AOGCM, respectively. For consistency with the anomalies and the reference time series, $\overline{\mathrm{Cld}}_{\mathrm{base}}$ needs to represent the simulated climatological mean for the year 2009. It is estimated by adding the cloudiness anomaly for a 0.9 K warming to the climatological mean of the control run (see section 6.2.2).

6.3.3. Precipitation

The application of precipitation anomalies is particularly challenging because of the importance of precipitation as key variable in impact assessments and the partially very large biases in simulated present-day precipitation. In cases where simulated precipitation

in the control run is very low, small absolute increases correspond to very large relative changes. When applied to significantly higher observed precipitation rates, the absolute changes can become unrealistically large. Other studies have therefore proposed to use absolute changes or limit the relative changes in such cases (Carter et al. 1994; Hulme et al. 1995). Füssel (2003) notes that the problem depends on the degree of underestimation of present-day precipitation rates by AOGCMs and proposes a seamless transition from a relative towards an absolute application of anomalies, depending on the degree of underestimation. Here we adopt the approach by Füssel (2003) with some modifications required for the application to time series (see also Gerten et al. 2011, where a similar approach was used). Anomalies are applied as relative change, but as the underestimation of present-day precipitation in the AOGCM increases, the applied relative change is reduced so that the resulting mean change in the scenario time series becomes increasingly similar to the absolute change:

$$P_{\mathrm{scen}}(y) = P_{\mathrm{ref}}(y) \cdot \left[1 + \left(\frac{\Delta\overline{P}_{\mathrm{scen}}(y)}{\overline{P}_{\mathrm{ref}}}\right)\left(\frac{\overline{P}_{\mathrm{ref}}}{\overline{P}_{\mathrm{base}}}\right)^{\lambda}\right] \tag{II.9}$$

with

$$\lambda = \begin{cases} \sqrt{\frac{\overline{P}_{\mathrm{base}}}{\overline{P}_{\mathrm{ref}}}} & \text{for } \overline{P}_{\mathrm{base}} < \overline{P}_{\mathrm{ref}} \\ 1 & \text{for } \overline{P}_{\mathrm{base}} \geq \overline{P}_{\mathrm{ref}} \end{cases} \tag{II.10}$$

with $P_{\mathrm{scen}}(y)$, $P_{\mathrm{ref}}(y)$, and $\Delta\overline{P}_{\mathrm{scen}}(y)$ denoting the precipitation time series of the scenario, the reference time series, and the time series of anomalies, respectively; and $\overline{P}_{\mathrm{ref}}$ and $\overline{P}_{\mathrm{base}}$ denoting the climatological means of the reference time series and the year 2009 in the AOGCM, respectively. Estimation of $\overline{P}_{\mathrm{base}}$ is analogous to estimation of $\overline{\mathrm{Cld}}_{\mathrm{base}}$ (see section 6.3.2). The exponent λ determines the degree to which an anomaly is applied as absolute or relative change. If $\lambda = 1$, Equation II.9 is equivalent to the relative interpretation of precipitation anomalies. If present precipitation is underestimated by the AOGCM, lower values of λ diminish the applied relative anomaly. If λ approaches zero, the factor applied to the values of the reference time series results in a shift of its mean equal to the absolute anomaly $\Delta\overline{P}_{\mathrm{scen}}(y)$. Because all anomalies are applied as a factor, the coefficient of variation is preserved in the scenario time series, which implies changes in interannual variability.

6.3.4. Rain month frequency

Based on the logistic regression model estimated from the AOGCM simulations, the probability of rain month occurrence was estimated for each month of the scaled scenario time series as follows:

$$p_{\text{scen}}(y) = \frac{e^z}{1+e^z} \quad \text{with} \quad z = \text{logit}\,(p_{\text{ref}}) + \beta^* \cdot \Delta T_{\text{glob}}(y) \tag{II.11}$$

where $p_{\text{scen}}(y)$ is the probability of year y in the scenario to be a rain month and p_{ref} the probability of rain month occurrence in the reference time series — i.e. the fraction of rain months in that series. In cases where p_{ref} is either 0 or 1, $\text{logit}\,(p_{\text{ref}})$ cannot be calculated and was set to a value of -7 and 7, respectively. This is equivalent to values for p_{ref} of about $1/1100$ and $1 - 1/1100$, respectively. The term $\beta^* \cdot \Delta T_{\text{glob}}(y)$ denotes the anomaly of the logit rain month probability estimated from the logistic regression model and T_{glob} anomalies (see section 6.2.2). Because the intercept and the slope of the logistic regression model are both estimated by fitting the model to the scenario data, extreme values are sometimes obtained for β^* where rain month probability is 0 or 1 and some singular dry or rain months occur towards the higher end of the temperature range. When used with the estimated intercept β_0, these slopes correspond to very small changes in rain month probability but produce unrealistically augmented probability changes when applied to p_{ref} in Equation II.11. In order to avoid this effect, only slopes with a corresponding estimate for the intercept between -7 and 7 were applied; otherwise no change was applied. This rule applied to about 5.5% of all significant estimates for β^*.

The application of p_{scen} to the reference time series entails the removal of excess and the introduction of additional rain months by means of a stochastic process. For this procedure, a random sequence $w(y)$ of uniformly distributed numbers between 0 and 1 is generated, which serves as a decision criterion on whether a rain month is introduced or removed in year y. If $p_{\text{scen}}(y)$ is smaller than p_{ref} a rain month is removed if

$$w(y) \geq \frac{p_{\text{scen}}(y)}{p_{\text{ref}}} \tag{II.12}$$

Conversely, if $p_{\text{scen}}(y)$ is larger than p_{ref}, a rain month is introduced if

$$1 - w(y) \geq \frac{1 - p_{\text{scen}}(y)}{1 - p_{\text{ref}}} \tag{II.13}$$

The precipitation event to be introduced is randomly chosen from the precipitation distribution of the respective reference time series. In cases where the reference time series has no rain month at all, a synthetic rainfall distribution is generated by interpolation from up to five neighbour cells with at least one precipitation event in their distribution. The selection criterion for these cells was taken to be the highest interpolation weight from all cells within a radius of 450 km. Interpolation weights were calculated as in New et al. (2000) with account for distance and angular separation.

In order to preserve the spatial and temporal coherence of the precipitation field, the same random number sequence $w(y)$ was used for all grid cells and months of the year. The rationale behind this procedure is that for neighbouring cells with similar $p_{\mathrm{scen}}(y)$ and p_{ref}, rain months get removed or inserted in the same year. In order to avoid an overlap with the removal of rain months, however, the reflected sequence $1 - w(y)$ was used as decision criterion for the introduction of rain months. The procedure was applied prior to the scaling of precipitation amounts described in the preceding sections. Average reference precipitation used in Equations II.9 and II.10 was calculated from this modified reference time series.

6.3.5. Wet-day frequency

An additional information required by many impact models is the number of wet days per month. Due to the sparse availability of daily rainfall data from AOGCMs and strong biases in frequency distribution of rainfall intensities in many AOGCMs, this information is hard to extract from these models. The number of wet days per month is therefore estimated based on New et al. (2000) using the relationship between monthly precipitation sum and number of wet days:

$$\mathrm{WD}(y) = \overline{\mathrm{WD}}_{\mathrm{obs}} \left(\frac{P(y)}{\overline{P}_{\mathrm{obs}}} \right)^{\gamma} \tag{II.14}$$

where $P(y)$ and $\mathrm{WD}(y)$ represent the time series for precipitation sum and the estimated number of wet days of a month and grid cell, respectively. The exponent γ is assumed to be 0.45, which was found by New et al. (2000) to yield best results. The values $\overline{\mathrm{WD}}_{\mathrm{obs}}$ and $\overline{P}_{\mathrm{obs}}$ represent the observed 1961–1990 mean monthly wet-day frequency and precipitation sum, respectively. The former was derived from CRU TS3.1 (Harris et al. 2014) and the latter from GPCC version 5 (Rudolf et al. 2010). The means

were calculated over the entire 30-yr period, including totally dry months. Because the datasets for wet days and precipitation are based on different station networks they are not fully consistent, i.e. there are cases where rain months have zero wet days (and vice versa). The absolute minimum for $\overline{\mathrm{WD}}_{\mathrm{obs}}$ is the fraction of rain months in the 30-yr period, which means that at least one wet day has to exist for each rain month. If the estimate of $\overline{\mathrm{WD}}_{\mathrm{obs}}$ is smaller than that, it was set to that minimum. This estimation procedure delivers conservative estimates of wet-day frequency for the scenario period, since the relationship between wet-day frequency and monthly precipitation sum is assumed to be constant over time.

7. Results and discussion

7.1. Properties of scaling patterns extracted from AOGCM simulations

The scaling patterns extracted from AOGCM simulations are the core component of the scenario-building described in this paper. They provide information on spatial and temporal heterogeneity of climate change signals for primary climate variables as projected by different AOGCMs. In this section, an overview is given of the spatial coverage of fits that are significant and of basic properties of the derived patterns (mean and standard deviation). The focus is primarily on a comparison of the different climate variables with some indication of the inter-model spread. A comprehensive overview with values for individual AOGCMs is presented in Table II.1.

An apparent difference between the climate variables is the spatial and temporal coverage of significant slope parameters of the regression models obtained from the AOGCM simulation. As described in section 6.2.2, only slope estimates with a statistical significance > 0.9 were accepted and used for the scaling. Each slope estimate is representative for a specific area (size of grid cell) and a specific time period of the year (length of month). In order to assess the spatial and temporal coverage of significant

Table II.1.: Overview over coverage of significant changes, pattern mean, and pattern standard deviation for temperature, cloudiness, precipitation, and rain month frequency for individual AOGCMs. Note that for precipitation coverage decreases refer to decreases of logarithmic precipitation. For calculation of pattern mean and standard deviation, decreases of logarithmic precipitation are converted to precipitation.

	Temperature			Cloudiness			Precipitation				Rain month frequency		
	coverage signif. change	Pattern mean (K)	Pattern stdDev (K)	coverage signif. change	Pattern mean (%)	Pattern stdDev (%)	coverage signif. increase	coverage signif. decrease	Pattern mean ($mm\,d^{-1}$)	Pattern stdDev ($mm\,d^{-1}$)	coverage signif. change	Pattern mean (K)	Pattern stdDev (K)
CCCMA-CGCM3.1	100.0 %	1.35	0.51	90.7 %	0.21	1.75	62.4 %	29.2 %	0.06	0.16	10.1 %	−0.0006	0.0194
CNRM-CM3	99.9 %	1.29	0.49	81.7 %	−0.75	1.67	48.0 %	29.8 %	0.03	0.20	7.5 %	−0.0017	0.0149
CSIRO-MK3.0	100.0 %	1.30	0.49	81.1 %	−0.91	1.72	37.0 %	29.3 %	0.00	0.19	7.8 %	−0.0038	0.0339
GFDL-CM2.0	100.0 %	1.40	0.50	78.7 %	−1.16	1.57	36.6 %	32.8 %	−0.01	0.27	13.8 %	−0.0063	0.0244
GFDL-CM2.1	99.7 %	1.43	0.58	77.7 %	−1.05	1.70	35.4 %	34.8 %	−0.02	0.27	13.5 %	−0.0074	0.0275
GISS-EH	99.3 %	1.33	0.50	81.9 %	0.37	2.09	45.3 %	30.9 %	0.04	0.32	5.0 %	−0.0017	0.0286
GISS-ER	99.9 %	1.37	0.44	75.6 %	−0.53	1.45	46.5 %	31.4 %	0.05	0.26	6.9 %	−0.0030	0.0215
IAP-FGOALS-g1.0	100.0 %	1.25	0.45	73.0 %	−0.37	0.97	39.0 %	32.5 %	0.03	0.15	4.0 %	0.0034	0.0287
INM-CM3.0	100.0 %	1.29	0.45	72.1 %	−0.40	1.39	46.3 %	31.2 %	0.03	0.18	5.8 %	−0.0016	0.0149
IPSL-CM4	100.0 %	1.37	0.40	87.5 %	−1.19	1.66	36.6 %	36.1 %	0.02	0.24	12.3 %	−0.0027	0.0209
MIROC3.2(hires)	100.0 %	1.23	0.42	85.3 %	−0.40	1.78	46.4 %	34.2 %	0.00	0.22	7.1 %	−0.0016	0.0154
MIROC3.2(medres)	100.0 %	1.36	0.55	91.6 %	−0.43	2.02	51.3 %	38.0 %	0.03	0.20	11.7 %	−0.0018	0.0161
MIUB-ECHO-G	100.0 %	1.40	0.59	87.3 %	−0.41	1.26	57.0 %	29.0 %	0.07	0.20	14.8 %	−0.0052	0.0253
MPI-ECHAM5	100.0 %	1.36	0.44	82.9 %	−0.62	1.33	46.3 %	28.0 %	0.02	0.19	20.4 %	−0.0072	0.0230
MRI-CGCM2.3.2a	100.0 %	1.18	0.42	82.2 %	−0.08	1.27	51.8 %	31.4 %	0.03	0.17	14.2 %	−0.0029	0.0213
NCAR-CCSM3	100.0 %	1.27	0.58	87.2 %	0.02	1.39	61.0 %	24.9 %	0.07	0.17	10.4 %	0.0018	0.0259
NCAR-PCM1	100.0 %	1.19	0.63	80.3 %	−0.13	1.22	55.1 %	25.5 %	0.06	0.17	10.5 %	−0.0003	0.0272
UKMO-HadCM3	100.0 %	1.39	0.47	79.7 %	−0.89	1.70	45.5 %	32.4 %	−0.01	0.29	8.5 %	−0.0034	0.0276
UKMO-HadGEM1	99.8 %	1.34	0.58	81.9 %	−0.50	1.44	43.6 %	32.2 %	−0.01	0.30	11.2 %	−0.0013	0.0197
min	99.3 %	1.18	0.40	72.1 %	−1.19	0.97	35.4 %	24.9 %	−0.02	0.15	4.0 %	−0.0074	0.0149
max	100.0 %	1.43	0.63	91.6 %	0.37	2.09	62.4 %	38.0 %	0.07	0.32	20.4 %	0.0034	0.0339
median	100.0 %	1.34	0.49	81.9 %	−0.43	1.57	46.3 %	31.4 %	0.03	0.20	10.4 %	−0.0018	0.0230
mean	99.9 %	1.32	0.50	82.0 %	−0.49	1.55	46.9 %	31.3 %	0.03	0.22	10.3 %	−0.0025	0.0230

slope estimates, the product of area and duration for each significant slope is calculated and summed up. The sum is related to the product of total land area and length of the year to arrive at a percentage of spatial and temporal coverage.

Averaged over all AOGCMs, spatial and temporal coverage of significant slopes is 99.9%, 82.0%, and 78.2% for temperature, cloudiness and precipitation, respectively (value for precipitation composed of 46.9% significant increases in the linear case and 31.3% significant decreases in the logarithmic case; Table II.1). The average coverage of significant slopes for the logistic regression models for rain month probability is 10.9% and 10.3% if regression models with extreme intercepts are excluded (see section 6.3.4). Although there is considerable variation in spatial coverage of significant fits among individual AOGCMs (see Table II.1), the relative magnitude of coverage for the different variables is consistent over all models. Near full coverage is found for temperature, followed by moderate to high coverage for cloudiness and precipitation (including both increases and decreases). Coverage of significant precipitation increases is in all cases higher than for decreases although values are similar in some cases. In all cases, coverage of significant changes of rain month frequency is smallest.

Although the coverage of significant changes for cloudiness, precipitation, and rain month frequency is significantly lower than for temperature, this must not be interpreted as an indication of limited applicability of the pattern-scaling approach for these variables. A major difference between temperature and the other variables is that for the former only positive trends occur, while the other variables display a mixture of positive and negative trends (see Figures II.3–II.6). This implies the existence of transition zones between areas with positive and negative trends in the monthly fields where trends are de facto zero and therefore no significant slopes can be found. In addition, cloudiness and precipitation both exhibit strong interannual variability that tends to mask weak trends that primarily occur around such transition zones. Similarly, the estimation of parameters of the logistic regression model for change of rain month frequency is hampered by the stochastic nature of this variable. Moreover, vast areas with a rain month frequency of 100% (e.g. in the high latitudes and the wet tropics) remain unaffected by the occurrence of dry months under climate change (Figure II.6).

For each derived anomaly pattern two statistics — mean and standard deviation — are calculated in order to characterise the patterns. We took into account the spatial and temporal coverage of the individual slopes — i.e. by weighting them with the respective

cell area and length of month. Because the aim is to illustrate the properties of the entire pattern as it is applied, grid cells and months without a significant slope are included as zero values.

Averaged over all AOGCMs the mean anomaly of temperature increase over land is estimated to be 1.32 K per 1 K increase of T_{glob} (from 14.0 °C in the reference time series). Because T_{glob} anomalies and local temperature anomalies used in the regression are estimated from the same data, the value demonstrates that the land surface heats up much more than the whole of the global surface. This phenomenon is well known and is caused by the higher heat storage capacity of the oceans, which cause them to heat up less (Lambert and Chiang 2007). Although temperature trends are found to be always positive over land (Figure II.3), there is considerable heterogeneity in the degree of warming in different regions and times of the year. This heterogeneity is captured by the pattern's standard deviation, which on average over all AOGCMs is 0.5 K. The mean and standard deviation for individual models are in the range of 1.18–1.43 and 0.40–0.63, respectively (Table II.1).

The prevalence of a clear mean signal in the pattern is unique to temperature among the variables considered here. For cloudiness the average pattern mean is −0.49% — less than 1% of the mean cloudiness over land in the reference time series (55.3%). The relatively small mean change is contrasted by a higher standard deviation of 1.55%, which reveals the distinct spatial and temporal pattern of changes in cloudiness. This is consistent over all individual AOGCMs, which are characterised by mean changes between −1.19 and 0.37%, and pattern standard deviations between 0.97 and 2.09%, respectively.

For the calculation of pattern mean and standard deviation for precipitation, the decreases of logarithmic precipitation that make up the decreasing part of the pattern need to be converted to absolute changes in precipitation. Although the nonlinearity of exponential decrease may lead to an augmentation of precipitation decreases, the effect remains small due to the small magnitude of slopes of logarithmic precipitation decrease (−0.10, average over all AOGCMs). Averaged over all AOGCMs a mean precipitation change of 0.026 mm d^{-1} (millimetre per day) is found, which is equivalent to $\sim$ 1% of the mean precipitation rate over land in the reference time series (2.27 mm d^{-1}). Similar than for cloudiness, this small mean change is contrasted by a much larger standard deviation of 0.22 mm d^{-1} (averaged over all AOGCMs). Corresponding values

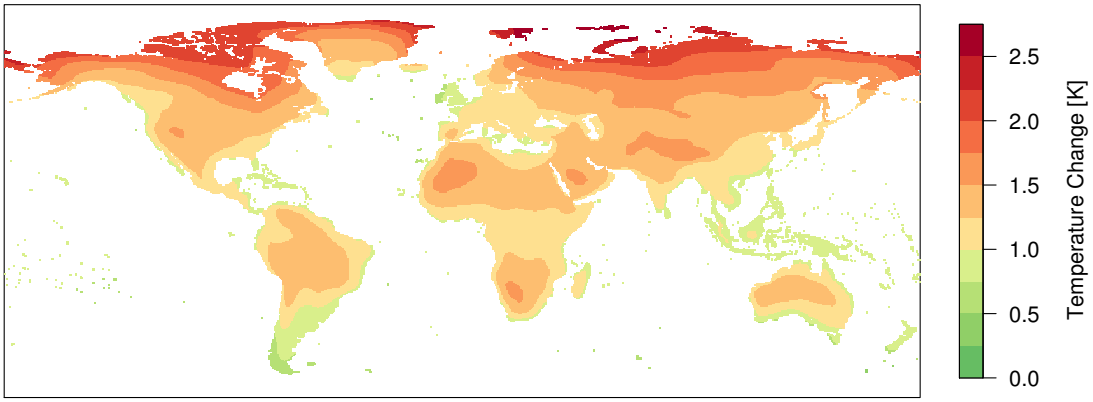

Figure II.3.: Multi-model mean of the actual applied annual mean change in near surface air temperature in K per 1 K of ΔT_{glob} (Equation II.16).

for individual AOGCMs range between -0.016 and $0.069\,\mathrm{mm\,d^{-1}}$, and between 0.15 and $0.32\,\mathrm{mm\,d^{-1}}$ for mean and standard deviation, respectively (Table II.1).

The slopes of the logistic regression for changes in rain month frequency are difficult to interpret in their original form and were therefore converted to changes in the fraction of rain months for the calculation of statistics. Averaged over all AOGCMs the mean change is -0.0025 rain months per month, which corresponds to an average loss of one rain month in about 33 yr on the entire land surface (including areas with no change). Average standard deviation of rain month changes is 0.028 rain months per month. For individual AOGCMs mean rain month frequency changes are between -0.0074 and 0.0034 rain months per month with standard deviations between 0.015 and 0.034.

7.2. Significance of scaling patterns extracted from AOGCM simulations

The assumption of a linear relationship between change in T_{glob} and mean local change of a climate variable V considered is central to pattern scaling. Although it is generally accepted that this assumption holds well for temperature (Mitchell 2003), it may not be fully valid for other climate variables. The focus of this section is therefore on a comparison between the different variables rather than between the different AOGCMs. However, values for individual AOGCMs are presented in Table II.2.

For ordinary linear square models, such as those fitted to the AOGCM data for pattern extraction, the total sum of squares (TSS) equals the sum of explained sum of squares (ESS) and residual sum of squares (RSS). For the pattern extraction, this is described in Equation II.15.

$$\sum_{y=1}^{N}[\Delta V(x,m,y)]^2 = \sum_{y=1}^{N}[V^*(x,m)\cdot\Delta T_{\mathrm{glob}}(y)]^2 + \sum_{y=1}^{N}[\Delta V(x,m,y) - V^*(x,m)\cdot\Delta T_{\mathrm{glob}}(y)]^2 \tag{II.15}$$

Based on this relationship, it is possible to evaluate the significance of the extracted patterns by comparing the explained sum of squares $\sum_{y=1}^{N}[V^*(x,m)\cdot\Delta T_{\mathrm{glob}}(y)]^2$ to the total sum of squares $\sum_{y=1}^{N}[\Delta V(x,m,y)]^2$ to provide a measure of explained variance. However, this measure is incomplete without an analysis of how much of the residual sum of squares $\sum_{y=1}^{N}[\Delta V(x,m,y) - V^*(x,m)\cdot\Delta T_{\mathrm{glob}}(y)]^2$ can be attributed to interannual variability inherent to the climate system. This variability cannot be captured by the linear regression, and the separation of the climate signal from the background variability is in fact the basic principle of the pattern-scaling approach. For the analysis of the residual sum of squares the variance of the control run $\mathrm{Var}_{\mathrm{cntrl}}(x,m)$ was multiplied with the number of values N in the residual sum of squares to obtain an estimate of the total sum of squared interannual variability to be expected in the scenario data.

Because Equation II.15 is valid for every single regression model, the evaluation metrics derived from its terms can be calculated for every model, grid cell, and month. In order to facilitate a comparison of the performance for different variables, area-weighted means over all land cells for the different square sums are calculated for each model and month and then again averaged.

For the ratio of explained sum of squares to total sum of squares (ESS/TSS), ensemble means of 0.78, 0.20, 0.16, and 0.15 are found for temperature, cloudiness, precipitation (increases only), and logarithmic precipitation (decreases only), respectively. Corresponding ensemble means for ratios of residual mean of squares to control run variance ($\mathrm{RSS}/(N\cdot\mathrm{Var}_{\mathrm{cntrl}})$) are 0.93, 1.01, 1.29, and 1.13, respectively. Although ratios of

Table II.2.: Overview of individual AOGCMs' ratios of explained sum of squares (ESS) to total sum of squares (TSS) and ratios of residual sum of squares (RSS) to scaled control run variance ($N \cdot \mathrm{Var}_{\mathrm{cntrl}}$) for temperature, cloudiness, increasing precipitation, and decreasing logarithmic precipitation. In all cases, only significant linear regression models are included. The scaling of control run variance is necessary to make it comparable to RSS, which is calculated for N values.

	Temperature		Cloudiness		Increasing Precipitation		Decreasing Log. Precipitation	
	ESS/TSS	RSS/($N \cdot \mathrm{Var}_{\mathrm{cntrl}}$)	ESS/TSS	RSS/($N \cdot \mathrm{Var}_{\mathrm{cntrl}}$)	ESS/TSS	RSS/($N \cdot \mathrm{Var}_{\mathrm{cntrl}}$)	ESS/TSS	RSS/($N \cdot \mathrm{Var}_{\mathrm{cntrl}}$)
CCCMA-CGCM3.1	0.86	0.88	0.28	0.92	0.19	1.31	0.18	1.09
CNRM-CM3	0.81	0.87	0.21	0.96	0.15	1.28	0.16	1.14
CSIRO-MK3.0	0.72	0.98	0.20	1.34	0.10	1.23	0.12	1.12
GFDL-CM2.0	0.69	0.99	0.18	1.04	0.12	1.37	0.13	1.18
GFDL-CM2.1	0.70	0.98	0.18	1.01	0.10	1.30	0.16	1.15
GISS-EH	0.66	0.89	0.18	1.01	0.24	1.20	0.21	1.03
GISS-ER	0.74	0.96	0.16	0.97	0.25	1.26	0.16	1.03
IAP-FGOALS-g1.0	0.70	0.82	0.11	0.93	0.15	1.09	0.09	0.96
INM-CM3.0	0.72	0.89	0.15	0.96	0.15	1.20	0.13	1.09
IPSL-CM4	0.83	0.95	0.32	1.00	0.27	1.53	0.18	1.20
MIROC3.2(hires)	0.86	0.98	0.28	1.00	0.14	1.40	0.13	1.17
MIROC3.2(medres)	0.86	0.97	0.28	1.01	0.17	1.37	0.13	1.15
MIUB-ECHO-G	0.87	0.89	0.21	0.97	0.24	1.38	0.16	1.22
MPI-ECHAM5	0.79	1.00	0.14	1.05	0.11	1.34	0.11	1.21
MRI-CGCM2.3.2a	0.82	1.01	0.23	1.01	0.14	1.25	0.13	1.15
NCAR-CCSM3	0.82	0.88	0.19	1.00	0.20	1.21	0.12	1.13
NCAR-PCM1	0.77	0.82	0.11	1.01	0.14	1.15	0.08	1.10
UKMO-HadCM3	0.79	0.98	0.25	1.01	0.15	1.33	0.22	1.22
UKMO-HadGEM1	0.81	0.95	0.19	1.00	0.13	1.34	0.19	1.19
all	0.81	0.92	0.21	1.00	0.17	1.30	0.14	1.14
min	0.66	0.82	0.11	0.92	0.10	1.09	0.08	0.96
max	0.87	1.01	0.32	1.34	0.27	1.53	0.22	1.22
median	0.79	0.95	0.19	1.00	0.15	1.30	0.13	1.15
mean	0.78	0.93	0.20	1.01	0.16	1.29	0.15	1.13

explained variation for cloudiness, precipitation, and logarithmic precipitation appear to be very small, the comparison of residual variance to the control run variance reveals that most of the unexplained variation can be attributed to the high interannual variability of these variables. This is a clear indication that the derived patterns have a strong significance and can be used in a scenario-building framework such as the one applied here. Even the relatively high value of $(\mathrm{RSS}/(N \cdot \mathrm{Var}_{\mathrm{cntrl}}))$ for increasing precipitation (1.29) is not critical if one considers that increases of mean precipitation are usually accompanied by increases in variability. Because a transformation to logarithmic values diminishes this effect, the ratio of residual variance to control run variance is very close to unity (0.98) if it is calculated for increasing logarithmic precipitation. It should be mentioned, however, that precipitation change in the AOGCM simulations is also influenced by factors such as atmospheric aerosol loading, as these effects are not captured by the extracted patterns and therefore contribute to higher $(\mathrm{RSS}/(N \cdot \mathrm{Var}_{\mathrm{cntrl}}))$ ratios. The ratio of residual variance to control run variance smaller than unity for temperature means that the residual variation is generally slightly smaller than expected from the interannual variability estimated from the control run. This is an indicator for the strong relationship between local temperature anomalies and T_{glob} anomalies captured by the derived patterns. When using these patterns to predict local temperature anomalies in conjunction with actual $\Delta T_{\mathrm{glob}}(y)$, the part of interannual variability that can be explained by interannual variability of $\Delta T_{\mathrm{glob}}(y)$ is included which reduces the residual error. In contrast, the estimation of control run variance is based on a constant mean climatology and therefore includes the part of variability that is correlated to the variability in $\Delta T_{\mathrm{glob}}(y)$.

7.3. Applied local anomalies for 1 degree of global warming

The dataset for systematic climate impact assessment presented here is a combination of extracted patterns and the reference time series of temperature, precipitation, and cloudiness. While properties of the scaling patterns were discussed in the preceding section, this section explores the actual anomalies by which the scenario time series are shifted. For each variable the scaling patterns that represent the anomalies for a 1-degree increase in T_{glob} are applied to the reference time series according to the methodology described in section 6.3. Thereby, the absolute change $V^*(x,m) \cdot 1\,\mathrm{K}$ is

altered, depending on the application method and the degree of disagreement between observed and simulated present-day climate. From the obtained time series multi-model means of the actual applied annual mean change are calculated:

$$\overline{\Delta\overline{V}}_{\mathrm{appl,1\,K}}(x) = \frac{1}{19 \cdot 12} \sum_{i=1}^{19} \sum_{m=1}^{12} \left[\overline{V}_{\mathrm{scen,1\,K}}(x,m,i) - \overline{V}_{\mathrm{ref}}(x,m) \right] \tag{II.16}$$

where $\overline{V}_{\mathrm{scen,1\,K}}(x,m,i)$ is the long-term climatological mean of the scenario time series for a T_{glob} increase by 1 K in location x, month m, and AOGCM i.

The alteration of anomalies by the application procedure is an important aspect of the methodology described in this paper. It is, however, a very general problem how to interpret and apply AOGCM-derived changes in climatological means when these means are biased. If the observed climatology is underestimated the simulated change may underestimate the actual change and vice versa, providing that changes derived from a biased representation of reality are a meaningful source of actual change at all. All assessments that are based on anomalies obtained from AOGCM simulations are confronted with this problem and have to deal with the question whether to use the unchanged absolute anomalies or adjust them according to the biases in the AOGCM's presentation of actual conditions. In cases where anomalies are combined with observations, an adjustment is often inevitable, as a direct use of anomalies can cause an exceedance of valid ranges for some variables (e.g. most variables have a positivity constraint). In these cases a relative application of anomalies provides a convenient and plausible way of accounting for the different base levels in simulations and observations. There are, however, no objective criteria on whether and how to perform this adjustment. Hence, any solution represents a choice that cannot be validated in a meaningful way. Our methodology is no exception from that. It is grounded on common practice found in the impact literature, aiming to fulfil the particular requirements of the pattern-scaling approach, while minimising alterations of the original signal. In place of a validation, we here complement the presentation of applied anomalies in the end product by a presentation of the alteration of the original anomalies. Multi-model means of the alteration of the original anomalies $V^*(x,m) \cdot 1\,\mathrm{K}$ in $\overline{V}_{\mathrm{scen,1\,K}}(x,m,i)$ are calculated as

$$\overline{\Delta\overline{V}}_{\mathrm{alt,1\,K}}(x) = \frac{1}{19 \cdot 12} \sum_{i=1}^{19} \sum_{m=1}^{12} \left[\left| \overline{V}_{\mathrm{scen,1\,K}}(x,m,i) - \overline{V}_{\mathrm{ref}}(x,m) \right| - \left| V^*(x,m,i) \cdot 1\,\mathrm{K} \right| \right] \tag{II.17}$$

The omission of the sign of change by the modulo function in Equation II.17 ensures that augmentations always have a positive sign and attenuations always have an negative sign, regardless of the sign of change.

For temperature, the actual applied anomalies for a 1-degree increase in T_{glob} (Figure II.3) are identical to the scaling pattern, as temperature anomalies are applied as absolute changes (Equation II.7). The spatial distribution of mean annual temperature changes across all AOGCMs exhibits the same overall behaviour as presented and discussed for the CMIP3 ensemble in IPCC (2007b). For the considered land area there are no incidents of decreasing local temperature with increasing T_{glob}. Below average warming (green colours) is only found in the vicinity of oceans, which is the result of the thermal inertia of the oceans. Overall, warming on the land surface is above average with a distinct pattern of polar amplification (stronger warming towards higher latitudes). Behind the multi-model annual mean change there is substantial variation in regional temperature change both among different AOGCMs and during the course of the year (see Appendix A). Disparity among AOGCMs is lower than the projected mean change — i.e. there is some disagreement in the magnitude but not in the direction of change. Seasonality of change is particularly strong in the high northern latitudes and broadly follows the pattern of polar amplification. Hence, the strong average increase projected for these areas does not occur uniformly over the year.

Actual applied anomalies for cloudiness are a mix of cloud cover increases and decreases (Figure II.4). Strong decreases are found in the Mediterranean, the Middle East, southern Africa, southern Australia, Central America, and the Amazon region. Increases are constrained to the higher northern latitudes and the Horn of Africa. In some areas, such as the northernmost latitudes, the Amazon, and some parts of Africa, variation of projected annual cloud cover change among AOGCMs is high with inter-model standard deviation exceeding the mean change (see Appendix A). Significant seasonality in the multi-model mean is limited to a few regions such as the Amazon, Central Asia and northeastern Canada only (see Appendix A). Regions with pronounced seasonality do not always coincide with regions of strong mean change, which indicates a mix of increases and decreases throughout the year that cancel out each other in the annual mean.

Alteration of the absolute signal, averaged over all months and AOGCMs, by the application method described in section 6.3.2 is depicted in the lower panel of Figure II.4.

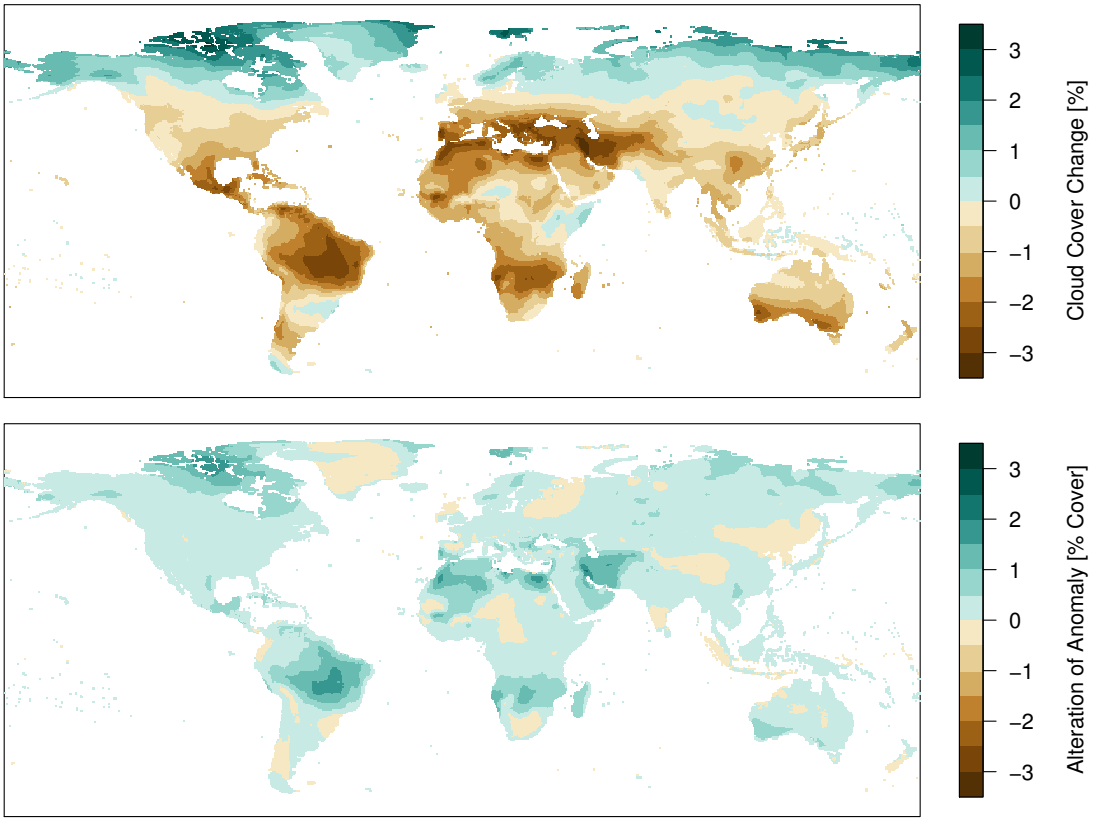

Figure II.4.: Upper panel: multi-model mean of the actual applied annual mean change in cloudiness in % cloud cover per 1 K of ΔT_{glob} (Equation II.16). Lower panel: multi-model mean of the alteration of the original anomaly in % cloud cover for 1 K of ΔT_{glob} (Equation II.17); positive values indicate an augmentation and negative values indicate an attenuation, regardless of the direction of change.

In most cases the application method augments the original signal, which means that decreases of cloudiness tend to be associated by underestimation and increases by overestimation of present-day cloud cover. However, in most cases the average alteration of the original signal is less than ±0.5%. Significant alteration of the signal only occurs in northern Canada, the Amazon, the Middle East, and some parts of Africa — all of these regions being characterised by strong mean changes (Figure II.4, upper panel).

The multi-model mean of annual precipitation change is shown in Figure II.5 (upper panel). As for temperature and cloudiness, precipitation changes are consistent with results presented in IPCC (2007b). Significant decreases prevail in the Mediterranean,

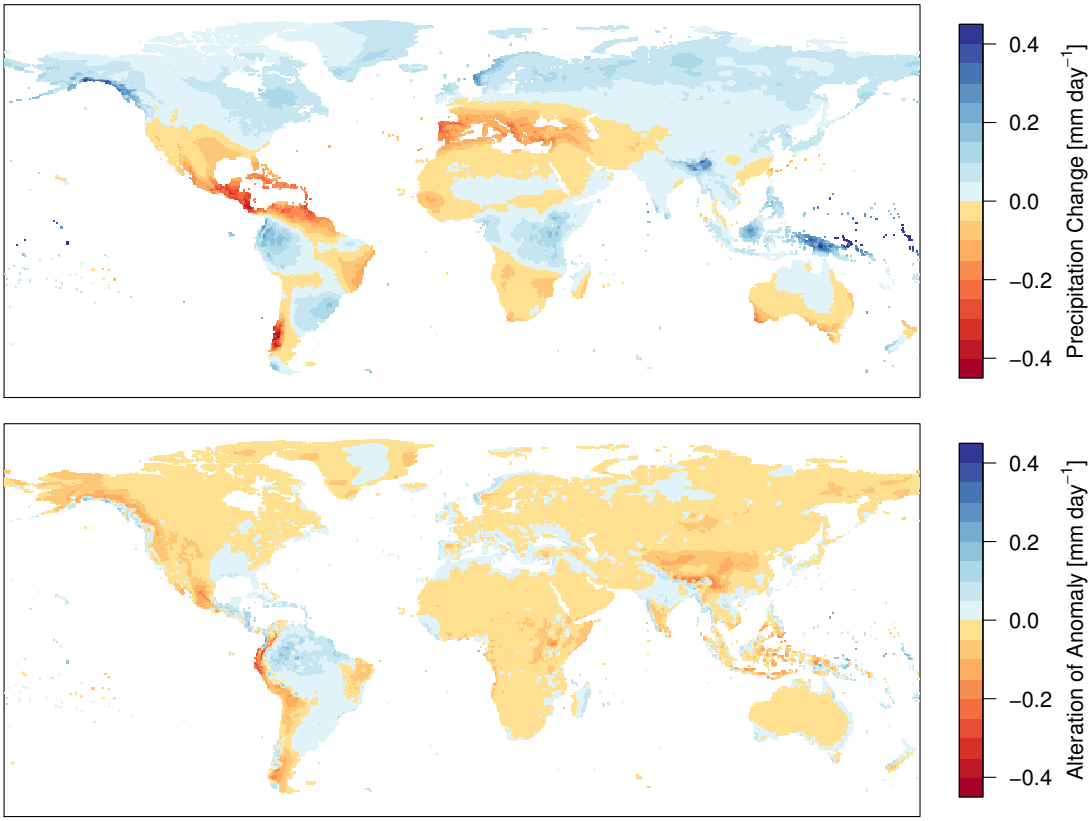

Figure II.5.: Upper panel: multi-model mean of the actual applied annual mean change in precipitation rate in mm d^{-1} per 1 K of ΔT_{glob} (Equation II.16). Lower panel: multi-model mean of the alteration of the original anomaly in mm d^{-1} for 1 K of ΔT_{glob} (Equation II.17); positive values indicate an augmentation and negative values indicate an attenuation, regardless of the direction of change.

the Middle East, South Africa, southern Australia, Central America and Patagonia; increases are projected for the Boreal zone, South and Southeast Asia, East Africa, and parts of South America. For some regions such as the Amazon, Sub-Saharan Africa, and Southeast Asia inter-model standard deviation is high (see Appendix A), indicating considerable disagreement in the magnitude and in some cases even sign of mean annual precipitation change for the different AOGCMs. Seasonality of change is less pronounced but seems to occur in regions where the inter-model spread is high — i.e. the wet tropics but also in temperate North America and Europe (see Appendix A).

Although large biases in the AOGCMs impair the applicability of derived anomalies

the alteration of the scaled anomalies by the application method is well controlled and rarely exceeds $\pm 0.05\,\mathrm{mm\,d^{-1}}$. Significant alterations primarily occur in mountainous regions (Andes, Rocky Mountains, Himalayas) where the AOGCMs' coarse spatial resolution impedes the correct representation of sub-grid orographic effects. In average, our application method attenuates rather than augments the original anomaly, which indicates that AOGCMs tend to overestimate observed precipitation rates. It is not the progressive reduction of the relative anomaly by the λ exponent with increasing underestimation in the AOGCM (Equation II.9) that causes the overall attenuation. The reduction of the relative anomaly applies to both increases and decreases and merely compensates for the asymmetry in the relative application of anomalies derived from differently biased AOGCM baselines. While the attenuation in case of overestimation can never exceed the original anomaly when applied as relative change, the augmentation in case of underestimation in the AOGCM can become many times bigger than the original anomaly. With our approach, in contrast, the original anomaly is also augmented with increasing underestimation in the AOGCM, but reaches a maximum augmentation by a factor of about two for a five-fold underestimation and then declines towards unity for a completely rain-free AOGCM baseline.

Changes in rain month frequency are rarely analysed and here their explicit consideration in a pattern-scaling framework is unique. The rain month frequency changes, averaged over all AOGCMs and months, shown in the upper panel of Figure II.6, exhibit both increases and decreases although decreases prevail. As already discussed in section 7.1, changes occur predominately in areas that are already today characterised by intermittent rainfall occurrence while regions such as North America, northern Europe, and Siberia remain unaffected. Regions of strong rain month frequency decrease broadly agree with key regions of decreases in average rainfall, but some noteworthy differences exist. Almost entire South America and Australia are, on average, affected by rain month frequency decrease while the picture for change in rainfall amount is much more mixed. In the Mediterranean, southern Europe is much less affected by rainfall amounts, while the opposite can be stated for North Africa. In southern Africa decreases in rain month frequency stretch much further up north along the east coast.

Variation of rain month frequency change among AOGCMs is pronounced but generally follows the pattern of strong decreases (see Appendix A). Thus, different models disagree primarily in the magnitude rather than in the direction of change. Seasonality of change

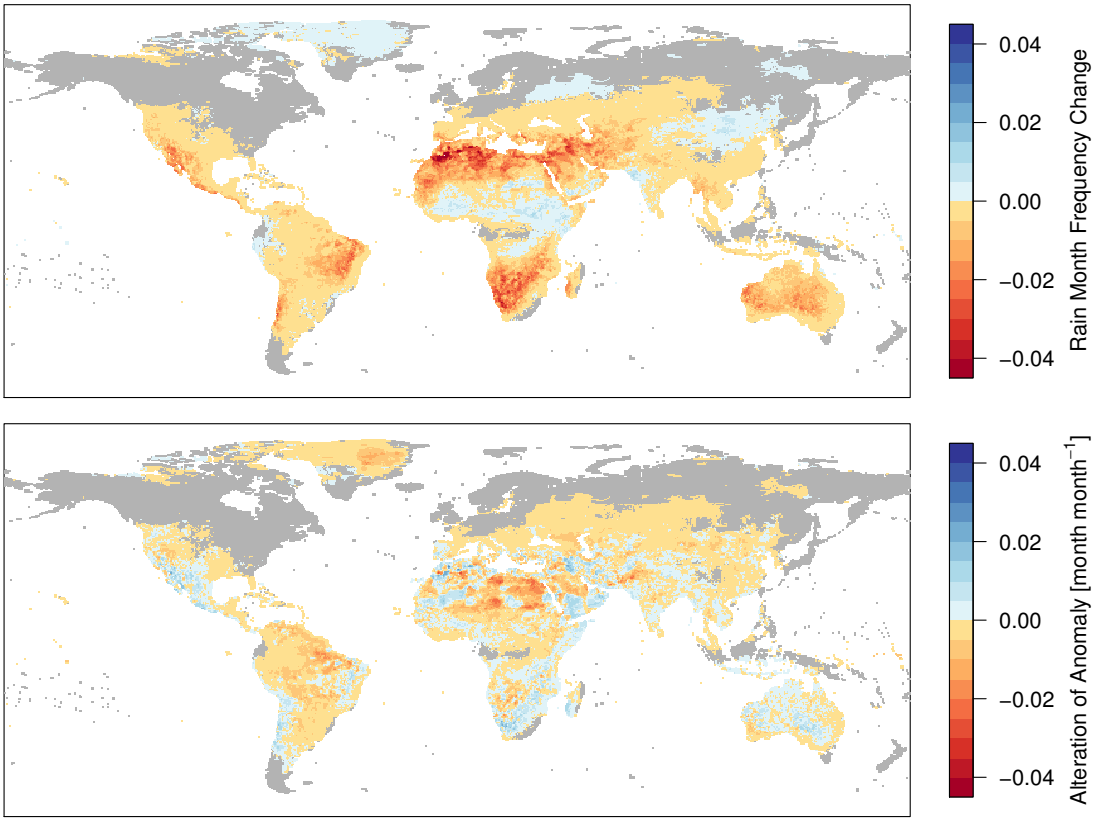

Figure II.6.: Upper panel: multi-model mean of the actual applied annual mean change in rain month frequency in month/month for a ΔT_{glob} of 1 K (Equation II.16). Lower panel: multi-model mean of the alteration of the original anomaly in month/month for 1 K of ΔT_{glob} (Equation II.17); positive values indicate an augmentation and negative values indicate an attenuation, regardless of the direction of change.

is in the same magnitude as the inter-model variation and also exhibits a similar pattern (see Appendix A). Hence, decreases in rain month frequency in some months can be very high, while little change occurs in others.

Anomalies of rain month frequency are significantly altered by the application method (see Figure II.6, lower panel). Although logit-transformed frequency anomalies are applied as absolute changes (see section 6.3.4), the different reference levels in the AOGCM and the observations result in very different actual frequency anomalies when transformed back. Equation II.11 implies a sigmoid shape for the relationship between rain month frequency and ΔT_{glob}, which means that a given $\beta^* \cdot \Delta T_{\text{glob}}(y)$ produces the

strongest change in rain month frequency when applied to a rain month frequency of 0.5; with reference values closer to 0 and 1 the effect progressively decreases. Consequently, augmentations of the signal occur when frequencies in the AOGCM are close to 0 or 1 and projected changes are applied to observed rain month frequencies closer to 0.5. Attenuations occur in cases where changes are estimated from intermediate rain month frequency levels in the AOGCM and applied to reference frequencies closer to 0 or 1.

In summary, the multi-model mean of applied annual change for the different variables presented here are — where applicable — consistent with the results presented in IPCC (2007b). Although the application method can significantly alter the absolute anomaly for some variables, these alterations are not arbitrary but a consequence of the biases in AOGCMs. We believe that the application methods chosen for the different climate variables are well justified and fulfil the aim of providing the necessary adjustment while minimizing unnecessary alterations.

8. Conclusions

Here we present a newly composed dataset of climate change scenarios for systematic assessments of climate change impacts as a function of T_{glob} increase. The dataset combines observations, information extracted from AOGCM simulations, and results from a reduced complexity climate model into physically plausible climate change scenarios for a wide range of global mean temperature increases. The scenarios are designed to reach global mean temperature increases above pre-industrial levels between 1.5 and 5 degrees (in 0.5 degree steps) around the year 2100. The scaling patterns extracted for 19 AOGCMs from the CMIP3 data base for temperature, cloudiness, and precipitation represent the key component for linking local climate change to changes in T_{glob}. We discuss the properties of these patterns and demonstrate that they preserve the original AOGCM climate change properties with sufficient accuracy. The methodology for combining the local climate anomalies (derived from the scaling patterns and ΔT_{glob} trajectories) with observations is extensively discussed as it has the potential to alter the derived raw anomalies. We show that alterations of climate anomalies by the application

method are a necessary adjustment of anomalies obtained from biased AOGCM baselines. The additional material used for creating the dataset — global datasets on observed historical climate and the reduced complexity climate model MAGICC6 — are not further discussed in this paper. They are well documented in other literature.

Supplementary material related to this part is available in Appendix A.

Acknowledgments

This work was supported by ILRI and the CGIAR research program on Climate Change, Agriculture and Food Security (CCAFS). Further support was given by GLUES (Global Assessment of Land Use Dynamics, Greenhouse Gas Emissions and Ecosystem Services), a scientific coordination and synthesis project of the German Federal Ministry of Education and Research's (BMBF's) 'Sustainable Land Management' programme (Code 01LL0901A), and the WATCH (FP6, grant no. 036946), CLIMAFRICA (FP7, grant no. 244240) and ERMITAGE (FP7, grant no. 265170) projects funded by the European Commission.

We acknowledge the modelling groups, the Programme for Climate Model Diagnosis and Intercomparison (PCMDI) and the WCRP's Working Group on Coupled Modelling (WGCM) for their roles in making available the WCRP CMIP3 multi-model dataset. Support of this dataset is provided by the Office of Science, US Department of Energy.

Edited by: M. Kawamiya

Part III.

Critical impacts of global warming on land ecosystems[1]

Sebastian Ostberg, Wolfgang Lucht, Sibyll Schaphoff, and Dieter Gerten

Abstract

Globally increasing temperatures are likely to have impacts on terrestrial, aquatic and marine ecosystems that are difficult to manage. Quantifying impacts worldwide and systematically as a function of global warming is fundamental to substantiating the discussion on climate mitigation targets and adaptation planning. Here we present a macro-scale analysis of climate change impacts on terrestrial ecosystems based on newly developed sets of climate scenarios featuring a step-wise sampling of global mean temperature increase between 1.5 and 5 K by 2100. These are processed by a biogeochemical model (LPJmL) to derive an aggregated metric of simultaneous biogeochemical and structural shifts in land surface properties which we interpret as a proxy for the risk of shifts and possibly disruptions in ecosystems.

Our results show a substantial risk of climate change to transform terrestrial ecosystems profoundly. Nearly no area of the world is free from such risk, unless strong mitigation limits global warming to around 2 degrees above pre-industrial level. Even then, our simulations for most climate models agree that up to one fifth of the land surface may experience at least moderate ecosystem change, primarily at high latitudes and high altitudes. If countries fulfil their current emissions reduction pledges, resulting in roughly 3.5 K of warming, this area expands to cover half the land surface, including the majority of tropical forests and savannas and the boreal zone. Due to differences in regional patterns of climate change, the area potentially at risk of major ecosystem change considering all climate models is up to 2.5 times as large as for a single model.

9. Introduction

One of the most critical consequences of globally increasing temperatures is the potentially unmanageable impact on terrestrial, aquatic and marine ecosystems, as climate is a prime determinant of ecosystem composition and functioning and explains much of their spatial variation (Woodward et al. 2004). In turn, through their material cycles, ecosystems and land surfaces are fundamental to the functioning of the Earth as a system of planetary chemical cycles, and they provide a multitude of ecological functions and services that human societies depend upon socially, culturally and economically (MEA 2005). Nonetheless, the potential of climate change to transform landscapes is less frequently addressed as a principal element of 'dangerous climate change' than more physical impacts such as sea level rise or direct damages from extreme weather events. This is partially due to the inherent complexity of ecosystems, rendering it difficult to systematically project their macroscopic response to multidimensional climate change. In fact, ecosystems are characterised by numerous internal feedbacks occurring in interlinked, multi-layered networks across various scales (both in space and time). While each layer is able to absorb some degree of change, reaching the limit of its adaptive capacity may trigger destructive cascades in successive hierarchical levels (Holling 2001). Unfortunately, comprehensive theories and computer models of such complex systems and their dynamics up to the global scale are not available at present. Complicating the matter, there is considerable uncertainty in climate projections, due primarily to climate model-structural and emissions scenario uncertainty (Hawkins and Sutton 2011).

Notwithstanding these methodological challenges, quantifying climate change impacts on ecosystems worldwide and systematically as a function of global warming is critical to substantiating the ongoing international negotiations on climate mitigation targets, as well as planning adaptation to unavoidable change. While the negotiations focus on a target of a maximum warming of 2 K (cf. Cancun Agreements, UNFCCC 2011), actual commitments by nation states to reduce greenhouse gas emissions currently add up to a warming well above 3 K (Rogelj et al. 2010, 3.3 K according to `www.climateactiontracker.org`, retrieved 20 August 2013). Given the inconclusive political debates on climate change in many industrialised countries, the robust economic growth in major developing countries, and a non-negligible possibility of high climate sensitivity of the Earth system (IPCC 2007b, ch. 8.6), an increase of global mean temperature

(GMT) of 5 K above pre-industrial by the end of this century is not out of the question (Rogelj et al. 2012). Therefore, assessing and illustrating the incremental impacts of a GMT rise of e.g. 2, 3.5 or 5 K and the associated uncertainties is of crucial importance.

Here we present a systematic macro-scale analysis of climate change impacts on terrestrial ecosystems and land surface properties as a function of GMT increase, which addresses the methodological challenges raised above. Our quantitative assessment is based on a consistent modelling framework composed of (1) newly developed sets of climate scenarios that sample the range of GMT increase uniformly (between 1.5 and 5 K), which are processed by (2) a state-of-the-art global biogeochemical model simulating climate-dependent vegetation-soil dynamics to derive (3) an aggregated metric of simultaneous biogeochemical and structural shifts in land surface properties. We interpret this metric as a numerical proxy for the risk of shifts and possibly disruptions in fundamental ecosystem properties and underlying finer-scale processes in response to climate change. As there is no simple impact equivalent of ecosystem macro-variables as those characterising the global climate (such as GMT increase or globally mixed atmospheric CO_2 concentration), the metric is designed to be spatially explicit.

10. Quantification of complex ecosystem change

On a fundamental level, ecosystems are characterised by their carbon exchange with the atmosphere and soil and by the water flowing through living tissues (Chapin et al. 2011; Ripl 2003). These properties, determined by the primary process of photosynthetic conversion of sunlight into biomass, constitute the base of the ecological food chain upon which trophic cascades and complex community structures depend (Mooney et al. 2009). At landscape level, ecosystems can be characterised by the prevailing broad types of vegetation in terms of their functional strategies, their carbon content, and their carbon and water exchange.

We argue that a climate-driven shift in these broad biogeochemical (water, carbon) and structural properties (vegetation type) implies corresponding impacts on the under-

lying, much more complex ecosystems (Heyder et al. 2011). In other words, changes in vegetation abundance and in the magnitude of exchange fluxes (in absolute terms and relative to each other) are taken to alter more detailed hierarchical structures, such as predator-prey and host-parasite relations (Parmesan 2006), complementarity and competition regarding resource use (Hooper et al. 2005), or mutual interactions like pollination (Mooney et al. 2009). To quantify these shifts, we combine changes in the magnitude and relative size of biogeochemical fluxes and stocks of the terrestrial vegetation and changes in its functional structure — which, in contrast to the more detailed ecosystem structures, are captured by spatially explicit simulation models — into one macro-level indicator which we treat as a proxy for the risk of ecosystem and landscape change.

This approach has two advantages. (1) Well-developed models of the impacts of climate change on terrestrial carbon and water biogeochemistry and vegetation structure are available in the form of dynamic global vegetation models (DGVMs; Murray et al. 2013). (2) Using a macro-level proxy that can be simulated with a DGVM in conjunction with climate change scenarios circumvents having to describe in-depth climate change impacts on concrete local ecological networks, or synthesising a large number of smaller-scale ecological studies into a coherent global picture, both of which are faced with nearly insurmountable methodological difficulties (Parmesan 2006; Williams and Jackson 2007).

10.1. Computation of the change metric

The generic change metric Γ developed by Heyder et al. (2011) is used to quantify overall biogeochemical and structural change and the implied risk of transitions in underlying ecosystem features. It calculates the difference between an ecosystem state under climate change and the current state. Ecosystem states are characterised as vectors in a multi-dimensional state space, with each dimension representing a specific exchange flux, stock or process variable. The distance between two state vectors represents the change an ecosystem is simulated to experience in terms of its biogeochemical properties. A larger distance implies a higher risk for underlying ecosystems to change, undergo restructuring, or collapse on short time scales. Ecosystem states for both the reference

Table III.1.: LPJmL model outputs (aggregated to 30 yr averages) used to compute present and future ecosystem states and the Γ metric.

Carbon exchange fluxes	Net primary production (NPP), heterotrophic respiration (rH), fire carbon emissions
Carbon stocks	Carbon contained in vegetation and soils
Water exchange fluxes	Transpiration (representing productive water use), soil evaporation and interception from vegetation canopies (representing unproductive water use), runoff
Additional parameters describing system-internal processes	Fire frequency, soil water content of the top-most layer (50 cm)
Vegetation structure	Composition of PFTs

period (1980–2009) and the future (2086–2115) are characterised by the variables specified in Table III.1. Γ is formulated to evaluate five dimensions of change:

$$\Gamma = \{\Delta V + c\,S\,(c,\ \sigma_c) + g\,S\,(g,\ \sigma_g) + b\,S\,(b,\ \sigma_b)\}\,/4 \tag{III.1}$$

where ΔV characterises changes in vegetation structure, c is the local change component, g is the global importance component, b is the ecosystem balance component and $S\,(x,\ \sigma_x)$ is a change to variability ratio.

Changes of vegetation structure in terms of major functional types representing different ecological strategies (woody vs. herbaceous, broadleaved vs. needleleaved, evergreen vs. deciduous) are quantified using a slightly modified version of the ΔV metric developed by Sykes et al. (1999) (see section B.2 in Appendix B for details). c and g are calculated as the length of the difference vector between state vectors characterised by all variables from Table III.1 except vegetation structure. Local change c quantifies changes in biogeochemical state relative to previously prevailing conditions at each location to quantify the magnitude of local ecosystem alterations. All state parameters are normalised to their grid cell-specific mean value during the reference period. Global importance g quantifies changes in the same parameters in absolute terms, i.e. their contribution to global-scale biogeochemistry. To achieve this, all state parameters are normalised to their global mean value during the reference period. g takes into account that even moderate (relative) changes on the local scale may significantly feed back to larger scales (global

carbon cycle, atmospheric circulation patterns, downstream water availability), possibly affecting ecosystems in other regions. Ecosystem balance b quantifies changes in the magnitude of stocks and fluxes relative to each other. It is computed as the angle between state vectors (using local normalisation of all parameters). Such shifts in the balance of biogeochemical properties indicate changes in the contributing dynamic processes and hence ecological functioning. Change to variability ratios S are computed for c, g and b. They relate changes in ecosystem state x to present-day variability σ_x and reflect the expectation that ecosystems are adapted to the range of previously encountered year-to-year variations. Since changes in vegetation structure usually take place on far longer time scales no such ratio is computed for ΔV. All terms in Equation III.1 are scaled between 0 (no change) and 1 (very strong change) and combined into the full metric Γ based on the assumption that simultaneous changes in several of the dimensions imply a higher risk of ecosystem destabilisation than changes in just one. See Heyder et al. (2011) for the specific scaling rules for each term.

10.2. Biosphere model

We use the well-established LPJmL DGVM (Lund-Potsdam-Jena model with managed land) to calculate the biogeochemical and vegetation-structural process dynamics required to quantify Γ. LPJmL simulates key physiological and ecological processes for 9 plant-functional types (PFTs) representing natural ecosystems at biome level (Sitch et al. 2003). Climate-dependent carbon and water cycles are directly coupled through photosynthesis based on a modified Farquhar approach (Farquhar et al. 1980; Collatz et al. 1992). Carbon taken up from the atmosphere is allocated to different vegetation carbon pools and subsequently converted to litter, forming soil carbon pools that decompose at various rates. PFTs coexisting within a grid cell compete for space, light and water, with establishment depending on climatic suitability and density of existing vegetation, mortality rates depending on growth efficiency, plant density and climatic stress, and fire disturbance depending on climate, fuel availability and PFT-specific fire resistance. The model is forced by monthly fields of temperature, precipitation and cloud cover, yearly values of atmospheric CO_2 concentration, and information on soil properties. All processes are calculated at a daily time step on a spatial grid of 0.5° longitude by 0.5° latitude resolution, with monthly climate data disaggregated as described in Gerten et al.

(2004). Human land cover/land use changes and their potential effects are neglected here, but areas under cultivation (shown in Figure B.1 in Appendix B) are excluded when computing the absolute area affected (see *Model settings and simulation protocol* in Appendix B for more details).

10.3. Interpretation of the change metric

In order to provide a better understanding of what a certain value of Γ signifies, we calculate the metric for the difference between present-day biomes, i.e. substituting space for time (Blois et al. 2013). Potential natural vegetation during the reference period is categorised into 16 different biome classes based on the simulated composition of PFTs (see Figure B.3a in Appendix B for the biome map and Figure B.4 in Appendix B for the classification scheme) and Γ is computed as the difference between average biome states (rather than between a future and the present state of a grid cell). The difference between present biomes typically adopts values of $\Gamma > 0.3$, corresponding to fundamentally different underlying ecological systems (Figure B.2 in Appendix B). For example, an average evergreen tropical rainforest differs from a tropical seasonal forest by a Γ value of 0.31; a shift to an average savanna gives 0.51, and a shift to a C4 grassland 0.86. A shift from a boreal evergreen to a boreal deciduous forest amounts to ≈ 0.21, to a temperate coniferous forest 0.37 and to a tundra 0.66. Only shifts between similar but still distinct biome types, such as a temperate mixed forest transforming into a temperate broadleaved or temperate coniferous forest, have smaller Γ values. Overall, $\Gamma < 0.1$ implies that despite biogeochemical shifts possibly affecting community composition, biomes remain roughly the same in terms of their defining characteristics. Values of Γ between 0.1 and 0.3 signal a change that produces a different, but related biome. In this study, we consider such changes to reflect risk of 'moderate' climate change impacts on ecosystems. Values of $\Gamma > 0.3$ are considered a risk of 'major' change. Figure B.2 in Appendix B compares biome averages. Since biomes aggregate an often continuous spectrum of actual vegetation composition into discrete categories, ecosystems may change their biome at lower Γ values than those in Figure B.2. Also, biomes can be rather broad categories. For example, the term savanna is used loosely in the literature to refer to very different ecological communities, covering a wide range of tree canopy cover anywhere between 5 and 80 % (Anderson et al. 1999). Owing to this

high variability within biomes our definition of what constitutes major change does not necessarily call for a change in biome class. Large shifts in biogeochemical functioning within a biome also qualify.

11. Climate uncertainty

Previous studies encountered several problems hampering a systematic quantification of climate change impacts for different GMT levels. (1) Considerable differences are found in the magnitude and spatial pattern of projected climatic changes from different Atmosphere-Ocean General Circulation Models (AOGCMs) for a given future time period or GMT increase. This is particularly true for changes in precipitation patterns, with AOGCM differences not just in the magnitude, but even in the sign of change for a number of regions (IPCC 2007b, ch. 11). Internal variability within different realisations of the same AOGCM is another source of uncertainty that has been estimated to account for at least half of the inter-model spread in projected climate trends during 2005–2060 (Deser et al. 2010). This necessitates the use of inputs from multiple AOGCMs and possibly multiple realisations per climate model in impact studies and to treat the differences as uncertainty. (2) Available climate scenarios do not sample the range of future GMT increase uniformly. For a given emission scenario the temperature reached by the end of this century differs between climate models due to differences in their climate sensitivity (IPCC 2007b, ch. 8.6). Combined with the limited number of emissions scenarios processed by AOGCMs and available in the CMIP3 archive[1] (Meehl et al. 2007), this introduces significant inconsistencies when attempting to compare multi-AOGCM impacts for different levels of GMT increase, because some future GMT ranges are reached by more (and different) climate models than others, or they are reached at different points in time.

We address these challenges with a new dataset of temperature-stratified climate scenarios. The 'PanClim' climate dataset described in Heinke et al. (2012) is created from

[1] World Climate Research Programme's (WCRP's) Coupled Model Intercomparison Project phase 3 (CMIP3) multi-model dataset

existing AOGCM runs available in the CMIP3 archive, but processed to reach specific GMT levels around the year 2100. The scenarios are created using a pattern-scaling approach (Huntingford and Cox 2000) and are based on two pillars: (1) temporal trajectories of GMT increase and (2) spatial patterns relating local AOGCM-specific climate change to GMT change. To cover emissions scenario uncertainty – ranging from ambitious mitigation to current commitment and continued emissions growth throughout the 21st century – trajectories of emissions and resulting GMT increases above pre-industrial level are computed by the fast, reduced-complexity carbon cycle-climate model MAGICC6 that has been shown to closely emulate the full range of C^{4}MIP carbon cycle models[2] and CMIP3 AOGCMs (Meinshausen et al. 2011a). These warming trajectories are physically and systemically plausible, with carbon cycle parameters adjusted to reproduce the Bern carbon cycle model and model parameters chosen to reproduce the median responses of the CMIP3 AOGCM ensemble, with a climate sensitivity of 3.0 K (Heinke et al. 2012).

The selected emissions trajectories result in global warming of 1.5, 2, 2.5, 3, 3.5, 4, 4.5 and 5 K during the 30 yr mean around the year 2100 (2086-2115), respectively. To explicitly incorporate climate pattern uncertainty, these 8 GMT trajectories are combined with the spatial characteristics of 19 CMIP3 AOGCMs. For each AOGCM, existing runs for at least two emissions scenarios (including multiple realisations where available) are used to extract a scaling pattern per month and climate variable. These patterns describe AOGCM-specific local changes in temperature, precipitation and cloud cover as a function of GMT change.

The combination of scaling patterns for each AOGCM and climate variable with GMT trajectories for the 8 warming scenarios results in 152 transient time-series of climate anomalies for the scenario period 2010 to 2115. Climate anomalies are then applied to a reference climate constructed from observed historical climate data (see below), which adds mean climatology and information on interannual variability. The process of anomaly application to the reference climate includes a bias correction, adjusting anomalies for regional biases found in the AOGCM data. The resulting climate scenarios allow for a smooth transition from historical data to future projections and therefore transient impact model runs across the whole 20th and 21st century. For a full documentation of

[2] C^{4}MIP, Coupled Climate Carbon Cycle Model Intercomparison Project

the methodology see Heinke et al. (2012). A flow chart illustrating the data processing steps is supplied as Figure B.5 in Appendix B.

For the historical simulation period the CRU TS 3.1[3] climatology (Harris et al. 2014) is used for temperature and cloud cover; and the GPCC[4] Full Data Reanalysis version 5 data for precipitation (Rudolf et al. 2010), extended to cover the full CRU grid. The number of wet days per month, used to distribute monthly sums, is created synthetically using the CRU approach (New et al. 2000) in order for the wet-day frequency to be consistent with GPCC precipitation. Historical climate data span from 1901 to 2009 and are followed seamlessly by climate scenario data. The resulting 152 climate scenarios (8 warming levels $\times$ 19 AOGCMs) provide a thorough and systematic sampling of the space of potential future GMT increase, retaining the key spatial properties of available AOGCMs while removing regionally distinct model-inherent biases. They provide a considerable step forward compared to up to 58 partially inconsistent scenarios used in previous DGVM-based, multi-climate-model, global ecosystem impact assessments (Heyder et al. 2011; Scholze et al. 2006).

Γ values are computed for impact simulations under each of the 152 climate scenarios separately. A grid cell is considered 'at risk' if at least one out of 19 AOGCMs demonstrates moderate or major ecosystem change at the respective GMT level. We determine the confidence in the projected severity of change based on the number of AOGCMs in agreement, using IPCC guidelines on uncertainty, i.e. about 2 out of 10 chance (4/19 AOGCMs), low confidence; about 5 out of 10 chance (10/19 AOGCMs), medium confidence; about 8 out of 10 chance (16/19 AOGCMs), high confidence (IPCC 2007b, ch. 1.6). However, we acknowledge that the 19 AOGCMs used in our study do not allow a full probabilistic assessment of the risks to ecosystems.

[3] Climatic Research Unit's time-series data available from British Atmospheric Data Centre (BADC), http://badc.nerc.ac.uk/data/cru/

[4] Global Precipitation Climatology Centre operated by Deutscher Wetterdienst, http://gpcc.dwd.de

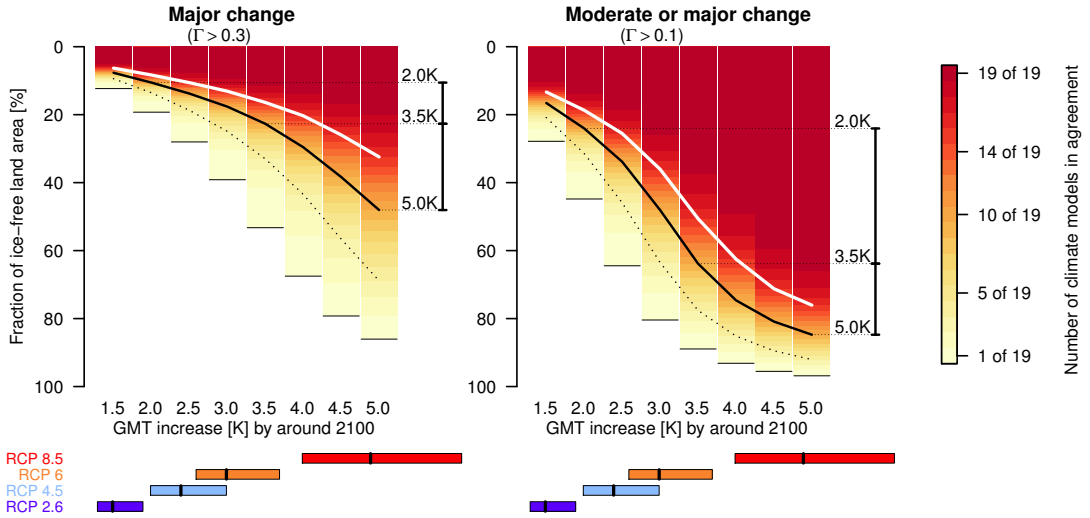

Figure III.1.: Global land-surface area at risk of major ($\Gamma > 0.3$, left panel) or at least moderate ($\Gamma > 0.1$, right panel) ecosystem change by around 2100. Black and white lines denote confidence based on AOGCM agreement: solid white, high; solid black, medium; dotted black, low confidence. Range bars to the right of each panel illustrate the difference in affected area (with medium confidence) between 2, 3.5 and 5 K of warming. Colored boxes below main figure compare results to the 66 % range of warming expected from four Representative Concentration Pathways (RCPs) after Table 2 in Rogelj et al. (2012).

12. Results: major and moderate ecosystem changes as a function of global warming

Our simulations show that the extent of global land area affected by either moderate or major ecosystem change is substantial and increases strongly with global warming. Assuming business-as-usual emissions leading to a GMT increase of 4–5 K above pre-industrial by 2100, more than two thirds of the global, ice-free land surface not currently used for agriculture are at risk of major ecosystem change ($\Gamma > 0.3$, 68 % at 4 K warming and up to 86 % at 5 K, left panel in Figure III.1). The uncertainty caused by differences in spatial patterns between climate models is large, however. For a global warming of 4 K, there is less than low confidence (less than 4 out of 19 AOGCMs in agreement) on 24 % of the land area, low to medium confidence on 23 % and high confidence (at least 16 of 19 models) on 20 % of the land area (dotted black and solid white lines in Figure III.1). At 5 K, the affected areas are 17, 36 and 32 % of the land area with less

than low, low to medium and high confidence, respectively.

Figure III.2 shows the regions affected by either major or moderate change, with colors indicating the degree of model agreement. Already for a warming of 2 K above pre-industrial — the target agreed upon in the Cancun accords following the UNFCCC's objective to prevent dangerous interference with the climate system (UNFCCC 1992) — major ecosystem shifts are projected under a majority of the AOGCM simulations for the temperature-sensitive high northern latitudes and some high-altitude regions (Figures III.2a and III.3a). These changes are associated primarily with migrations of the tree line and increased vegetation productivity, both of which have already been observed to some extent in recent decades (Lloyd 2005; Walker et al. 2012). Significantly larger areas, equalling 23 % of the global land area with at least medium confidence (Figure III.1), would be affected by major change at a global warming of 3.5 K — i.e. if countries restricted their greenhouse gas emissions according to their current pledges. In a 5 K world, vast areas on each continent and most biomes are likely to be affected in a major way (Figures III.2c and III.3a). They expand into the Sahel region and eastern Africa, cover large portions of southern Africa, most of the Australian interior, the eastern flanks of the Andes and the Brazilian northeast, areas of the central United States, the temperate-to-boreal ecotone in North America, most of India and the northern part of Southeast Asia, the Tibetan Plateau and extensive areas of the boreal-steppe ecotone in the Asian continental interiors of Mongolia, Kazakhstan, southern Russia and northern China, as well as all of the circumpolar region presently covered by tundra. Many of these large-scale patterns are already partly realised at 3.5 K of warming, such as along the southern edge of the boreal zone, the forest transition zone in tropical Africa, East India, and the Chaco region in South America (Figure III.2b).

In addition to areas affected by major change there are regions for which our simulations project moderate ecosystem changes ($0.1 < \Gamma < 0.3$). Moderate change as defined here may still correspond e.g. to a tropical seasonal forest changing into a densely wooded savanna or may signal significant changes of tree composition in temperate forests (Figure B.2 in Appendix B). Taking these into account, the total global area at risk more than doubles in the low emissions scenarios; for example, 45 % of the land area is at risk of at least moderate change compared to 19 % at risk of major change in the 2 K scenarios (Figure III.1). The area for which we project moderate ecosystem change is largest at 4 K and actually decreases in the higher warming scenarios as more and

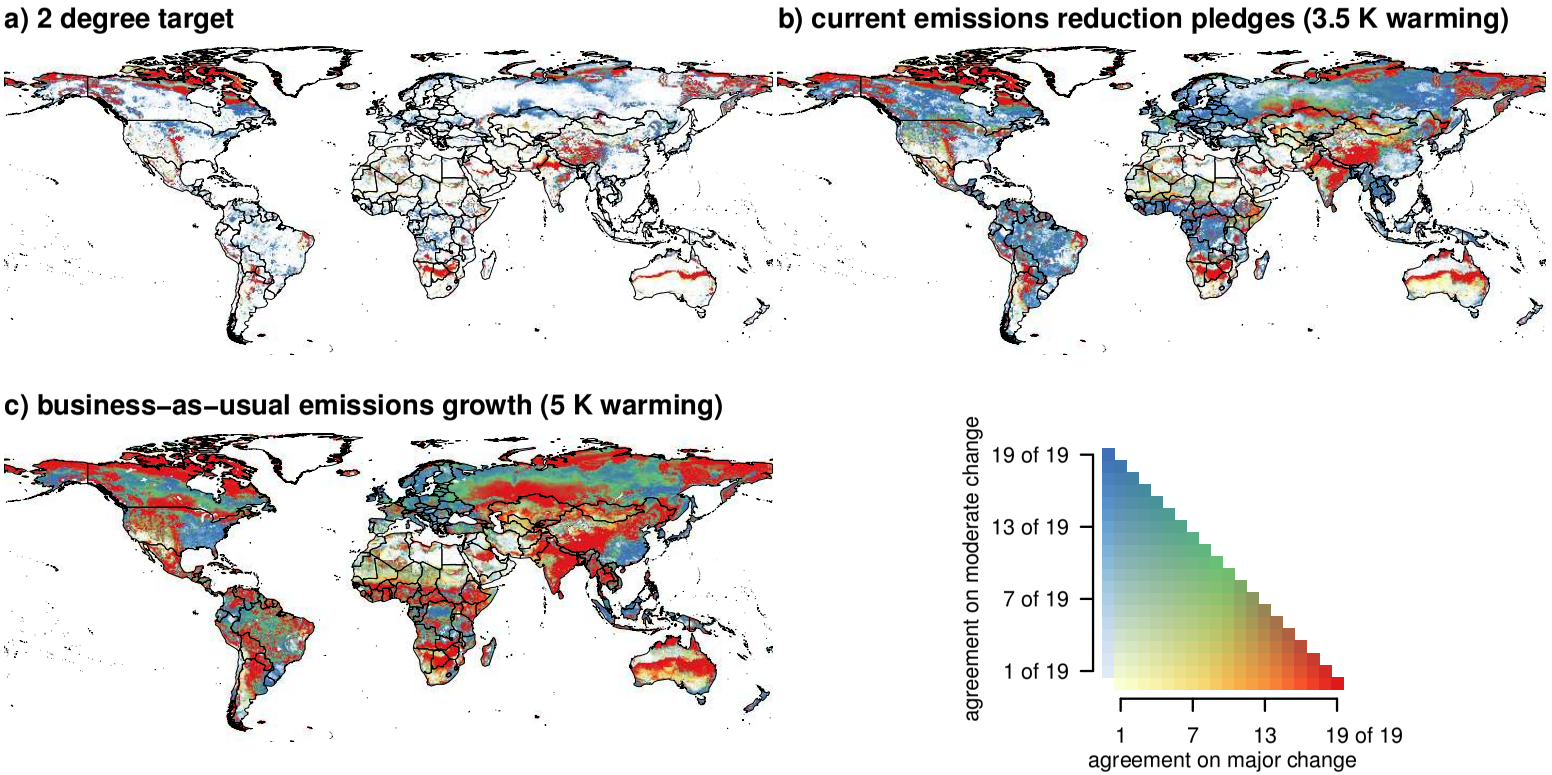

Figure III.2.: Regional patterns of simulated ecosystem change by 2100 and their confidence, for different climate policies leading to a GMT increase of 2, 3.5 and 5 K above pre-industrial, respectively. Colours indicate the number of simulations agreeing on either major ($\Gamma > 0.3$) or moderate ecosystem change ($0.1 < \Gamma < 0.3$) in each grid cell.

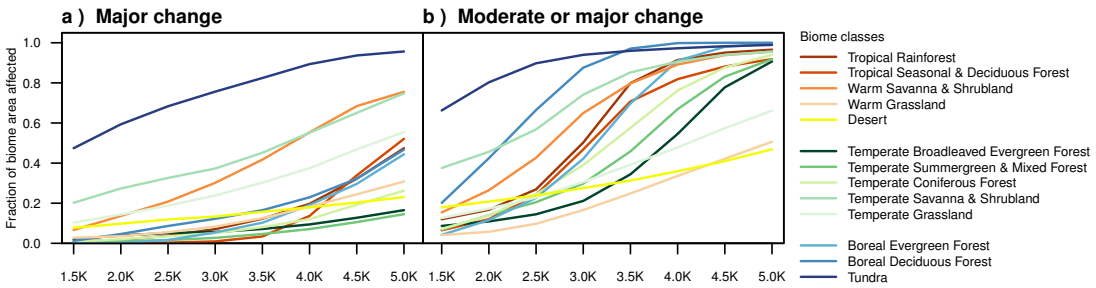

Figure III.3.: Biome area affected by **(a)** major ($\Gamma > 0.3$) or **(b)** at least moderate ($\Gamma > 0.1$) ecosystem change by around 2100 with at least medium confidence ($\geq 10/19$ AOGCMs in agreement). For other levels of confidence see Figure B.6 in Appendix B.

more regions go from moderate to major change. As a result, the increment between GMT steps of the total area at risk — i.e. affected by either moderate or major change under at least one AOGCM — tapers off beyond 3–3.5 K warming. On the other hand, confidence, based on AOGCM agreement, that ecosystems will be subjected to either moderate or major change continues to grow (Figure III.1, right panel). The remaining model disagreement is located primarily in some deserts and grasslands – the only biomes that still have non-negligible parts where under no AOGCM moderate or major change is projected at 5 K global warming (16 % of deserts, 7 % of warm grasslands, 5 % of temperate grasslands, Figure B.6 in Appendix B). Moderate changes are projected predominantly for the forest biomes. Changes in the tundra and in savannas tend to be major, with smaller surrounding areas experiencing moderate change. This is reflected in the shape of the curves in Figure III.3, which are markedly different in a) and b) for forests but have quite similar shapes for the other biomes.

12.1. Dimensions of ecosystem change

By using the Γ metric as a proxy our analysis specifically focuses on the overall magnitude of change instead of the individual processes driving that change, which differ between regions and sometimes even between AOGCMs for the same region. Still, it is possible to derive some generalisations as to which dimensions of change covered by Γ dominate in different biomes. For Figure III.4 and Figure B.7 in Appendix B we separate the full metric into the local change, global importance, ecosystem balance and vegetation structure component. c, g and b are scaled with their respective change to variability

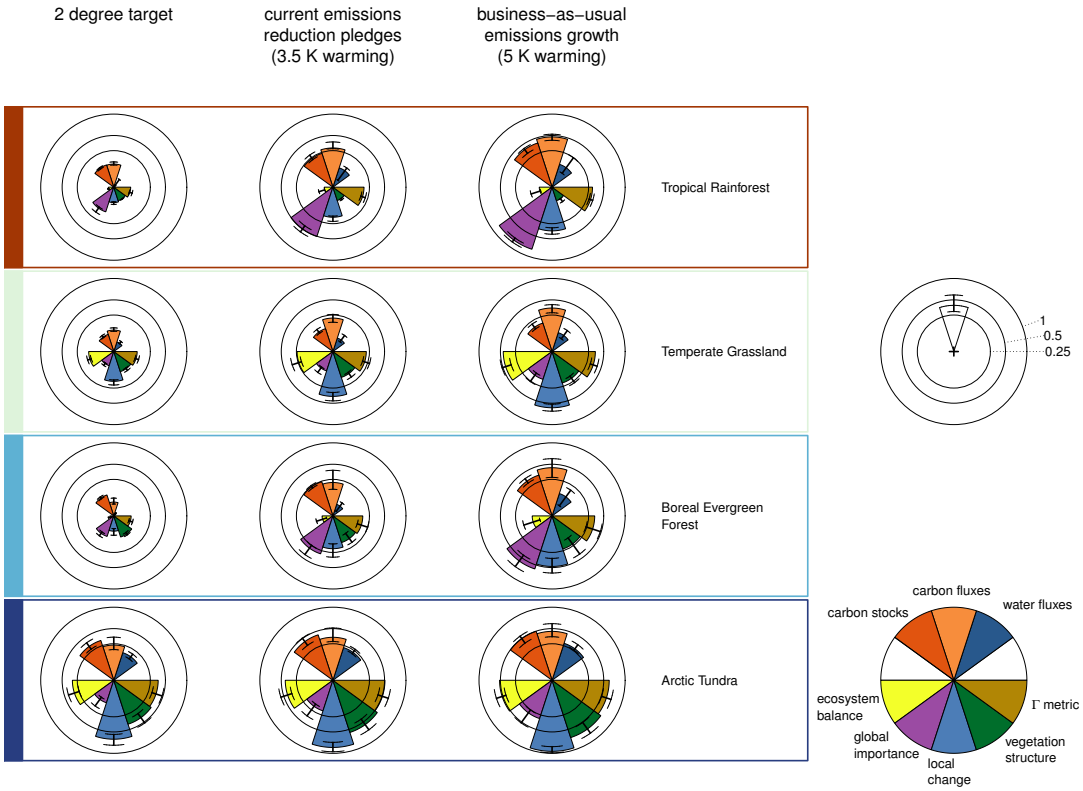

Figure III.4.: Dimensions of ecosystem change for select biomes. Components of Γ are averaged over all grid cells belonging to the biome during the reference period. Vegetation structure: ΔV; local change: $c \cdot S\,(c,\ \sigma_c)$; global importance: $g \cdot S\,(g,\ \sigma_g)$; ecosystem balance: $b \cdot S\,(b,\ \sigma_b)$. Carbon stocks, fluxes and water fluxes refer to parameter subsets in Table III.1. Error bars denote the range across the 19 climate patterns per GMT level. The four largest biomes (except deserts) are presented. For all 16 biome classes see Figure B.7 in Appendix B.

ratio S. In addition, we compute biogeochemical change separately for the carbon stocks, carbon exchange fluxes and water exchange fluxes subsets of parameters in Table III.1. Figure III.4 presents results for the four largest present-day biomes (except deserts), while Figure B.7 includes all biomes.

Tundra regions are projected to experience the strongest relative changes in biogeochemistry (local change component), moving from a value of 0.65 at 2 K to 0.95 at 5 K of global warming — note that local temperature increases in these regions are much higher than the global average. These shifts in biogeochemistry are accompanied by large shifts in vegetation structure (0.4 at 2 K, almost 0.7 at 5 K). The complete restructuring

of tundra ecosystems is also represented in strong changes of the ecosystem balance component, the highest of any biome. Changes in warm savannas are of similar overall magnitude as changes in the tundra, starting out slightly lower in the low warming scenarios and ending slightly higher in the high warming scenarios (Figure B.7). The higher total Γ values are primarily due to a higher global importance of savannas (0.3 versus 0.8 at 5 K). In general, changes in tropical forests and savannas have the highest global importance of all biomes, once global warming exceeds 2 degrees. This means that they have more impact on global biogeochemistry than changes in other biomes that may be stronger on the local level.

Our results show very little change in vegetation structure for all tropical and temperate forest biomes, with slightly higher values in boreal deciduous forests (Figure B.7). More importantly, what little changes are found are independent of the level of GMT increase and stay fairly constant between 1.5 and 5 K warming. All other biomes show a clear trend of increasing ΔV with increasing global warming. Boreal evergreen forests differ from the other forest biomes in that projections show increasing areas of forest decline in the boreal-steppe ecotone as well as an invasion of temperate broadleaved trees with increasing warming. Temperate grasslands are characterised by a temperature-driven shift from temperate (C3) to tropical (C4) grasses along their warm edge. Due to better water use efficiency of C4 photosynthesis this shift has strong implications on biogeochemistry. There is desertification in some grassland areas, although spatial patterns vary between climate models. Looking at the different stocks and fluxes describing biogeochemical states the general pattern is: Change in carbon stocks is usually more substantial than change in carbon fluxes in the low warming scenarios. Higher warming tends to lead to stronger increase of carbon flux changes while carbon stocks have a higher tendency to saturate. Projected changes in water exchange fluxes are considerably weaker than changes in carbon stocks and fluxes across all biomes. While of smaller magnitude from a biogeochemical standpoint, changes in freshwater availability have considerable effects on chronic supply-side water scarcity, as demonstrated by Gerten et al. (2013) for the 'PanClim' set of climate scenarios.

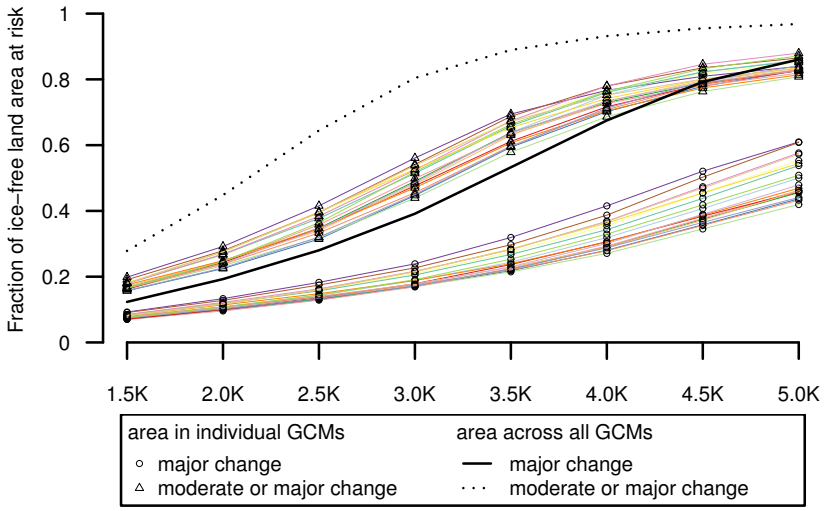

Figure III.5.: Importance of climate ensemble analysis. Circles and triangles denote the area projected at risk of major or at least moderate change, respectively, by individual AOGCMs. The black solid and dashed lines mark the total area at risk across all AOGCMs. Higher total areas result from regional differences between AOGCMs.

12.2. Climate pattern uncertainty

Comparing changes in impact simulations under individual AOGCMs reveals the importance of using a large ensemble of climate models. Affected areas at a specific GMT level vary between AOGCM projections. In addition — because affected areas in different AOGCMs may lie in different regions (see Figure B.8 in Appendix B for maps of Γ values from individual model runs) — the total area at risk across all models is consistently higher than the model with the largest affected area (Figure III.5). For example, the total area where at least 1 AOGCM shows major change is between 33 % (1.5 K warming) and 67 % (3.5 K) higher than the largest area simulated by any individual AOGCM (compare individual circles in Figure III.5 to solid black line). Even at 5 K, using the less strict criterion of $\Gamma > 0.1$ where AOGCM agreement is much higher, the total area taking into account the whole ensemble is at least 10 % higher than for any individual AOGCM. While the total area at risk represents a worst case that is extremely unlikely to come to pass, major or at least moderate changes cannot be precluded in these regions based on the climate scenarios used.

13. Discussion and conclusions

This paper shows that there is a substantial risk of climate change to transform the world's terrestrial ecosystems profoundly, as judged by shifts in basic biogeochemical functioning. Nearly no area of the world is free from such risk, unless strong mitigation limits global warming to around 2 degrees above pre-industrial level. Even then, most climate models agree that up to one fifth of the world's ice-free, non-agricultural land surface is under a risk of at least moderate change.

The results presented here are snapshots of the projected changes at the end of the 21st century. GMT is likely to continue to rise beyond the simulation period, which means that pressure on ecosystems will continue into the 22nd century. Because of time-lags in their response ecosystems may also continue to change if GMT is stabilised by 2100. Adaptation can take place at the scale of years to decades in the case of vegetation decline, but time-lags may extend to centuries or even millennia where adaptation entails the migration and regrowth of forests (Leemans and Eickhout 2004). The different speeds of adaptation processes mean that ecosystem changes projected for the low warming scenarios cannot simply be taken to represent transitional states that happen at an earlier point in time of the higher warming scenarios.

The Γ metric goes beyond commonly used indexes like the Köppen-Geiger climate classification system and the Holdridge life zones system which map the state of land areas (and their biomes) based on climatic indicators. In contrast, Γ particularly measures changes in the biogeochemical as well as structural state of the land surface. This means that our metric can have values even without a change of either Köppen or Holdrige class (i.e. without changing to a different climate zone or biome).

Since Γ measures the amount of change regardless of the direction of change (increase or decrease) in the individual parameters describing ecosystem states, a high confidence in projected moderate or major ecosystem change does not necessarily imply agreement on the type of change. For example, a tropical savanna may change into a seasonal forest following reduced water limitation or into a grassland if precipitation is reduced, both of which would be considered major change in this analysis. From the view of the Γ metric, in either case the present ecosystem 'as we know it' would be affected in a major way and likely disappear. This focus on the magnitude of change instead of the individual

processes driving that change can be considered a disadvantage. On the other hand, the ability to capture many types of changes at once is important in the context of a risk assessment. The metric does not categorise changes as positive or negative, as such evaluations often depend on the perspective taken (Leemans and Eickhout 2004). Any significant change in the underlying biogeochemistry is considered an ecological adaptation challenge that puts pressure on species and communities to either adapt, migrate or disappear entirely (Mooney et al. 2009). Combining the Γ metric with maps of present-day species endemism richness, Gerten et al. (2013) expand on our analysis of affected areas and attempt to assess climate change risks to biodiversity.

While possibly the most comprehensive sampling of climate uncertainty with respect to projected changes in biogeochemical functioning to date, this study is based on one impact model only. Previous DGVM intercomparison studies found that model results matched quite well for contemporary, observed climatology, but diverged in their response to climate change (Cramer et al. 2001; Sitch et al. 2008). The ongoing Inter-Sectoral Impact Model Intercomparison Project (ISI-MIP, `http://www.isi-mip.org`) compiled impact simulations from more than 30 impact models within a consistent modelling framework covering the agricultural, biome, health and water sector. The ISI-MIP archive includes simulations from 7 global vegetation models including LPJmL which are analysed with the Γ metric. While using a different model setup and different climate scenarios, these results provide an indication of the representativeness of LPJmL as used here in comparison to other vegetation models. Overall, LPJmL results are found to fall well within the range of the other biogeochemical models participating in ISI-MIP (Piontek et al. 2014; Warszawski et al. 2013), although analysis suggests that uncertainty from differences in impact models is larger than that caused by climate model differences. However, biome sector results in the ISI-MIP archive are based on climate scenarios from only three AOGCMs. Also, they directly relate ecosystem changes to changes in GMT regardless of emissions scenario and therefore timing, ignoring possible time-lag effects. Several of the participating models lack dynamic vegetation and there are other differences regarding included processes (e.g. fire disturbance, nutrient limitation). While the Γ metric can be computed for different sets of parameters describing ecosystem states this hampers comparability of results.

Processes determining species composition in ecosystems are highly complex and in many cases poorly understood, especially in connection with novel climates (Williams and

Jackson 2007). While simulated dynamics in LPJmL constitute best current knowledge, further model development is required to improve the reliability of projected change in vegetation structure (see section B.4 in Appendix B for further discussion). Climate change is closely linked to increasing CO_2 concentrations in the atmosphere which have a fertilisation effect on vegetation growth. Both drivers act together to produce the biogeochemical shifts in the biosphere measured by Γ. Compared to just the climate effect, CO_2 fertilisation increases the magnitude of change in many regions, while in others it partially counteracts climate-driven changes, resulting in lower Γ values. While there is still some debate about the long-term magnitude of CO_2 fertilisation and the potential role of nutrient co-limitations in some biomes (e.g. Hickler et al. 2008) a complete absence of fertilisation effects is not realistic and therefore not investigated here.

In addition to the effects of climate change and CO_2 fertilisation, land use change is a concurrent pressure acting upon ecosystems. This is expected to increase, as a rising global population and growing economic wealth will increase demand for food and feed, combined with a potentially substantial future demand for bio-energy production to achieve energy independence and climate mitigation targets (Lotze-Campen et al. 2010; van Vuuren et al. 2010). Ecosystem protection in the 21st century will therefore face both of these interacting pressures, global climate and land use change.

In view of the substantial risks of ecosystem change from global warming found in this study, advancing systematic, comprehensive numerical analysis of terrestrial climate change impacts should be a focus of scientific research in the next years with the aim of reducing the large present uncertainty in the quantification of impacts. This would provide a better foundation for policy processes considering tradeoffs with the political, social and economic transformations implied in managing global change. Despite the remaining uncertainties, our findings demonstrate that there is a large difference in the risk of global ecosystem change under business as usual or limited as compared to effective mitigation.

Supplementary material related to this part is available in Appendix B.

Acknowledgements

This study was supported by GLUES (Global Assessment of Land Use Dynamics, Greenhouse Gas Emissions and Ecosystem Services), a scientific coordination and synthesis project of the German Federal Ministry of Education and Research's (BMBF's) 'Sustainable Land Management' programme (Code01LL0901A), and by the EU-FP7 research project ERMITAGE (grant no. 265170).

The 'PanClim' climate dataset, the Γ metric results for all our 152 scenarios and the source code for the Γ metric software and related analysis tools are available for download at http://www.panclim.org. LPJmL can be obtained through the LPJ & LPJmL Web Distribution Portal at http://www.pik-potsdam.de/research/projects/lpjweb.

Part IV.

Asynchronous exposure to global warming: freshwater resources and terrestrial ecosystems[1]

Dieter Gerten, Wolfgang Lucht, Sebastian Ostberg, Jens Heinke, Martin Kowarsch, Holger Kreft, Zbigniew W. Kundzewicz, Johann Rastgooy, Rachel Warren, and Hans Joachim Schellnhuber

Abstract

This modelling study demonstrates at what level of global mean temperature rise (ΔT_g) regions will be exposed to significant decreases of freshwater availability and changes to terrestrial ecosystems. Projections are based on a new, consistent set of 152 climate scenarios (eight ΔT_g trajectories reaching 1.5–5 °C above pre-industrial levels by 2100, each scaled with spatial patterns from 19 general circulation models). The results suggest that already at a ΔT_g of 2 °C and mainly in the subtropics, higher water scarcity would occur in >50% out of the 19 climate scenarios. Substantial biogeochemical and vegetation structural changes would also occur at 2 °C, but mainly in subpolar and semiarid ecosystems. Other regions would be affected at higher ΔT_g levels, with lower intensity or with lower confidence. In total, mean global warming levels of 2 °C, 3.5 °C and 5 °C are simulated to expose an additional 8%, 11% and 13% of the world population to new or aggravated water scarcity, respectively, with >50% confidence (while ~1.3 billion people already live in water-scarce regions). Concurrently, substantial habitat transformations would occur in biogeographic regions that contain 1% (in zones affected at 2 °C), 10% (3.5 °C) and 74% (5 °C) of present endemism-weighted vascular plant species, respectively. The results suggest nonlinear growth of impacts along with ΔT_g and highlight regional disparities in impact magnitudes and critical ΔT_g levels.

14. Introduction

Countries' current pledges to reduce greenhouse gas emissions would set global mean temperature increase (ΔT_g) on a trajectory of ~3.5 °C above pre-industrial levels by the end of this century (Rogelj et al. 2010) — far above the 2 °C target adopted

in the Cancún Agreements (UNFCCC 2011). The tensions about the climate policy goal of limiting ΔT_g to 2 °C require that policymakers be informed about possible consequences of their decisions. This can be accomplished by solid scientific assessments of the presumably high costs, the implementation risks and the benefits (in terms of avoided climate change impacts) of low-stabilization targets on the one hand and of consequences of less ambitious mitigation (i.e. global warming above 2 °C) on the other hand (Knopf et al. 2012). To contribute to a better understanding of the latter, this study quantifies — spatially explicitly at global scale — how freshwater availability and terrestrial ecosystems might change in response to different levels of ΔT_g.

Previous assessments of (exposure to) impacts associated with different ΔT_g levels were compromised by a number of methodological inconsistencies, as pointed out e.g. by Lenton (2011) and Warren et al. (2011). 'Reasons for concern' (Smith et al. 2009) and 'burning ember' diagrams (Schneider and Mastrandrea 2005) often combine heterogeneous, partly qualitative impact estimates that lack spatial and temporal detail and do not systematically account for available climate change scenarios. Simulation models or other internally consistent balancing schemes, applied for the whole land surface and forced by simulations from a large ensemble of general circulation models (GCMs), can in principle overcome these inconsistencies. However, respective studies either focused on single, though politically relevant ΔT_g levels (Fung et al. 2011; Zelazowski et al. 2011) or could not consider the structural uncertainty among GCMs — which is sizeable due to the large spread especially in precipitation projections (e.g. Knutti and Sedláček 2012). Often projections from only a few GCMs were used (Arnell et al. 2011) or ensemble projections were grouped according to the warming level reached by the end of this century (Scholze et al. 2006), which strongly reduces the sample size for higher ΔT_g levels due to differences in the GCMs' climate sensitivity (see Rogelj et al. 2012). Other studies (Tang and Lettenmaier 2012) selected those future time periods when a given ΔT_g value was exceeded, which means that the timing of the T_g changes differed among GCMs. Yet other studies only investigated when and where specific temperatures or warming rates are likely to be reached, without quantifying resulting impacts (Joshi et al. 2011; Mahlstein et al. 2013).

To overcome many of these problems, we here employ a newly generated ensemble of 152 climate scenarios (Heinke et al. 2012), constructed by performing a 'pattern-scaling' of stylized ΔT_g trajectories (reaching 1.5–5 °C above pre-industrial levels around year

2100, in 0.5° steps) with 19 GCMs from the CMIP3 archive. Used as forcing for the well-validated LPJmL biosphere and water balance model (Sitch et al. 2003; Gerten et al. 2004; Bondeau et al. 2007), this setup enables consistent quantification of impacts for different ΔT_g levels and underlying climate policies, respectively. The local–global scaling factors are nearly independent of the considered emissions scenarios and are sufficiently accurate over a wide range of ΔT_g, especially in case of temperature but less so in case of precipitation (Mitchell 2003; see Heinke et al. 2012 for details on this approach).

We present our results acknowledging that climate change proceeds asynchronously across the globe (i.e. some regions are affected earlier by significant changes than others; Joshi et al. 2011; Mahlstein et al. 2011) and that regions differ with respect to their vulnerability to such change (Füssel 2010). In so doing, we highlight which regions are likely to experience the here considered critical changes to water availability and ecosystems 'earlier' (i.e. at lower ΔT_g levels around 2100) than others. To communicate these spatiotemporal patterns of exposure — and of implied global inequalities — we directly map the ΔT_g level at which the local impacts on water and ecosystems first occur. We also demonstrate the incremental changes between different ΔT_g levels.

15. Methods

15.1. Climate scenarios

We rearranged pre-existing GCM simulations using a pattern-scaling approach to allow for analysis of impacts under different levels of ΔT_g while accounting for differences among GCMs. The principle of pattern-scaling is to calculate scaling coefficients that statistically link local changes in climate variables to ΔT_g, global fields of which can be used in spatially resolved impact models.

The scaling coefficients were derived for each calendar month, for each grid cell over land ($0.5° \times 0.5°$ spatial resolution), and for each of 19 GCMs that participated in

the World Climate Research Programme's Coupled Model Intercomparison Project (CMIP3) (Meehl et al. 2007) to account for the large differences in GCM projections (see e.g. Knutti et al. 2010). For each GCM and month, this procedure yielded the local change in climate variables (air temperature, precipitation amount, degree of cloudiness) per degree of ΔT_g. These response patterns were then combined with time series of annual ΔT_g derived from the reduced-complexity climate model MAGICC6 (Meinshausen et al. 2011a). Greenhouse gas emissions were tuned in MAGICC6 in a way that ΔT_g levels of 1.5, 2.0, 2.5, 3.0, 3.5, 4.0, 4.5 and 5 °C above pre-industrial levels (from the GCMs' unforced control runs) are reached by around year 2100 (2086–2115 average). Corresponding atmospheric CO_2 concentrations range between ∼400 ppm (for the 1.5 °C trajectory) and ∼1400 ppm (for the 5 °C trajectory). As a result of this data fusion, 19 climate change patterns were obtained for each ΔT_g step — 152 scenarios altogether. The patterns were applied as anomalies to 1980–2009 observed climate (CRU TS3.1 for temperature and cloudiness, Mitchell and Jones 2005; and GPCC dataset version 5 for precipitation, Rudolf et al. 2010), yielding the 152 monthly time series up to year 2115. These data were subsequently interpolated to daily values using stochastic procedures as in Gerten et al. (2004) and then used to force the LPJmL model for assessing potential impacts (see following sections). A comprehensive description of the generation of the scaling patterns and of the anomaly approach is provided by Heinke et al. (2012). While biases in GCM projections have been accounted for in this data processing, we recognize that the skill of GCMs to project climate changes at regional scale is limited, as has been shown in a number of studies for CMIP3 models (e.g. Pincus et al. 2008; Hawkins and Sutton 2011). Thus, the present scenarios are suited to identify the broad patterns of climate changes and their impacts (presented in global- and continental-scale plots and tables), but results for individual grid cells (presented in maps) should be interpreted with caution.

15.2. The LPJmL model

For quantifying the below-specified changes to water availability and ecosystems for each climate scenario, we employed the process-based LPJmL dynamic global vegetation and water balance model (Sitch et al. 2003; Gerten et al. 2004; with recent overall improvements by Bondeau et al. 2007 and Rost et al. 2008a but with crop, irrigation and

river routing modules switched off — see section 15.3.1). LPJmL computes the growth and productivity of the world's major vegetation types (here, nine plant functional types) in direct coupling with associated fluxes of water and carbon in the vegetation-soil system. The model was run at daily time step and $0.5° \times 0.5°$ spatial resolution globally, forced by the pattern-scaled time series of daily climate (air temperature, precipitation amount, number of wet days per month, cloud cover) and yearly atmospheric CO_2 concentration. The model has been shown to well reproduce observed vegetation distribution, biomass production and carbon fluxes (Lucht et al. 2002; Sitch et al. 2003; Hickler et al. 2006; Bondeau et al. 2007), fire regimes (Thonicke et al. 2001) and water fluxes (Gerten et al. 2004; Rost et al. 2008a; Fader et al. 2010). Hence, although individual process representations require continuous improvement in this model and others of its type (e.g. Sitch et al. 2008; Li et al. 2012; Murray et al. 2013; Piao et al. 2013), LPJmL is a suited tool for assessing climate change effects on water resources and ecosystems alike.

15.3. Change metrics

We consider local changes in water availability/scarcity and terrestrial ecosystems as expressed by two metrics, and subsequently relate these changes to the in situ human population size and 'species endemism' of vascular plants, respectively (see following paragraphs). The metrics are calculated for each 0.5° grid cell, ΔT_g step and GCM pattern. The global warming level deemed critical from a local perspective is given by the lowest ΔT_g value at which the metrics cross specific thresholds in the 2086–2115 average. We focus on changes projected to be 'more likely than not' (found in >50%, i.e. at least 10 out of the 19 climate change scenarios) but also address 'likely' (>66%) and 'unlikely' (<33% but >0%) impacts, following IPCC guidance notes (Mastrandrea et al. 2010). We also focus on three policy-relevant ΔT_g levels: the 2 °C mitigation target; the likely outcome of current national emissions reduction pledges (3.5 °C); and a business-as-usual case (5 °C, near to the average ΔT_g simulated by GCMs under high-emission SRES A1FI and RCP8.5 scenarios; Rogelj et al. 2012). Since there are interdependencies among GCMs (Masson and Knutti 2011; Pennell and Reichler 2011), actual confidence may be narrower than stated herein. Moreover, although we have integrated all GCM runs with different initial conditions available from the CMIP3 archive (see Heinke et al. 2012), they embody only a fraction of possible climate developments in the future (Rowlands

et al. 2012).

15.3.1. Water scarcity

Chronic supply-side water scarcity — likely to increase competition among water users and to constrain food production, economic development and environmental integrity — is defined to prevail if $<1000\,m^3\,cap^{-1}\,yr^{-1}$ are available within a given spatial unit (Falkenmark and Widstrand 1992). This analysis uses river basins as the spatial unit, delineated as in Haddeland et al. (2011), which implicitly assumes that any water demand is to be met within each basin, neglecting e.g. import of water-intensive products from other regions (Fader et al. 2011). Furthermore, we consider only 'blue' water resources, i.e. renewable surface and subsurface runoff useable for irrigation, industries and households. Applying more complex water scarcity indicators and of other mapping units may yield different results (Gerten et al. 2011). Runoff was computed under conditions of potential natural vegetation, for reasons of consistency with the assessment for ecosystems; irrigation, reservoir operation and land use change effects are thus not considered in this study. We distinguish four types of change to water resources and scarcity.

1. *Regions already chronically water-scarce experience aggravated scarcity.* This is the case if the simulated annual and/or monthly runoff is significantly lower in the future (2086–2115 period) than presently (1980–2009). A significant decrease in the average annual runoff is assumed if its change is greater than present standard deviation (Gosling et al. 2010; Arnell et al. 2011), which can be regarded as a challenge to water management systems attuned to historic flow experience. A significant decrease in monthly runoff — taken as a proxy for increased drought frequency on top of the change in mean annual flow (Lehner et al. 2006) — is assumed if the median of calendar months in the future is lower than the respective present-time median in more than 10% (i.e. 36) of the future months.
2. *Regions not yet chronically water-scarce move into a water-scarce status* — i.e. $<1000\,m^3\,cap^{-1}\,yr^{-1}$ are simulated to be available in the future in regions that are above this threshold today.
3. *Regions not chronically water-scarce experience lower water availability.* In this case the decrease in water availability is defined as in (1), yet applied to regions

with $>1000\,\mathrm{m^3\,cap^{-1}\,yr^{-1}}$ both presently and in the future.

4. *Regions that are water-scarce but do not experience aggravated scarcity*; i.e. regions where present water availability is $<1000\,\mathrm{m^3\,cap^{-1}\,yr^{-1}}$ but does not cross the thresholds cf case (1). Human populations are either held constant at year 2000 values or assumed to change according to the SRES B1 or A2r population projections, respectively (Grübler et al. 2007). Increases in runoff are also analysed, but for reasons of brevity we do not relate them to the number of people living in areas affected by such increases.

15.3.2. Ecosystem change

Severe ecosystem changes are assumed if the change in a generic ecosystem stability index 'Γ' developed by Heyder et al. (2011) adopts a value ≥ 0.3 (moderate changes, $\Gamma > 0.1$). This can be interpreted as simultaneous shifts in several ecosystem features as large as those associated with e.g. a transition from temperate forest to boreal forest. The Γ metric is composed of a suite of biogeochemical and vegetation structural variables, changes in which either represent alterations in the entire ecosystem status or in a specific subset of variables. Using such an aggregated index advances earlier studies focused solely on biome area changes (Leemans and Eickhout 2004) or individual ecosystem properties (Gerber et al. 2004; Scholze et al. 2006; Sitch et al. 2008).

Specifically, Γ encompasses the following components: (1) carbon fluxes (net primary production, heterotrophic soil respiration, carbon release from natural fires), (2) water fluxes (runoff, evaporation, transpiration), (3) carbon stocks (in plants and soils), and (4) vegetation composition ('ΔV' metric measuring structural dissimilarity of ecosystems based on life forms (trees, grass, bare ground) and their leaf architecture and phenology (needle-leaved or broadleaved, evergreen or deciduous; Sykes et al. 1999)). Γ combines relative and absolute changes in these variables as well as changes in the proportional relation of carbon and water fluxes to each other. Some components are also scaled according to their signal-to-noise ratio. The overall Γ metric is finally normalized to values between 0.0 meaning no change and 1.0 meaning total restructuring of the considered basic ecosystem features. It was calculated for the uncultivated fraction of grid cells, thus maps and aggregated global values refer to the respective fractions of grid cells only. For a complete description of Γ see Heyder et al. (2011), and also Ostberg

et al. (2013b) who analyse it in more detail for the same climate scenarios as used here.

While Γ can be interpreted as overall habitat changes, the simulations do not contain information at species level. To frame the model results in the context of floral biodiversity (rather than merely counting the total area affected by $\Gamma > 0.3$ or > 0.1 as in Ostberg et al. (2013b), we linked them to an independent global dataset of vascular plant (ferns, gymnosperms, angiosperms) biodiversity (Kier et al. 2009). The dataset contains information on the current fractional distribution, species richness and endemism for each of 90 unique terrestrial (island and mainland) biogeographic regions — 315903 species altogether. The here used 'endemism richness' is the weighted product of the number of species within a biogeographic region and the region's share (0–1) of each species' global distribution range. For example, if 20% of a species' distribution range falls into a region, 20% of the total species number is attributed to it.

We determined, for each ΔT_g step, which biogeographic regions experience changes in Γ on more than a third of their respective area, and counted how many of the 19 climate scenarios show this. We then determined the endemism richness of each of those regions from the Kier et al. (2009) dataset, and aggregated the values to continental and global sums. Note that endemism richness refers to the present situation, whilst climatic and land cover changes may concurrently alter species richness and endemism (Sommer et al. 2010). That is, our results do not indicate the climate effects on future endemism richness; they rather indicate the changing biogeochemical boundary conditions.

16. Results

16.1. Aggravation or new establishment of water scarcity

Figure IV.1 illustrates that certain regions are affected by the here assessed changes at low ΔT_g levels already, under >50% of the climate change patterns, whereas others are affected not before higher ΔT_g levels are reached. People inhabiting river basins

particularly in the Middle East and Near East become newly exposed to chronic water scarcity or experience an aggravation of existing scarcity even if highly ambitious mitigation policies could constrain ΔT_g to $\leq 2\,°C$ (Figure IV.1a). For these regions, GCMs project significantly lower rainfall even in low-emission scenarios (Bates et al. 2008), resulting in less runoff (Figure IV.2a). Of the ∼1.3 billion contemporary population exposed to water scarcity (Table IV.1), 3% (North America) to 9% (Europe) are prone to aggravated scarcity at $\Delta T_g \leq 2\,°C$. An additional 0–2% of each continent's population live in basins simulated to become water-scarce (Figure IV.3a, top panel). In total, 486 million people — about 8% of the world population in 2000 (equalling almost that year's population of the US and Indonesia together) — are affected by either of these changes at $\Delta T_g \leq 2\,°C$.

Conversely, more runoff is simulated especially for high latitudes and parts of the tropics at $\Delta T_g > 3.5\,°C$ (Figure IV.2b). Associated shifts in seasonal hydrographs and higher flood risk compared to historical experience cannot be ruled out for those regions (Kundzewicz et al. 2008), but this is not investigated in detail here as we focus on regions with decreases in runoff.

Many of the regions not significantly affected at $\Delta T_g \leq 2\,°C$ are projected to become (more) water-scarce if T_g increased by up to 3.5 °C — a scenario that cannot be dismissed, if no further commitments were made than current emissions reduction pledges. This concerns e.g. the Middle East, North Africa and South Europe (Figure IV.1a), i.e. regions inhabited by another 3% of the world population (adding to the 8% increase at 2 °C; see Figure IV.4a). At $\Delta T_g > 3.5\,°C$, the climate change effects expand further into these regions, such that 12–15% of each continent's population (Australasia, 23%) and 13% of the world population are exposed to aggravated or newly established water scarcity at $\Delta T_g = 5\,°C$ under >50% of the climate patterns (Figure IV.3a). This increase is attributable primarily to Asia (see Figure IV.3a, bottom panel), while contributions from other continents are comparatively minor. Given the SRES B1 and A2r demographic projections, a higher fraction of the future world population would be exposed to water scarcity than around year 2000, i.e. 30–43% (∼2–5 billion cf Table IV.1; also see Figure C.5 in Appendix C). Note that the relative increase in the number of people exposed to new or aggravated water scarcity due to climate change only is largely independent of the population scenario, as was also found by Gosling et al. (2010).

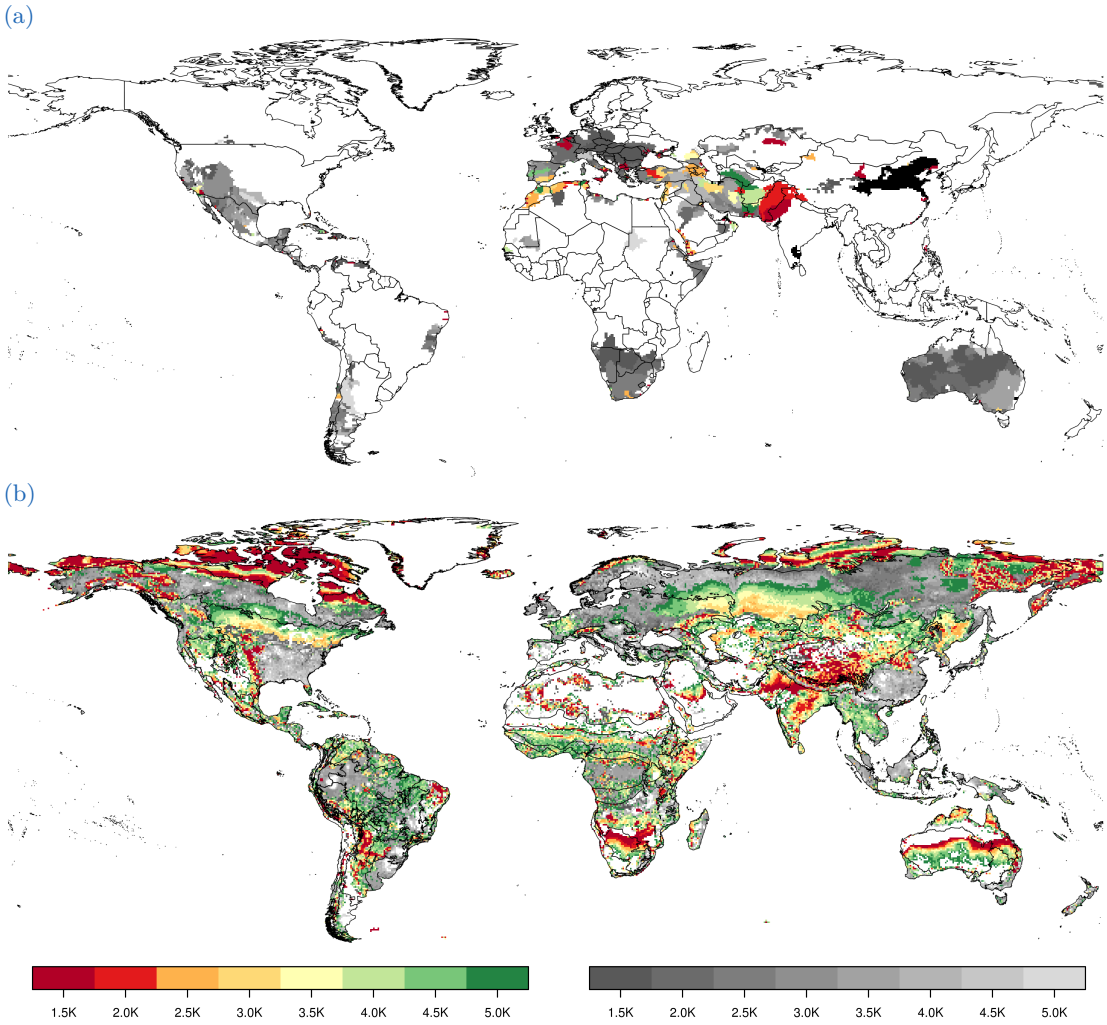

Figure IV.1.: Threshold level of ΔT_g leading to significant local changes in water resources (a) and terrestrial ecosystems (b). (a) Coloured areas: river basins with new water scarcity or aggravation of existing scarcity (cases (1) and (2), see section 15.3.1); greyish areas: basins experiencing lower water availability but remaining above scarcity levels (case (3)); black areas: basins remaining water-scarce but without significant aggravation of scarcity even at $\Delta T_g = 5\,^{\circ}\mathrm{C}$ (case (4)). No population change is assumed here (see Figure C.5 in Appendix C for maps including population scenarios). Basins with an average runoff $<10\,\mathrm{mm\,yr}^{-1}$ per grid cell are masked out. (b) Regions with severe (coloured) or moderate (greyish) ecosystem transformation; delineation refers to the 90 biogeographic regions. All values denote changes found in >50% of the simulations.

16.2. Severe changes to terrestrial ecosystems

Substantial biogeochemical and vegetation structural shifts in terrestrial ecosystems are simulated under more than half of the climate patterns for a mean global warming of 2 °C (Figures IV.1b and IV.3). In particular, this concerns high latitudes (reflecting higher primary production and northward migration of the treeline), and also semiarid regions on all continents (reflecting CO_2-induced improvements in plant water use efficiency and expanding vegetation cover) (Heyder et al. 2011). These areas represent 11% of the ice-free, unmanaged global land surface (details in Ostberg et al. 2013b). But, due to the highly uneven distribution of species richness around the world, they represent only 4 — albeit spatially quite extensive — unique biogeographic regions that altogether entail 1% of global endemism richness of vascular plants (Table IV.1, Figure IV.4b). The number of biogeographic regions exposed to severe habitat changes is found to quadruple at $\Delta T_g = 3.5\,°C$, then affecting 10% of endemism richness. The incremental exposure steeply rises further if warming continued above this level: our simulations suggest that 68 out of the 90 distinct biogeographic regions — presently containing $\sim 3/4$ of today's vascular plant endemism richness — would be subject to pronounced habitat transformation at 5 °C (Figure IV.4b). Even higher shares of continental endemism richness are reached in Africa and the Americas at 5 °C (Figure IV.3b, top panel). Severe ecosystem changes on these two continents are simulated for regions presently containing half of the world's vascular plant endemism richness (see Figure IV.3b, bottom panel). Results tend to concur with regional studies that suggest significant declines in floral and faunal species richness at ΔT_g above ~3 °C (Hare et al. 2011).

16.3. Moderate or less confident changes

When choosing lower 'critical' thresholds (including non-water-scarce basins and, respectively, areas with $0.1 < \Gamma < 0.3$) or considering changes simulated under less than 50% of the climate patterns, exposure to change generally occurs at lower ΔT_g and covers larger areas. This is indicated by the following examples (figures compiled in Appendix C). The incremental impact on ecosystems between 2 and 3.5 °C is significantly stronger when accounting for moderate ecosystem changes in addition to severe ones, in terms of both the size of the affected area (Figure C.6d in Appendix C) and the number and

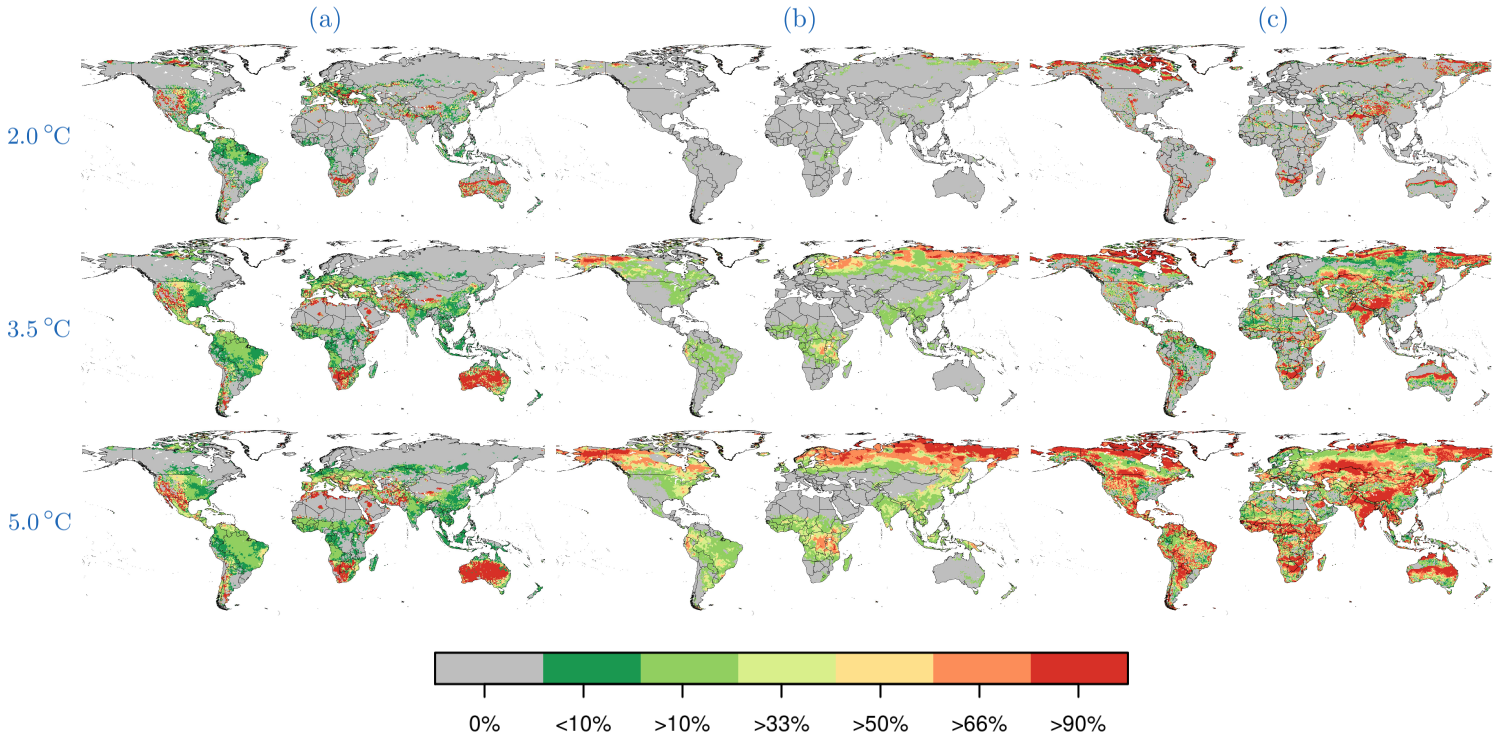

Figure IV.2.: Likelihood of a decrease in runoff (a), an increase in runoff (b) and a severe change in ecosystems (c) for selected ΔT_g levels. (a) and (b) show whether the simulated decrease (increase) in average annual runoff exceeds present (1980–2009) standard deviation, or whether monthly runoff is >10% more frequently below (above) its present median. Areas with presently $<10\,\mathrm{mm\,yr^{-1}}$ are masked out. The likelihoods are derived from the 19 climate change patterns. See Figures C.1–C.4 in Appendix C for all eight ΔT_g levels.

Table IV.1.: Continental and global effects of different ΔT_g levels. Top: millions of people living in river basins characterized by chronic water scarcity ($<1000\,m^3\,cap^{-1}\,yr^{-1}$) (cases (2) and (4)), either with or without B1 and A2r future population change. People in water-scarce basins that show an aggravation of scarcity according to case (1) (see Figure IV.3a) are not counted here. Numbers in brackets denote the changes (relative to the present) that are solely due to climate change. Bottom: number of unique biogeographic regions (out of 90) exposed to severe biogeochemical or vegetation structural shifts. All values refer to changes with $> 50\%$ confidence, simulated under at least 10 of the 19 GCM patterns.

	Around 2000		Climate change only			Climate and B1 population change				Climate and A2r population change			
	Total	Affected	Affected			Total	Affected			Total	Affected		
			+2 °C	+3.5 °C	+5 °C		+2 °C	+3.5 °C	+5 °C		+2 °C	+3.5 °C	+5 °C
People living in water-scarce basins													
Europe	505	110	118	123	133	465	143	145	133	531	258	237	186
Asia	3879	870	988	985	970	3733	1424	1480	1442	6929	3463	3440	3,401
Africa	775	115	115	115	126	1647	313	304	295	3145	1084	925	867
N America	479	83	81	86	87	712	137	121	127	891	270	274	259
S America	345	77	82	82	82	407	87	89	89	747	198	167	165
Oceania	29	13	13	13	14	44	16	18	18	55	19	20	20
Globe	6012	1267	1397	1404	1412	7009	2120	2157	2103	12 298	5294	5063	4897
			(+130)	(+137)	(+145)		(+628)	(+665)	(+611)		(+293)	(+62)	(-104)
Number of unique biogeographic regions with severe ecosystem changes on $> 33\%$ of their area													
Europe	3	—	—	—	2								
Asia	22	—	1	6	16								
Africa	18	—	1	4	13								
N America	10	—	1	2	10								
S America	26	—	1	3	21								
Oceania	10	—	—	1	6								
Globe	90	—	4	16	68								

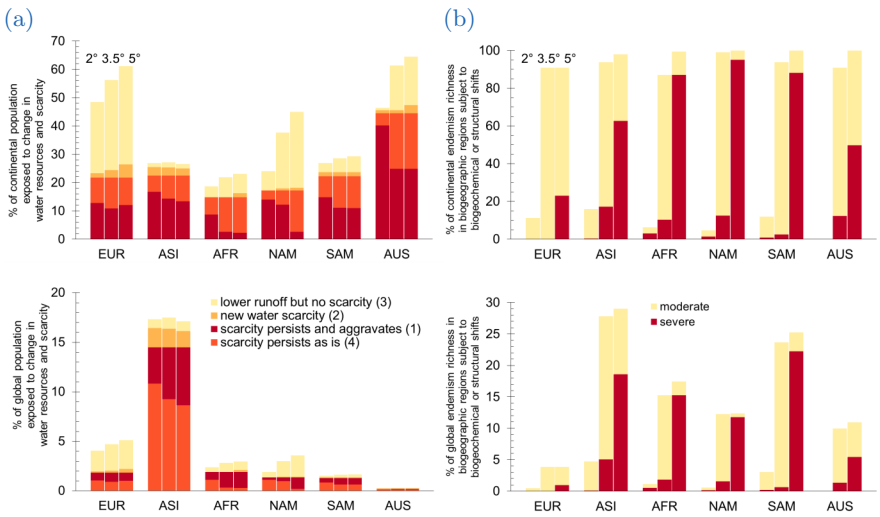

Figure IV.3.: Continental-scale effects of selected ΔT_g levels (2 °C, left bars; 3.5 °C, middle bars; 5 °C, right bars), simulated under >50% of the climate change patterns. (a) Percentage of continental population exposed to new or aggravated water scarcity, or lower water availability outside water-scarce river basins, assuming unchanged population. (b) Percentage of continental endemism-weighted species richness of vascular plants in biogeographic regions exposed to substantial habitat shifts ($\Gamma > 0.3$ on $> 33\%$ of the regions' area). The upper panel shows values relative to the continental totals, whereas the bottom panel shows values relative to the global totals. Numbers in brackets refer to the four cases of hydrologic change (see section 15.3.1 and Figure IV.1). EUR, Europe; ASI, Asia; AFR, Africa; NAM, North America; SAM, South America; AUS, Australasia.

endemism richness of the underlying biogeographic regions (Figure C.7 in Appendix C). If reductions in water availability are computed also for non-water-scarce basins in addition to the reductions in water-scarce regions, many regions especially in Europe, Australia and southern Africa appear to be affected already at 1.5 °C (Figure C.6a). For a 5 °C warming, this would mean that $\sim 20\%$ of the world population is exposed to some form of significantly reduced water availability (Figure C.7). Finally, inclusion of unlikely changes ($< 33\%$ of the simulations) suggests a substantially larger globally affected population (water scarcity) and area (ecosystem change) compared to the $> 50\%$ case, for all ΔT_g levels (Figure C.6). Note that 'unlikely' here represents changes that cannot be ruled out scientifically, as they occur under simulations from at least one of the 19 GCMs — each of which we here consider equally plausible.

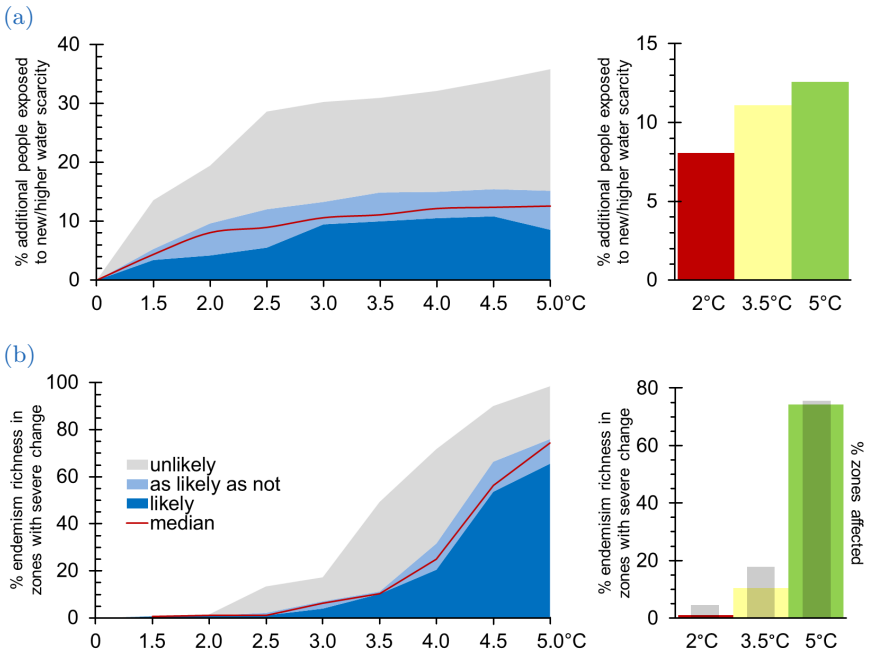

Figure IV.4.: Simulated exposure of world population to water scarcity (a) and of global endemism richness to severe habitat changes (b), plotted as functions of ΔT_g. Left panel: function for all $8\Delta T_g$ levels and three confidence levels (stacked plot); right panel: results highlighted for 2, 3.5 and 5 °C and the >50% case. Specifically, (a) shows the additional percentage of current world population exposed to new or aggravated water scarcity (cases (1) and (2); see section 15.3.1); (b) shows the percentage of global vascular plant endemism richness presently residing in regions that will be exposed to substantial habitat shifts (>33% of a region's area with $\Gamma > 0.3$). Grey bars in (b) show the corresponding number of affected regions (% out of the 90 regions; plotted on the same axis).

17. Discussion

Albeit confined to selected change metrics, the present assessment accentuates asynchronies in exposure to climate change. That is, different regions are exposed to hydrologic or ecosystem changes at different ΔT_g levels, as displayed in Figure IV.1. Moreover, the study suggests that global and continental impacts accrue — in part nonlinearly — with ΔT_g and that the shape of this growth curve differs between impact sectors.

For ecosystems, the climate response functions tend to display a sigmoidal shape with a slow initial increase, a rapid expansion in a critical range at intermediate ΔT_g levels,

and a plateau at high ΔT_g when changes cover most regions (Figure IV.4b; note that the shape hardly depends on the confidence level, i.e. the number of climate scenarios). Regarding the additional population in water-scarce regions, the curve is much flatter, i.e. the incremental global effect of high ΔT_g levels is weaker. It can also be noted, for Asia, that the population exposed to water scarcity slightly decreases at high ΔT_g (Table IV.1, representing case (2) category in Figure IV.3a and possibly also basins that move out of the water-scarce category). This is probably due to nonlinearities in the relationship between forcing and hydrological response in a few, densely populated regions where e.g. effects of higher precipitation at high ΔT_g may outdo effects of higher evapotranspiration. Detailed explanation of such developments would require model runs in which different driving forces are held constant. In general, different shapes of impact functions are found for change metrics other than those studied here, and also for individual regions (compare e.g. Levermann et al. 2012; Schaphoff et al. 2013).

Expert judgements suggest that abrupt, potentially irreversible biospheric 'tipping points' may be reached if ΔT_g exceeds a critical range (Amazonian forest decline, +3–4 °C; boreal forest decline, +3–5 °C; Lenton et al. 2008). While such events are not studied here, our results partly support these concerns. As shown in Figure IV.1b, widespread ecosystem changes and implied forest die-back in the southern boreal zone and some other regions are simulated under $> 50\%$ of the climate patterns if ΔT_g exceeded $\sim$3.5 °C, due primarily to heat stress and also droughts (as is already evident in some regions; Allen et al. 2010). However, large-scale change to Amazonian ecosystems — characterized by high endemism richness — is simulated only for ΔT_g levels close to the maximum range considered here, i.e. 5 °C (Figure IV.2c). Recent findings also suggest that Amazonian die-back is found under a few climate change scenarios only, and that the (highly uncertain) CO_2 effects on vegetation play a major role (Rammig et al. 2010; Huntingford et al. 2013). The simulated system transition in savannah-dominated regions agrees with recent evidence for local regime shifts (Higgins and Scheiter 2012), with C4 grass benefitting from low ΔT_g and woody encroachment benefitting directly from the elevated CO_2 concentration associated with higher ΔT_g. Furthermore, in the boreal zone, permafrost thawing (not considered in the present model setup) will, due to higher microbial activity, augment soil carbon release even further than implied in our simulations, probably producing a positive feedback to warming (Schneider von Deimling et al. 2012; Schaphoff et al. 2013).

The here used climate change scenarios were constructed so that different ΔT_g levels are reached around year 2100. In current high-emission scenarios, however, the prospective timing of $\Delta T_g = 2\,°C$ is around 2050 and that of $\Delta T_g = 3.5\,°C$ around 2080 (Rogelj et al. 2012). Hence, in case such scenarios will come true, the demonstrated changes in water scarcity and Γ would occur some decades earlier than assumed herein. A related caveat, which merits quantification in further studies, is that the timing of ΔT_g and associated local climate changes could be of importance. This is particularly true for ecosystems, whose adaptation capacities may be weaker or whose response to climate change may be slower than assumed in our model (Loarie et al. 2009; Sandel et al. 2011; Diffenbaugh and Field 2013). There is also scope to investigate how much of the difference in impacts between ΔT_g levels is due only to the corresponding differences in atmospheric CO_2 concentration. In fact, besides the radiative (climate) effects of CO_2, there are direct physiological and structural effects on plants, with implications for both water scarcity and Γ. These effects are accounted for in the LPJmL model (Leipprand and Gerten 2006), but different assumptions about the relationship between CO_2 and ΔT_g (e.g. due to other emissions trajectories and climate sensitivities) may produce somewhat different responses. Furthermore, not only GCMs but also impact models (including vegetation models such as the one used here) differ in terms of model structure and parameterization, thus introducing a further level of uncertainty. Resulting uncertainties regarding the Γ metric and variants of the hydrologic metric used herein have been analysed recently (Piontek et al. 2014; Schewe et al. 2014).

18. Conclusions

Our comprehensive simulations show that both freshwater availability and ecosystem properties will change significantly in the future if no efforts were made to abate global warming. The impacts seem to accrue in nonlinear ways, though the shape of impact functions differs among the considered variables. Even if global warming was limited to 1.5–2 °C above pre-industrial level in accordance with current negotiations, almost 500 million people might be affected by an aggravation of existing water scarcity or be

newly exposed to water scarcity. Concurrent population growth would further increase this number to up to around 5 billion people. This outlook is basically supported by findings from Schewe et al. (2014) based on a large suite of global hydrological models. Strongest effects on terrestrial ecosystems appear to occur at somewhat higher global warming levels, with the sharpest increase in the affected area (and underlying plant biodiversity) beyond 3–3.5 °C. These global changes are simulated to be made up by a heterogeneous spatial pattern of change (which differs among impact variables), and different regions will be affected at different ΔT_g levels (as summarized in Figure IV.1).

Besides their obvious relevance for the affected regions themselves, the complex patterns of exposure to climate change might be of political and ethical concern when considering global mitigation targets and related impacts. For example, they shed interesting light on the ethical responsibility of high-emission countries, which — if accepted — could have bearing on both mitigation and adaptation burden sharing (Srinivasan et al. 2008). Furthermore, the present results inform, but also complicate decisions about a fair allocation of international adaptation funds to different regions today. Such aspects will have to be explored in future studies, possibly relating the patterns of exposure to patterns of emissions underlying the climate change scenarios.

We emphasize that the here simulated changes to terrestrial ecosystems cover vast areas, which poses the question whether these changes are manageable, especially under conditions of rapid change and continued anthropogenic landscape modifications (Millar et al. 2007). Decreases in water availability appear to be less widespread and may partly be buffered through adaptive management (not quantified here), even though climate change undermines the conventional assumption of stationary water resources (as reflected in our analysis of whether future changes exceed present variability; also see Milly et al. 2008). At any rate, it is questionable whether adaptive water management will be sufficient to meet increasing water and food demands of a growing world population (Rost et al. 2009). As a consequence, further expansion of irrigated or rainfed cropland may be needed, which would, in turn, amplify the climate change impact on Γ on those areas.

In sum, the present results plea for more comprehensive studies of whether critical ranges for a larger selection of impacts do cluster around a certain ΔT_g level (as suggested already by Parry et al. 2001; Schellnhuber et al. 2004). Ultimately, this requires multi-

sectoral impact model intercomparisons in an interdisciplinary scientific community effort, now under way (Arnell et al. 2013; Piontek et al. 2014).

Supplementary material related to this part is available in Appendix C.

Acknowledgments

This research was supported by the 6th and 7th Framework Programmes of the European Communities under grant agreements no. 036946 (WATCH) and 265170 (ERMITAGE), the BMBF-funded project GLUES, and the CGIAR research program on Climate Change, Agriculture and Food Security. We thank Katja Frieler and Malte Meinshausen for preparing the MAGICC6 data, Sibyll Schaphoff and Werner von Bloh for technical support, and anonymous reviewers for constructive comments.

Part V.

Three centuries of dual pressure from land use and climate change on the biosphere[1]

Sebastian Ostberg, Sibyll Schaphoff, Wolfgang Lucht, and Dieter Gerten

Abstract

Human land use and anthropogenic climate change (CC) are placing mounting pressure on natural ecosystems worldwide, with impacts on biodiversity, water resources, nutrient and carbon cycles. Here, we present a quantitative macro-scale comparative analysis of the separate and joint dual impacts of land use and land cover change (LULCC) and CC on the terrestrial biosphere during the last ca. 300 years, based on simulations with a dynamic global vegetation model and an aggregated metric of simultaneous biogeochemical, hydrological and vegetation-structural shifts. We find that by the beginning of the 21st century LULCC and CC have jointly caused major shifts on more than 90% of all areas now cultivated, corresponding to 26% of the land area. CC has exposed another 26% of natural ecosystems to moderate or major shifts. Within three centuries, the impact of LULCC on landscapes has increased 13-fold. Within just one century, CC effects have caught up with LULCC effects.

19. Introduction

The Earth system is currently undergoing a large-scale transformation of many of its components, including the terrestrial biosphere, that has prompted the declaration of a new geological epoch: the Anthropocene (Steffen et al. 2007). Natural ecosystems across the globe face mounting pressure from two anthropogenic processes, one direct, land use and land cover change (LULCC), and one indirect, climate change (CC). The transformation these two pressures cause is on-going, with wide-ranging implications from biodiversity, food security and human health to feedbacks with other components of the earth system. Two questions emerge: (1) What is the comparative strength of CC

effects, which are a phenomenon largely of the recent decades, and LULCC effects, which have emerged in their current form over the course of the last 300 years mainly? (2) What is the combined magnitude of biosphere transformation caused by these pressures until today?

In light of the pervasiveness of present-day LULCC it has been suggested to characterize the land surface in terms of 'anthromes' instead of (natural) biomes (Ellis and Ramankutty 2008). Historical reconstructions trace back the spread of agriculture over several millennia (e.g. Kaplan et al. 2010; Klein Goldewijk et al. 2011), and the combination of satellite and census data helps to distinguish which crops are grown where (e.g. Portmann et al. 2010). Biospheric impacts of CC have been documented on every continent and in most major taxonomic groups (Parmesan 2006) and were reviewed extensively, e.g., in IPCC (2014a, ch. 4,18) and with regional focus in IPCC (2014b, ch. 22–30).

We use multidimensional shifts in a number of basic biospheric properties as a proxy for more complex changes happening in ecosystems in response to LULCC and CC. The rationale behind this proxy approach is that significant changes of the fundamental building blocks, e.g. carbon and water exchanges with the atmosphere and soil, or broad types of vegetation in terms of their functional strategies, imply impacts on more detailed hierarchical structures, such as predator-prey and host-parasite relations (Parmesan 2006), complementarity and competition regarding resource use (Hooper et al. 2005), or mutual interactions like pollination (Mooney et al. 2009) that cannot be readily modelled at the global scale (Ostberg et al. 2013a).

Impacts of LULCC and CC on individual biospheric properties have been studied extensively, usually focussing on only one of the two pressures or modelling them at drastically diverging levels of complexity. For example, LULCC has reduced global transpiration by ≈10%, while increasing river discharge by 7%, as was found in a modelling study comparing present land use patterns to conditions of potential natural vegetation (Rost et al. 2008b). The human appropriation of terrestrial net primary production (HANPP) has been estimated at 24% of total potential productivity (Haberl et al. 2007), and has doubled over the course of the 20th century (Krausmann et al. 2013). Emissions from LULCC have likely amounted to 156 PgC (or 35% of all anthropogenic CO_2 emissions) between 1850 and 2000 (Houghton 2003; Pongratz et al. 2008) and to 1.1 ± 0.7 PgC/yr during the first decade of the 21st century, although their share of the

total emissions has gone down considerably due to the increasing contribution from burning of fossil fuels (Friedlingstein et al. 2010).

Observed CC impacts in terrestrial natural ecosystems include changes in phenology (e.g. spring advancement of ≈3 days per decade, Parmesan 2007), productivity and mortality as well as shifts in geographical ranges (on average 6 km per decade poleward, Parmesan and Yohe 2003), often combined with changes in species distributions and biodiversity. Based on modelling, CC and increased CO_2 concentrations have resulted in a long-term increasing trend in global river discharge of $+26\,km^3/yr^2$ during the 20th century (Gerten et al. 2008) and a cumulative land uptake of 70–110 PgC during the second half of the 20th century (Sitch et al. 2008). CO_2 fertilisation alone has lead to an 11% increase of vegetation cover across warm, arid environments during recent decades (Donohue et al. 2013).

Comparability between impact studies is often limited owing to a lack of a common baseline and lack of common or at least comparable indicators, and attribution of observed impacts is often difficult in the presence of multiple drivers of change (Stone et al. 2013).

Here, we present an analysis of the impacts of LULCC and climate/CO_2 change for the last ≈300 years, based on a consistent framework composed of (1) observation-based global gridded climate data, (2) historical reconstructions of cropland and managed grassland areas, (3) a Dynamic Global Vegetation Model (DGVM) capable of simulating vegetation-soil dynamics of both natural vegetation and agricultural ecosystems, both at comparable levels of complexity, and (4) an aggregated metric of simultaneous biogeochemical, hydrological and structural shifts at the landscape (grid cell) scale.

We produce a time-series of human intervention with the terrestrial biosphere from 1700 and present results for the joint and separate effects.

20. Materials and Methods

Changes of the biosphere are quantified using the Γ metric of biogeochemical and vegetation-structural change (Heyder et al. 2011). While Γ was originally designed to assess the risk of future CC to natural ecosystems, we extend it here to also analyse LULCC effects. The metric characterizes ecosystem states as vectors in a multidimensional state space where each dimension represents one exchange flux, pool or process variable (listed in Table V.1). The change between two states is then expressed as the length of the difference vector and the angle between state vectors (Heyder et al. 2011). Γ is formulated to evaluate four equally weighted components of change:

$$\Gamma = \Big(\Delta V \cdot S\left(\Delta V, \sigma_{\Delta V}\right) + c \cdot S\left(c, \sigma_c\right) + g \cdot S\left(g, \sigma_g\right) + b \cdot S(b, \sigma_b)\Big) / 4 \tag{V.1}$$

where ΔV characterizes changes in vegetation structure, c is the local change component, g is the global importance component, b is the ecosystem balance component, and $S\left(x, \sigma_x\right)$ is a change to variability ratio.

Table V.1.: Parameters in the Γ metric describing landscape states

Group	Individual parameters[a]
Carbon exchange fluxes	Net primary production, heterotrophic respiration *and harvest (from crops and grasslands)*, fire carbon emissions
Carbon stocks	Carbon contained in vegetation, sum of soils and litter
Water exchange fluxes	Transpiration, sum of soil evaporation and interception loss from vegetation canopies, runoff
Other system-internal processes	Fire frequency, soil water content *(upper 1 m, 3 layers)*
Vegetation structure	Composition of PFTs *and CFTs*

[a] Changes to original metric implementation marked in italics.

Vegetation changes in terms of major ecological strategies (herbaceous vs. woody, broadleaved vs. needleleaved, evergreen vs. deciduous) are expressed by ΔV, based on Sykes et al. (1999), but with modifications to accommodate PFTs in LPJmL (Ostberg et al. 2013a). For this study, we add a new attribute *naturalness* to distinguish between natural and managed ecosystems (see section D.1 in Appendix D).

Local change c quantifies biogeochemical changes relative to previously prevailing conditions at each location and therefore the magnitude of local landscape transformation. In contrast, g captures the contribution of local changes to global biogeochemistry, assuming that even moderate (relative) changes on the local scale may feed back to larger scales (global carbon cycle, atmospheric circulation patterns, downstream water availability). Ecosystem balance b is computed as the angle between state vectors and represents changes in the magnitude of biogeochemical properties relative to each other, which indicate alterations in the contributing dynamic processes and hence ecological functioning. S relates the change of each component $x \in (\Delta V, c, g, b)$ to its variability σ_x under reference conditions, reflecting the expectation that ecosystems are adapted to the range of year-to-year variability. All terms in Equation V.1 are scaled between 0 (no change) and 1 (very strong change) using sigmoid transformation functions as described in Heyder et al. (2011).

Each grid cell in the model represents a landscape unit characterized by homogeneous forcing conditions (climate, soil, CO_2). Unless stated otherwise, LULCC and CC effects are assessed at grid cell level even though land use change has a direct effect only on the cropland or managed grassland portion of the cell. Parameters in Table V.1 are averaged across natural and managed parts before quantification of the total landscape state which is then used to derive landscape change.

Previous studies of CC impacts on natural vegetation used thresholds of $0.1 < \Gamma < 0.3$ and $\Gamma > 0.3$ to denote risk of moderate and major ecosystem transformation, respectively (Heyder et al. 2011; Ostberg et al. 2013a; Warszawski et al. 2013). For example, moderate changes in the Γ metric are comparable to the difference between similar, yet distinct biomes under present climate, such as temperate coniferous and temperate broadleaved forests, whereas a boreal evergreen forest differs from temperate forests by a Γ of 0.3–0.4 and a shift from a temperate forest to a savanna would result in Γ of ≈0.4–0.6 (see Figure B.2 in Appendix B). None of these studies considered human land use. Quantified

at the landscape scale, LULCC impacts scale with both the magnitude of change on the managed land and the fraction of the grid cell transformed.

20.1. Model description

The LPJmL DGVM simulates natural vegetation, represented by 9 plant functional types (PFTs) (Sitch et al. 2003), as well as agriculture, represented by 13 crop functional types (CFTs) and managed grasslands (Bondeau et al. 2007). The current model version includes a permafrost module and a new hydrology scheme (Schaphoff et al. 2013).

PFT composition within a grid cell is the result of competition between plant types for light, space and water. Establishment depends on climatic suitability and the density of the existing vegetation. Mortality rates depend on growth efficiency, plant density and climatic stress. For fire disturbance, daily fire probability is calculated based on fuel load and litter moisture, the annual burnt area fraction is derived from the length of the fire season, whereas the fraction of killed individuals within burnt areas depends on PFT-specific fire resistance (Thonicke et al. 2001).

Crops and managed grasslands are grown on prescribed areas, and irrigation is possible on areas equipped for irrigation (section 20.2). Irrigation water demand is determined from the soil water deficit below optimal growth (Rost et al. 2008b). We assume that irrigation water withdrawal equals demand and is not limited by the local renewable water resource. Sowing dates for annual crops are computed within the model based on a set of rules depending on crop- and climate-specific characteristics (Waha et al. 2012). Crops are harvested when they reach maturity, which is defined as a crop-specific phenological heat unit sum, at which point carbon from the storage organ pool is extracted. For annual crops, extensive grass growth is simulated outside the growing period as a proxy for inter-cropping practices. Managed grasslands are harvested whenever the above-ground carbon pool reaches a threshold, at which point 50% are extracted.

Plant growth of both natural vegetation and crops in LPJmL is constrained by temperature, radiation, water and CO_2 availability. Nutrients such as nitrogen and phosphorus are not explicitly modelled.

The model setup for this study assumes good management of crops everywhere instead of applying different management intensities per crop and country, which are not well-documented historically. Although management has an impact on Γ, we found its effect to be minor compared to the first-order effect of changing natural vegetation to cropland/managed grassland (see section D.2 and Figure D.1 in Appendix D).

The model runs on a spatial grid of 0.5° longitude by 0.5° latitude and a daily time step. It is driven by monthly temperature, precipitation, cloud cover and number of wet days (section 20.3) which are disaggregated according to Gerten et al. (2004). Additional inputs include information on soil properties, country-specific irrigation efficiencies (Rohwer et al. 2007), and annual atmospheric CO_2 concentrations (section 20.3).

Individual processes in LPJmL have been validated extensively before, e.g. Sitch et al. (2003, 2008) for carbon cycling and plant geography of the natural vegetation, Bondeau et al. (2007) and Fader et al. (2010) for crop production, Rost et al. (2008b) for irrigation water use and Schaphoff et al. (2013) for permafrost, river flow, carbon and water fluxes. LPJmL participates in model intercomparison projects, such as AgMIP (`http://www.agmip.org`), ISI-MIP (`http://www.isi-mip.org`), and the already finished WaterMIP (`http://www.eu-watch.org/watermip`).

20.2. Land use data

Annual fractions of 13 CFTs (12 distinct types and one mixed class of other annual and perennial crops) and managed grasslands in each 0.5° grid cell are prescribed with a distinction between irrigated and rain-fed areas. Data for the year 2000 are taken from the MIRCA2000 dataset (Portmann et al. 2010) and are extrapolated historically to the year 1700 based on the relative changes of cropland and pasture extent from the HYDE3 database (Klein Goldewijk and van Drecht 2006). The temporal evolution of irrigated areas is estimated from global trends (Hoekstra 1998). Compared to the documentation in Fader et al. (2010) the current dataset version has been extended to include sugarcane as a separate CFT. Areas not covered by managed lands are assumed to be covered with natural vegetation or barren, as dynamically simulated by LPJmL.

In the context of this study, LULCC refers to the conversion and use of land as cropland or managed grassland. Other forms of land use such as forest management are not considered.

20.3. Climate data

We use observation-based monthly temperature and cloud cover time-series provided by the Climatic Research Unit (CRU TS version 3.21) and spanning 1901–2012 (University of East Anglia Climatic Research Unit (CRU) et al. 2013; Harris et al. 2014). These are combined with gridded precipitation provided by the Global Precipitation Climatology Centre (GPCC Full Data Reanalysis Version 6.0), spanning 1901–2010 (Schneider et al. 2011; Becker et al. 2013), which is extended to cover the full CRU land mask. The corresponding number of wet days per month, used to distribute monthly precipitation sums, is derived synthetically using the CRU approach (New et al. 2000; Heinke et al. 2013).

We use early 20th century (1901–1930) observations before 1900. Since detection and attribution studies have identified human activities as the dominant driver of observed climate changes during the second half of the 20th century (IPCC 2013b), early 20th century is a suitable reference to calculate climate-driven changes. For this, the first 30 years of observation-based data are randomly reshuffled into a new sequence spanning 1700–1900. Since reshuffling may change some properties of the original statistical distribution, we produce 20 different realizations and run simulations for all of them. Atmospheric CO_2 concentrations are based on merged ice-core record data for 1830 to 1958, provided by Scripps Institution of Oceanography (http://scrippsco2.ucsd.edu/data/atmospheric_co2.html, Keeling et al. 2001), and on direct observations from the Mauna Loa Observatory after 1958, provided by NOAA/ESRL (http://www.esrl.noaa.gov/gmd/ccgg/trends/, both datasets as of 31 March 2014). A constant concentration of 282 ppm is used before 1830. No distinction between anthropogenic and natural contributions to CC is made in the analysis of impacts.

Table V.2.: Scenario setup. Each scenario is simulated with 20 different climate realizations as described in section 20.3.

Name	Description
PNV_{noCC}	Control scenario without any human impact, potential natural vegetation only, constant climate at 1901–1930 level and CO_2 at 282 ppm; reference run for full impact
PNV_{CC}	Scenario without land use (potential natural vegetation only), but with transient climate and CO_2; reference run for land use change effect
LUC_{noCC}	Scenario with transient land use, but with constant climate at 1901–1930 level and CO_2 at 282 ppm; reference run for climate change effect
LUC_{CC}	Representation of actual, transient land use, climate and CO_2; comparison with reference runs gives full impact, land use change effect, climate change effect

20.4. Simulation setup

LPJmL simulations require a spin up of 5000 years for vegetation and soil carbon pools to reach an equilibrium state. Spin up is performed for potential natural vegetation (PNV) without any land use, but with fire disturbance and dynamic vegetation, recycling the 200-year climate sequence and constant CO_2 concentration described above. We run four scenarios from 1700–2010, as described in Table V.2. The LUC scenarios are preceded by another 100 years of spin up using the land use pattern from 1700 to adjust carbon stocks from the PNV spin up and train sowing dates, which are based on climate experienced in the past. All four scenarios are simulated for each of the 20 climate realizations. LUC_{CC} and PNV_{CC} runs use transient atmospheric CO_2 from 1830 and transient CRU/GPCC climate data from 1901. In contrast, LUC_{noCC} and PNV_{noCC} runs use a constant CO_2 concentration of 282 ppm and continue using the reshuffled constant climate sequence after 1900. The difference between the various simulations allows us to separate the individual effects of LULCC and CC (cf. Table V.2).

Landscape states for the Γ metric are compared using 30 year averages of the state variables to avoid noise from inter-annual variability. We derive the full impact of human land use and CC (we include increasing CO_2 in the latter) on landscapes by comparing

the LUC_{CC} (real world) scenario to the PNV_{noCC} control scenario. The difference between LUC_{CC} and LUC_{noCC} gives the CC effect, while a comparison between LUC_{CC} and PNV_{CC} provides an estimate of the land use change effect (Table V.2). Time series of these effects are derived from concurrent time frames of the respective scenarios. Global and biome aggregates are calculated as area-weighted means of the grid cell values.

Γ values for the separated effects do not necessarily add up to the full impact value. This is due to possibly opposing impacts of climate and LULCC. Only the full impact is based on constant reference conditions (PNV_{noCC}, Table V.2), whereas reference conditions for the CC effect (LUC_{noCC}) and land use change effect (PNV_{CC}) are themselves impacted by land use and CC, respectively.

21. Results and Discussion

21.1. Global development

By the beginning of the 21st century, humans have transformed almost 30% of the global ice-free land area for agricultural production, replacing the original natural ecosystems. Quantifying Γ separately on the cultivated areas, more than 90% of croplands and pastures, corresponding to 26% of the global land area, have experienced major biogeochemical and structural shifts ($\Gamma > 0.3$), with moderate changes ($0.1 < \Gamma < 0.3$) on the rest (Figure V.1a). These changes were driven mainly by LULCC, but also include CC impacts on cultivated lands. Natural ecosystems covering an additional 26% of the land surface have experienced major or at least moderate climate-driven changes (Figure V.1a).

The majority of landscapes contain a mixture of natural and agricultural ecosystems. Within landscapes, effects of land use may be partially offset by CC and vice versa. For example, forest clearing reduces carbon stocks on the cultivated fraction, but enhanced productivity through warming or CO_2 fertilisation may increase carbon stocks in the

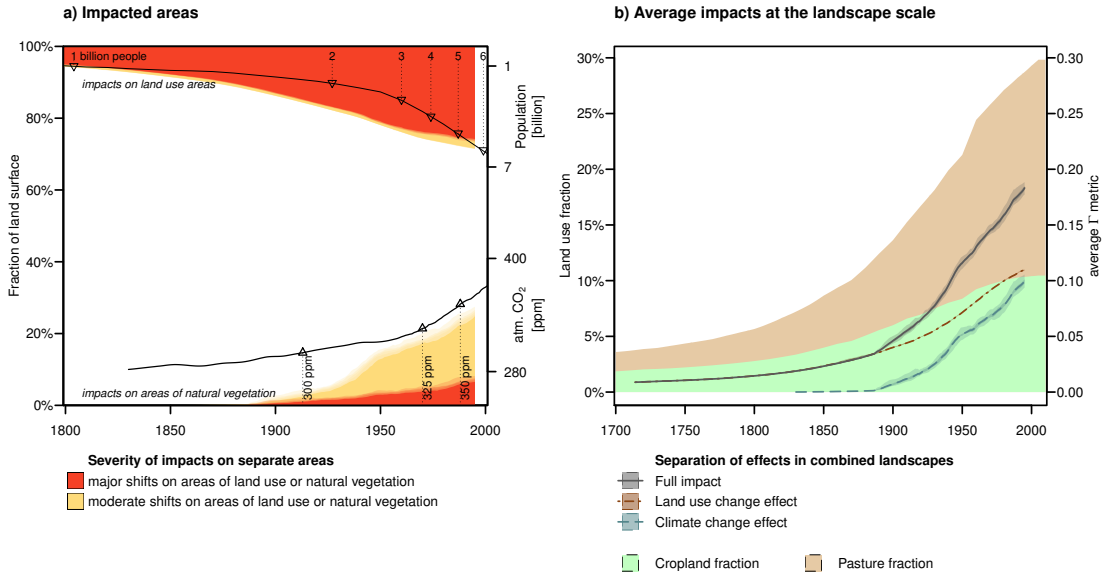

Figure V.1.: Transformation of natural ecosystems through land use and climate change. (a) Impacts on land use areas shown from above, impacts on remaining natural ecosystems shown from below. Remaining white area represents natural vegetation with only minor climate change impacts. World population and atmospheric CO_2 concentration added for illustrative purposes. (b) Average impacts (full, LULCC, CC) quantified at the landscape scale. Lines and coloured shading depict ensemble mean and ensemble range, respectively. Background shading shows land use fraction.

remaining natural vegetation. The full impact within these landscapes is therefore the combined effect of LULCC and CC. As a global average, LULCC and CC together have transformed landscapes worldwide by a value of $\Gamma = 0.18$ (full impact, Figure V.1b). This includes major impacts in 24% in addition to moderate changes in 31% of all landscapes (Table V.3, Figure V.2b).

Our simulation setup allows us to separate the LULCC effect from the CC effect within landscapes / grid cells where they co-occur. During the time frame of our analysis, total agricultural area has expanded from roughly 500 Mha to almost 4300 Mha. Compared to the PNV_{CC} world, land use change has caused an average impact on landscapes of $\Gamma = 0.009$ during 1700-1729 and $\Gamma = 0.11$ today in the LUC_{CC} simulations (Figure V.1b).

In parallel, atmospheric CO_2 concentration has risen from 282 ppm in 1830 to 390 ppm in 2010, and long-term annual mean temperature on land (computed as an area-weighted

Table V.3.: Global impacts and affected areas quantified at the landscape scale. Values provided for two 30-year time slices centred on 1915 and 1995, as in Figure V.2.

Impact	1901–1930	1981–2010
Full impact		
Global average Γ	0.06	0.18
Fraction of land area with:		
$0.1 < \Gamma < 0.3$	12%	31%
$\Gamma > 0.3$	6%	24%
Land use change effect		
Global average Γ	0.05	0.11
Fraction of land area with:		
$0.1 < \Gamma < 0.3$	10%	16%
$\Gamma > 0.3$	5%	15%
LUC effect dominant	44%	40%
Climate change effect		
Global average Γ	0.01	0.1
Fraction of land area with:		
$0.1 < \Gamma < 0.3$	2%	23%
$\Gamma > 0.3$	2%	10%
CC effect dominant	56%	60%
of which free of agriculture	62%	53%

30-year mean across all simulated grid cells) has risen by almost 0.8 K within 80 years. This has resulted in an average change of $\Gamma = 0.1$ today (Figure V.1b).

Hence, LULCC and CC have reached the same level, although marked differences underlie the global aggregate impact.

CC is currently the dominating effect on 60% of the land surface (Table V.3, Figure V.2f).

Half of this area is virtually agriculture-free (< 1% of grid-cell area used), while the other half contains on average 27% managed lands. In the remaining 40% of landscapes (of which on average 52% are used as cropland or pasture), the LULCC effect exceeds the CC effect (Table V.3, Figure V.2d). At the beginning of the 20th century (1901–1930), the share between landscapes with dominant climate or land use change effects was similar (56% and 44% of the land surface, Table V.3), but average impacts were one order of magnitude smaller for climate and less than half for land use.

It is worth noting that in the vast majority of landscapes the dominant effect is at least 5 times as strong as the secondary effect. There are very few landscapes where climate and land use effects are of similar magnitude. Examples include some boreal and tropical forests with minor CC impacts and low fractions of land use, or some Chinese steppe regions with mostly moderate CC and moderate to major LULCC impacts (Figure V.2b, d and f).

21.2. Historical evolution of LULCC impacts

Although humanity has practiced agriculture at least since the early Holocene (Kirch 2005), almost 90% of the current cropland and managed grassland extent have been converted within the last 300 years. In 1700, almost 60% of all landscapes were still virtually free of agriculture (< 1% of their area transformed), and in most other landscapes land use density was low (98% of all landscapes with < 25% use, Figure D.2 in Appendix D). Regions with higher land use density were limited to Western and Central Europe and parts of China. Major change at the landscape scale (land use change effect, $\Gamma > 0.3$) was limited to < 1% of the land surface, mostly in Ireland and France, but also along the Nile river in Egypt and in some parts of Pakistan, while land use caused only minor changes ($\Gamma < 0.1$) in the majority of landscapes.

By 1800, areas with major land use impacts had expanded to Northern India and parts of Western China, but still encompassed only 1.2% of the land surface. Although half of all landscapes were already partly cultivated, land use density was low in most of them, causing only minor impacts.

Land use expansion accelerated during the 19th century, and by 1900 5% of all landscapes were dominated by land use (> 50% of their area transformed), while a quarter of all

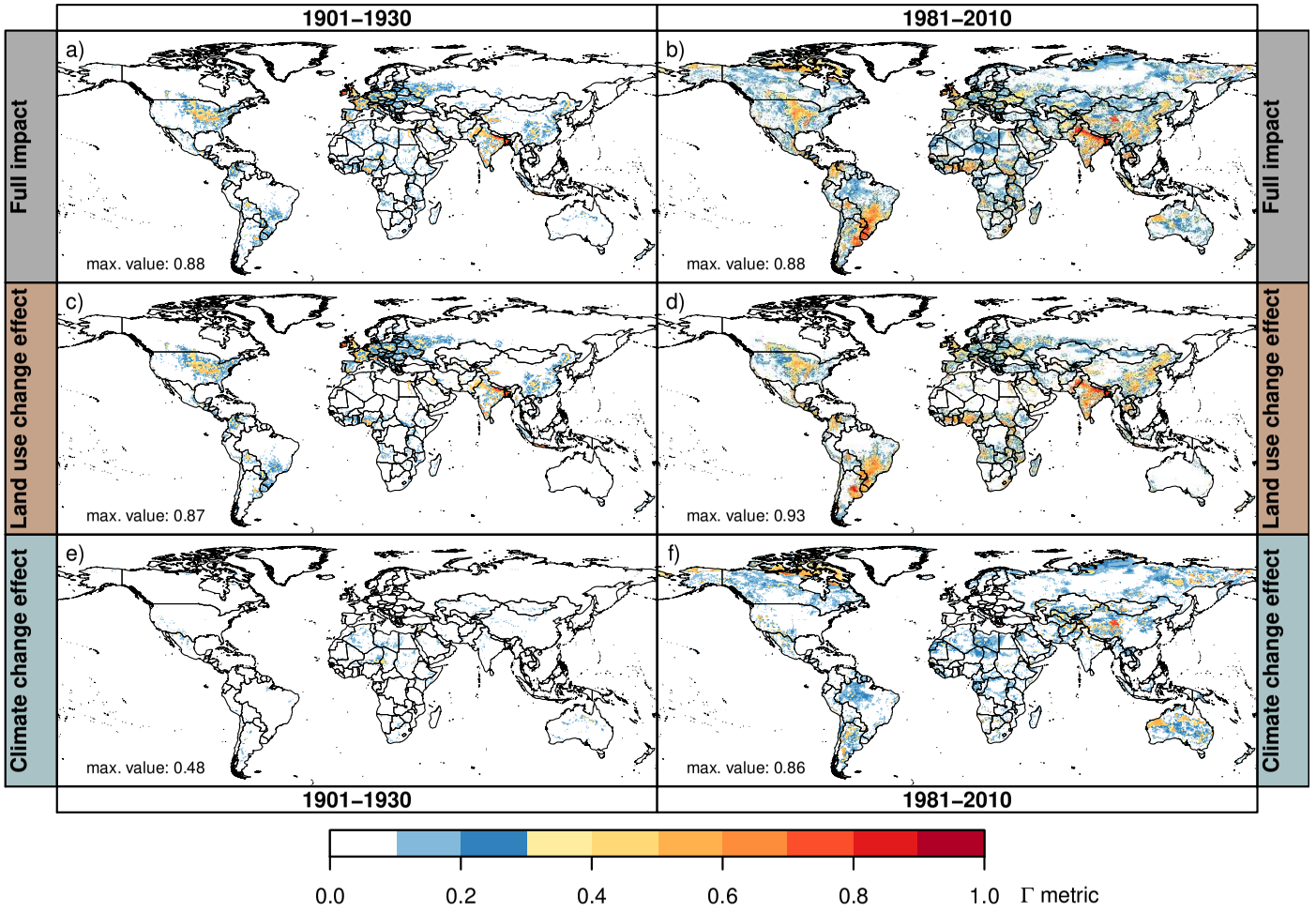

Figure V.2.: Spatial patterns of impacts on the biosphere. Full impact (a), (b), land use change effect (c), (d) and climate change effect (e), (f) shown for two 30-year time slices centred on 1915 and 1995 (left and right, respectively). All effects quantified at the landscape (i.e. grid cell) scale. Maps depict ensemble mean from 20 climate realizations.

landscapes contained at least 25% land use. This caused at least moderate changes ($\Gamma > 0.1$) in 13% of all landscapes. Agriculture had also expanded into new regions, especially North America, with now only about one third of global landscapes left agriculture-free. However, croplands and managed grasslands had still only achieved roughly half of their present-day global extent.

During the 20th century, agricultural expansion mainly took place in landscapes that already contained some portion of land use. The share of landscapes with more than 25% croplands and pastures doubled, and the share of landscapes with more than 50% use increased six-fold. This is reflected in the here studied LULCC effect: while the global average Γ increased from 0.04 to 0.11, the fraction of landscapes with major change ($\Gamma > 0.3$) almost quadrupled from 4 to 15%. Today, only one third of all landscapes can still be considered free of agriculture ($< 1\%$ of their area transformed), while almost as many landscapes are now dominated by managed lands ($> 50\%$ of their area transformed, Figure D.2 in Appendix D).

As with any historical reconstruction, a caveat of the HYDE database used here is that it has considerable uncertainties based on input data (primarily population data) and assumptions and parameters (primarily change in land use per capita over time) used in its construction (Ellis et al. 2013; Klein Goldewijk and Verburg 2013). For example, based on a scenario of adaptive changes in land use systems, the KK10 model (Kaplan et al. 2010) produces consistently higher levels of pre-industrial land cover change, and roughly twice as much land use change in 1850 as HYDE. However, both reconstructions converge towards the present. Naturally, the uncertainty of historical LULCC patterns translates into the evolution of the here studied LULCC effect. Given their convergence, our results for the second half of the 20th century and the comparison with recent CC impacts should remain relatively unaffected by the choice of land use reconstruction.

21.3. Biome-level changes

At present, temperate broadleaved deciduous and evergreen forests show the highest full impact with values of $\Gamma = 0.39$ and $\Gamma = 0.30$, respectively (Figure V.3). Land use change is the main driver of Γ in temperate forests, where the average LULCC effect is roughly 4–9 times higher than the CC effect. The impact of land use decreases from temperate

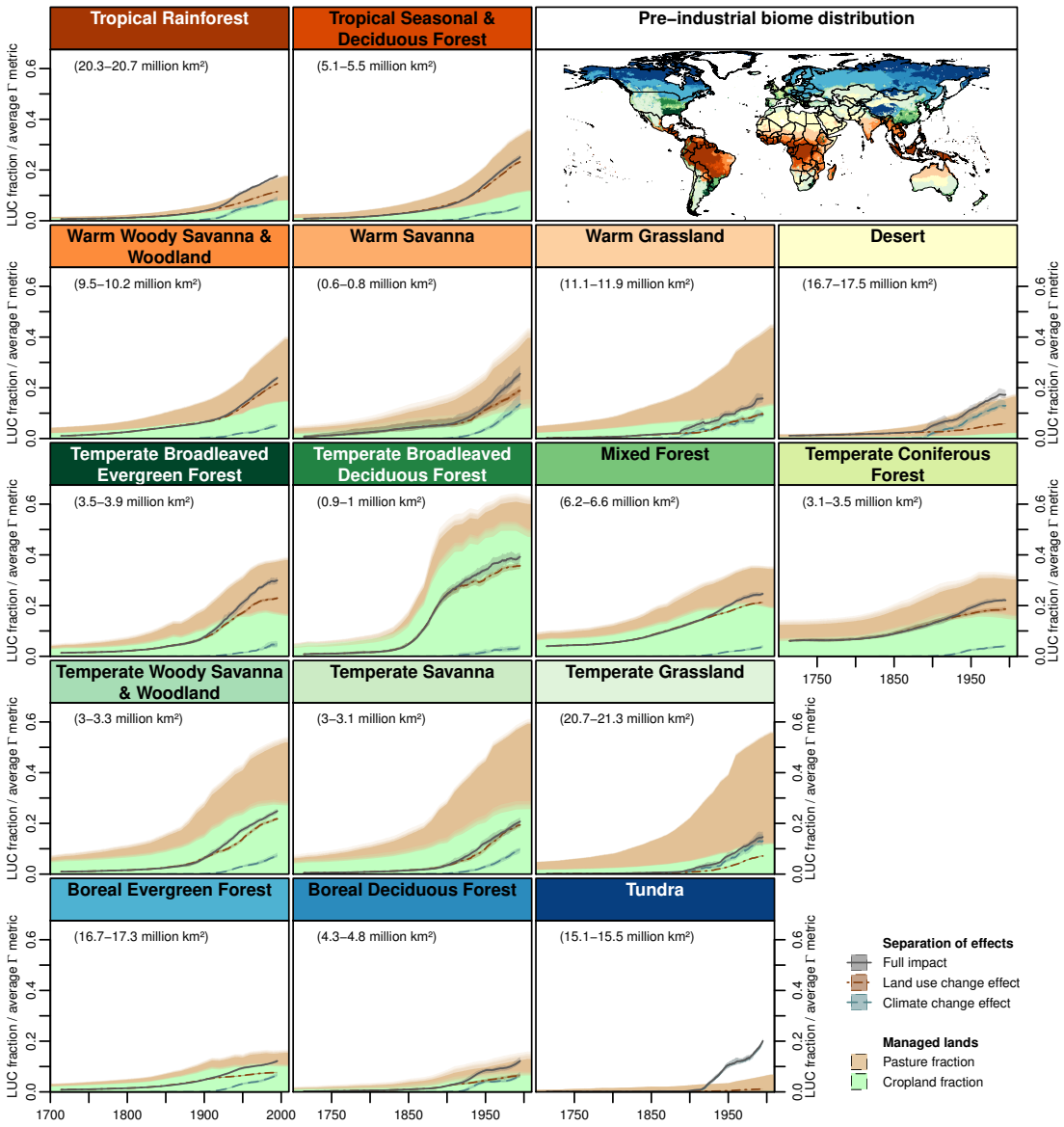

Figure V.3.: Impact of land use and climate change across biomes. Separate and combined effects at the landscape scale. Map shows potential natural biome distribution under pre-industrial conditions (dominant class from climate ensemble), and numbers in brackets denote ensemble range of biome areas without any land use.

forests to savannas to grasslands, the latter having a land use change effect of only $\Gamma = 0.07$ despite 54% of their area being used predominantly as managed grasslands. On the other hand, there is a sharp increase of the CC effect along this gradient, with

forests experiencing an average Γ of 0.04–0.05 compared to $\Gamma = 0.13$ in grasslands.

In the tropics, the average CC effect is almost equal between tropical rainforests and warm grasslands ($\Gamma = 0.09$), with slightly lower impacts in warm woody savannas and tropical seasonal forests and considerably higher impacts ($\Gamma = 0.14$) in open savannas. In terms of the LULCC effect, there is a similar increasing trend from warm grasslands to savannas to tropical seasonal forests as in the temperate zone. Tropical rainforests have less than half as much land use share as the other tropical biomes, resulting in a lower land use $\Gamma = 0.12$ (Figure V.3).

Averaged across the whole biome, LULCC and CC effects are at an equal level in boreal forests. Climate impacts are higher than in other forests (except tropical rainforests), but land use effects are low given that only 14–16% of their potential natural extent have been converted to croplands and pastures. Overall, boreal forests have the lowest average full impact of all biomes with $\Gamma = 0.12$. While tundra regions have the lowest land use share with only 6% of their pre-industrial extent, they have been exposed to the strongest CC impacts, with an average CC effect of $\Gamma = 0.2$ (Figure V.3).

Figure D.3 and section D.3 in Appendix D illustrate the different ways in which LULCC and CC affect the components that constitute Γ in each biome.

Comparing the temperate and tropical zone illustrates that the land use change effect depends not only on the fraction of the landscape that is transformed, but also on the type of natural ecosystem that is replaced. Extensive grazing on many semiarid grasslands, e.g. in Australia and Central Asia, causes relatively small biogeochemical and structural change despite large managed land shares (Figure V.2c and d, Figure D.4 in Appendix D). On average, Γ values increase with increasing woody vegetation cover, which is why high fractions of land use usually cause lower land use impacts in a grassland or savanna than in a forest landscape. In addition to vegetation structure, grasslands and savannas also differ from forests in regard to their contribution to the global carbon and water cycles, reflected by the global importance component of Γ (Figure D.3 in Appendix D). Differences in global importance also explain why similar land use fractions usually cause higher impacts in tropical than in temperate landscapes (Figure V.3, Figure D.3 in Appendix D).

Table V.4 provides lower thresholds of managed land fractions that we have found to cause moderate and major LULCC impacts in each biome today. Numbers represent the

5% quantile of all managed land fractions encountered in grid cells of the biome that result in the respective level of change during the time-frame 1981–2010. On the one hand, these numbers serve to illustrate the different extent to which land use impacts various biomes discussed above. On the other hand, they may act as a guideline of the severity of impacts to expect in case of land expansion in landscapes that have little or no land use today. For forest biomes, our results show a risk of moderate LULCC impacts if the managed land fraction exceeds 15–28%, and of major impacts if more than 39–69% of the grid cell is used for agriculture. For savannas and grasslands, the threshold for (moderate) major change is (25–46%) 44–55% managed area. Besides the current land use fraction, climate conditions and land use history also affect the realized LULCC impact in a given landscape. In some regions, such as temperate grasslands, tundra and deserts, climate conditions seem to be a more reliable predictor of land use impacts than the managed land fraction.

21.4. Examples of CC impacts

Changes in vegetation greenness (e.g. Walker et al. 2012) and advances of the tree line (e.g. Lloyd 2005; MacDonald et al. 2008) have been observed in both the American and Eurasian tundra. We define any ecosystem with less than 60% tree cover and an annual mean temperature below −2 °C as tundra (see Figure D.5 in Appendix D) and find that almost 60% of the modelled pre-industrial tundra area is exposed to at least moderate climate-driven changes, with 24% exposed to major shifts, mostly in treeless regions (Figure V.2f, Figure D.6 in Appendix D). Along the boreal-tundra ecotone, infilling of sparse tree populations has transformed about one fifth of the tundra into boreal forest (> 60% tree cover). Lacking a seed dispersal model, tree establishment in LPJmL is constrained by climatic suitability, not seed availability. Over the course of 100 years, our arctic tree line has shifted by 0 to 2 grid cells (at 0.5° spatial resolution) and fits well to available maps (Figure D.7 in Appendix D).

Many regions in northern and central Australia have experienced an increase of long-term mean precipitation while the South has generally gotten drier (Jones et al. 2009b). Based on our simulations, wetter conditions combined with the effects of increasing CO_2 concentrations have boosted vegetation productivity over large semiarid and arid areas by a factor of 2 to more than 5, with long-term impacts also on carbon stocks. Plant

Table V.4.: Lower thresholds of managed land fraction leading to moderate ($0.1 < \Gamma < 0.3$) or major ($\Gamma > 0.3$) LULCC impacts in each biome.

Biome	**Land use 1981-2010**	
Impact	moderate	major
Tropical Rainforest	17%	39%
Tropical Seasonal Deciduous Forest	20%	42%
Warm Woody Savanna Woodland	25%	44%
Warm Savanna	30%	48%
Warm Grassland	35%	45%
Temperate Broadleaved Evergreen Forest	24%	47%
Temperate Broadleaved Deciduous Forest	28%	61%
Mixed Forest	19%	44%
Temperate Coniferous Forest	15%	47%
Temperate Woody Savanna & Woodland	31%	55%
Temperate Savanna	39%	47%
Temperate Grassland	46%	46%
Boreal Evergreen Forest	20%	54%
Boreal Deciduous Forest	28%	69%
Tundra	6%	–*
Desert	1%	2%

* Values are only provided for biomes with at least 1% of their landscapes affected by moderate or major LULCC impacts.

transpiration has increased with a similar pattern and rate as NPP, whereas changes to evaporation, interception and runoff have been smaller or even showed an opposite sign. Increased fuel load has also increased risk of wildfire in our simulations, especially in more productive grasslands and savannas. Both our model results and observations suggest an expansion of forests into tropical savannas (Brook and Bowman 2006). All of these changes are combined in the Γ metric, leading to major or at least moderate CC effects over much of Australia. Note that many of the affected regions have high

fractions of human land use, so other effects such as grazing intensity and prescribed burning practices that are not represented in our model may interfere with the climate signal (Fensham et al. 2005). These model limitations may also contribute to the very low simulated land use change effect, i.e. why managed lands in much of Australia are biogeochemically very similar to PNV conditions.

We do not explicitly account for impacts of land use change on the climate system. Since our PNV_{CC} and LUC_{CC} simulations use the same observation-based climate data after 1900, we cannot distinguish between LULCC, other anthropogenic and natural forcing on climate. The use of a constant reference climate before 1900 obscures any effect LULCC has had on climate before the onset of modern-day global warming. At the global scale, deforestation has a warming effect through CO_2 emissions, a cooling effect through changes in albedo, and additional effects (both warming and cooling) through reduced emissions of biogenic volatile organic compounds that control other climate pollutants (Unger 2014). Because of additional non-radiative impacts of LULCC, especially through changes to the hydrological cycle, the overall impact of LULCC on global temperatures is unclear, with a likely dominance of the cooling effect in the high latitudes and warming in the tropics and even more complex impacts on precipitation patterns (IPCC 2013b).

22. Conclusion

We have quantified human intervention with the terrestrial biosphere through both climate and land use change in a consistent way across the globe and over time. The Γ metric brings together quantitative changes in a high number of system-dynamical parameters, that were previously studied only separately, and allows for the first time to compare the relative strength of these two pressures despite considerable differences in the mechanisms, affected processes and spatial patterns. We have shown that LULCC and CC have now reached a similar level at the global scale, causing average impacts of $\Gamma = 0.11$ and $\Gamma = 0.1$, respectively. In their interaction at the landscape scale, both effects have jointly exposed 55% of the global land surface to at least moderate

biogeochemical and vegetation-structural changes of a magnitude comparable to the difference between distinct biomes. CC is the dominant driver of biospheric change on 60% of the land surface. While LULCC is not as widespread as CC, with roughly one third of all landscapes still free of any land use, it has exposed 1.5 times as many landscapes to major impacts as CC.

Land use intensification and industrialization during the 20th century have allowed a rapidly growing world population to shift to a richer diet while per capita demand for arable land has stabilized or even declined (Ellis et al. 2013). The future development of land use and its impacts will strongly depend on how much of the anticipated increase in demand for food, feed, fuel and fibre can be met through intensification on existing lands versus expansion of cultivated areas (Foley et al. 2011; Tilman et al. 2011; Johnson et al. 2014). Most land use scenarios project an expansion of cropland which is taken to varying degrees from existing managed grassland or conversion of natural vegetation (van Vuuren et al. 2011a). These choices would result in very different biogeochemical impacts, especially in case of tropical deforestation.

Also, even if the target of limiting global warming to at most 2 K above pre-industrial conditions were met, this would still translate to more than double the warming ecosystems have been exposed to during the 20th century, along with the associated elevated CO_2 concentration and changes in precipitation. In case of continued emissions growth, even 6 K of warming until 2100 seem likely (Rogelj et al. 2012), putting the majority of ecosystems at risk of major climate-driven transformation (as studied using our Γ metric by Ostberg et al. 2013a; Warszawski et al. 2013).

The combined impact of possible future changes in land use and climate on landscapes remains to be studied. Our results highlight the importance of considering both drivers in impact assessments, given their comparative magnitude and the potential need for trade-offs in limiting one or the other. For example, land-based climate mitigation measures such as large-scale biomass plantations to substitute fossil fuels, which are often considered crucial to achieving low climate stabilization targets (Rose et al. 2013), need to be carefully designed to avoid just substituting climate impacts with land use impacts. Overall, the dual pressures of anthropogenic land use expansion and CC have launched a process of global-scale transformation of the Earth's land surface that is accelerating. The mounting shifts in biogeochemical properties of terrestrial landscapes

found in our study are likely an indication of developing larger systemic shifts in the Earth system as a whole.

Supplementary material related to this part is available in Appendix D.

Acknowledgements

This study was supported by GLUES (Global Assessment of Land Use Dynamics, Greenhouse Gas Emissions and Ecosystem Services), a scientific coordination and synthesis project of the German Federal Ministry of Education and Research's (BMBF's) 'Sustainable Land Management' programme (Code01LL0901A).

Part VI.

The biosphere under potential Paris outcomes [1]

Sebastian Ostberg, Lena R. Boysen, Sibyll Schaphoff, Wolfgang Lucht, and Dieter Gerten

[1] A revised version of this part has been published under the Creative Commons Attribution-NonCommercial-NoDerivatives 4.0 License as S. Ostberg et al. 2018. 'The Biosphere Under Potential Paris Outcomes.' *Earth's Future* 6 (1): 23–39. doi:10.1002/2017EF000628

Abstract

Rapid economic and population growth over the last centuries have started to push Earth out of its Holocene state into the Anthropocene. In this new era, ecosystems across the globe face mounting dual pressure from human land use change (LUC) and climate change (CC). With the Paris Agreement, the international community has committed to holding global warming below 2 degrees Celsius above pre-industrial levels, yet current pledges by countries to reduce greenhouse gas emissions appear insufficient to achieve that goal. At the same time, the sustainable development goals strive to reduce inequalities between countries and provide sufficient food, feed and clean energy to a growing world population likely to reach more than 9 billion by 2050. Here, we present a macro-scale analysis of the projected impacts of both CC and LUC on the terrestrial biosphere over the 21st century using the Representative Concentration Pathways (RCPs) to illustrate possible trajectories following the Paris Agreement. We find that CC may cause major impacts in landscapes covering between 16 and 65% of the global ice-free land surface by the end of the century, depending on the success or failure of achieving the Paris goal. Accounting for LUC impacts in addition, this number increases to 38–80%. Thus, CC will likely replace LUC as the major driver of ecosystem change unless global warming can be limited to well below 2 degrees. We also find a substantial risk that impacts of agricultural expansion may offset some of the benefits of ambitious climate protection for ecosystems.

23. Introduction

With the Industrial Revolution, humans have emerged as a major driver of change in the Earth system, prompting the advent of the Anthropocene (Steffen et al. 2007). Today, 7.5 billion people rely on the biosphere to supply them with a multitude of essential ecosystem services (MEA 2005; UNPD 2015). For the purpose of food production alone, roughly 1500 Mha of land are used to grow crops, and twice as much grazing land feeds cattle, sheep and other livestock (FAO 2016). Three quarters of the land surface show signs of human alteration as they are either used directly or have become embedded within agricultural land or settlements (Ellis et al. 2010). Land use in combination with humanity's utilization of fossil fuels has released a total of 565 ± 55 Gt carbon into the atmosphere between 1870 and 2016 and has increased atmospheric CO_2 concentration from ≈278 parts per million (ppm) at the beginning of the industrial era (1750) to 403 ppm in 2016 (Joos and Spahni 2008; Le Quéré et al. 2016; Dlugokencky and Tans 2017). The resultant global warming has crossed 1 K above the 1880–1900 global annual average surface temperature in 2015 (Hansen et al. 2010; GISTEMP Team 2017), reaching the half point to the 2-degree limit set by the international community in the Paris Agreement (UNFCCC 2016). Taking the Paris Agreement into account, three outcomes for the 21st century can be imagined: (1) assuming a full success, global warming will be limited to well below 2 degrees Celsius (°C) above pre-industrial, (2) emissions will be reduced, but not enough to limit global warming to 2 degrees, (3) in case of a widespread failure of the Paris Agreement emissions continue to rise unabated.

Given that global population and its food demand is still on the rise, and taking into account the inertia of the climate system, pressure on the biosphere from land use change (LUC) and climate change (CC) is likely to increase over the course of the 21st century even in the best of these three cases. Furthermore, as pointed out by Rockström et al. (2016), negative greenhouse gas (GHG) emissions are a key requirement of most recent scenarios assessed by the Intergovernmental Panel on Climate Change (IPCC) that attempt to limit warming to below 2 °C (IPCC 2014d). Usually, these scenarios rely on bioenergy with carbon capture and storage (BECCS) to deliver a carbon sink in the order of magnitude of the global ocean sink (Rockström et al. 2016). As such, reducing one pressure on the biosphere (CC) may directly exacerbate the other (LUC).

Although impacts of CC and LUC on ecosystems have been documented for every continent and major biome, quantifying them in a comprehensive, consistent and comparable manner across the globe for both past and future changes still poses methodological challenges. Ellis and Ramankutty (2008) proposed to map the historical anthropogenic transformation of the biosphere by way of anthropogenic biomes or 'anthromes', recognizing that human impacts extend beyond the land used directly to create a number of seminatural systems. Changes in 21st century land cover driven by CC and LUC have been studied before for a subset of the Representative Concentration Pathways (RCPs) (Davies-Barnard et al. 2015; Boit et al. 2016). For our study, a more complex model-based indicator of human interference with the biosphere at the landscape level (Heyder et al. 2011; Ostberg et al. 2015) is used to estimate how much CC and LUC impact landscapes worldwide individually and in their interaction during the historical period (20th century) and for a set of CC and associated LUC scenarios representative of the three outlined Paris outcomes (21st century). The analysis compares the relative strength of CC and LUC effects and their joint impact on the terrestrial biosphere and highlights the consequences of different levels of CC mitigation. We further investigate whether trade-offs between CC and LUC impacts emerge in the scenarios based on different strategies of future land use. This study expands on the comparison of historical CC and LUC impacts on the biosphere presented in Ostberg et al. (2015).

Emissions reductions pledged by countries in order to achieve the 2-degree target, so-called 'Intended Nationally Determined Contributions' (INDCs), only cover the period up to 2030, so any assessment of long-term climate impacts is highly dependent on assumptions about how emissions develop thereafter. Preliminary analysis of the INDCs suggests that they will likely not be sufficient to limit warming to below 2 °C unless mitigation efforts are stepped up considerably after 2030 (e.g. Fawcett et al. 2015; UNFCCC 2015; Rogelj et al. 2016). While simple reduced-complexity climate models have been used to estimate global average temperature rise resulting from a range of INDC extensions (e.g. Climate Action Tracker, `http://www.climateactiontracker.org/`), these do not provide spatial patterns of temperature change or changes in other climate variables which are required for an impact assessment. For this study, we use climate projections produced by a large number of climate and Earth system models as part of the fifth phase of the Coupled Model Intercomparison Project (CMIP5, Taylor et al. 2012) and based on the RCPs (van Vuuren et al. 2011a). Although developed independently of the Paris process, RCP2.6 is used here to represent a 'Paris success'. RCP4.5 is used

as a proxy for an 'INDC+' world where mitigation efforts are increased somewhat over INDC levels, but not enough to safely stay within the 2-degree limit. RCP6.0 is used to represent an 'INDC' world where efforts after 2030 continue the 2020–2030 trends. These three scenarios lead to 1.6 ± 0.4 K (multi-model mean and standard deviation), 2.4 ± 0.5 K and 2.8 ± 0.5 K of global warming in 2081–2100 compared to 1850–1900, respectively (Collins et al. 2013). Lastly, RCP8.5 is used as a proxy for a 'Paris failure' scenario. Assuming continued high GHG emissions in the absence of effective mitigation, this pathway leads to 4.3 ± 0.7 K of global warming by the end of the century.
The RCPs are based on a set of Integrated Assessment Model (IAM) scenarios which also include scenarios of future land use consistent with the climate projections (Hurtt et al. 2011). For this study, each RCP CC scenario is combined with the respective LUC scenario (see section 24.3 below for a characterization of LUC forcing in each scenario).

For the quantification of terrestrial biospheric change, each landscape is treated as a point in a multidimensional state space that gets shifted from its reference conditions to a new state by CC and LUC (Heyder et al. 2011; Ostberg et al. 2015). In this context, a landscape is defined as a contiguous area of land which may feature both natural vegetation and managed land — similar to the anthrome concept — but is characterized by homogeneous weather conditions and represented by a grid cell in the model (see 'Methods' below). The distance between two positions in the state space describes the level of human interference with the biosphere in each landscape. The Γ metric used here combines changes in biogeochemical processes and vegetation structure to quantify changes in landscape states (see Table E.1 in Appendix E for the full list of parameters). These parameters serve as a proxy for several ecosystem services, such as food production (harvest), carbon sequestration (carbon stocks), and freshwater provisioning (runoff). Although they represent rather broad biogeochemical and structural properties, changes to these fundamental building blocks imply a risk of substantial, potentially self-amplifying transformations in the underlying, much more complex system characteristics, food chains and species composition, with possible implications for biodiversity (Heyder et al. 2011).
The Γ metric is a unit-less number scaled between 0 (no change) and 1 (very strong change, see Methods below). Following previous applications (e.g. Heyder et al. 2011; Ostberg et al. 2013a, 2015), $\Gamma < 0.1$ is considered a minor, values between 0.1 and 0.3 a moderate and $\Gamma > 0.3$ a major landscape change. For illustrative purposes, the difference

between present-day biomes generally adopts values of $\Gamma > 0.3$, such as a tropical rainforest changing into a tropical seasonal forest (∼0.30), a tropical savanna (∼0.5–0.7) or a grassland (∼0.85); or a boreal forest changing into a temperate forest (∼0.3–0.4) or a temperate savanna (∼0.5–0.6), whereas moderate changes may be compared in magnitude to the difference between similar biomes, such as a temperate coniferous forest and a temperate broadleaved forest (∼0.1–0.2) (Ostberg et al. 2013a). For LUC impacts, the magnitude of change depends on a number of factors such as the fraction of the grid cell that is transformed, the vegetation type that is replaced, and land use type and history, with major impacts ($\Gamma > 0.3$) calculated for landscapes where more than 40–60% of the area have been converted to land use (Ostberg et al. 2015).

24. Methods

The Γ metric of the risk of landscape-level biogeochemical change is used here to assess systematically the dual pressure from LUC and CC on the biosphere. It captures five dimensions of change (Heyder et al. 2011; Ostberg et al. 2015):

$$\Gamma = \Big(\Delta V \cdot S\left(\Delta V, \sigma_{\Delta V}\right) + c \cdot S\left(c, \sigma_c\right) + g \cdot S\left(g, \sigma_g\right) + b \cdot S(b, \sigma_b)\Big)/4 \qquad \text{(VI.1)}$$

ΔV quantifies the structural dissimilarity between two landscape states in terms of basic plant life forms (trees, grass or bare ground) and their attributes (modified after Sykes et al. 1999, see section E.1 in Appendix E). S, c, g and b are calculated in the multi-dimensional state space characterized by the biogeochemical properties in Table E.1 in Appendix E.

Local change c quantifies relative changes in biogeochemical stocks and fluxes compared to local reference conditions in each landscape, represented by a grid cell in the model (see below).

By comparing local changes to the global mean reference conditions, global importance g captures the varying contribution of each grid cell to global biogeochemical cycles, taking into account that even moderate (relative) changes on the local scale may feed

back to larger scales if large enough in absolute terms.
Ecosystem balance b, which is calculated as the angle between state vectors, quantifies shifts in the relative magnitude of biogeochemical properties with respect to each other as an indicator for qualitative changes in the balance of dynamic processes, which may signal a breakdown of ecological functioning.
S evaluates the change in each of the previous four components in comparison to its interannual variability σ under reference conditions, based on the assumption that ecosystems are adapted to the variability they are regularly exposed to but may be vulnerable if it is exceeded.
For more details about the vector geometry and the sigmoid transformation functions used to scale S, c and g between 0 and 1, see section E.2 in Appendix E and Heyder et al. (2011).

The LPJmL dynamic global vegetation model (DGVM) is used to simulate landscape states and their evolution through CC and LUC, providing all parameters in Table E.1 in Appendix E. LPJmL is well-established and has been extensively documented before so the following is only a short summary. The model simulates key ecosystem processes such as photosynthesis, plant and soil respiration, carbon allocation, evapotranspiration and phenology for natural vegetation represented by 9 plant-functional types (PFTs) (Sitch et al. 2003), agricultural production represented by 12 crop-functional types (CFTs) and managed grassland (Bondeau et al. 2007), as well as dedicated biomass plantations (for bioenergy) using 2 woody and 1 herbaceous biomass-functional types (BFTs) (Beringer et al. 2011). In each grid cell PFTs compete for light, space and water. Their establishment is constrained by climatic suitability and the density of the existing vegetation, whereas their mortality depends on climatic stress (i.e. heat), plant density and growth efficiency (Sitch et al. 2003). Fire disturbance in natural vegetation is simulated using the Glob-FIRM fire model (Thonicke et al. 2001), which estimates day-to-day fire probability based on litter moisture and the annual burned fraction of the grid cell based on the length of the fire season. The LPJmL model version used here includes a 5-layer soil hydrology and permafrost module (Schaphoff et al. 2013). CFTs, managed grassland and BFTs are grown on prescribed areas (see section on land use data below), with a distinction between rain-fed and irrigated agriculture. Irrigation is possible on prescribed areas equipped for irrigation, with water demand derived from the soil water deficit below optimal growth (Rost et al. 2008b). To provide a better representation of irrigation efficiency, i.e. the partitioning of water

withdrawn into beneficial consumption by the plant and conveyance and application losses, the model distinguishes three major irrigation systems (surface, sprinkler, drip) (Jägermeyr et al. 2015). Sowing dates for annual crops are computed internally based on a set of rules depending on crop- and climate-specific characteristics (Waha et al. 2012), and crops are harvested after reaching a crop-specific phenological heat unit sum. Crop residues are left on the field, and extensive grass growth is simulated outside the growing period of annual crops as a proxy for inter-cropping practices (Bondeau et al. 2007). Other aspects of crop management, fertilizer application or soil fertility management are not explicitly modeled. To account for non-climatic factors influencing agricultural intensities maximum leaf area index (LAI_{max}) of each CFT is calibrated to best match FAOSTAT national yields at the country level (Fader et al. 2010). Managed grassland is harvested monthly, with global harvest tuned to fulfil present-day global feed demand for livestock production and harvest fraction in each grid cell dependent on local productivity. Depending on the scenario, bioenergy plantations are either stocked with highly productive C4 grasses or broadleaved trees (representative of willow/poplar for the temperate zone and eucalyptus for the tropics). 85% of the leaf mass of bioenergy grasses is harvested once or several times a year when leaf carbon stocks reach $400\,g/m^2$, whereas bioenergy trees are managed as short-rotation coppice systems harvested every 8 years (Heck et al. 2016). The model runs at a daily time step and a spatial resolution of 0.5° by 0.5°. It is driven by monthly fields of cloud cover, precipitation and temperature which are disaggregated to daily values following Gerten et al. (2004).

24.1. Input data

Climate input is created from all climate models from the CMIP5 archive that provide all required variables for the historical period and all four RCP scenarios (20 models in total, `https://pcmdi.llnl.gov/projects/cmip5/`, accessed April 2014). In a first step, raw climate model output is interpolated to a 0.5° by 0.5° resolution by bilinear interpolation. Next, simulated time series of each variable are corrected for systematic errors in mean and variance applying a quantile mapping approach based on the method described in Watanabe et al. (2012). While the original approach was developed for the bias correction of time slices, the required statistics (mean and variance) are calculated for each time step applying a moving 31-year window. Obtained statistics are compared to climate

observations for the reference period 1970–2000 to derive correction offsets (temperature) and correction factors (cloud cover, precipitation, all variances). Observational reference data is taken from the Climatic Research Unit's time-series (CRU TS) 3.21 datasets (University of East Anglia Climatic Research Unit (CRU) et al. 2013; Harris et al. 2014) for temperature and cloud clover and from the Global Precipitation Climatology Centre's (GPCC) full data reanalysis version 6 (Schneider et al. 2011; Becker et al. 2013) for precipitation. Wet-day frequency, which is used by LPJmL to distribute monthly precipitation sums, is created synthetically following Heinke et al. (2013) since it is not provided directly by the climate models. Annual midyear atmospheric CO_2 concentrations for both the historical period and all four RCP scenarios are taken from the RCP database (`http://tntcat.iiasa.ac.at/RcpDb`, accessed April 2014).

Land use input is based on the land use harmonization (LUH) products created for CMIP5 (Hurtt et al. 2011, available at `http://luh.umd.edu/data.shtml`). The LUH dataset provides gridded annual fractions of total cropland (LUH variable g_{crop}) and managed grassland (g_{past}) at a spatial resolution of 0.5° by 0.5°, which have been harmonized to provide a smooth transition from the historical period (1700–2004) to each of the four RCP scenarios (2005–2100). In addition, LUH provides gridded information on biofuels (g_{biof}) in each scenario. LPJmL distinguishes 12 CFTs and an 'others' category containing the remaining cropland, and also separates rain-fed from irrigated cropland. To add this information to the LUH dataset, it is combined with the default LPJmL historical dataset (Fader et al. 2010), which is derived from a combination of crop-specific rain-fed and irrigated harvested areas (MIRCA2000, Portmann et al. 2010), historical trends in cropland and managed grassland (HYDE3, Klein Goldewijk and van Drecht 2006) and historical trends in irrigated areas (Hoekstra 1998). In case of inconsistencies between both historical datasets, managed grassland fractions are taken directly from g_{past}. For cropland, relative CFT shares in each grid cell of the LPJmL default dataset $\text{CFT}_{\text{LPJmL}}$ are rescaled proportionally to match total cropland from LUH g_{crop}:

$$\text{CFT}_{\text{LUH}} = \frac{\text{CFT}_{\text{LPJmL}}}{\text{cropland}_{\text{LPJmL}}} \cdot g_{\text{crop}} \tag{VI.2}$$

To preserve irrigated areas, changes are preferentially applied to the rain-fed cropland share. Grid cells missing in the LPJmL default dataset but containing cropland in LUH are filled using the country-average CFT mix from the LPJmL default dataset. For the four RCP scenarios, the present-day CFT mix in each grid cell remains constant and is rescaled proportionally to match future total cropland g_{crop} following Equation VI.2.

Irrigated cropland is scaled proportionally with total cropland since the RCP scenarios do not include information on irrigated land. Future managed grassland fractions g_{past} are taken directly from LUH.

Sub-regional information on the global distribution of irrigation systems is available neither for the historical period nor the future scenarios. Following the approach in Jägermeyr et al. (2015), country-level shares of irrigation systems from AQUASTAT (FAO 2014) are disaggregated to grid cells and CFTs through a decision tree approach, using the extent of irrigated areas by CFT and an irrigation system suitability table (full description in Jägermeyr et al. 2015).

The LUH biofuel information g_{biof} was not part of the original harmonization process, but was added to the LUH dataset at a later stage. For RCP2.6, RCP4.5 and RCP6.0 g_{biof} represents a land fraction that has to be subtracted from total cropland g_{crop}. CFT fractions are scaled down proportionally to make room for bioenergy. In cases where g_{biof} is larger than g_{crop} (because of the missing harmonization), preference is given to g_{biof}, which is then expanded into g_{past} and (if not sufficient) into natural vegetation. For RCP2.6 and RCP6.0 g_{biof} in each grid cell is split equally between bioenergy grass and bioenergy tree (short-rotation coppice) plantations, except for cells where climate conditions prohibit tree growth (see section E.3 in Appendix E for details). For RCP4.5 the LUH documentation specifies bioenergy crops to be herbaceous so g_{biof} is assigned completely to the bioenergy grass BFT in LPJmL. For RCP8.5 g_{biof} represents gridded harvested biomass amounts instead of land fractions. Bioenergy fractions in each grid cell g^*_{biof} are derived under the assumption that they are proportional to the bioenergy harvest share of total wood harvest:

$$g^*_{\text{biof}} = \frac{g_{\text{biof}}}{\text{harvest}_{\text{wood}}} \cdot \text{frac}_{\text{wood}} \tag{VI.3}$$

with $\text{harvest}_{\text{wood}}$ the sum of LUH variables g_{sbh1}, g_{sbh2}, g_{sbh3}, g_{vbh1}, and g_{vbh2} (wood harvested from different sources) and $\text{frac}_{\text{wood}}$ the sum of LUH variables g_{fsh1}, g_{fsh2}, g_{fsh3}, g_{fvh1}, and g_{fvh2} (land fractions corresponding to harvested biomass). Short-rotation coppice plantations are simulated on all RCP8.5 bioenergy land fractions, which reduce the area available for natural vegetation. No irrigation is applied to bioenergy plantations in any of the RCP scenarios to avoid competition with food production for available irrigation water. Grid cell fractions not covered by cropland, managed grassland, bioenergy plantations or water are simulated with natural vegetation.

Additional inputs to LPJmL include a flow direction map (STN-30, Vörösmarty et

al. 2000) and a database of the location and storage capacity of dams and reservoirs (GRanD, Lehner et al. 2011), both of which affect the routing of discharge through the river network (Rost et al. 2008b; Biemans et al. 2011), a gridded dataset of lake and river fractions based on the Global Lakes and Wetlands Database (GLWD, Lehner and Döll 2004) which affects the land area available in each grid cell. Soil data describing the thermal and hydraulic characteristics are taken from the Harmonized World Soil Database (version 1.2) (FAO et al. 2012) and classified according to the USDA soil texture classification (http://ufdc.ufl.edu/IR00003107/00001).

24.2. Simulation setup

To allow for the individual evaluation of CC and LUC effects as well as their combined impact on the biosphere, four parallel lines of simulations are conducted for each climate model (bottom-left schematic in Figure VI.1): PNV_{CC} and PNV_{noCC} simulations feature no land use, with all the ice-free land surface covered with potential natural vegetation (PNV). LUC_{CC} and LUC_{noCC} simulations include land use using historical and future scenario land use patterns described above. PNV_{noCC} and LUC_{noCC} simulations use a constant historical climate and a constant pre-industrial CO_2 concentration of 278 ppm until 2099. They provide the reference conditions for the full impact and climate change effect, respectively. PNV_{CC} and LUC_{CC} simulations use transient climate and transient atmospheric CO_2 concentrations. PNV_{CC} provides reference conditions for the land use change effect, whereas LUC_{CC} represents the real world which is compared to each of the three reference simulations. Land use scenarios start to diverge in 2005, but because of the 31-year moving window used in bias correction climate scenarios may start to diverge slightly from as early as 1991. All scenarios are run until 2099.

All simulations are preceded by 5000 years of spin up to allow vegetation and soil carbon pools to reach an equilibrium state. Spin up is performed for each GCM separately with dynamic vegetation and fire disturbance enabled, but without any land use. The first 30 years of 20th century climate are randomly sampled into a 200-year sequence, which is recycled repeatedly during spin up, together with a constant pre-industrial CO_2 concentration of 278 ppm. From there, LUC_{CC} and LUC_{noCC} simulations add another 100 years of land use spin up using year-1700 land use patterns to adjust carbon pools before using transient historical land use patterns from 1700 onwards.

LAI_{max} calibration of yields is performed on a decadal basis for five decades from 1961–2010 for which FAOSTAT national yield statistics are available (FAO 2016), using the observational climate datasets from bias correction to drive the model. Historical trends in agricultural intensity are derived by linear regression for each country and each CFT and are then extrapolated into the future with a maximum upper limit of $LAI_{max} = 7$. For countries with negative historical trends, these are reversed in the future. This procedure introduces some agricultural intensification in the future, but is not intended to reproduce productivity increases assumed in each of the original IAM scenarios the RCPs are based on. While management intensity has an impact on the Γ metric Ostberg et al. (2015) showed that its effect is minor compared to the first-order effect of changing natural vegetation into cropland/managed grassland.

Time series of Γ for each climate model are derived by comparing 30-year moving windows of LUC_{CC} simulations to concurrent windows in the three reference runs LUC_{noCC}, PNV_{CC} and PNV_{noCC}. ΔV, c, g, and b from Equation VI.1 are calculated from the window mean while S is estimated from the interannual variability within the 30-year window.

24.3. CC and LUC forcing in the RCPs

Radiative forcing in the RCP2.6 scenario used here to represent a *Paris success* peaks before mid-century and then declines to $2.6\,W/m^2$ by 2100. CO_2 emissions in the less ambitious *INDC+* and *INDC* scenarios peak roughly 20 (RCP4.5) and 40 years (RCP6.0) later than in the *Paris success* case, and radiative forcing stabilizes only after 2100 at 4.5 and $6\,W/m^2$, respectively (van Vuuren et al. 2011a). Out of the three scenarios, only RCP2.6 is likely to achieve the ultimate goal of the Paris Agreement of limiting global warming to below 2 °C (Collins et al. 2013). CO_2 emissions in the illustrative *Paris failure* (RCP 8.5) scenario keep rising throughout the 21st century, and radiative forcing reaches $8.5\,W/m^2$ in 2100, with a stabilization only after 2200. All four scenarios analysed in this study project an increase of global population combined with an increase in per capita food demand and feature an increasing contribution of biofuels to the global energy mix (van Vuuren et al. 2011a). Despite these similarities, their global land use area varies between roughly 3700 and more than 6000 Mha in 2100 (Table VI.1). Besides total area, the scenarios differ in terms of the relative share of cropland, managed

Table VI.1.: Global land area (Mha) covered by major types of managed lands in 2004 and in 2100 under 4 studied Paris outcomes. Bioenergy refers to dedicated second-generation biomass plantations.

Year/Scenario	Pasture	Cropland	Bioenergy	Total
2004	3334	1519	0	4853
Paris success (RCP 2.6)	3149	1869	441	5459
INDC+ (RCP 4.5)	2861	783	295	3939
INDC (RCP 6.0)	1766	1582	338	3686
Paris failure (RCP 8.5)	3702	1800	543	6045

grassland and bioenergy plantations and regarding the placement of land use (Figure E.1 in Appendix E). Total managed land expands by 606 Mha compared to 2004 under the *Paris success* (RCP2.6) scenario, due to a 23% increase of global cropland and the introduction of almost 450 Mha of dedicated biomass plantations for bioenergy production (corresponding to ∼30% of current cropland). While the *INDC+* and *INDC* scenarios represent an assumption of half-way success in climate mitigation both RCPs exhibit extreme success in reducing the concurrent land use pressure, leading to a net abandonment of 913 and 1166 Mha of managed land, respectively. Strong increases in crop productivity and efficiency of food production assumed in the underlying IAM scenario allow for a reduction of global cropland by 48% under *INDC+* (RCP4.5) (Thomson et al. 2011), whereas *INDC* (RCP6.0) reduces grazing-based livestock production, leading to a net abandonment of 47% of global pastures (Masui et al. 2011). In addition to the highest CC forcing, the *Paris failure* (RCP8.5) scenario also features the largest expansion of managed land of all four scenarios (Table VI.1). The RCPs cover a wide range of assumptions regarding future yield gains, intensification of livestock production and dietary shifts (van Vuuren et al. 2011a). The land use patterns resulting from these assumptions are assessed here in terms of their impact on the biosphere.

25. Results

At the end of the historical period (1976–2005 time slice), human interference with the terrestrial biosphere through the interaction of climate change (CC) and land use change (LUC) has already caused major impacts ($\Gamma > 0.3$) in landscapes covering 25–30% of the ice-free land surface (full impact in Figure VI.1, range across 20 climate models). Given that more than 75% of all landscapes worldwide contain some amount of managed land (Ellis et al. 2010, see also Figure E.1 in Appendix E) the full impact is usually a combination of CC and LUC-driven changes, but values of the individual effects are not necessarily additive: major CC and LUC effects can co-occur within the same landscape, but the full impact may also attain values of $\Gamma > 0.3$ in landscapes where both individual effects are below that threshold. Because of the complex way in which CC and LUC affect the individual parameters describing landscape states it is even possible for the full impact to be smaller than the individual effects. Globally, LUC is the main driver of change, responsible for major impacts on 18–19% of the land surface compared to 5–10% subject to major CC impacts (land use change effect and climate change effect in Figure VI.1, respectively).

25.1. Paris success

In case of a *Paris success* (RCP2.6) — which would limit global warming to below 2 °C above pre-industrial level — major CC effects are limited mostly to cold (tundra, boreal forests) and dry regions (deserts and grasslands, Figure VI.2). They are still projected for 22% (16–27% model range) of the global land surface by 2070–2099 (climate change effect, Figure VI.1), which represents a 2 to 5 fold increase over the historical period. Even in this low warming scenario, tundra ecosystems may lose more than half of their pre-industrial extent (Figure VI.3). Boreal forests are simulated to expand into the tundra, while on the other hand tree composition shifts towards temperate species along

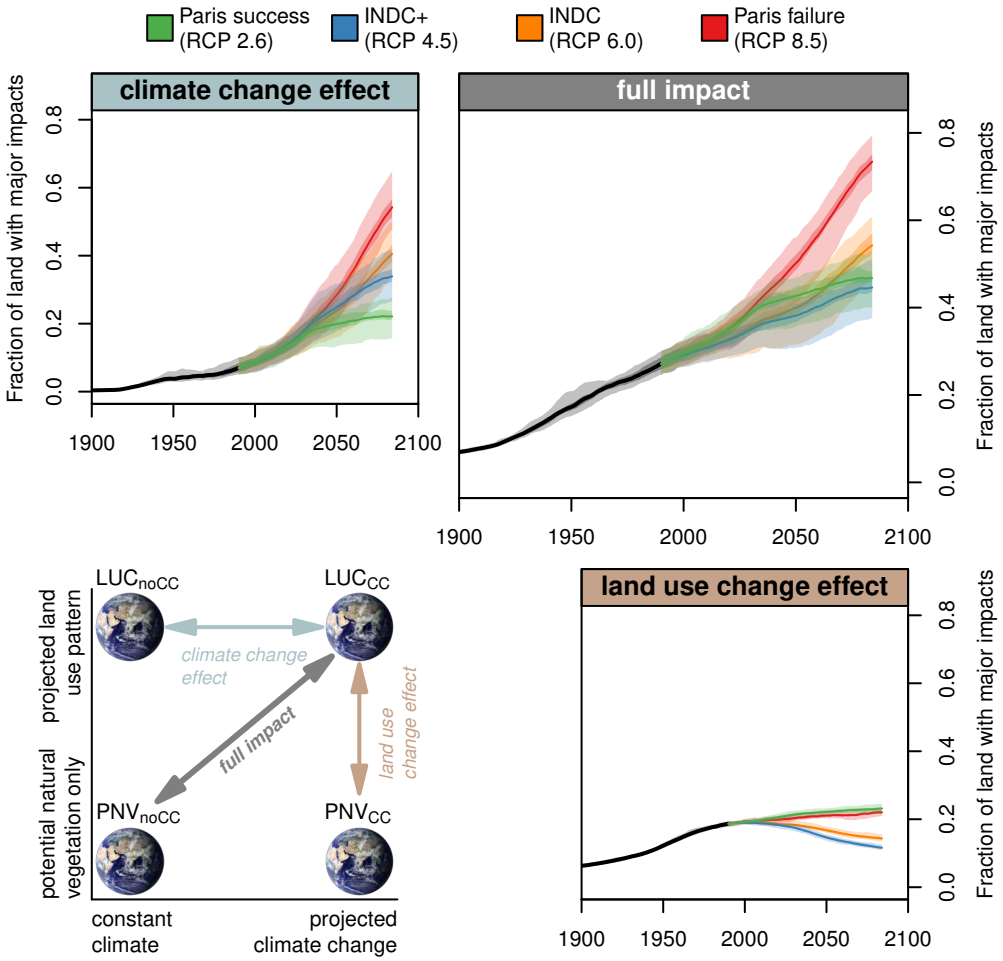

Figure VI.1.: Fraction of the global land surface exposed to major landscape change under 4 studied Paris outcomes. The climate change effect and land use change effect measure the impact caused by CC and LUC individually, while the full impact measures the combined effect, as illustrated by the schematic in the lower left and described in section 24.2 'Simulation setup'. Coloured lines show the ensemble mean of affected areas based on LPJmL simulations driven by 20 different climate models, while shaded areas show the inter-quartile range (dark shading) and full range (light shading) of simulations. Earth image by NASA Goddard Space Flight Center.

their warm edge (Figure E.3 in Appendix E). Based on the RCP2.6 land use scenario, LUC is estimated to expose landscapes covering 23% of the land surface to major impacts by 2070–2099 (22–25%, land use change effect, Figure VI.1), which roughly equals the

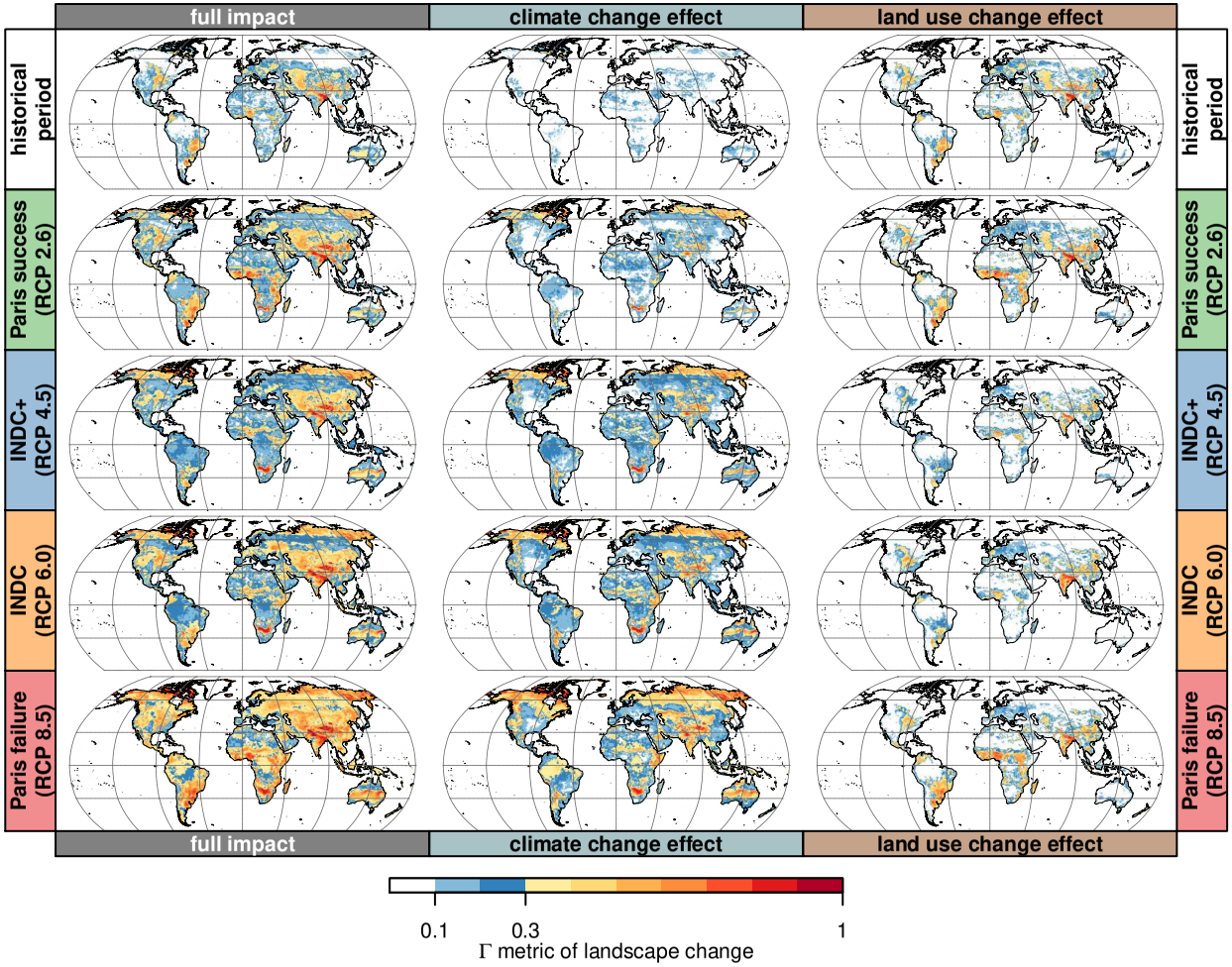

Figure VI.2.: Simulated landscape change under 4 studied Paris outcomes. Maps show the ensemble mean across LPJmL simulations driven by 20 different climate models. Historical period refers to 1976–2005 while all scenarios refer to 2070–2099. Blue colours depict moderate ($0.1 < \Gamma < 0.3$) and yellow to red colours depict major landscape changes ($\Gamma > 0.3$).

extent of major CC impacts. Land use expansion is concentrated in tropical forests as well as tropical savannas and grasslands, where areas of major LUC effects expand by 59% (33–74%) and 88% (51–140%), respectively, compared to the historical period (Figure E.5 in Appendix E). At the global scale, human interference with the biosphere through both CC and LUC is projected to cause major changes on 47% of the land surface by 2070–2099 (40–53%, full impact, Figure VI.1). At the biome level, the relative contributions of CC and LUC vary widely: For example, CC effects are generally low in tropical and temperate forests, but full impacts are in the same range as the global aggregate because of the high level of land use in these regions (Figure VI.3, Figures E.5 and E.6 in Appendix E). CC and LUC contribute roughly equally to major full impacts in tropical savannas and grasslands, but there is little spatial overlap between major impacts caused by both effects (Figure VI.2). In Asia and the western US, co-occurring minor or moderate CC and LUC effects amplify in temperate savannas and grasslands to cause major full impacts in roughly 46% more landscapes than the sum of both individual effects. A similar amplification effect is found in forests in Eastern Europe.

25.2. INDC+ scenario

Less ambitious climate change mitigation under *INDC+* translates into considerably higher numbers of landscapes with major CC effects, eventually covering 34% (27–42%) of the land surface by the end of the century (Figure VI.1). This represents a 54% (32–83%) increase over the *Paris success* scenario and a 4 to sevenfold increase over the historical period (1976–2005). In cold biomes three quarters of climate models agree on major CC effects for more than 80% of the tundra and more than 40% of all boreal forests (Figure E.6 in Appendix E). Changes in the high latitudes are not only driven by temperature rise, which extends the growing season length, but also by an increase in precipitation projected for that region. Major CC effects are also projected for roughly half of all tropical and one third of all temperate savannas and grasslands. For tropical forests, moderate CC effects ($0.1 < \Gamma < 0.3$) dominate, with major CC impacts projected for 14–29%. CC impacts in temperate forest regions are still widely below the moderate threshold ($\Gamma < 0.1$, Figure VI.2). The underlying RCP4.5 scenario has a strong afforestation/avoided LUC emissions component to its emissions mitigation strategy (Thomson et al. 2011). After some land use expansion during the early 21st

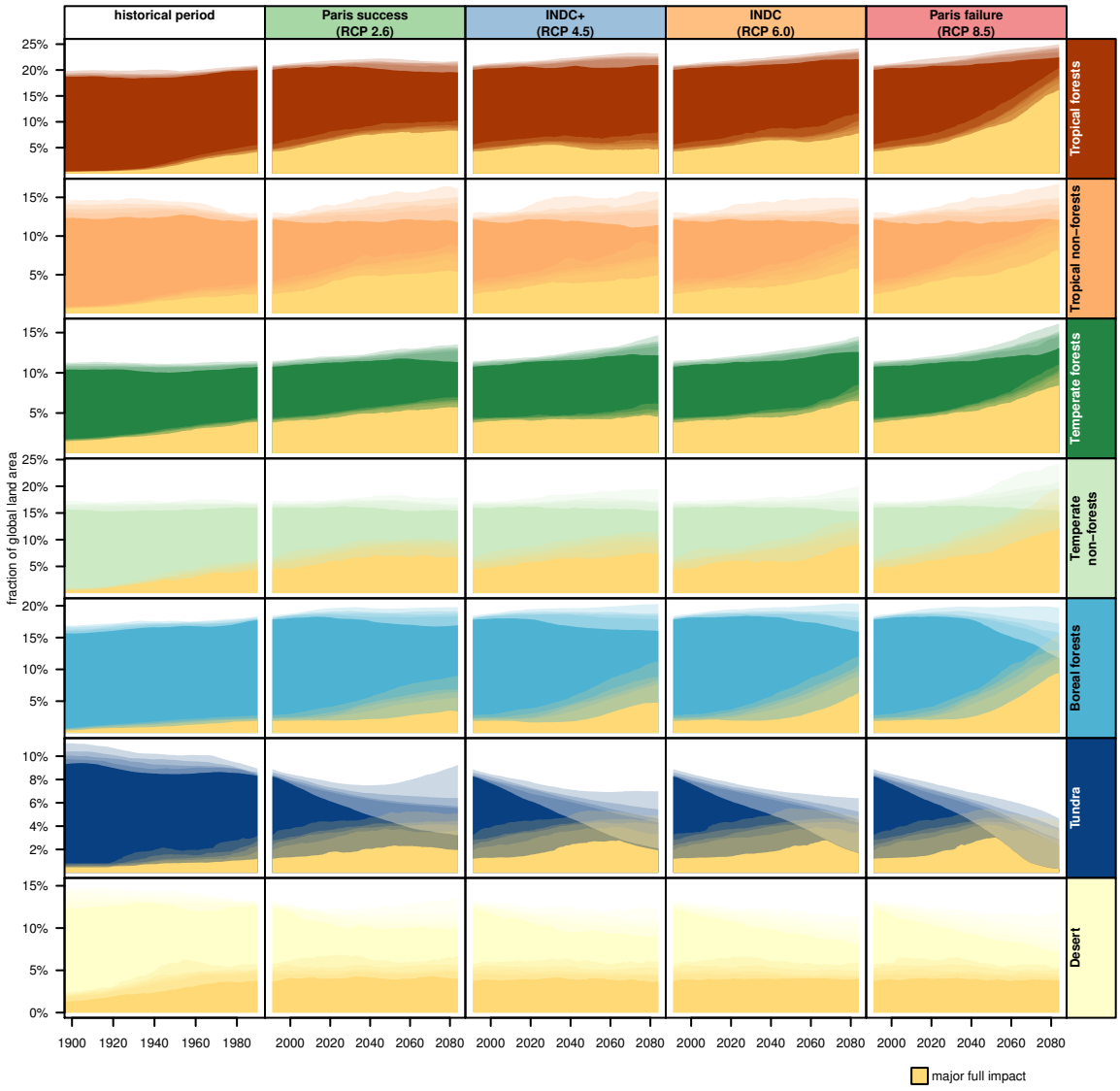

Figure VI.3.: Joint full impacts of CC and LUC in major biomes over time. Each plot shows the fraction of the global land area covered by the respective biome as well as the fraction of the biome projected to experience major change (yellow overlay). Biome classification of landscapes (grid cells) is based on their potential natural vegetation even if land has been converted to agriculture. Semitransparent shading denotes climate model uncertainty (maximum extent, 75%, 50% and 25% quantile and minimum extent with increasing opacity). See Figures E.5 and E.6 in Appendix E for corresponding versions showing the individual effects of LUC and CC.

century, managed land is reduced in all biomes except tropical savannas (Figure E.4 in Appendix E). At the global scale, landscapes with major LUC effects shrink from 18–19% of the land surface in 1976–2005 to 11–13% in 2070–2099. The fraction of the land surface exposed to major full impacts, i.e. the combination of CC and LUC, is almost identical in the *INDC+* and *Paris success* scenarios (45 and 47%, respectively, Figure VI.1) which can be traced back to the differences in land use: Compared to the *Paris success* scenario, *INDC+* reduces the extent of landscapes with major LUC effects by almost two thirds in tropical forests, and roughly 50% in most other biomes (Figure E.5 in Appendix E). This higher pressure from LUC under the *Paris success* scenario is reflected in the joint full impact: *Paris success* exposes 52% (22–81%) more tropical and 22% (11–36%) more temperate forest landscapes to major full impacts than *INDC+* (Figure VI.3), even though major CC effects are simulated for 2–5 times and 2–3 times as many landscapes in tropical and temperate forests, respectively under *INDC+* (Figure E.6 in Appendix E).

25.3. INDC scenario

Under *INDC* (RCP6.0), major CC effects are projected for 41% (34–50%) of the land surface by 2070–2099, an 83% (62–121%) increase over the *Paris success* scenario (Figure VI.1). The largest expansion of major CC effects is projected for tropical forests, especially in Africa and South America (Figure VI.2). Climate change causes an expansion of tropical seasonal forests at the expense of both tropical evergreen forests and tropical savannas (Figure E.3 in Appendix E). However, some of these areas, especially in Africa, are heavily used as pastures and cropland, which may suppress climate-driven forest expansion. In terms of LUC forcing, *INDC* has slightly less total managed land than *INDC+* (Table VI.1), but only the global pasture area is strongly reduced in this scenario, whereas croplands are relocated partially between biomes and overall expand by 4% globally. Cropland expansion takes place mostly in tropical and temperate forests (Figure E.4 in Appendix E). In addition to cropland expansion, land for dedicated bioenergy plantations is also located mostly in tropical forests and temperate forests and savannas. On the other hand, abandonment of pasture areas takes place mostly in tropical and temperate savannas and grasslands and tropical forests, leaving only temperate forests with a net increase of total agricultural area. At the

global scale, landscapes with major LUC effects cover 13–16% of the land surface by 2070–2099, slightly more than in the *INDC+* scenario (Figure VI.1). Major full impacts are projected for 54% (47–61%) of the global land surface. During the second half of the 21st century, relatively low LUC impacts (compared to today and the other scenarios) can no longer compensate for increasing CC impacts, and *INDC* is likely to expose more landscapes to major impacts than either *Paris success* or *INDC+* in all biomes by 2070–2099 (Figure VI.3).

25.4. Paris failure

More than half the land surface — 54% with a model range of 48-65% — is projected to experience major CC effects by 2070–2099 in the *Paris failure* scenario (Figure VI.1). This is roughly the same area as is projected to experience major impacts from both CC and LUC under the *INDC* scenario. Even though boreal forests may replace up to 97% of all tundra regions (Figure VI.3, ensemble mean 71%), increased mortality of boreal trees along their warm edge due to heat and water stress can often not be compensated fast enough by temperate tree recruitment, causing a wide-spread shift to a savanna-like state in both Russian and Canadian boreal regions (Figure E.3 in Appendix E). The extent of biome transitions between tundra, boreal forests and temperate savannas represents the largest area of climate-model related uncertainty in our simulations. Our findings are in general agreement with earlier studies that reported high risk of biome shifts in the high latitudes (e.g. Scholze et al. 2006; Gonzalez et al. 2010; Beck and Goetz 2011), but responses were also found to differ considerably between vegetation models (e.g. Sitch et al. 2008; Warszawski et al. 2013). Major CC effects are also projected under the majority of climate models in large parts of the Amazon and African equatorial rainforests and South-east Asia (Figure VI.2). The underlying RCP8.5 features the largest total managed land of all four scenarios, with an increase of nearly 25% over present day (Table VI.1). At the global scale, landscape changes from LUC are still slightly lower than in the *Paris success* scenario, causing major impacts on 22% (21–23%) of the land surface (Figure VI.1). They are particularly strong in South America, tropical Africa, India and China, while LUC impacts decrease below present-day levels in parts of Europe and North America. Human interference with the biosphere through both CC and LUC is projected to put 73% (67–80%) of the global land surface at risk of major

landscape change by 2070–2099. Moderate changes ($0.1 < \Gamma < 0.3$) are simulated for another roughly 20% of the land surface, leaving a mere 3–8% of ice-free landscapes worldwide with only minor biosphere changes.

While the Γ metric allows for a quantitative comparison of the magnitude of change its integrated value gives little indication of the type of change. Section E.5 and Figure E.7 in Appendix E provide a decomposition of Γ into its components and illustrate the contributing factors to landscape change in different biomes. All results presented here use the area affected by $\Gamma > 0.3$ to aggregate impacts of CC and LUC at the landscape level to the biome or global scale, which essentially ignores landscapes with moderate or only minor impacts. In Appendix E we test using the area-weighted global mean Γ as an alternative global measure (section E.6, Figure E.8). This does not affect the ranking of scenarios relative to each other, but it does reduce the spread between scenarios. It also reduces the relative increase of impacts between the present-day state and the end of the scenario period. We also test the sensitivity of our results to the threshold used for Γ and find that most results are robust, except that lower thresholds reverse the ranking of *Paris success* and *INDC+* in terms of the full impact (Figure E.9).

26. Discussion

We find that, with the exception of a full *Paris success*, CC is projected to take over as the main driver of major landscape change at the global scale by mid-century, and by the end of the century, major CC effects are projected for more than twice the area that experiences major LUC effects (Figure VI.1). In the *Paris success* case, CC roughly catches up with LUC. This finding is in qualitative agreement with earlier studies that found stronger effects of CC than LUC on biome distribution during the 21st century (Davies-Barnard et al. 2015; Boit et al. 2016). Two of the scenarios studied here, *Paris success* and *INDC+*, expose almost the same amount of areas worldwide to major change despite roughly 0.8 K difference in global mean temperature rise. CC impacts that are avoided under *Paris success* are compensated by LUC impacts which are higher than in all the other three studied scenarios. While this finding might suggest that strong

climate mitigation (*Paris success*) provides no benefits — and may even cause more harm — to the terrestrial biosphere compared to the less ambitious *INDC+* scenario it is important to have a closer look at the underlying scenarios to understand whether the differences are indeed a result of the level of climate mitigation ambition or caused by other factors. In the RCP development process, each RCP scenario was constructed by a different IAM modelling group (van Vuuren et al. 2011a). While RCP8.5 represents a high-emission 'baseline' scenario without any climate change policies (Riahi et al. 2011), all the other IAMs used their own unique baseline conditions and then added climate mitigation measures to limit global warming in the most cost-efficient way (Masui et al. 2011; Thomson et al. 2011; van Vuuren et al. 2011b). As such, the baseline scenarios differ regarding key socioeconomic driving forces such as population, economic and income development, energy and land use (van Vuuren et al. 2011a). For example, the reference scenario for RCP4.5 (*INDC+*) has ∼20% more agricultural land than the reference scenario for RCP2.6 (*Paris success*) (Thomson et al. 2011; van Vuuren et al. 2011b). RCP4.5 uses a universal carbon tax to induce reductions in GHG emissions from baseline conditions which applies equally to all emissions regardless of the source (industry, energy, land use) and creates a strong financial incentive in the IAM to avoid land use expansion and even leads to a large increase in forest extent (Wise et al. 2009b; Wise et al. 2009a), while still fulfilling food demand by shifting cropland to higher-yielding regions and shifting toward food products with a smaller carbon footprint (Thomson et al. 2010; Thomson et al. 2011). As such, the reductions in global cropland and pasture areas (see Table VI.1) are an integral part of the mitigation strategy of the *INDC+* scenario, working in addition to the use of bioenergy to reduce emissions. It appears that no similar mechanism is present in RCP2.6 (*Paris success*) because mitigation from baseline conditions leads to an overall increase of the agricultural area, caused by an expansion of bioenergy (and BECCS), which is higher than in *INDC+*, and cropland expansion to balance a climate-driven reduction of crop productivity assumed in the IAM (van Vuuren et al. 2011b). An assessment of the technological assumptions made in the IAMs or the general feasibility of mitigation strategies in the RCPs is far beyond the scope of this analysis, but the lower agricultural area in RCP4.5 does not appear to be caused by different baseline assumptions in RCP2.6 and RCP4.5, but rather by the question how land use policies are affected by climate policy in each IAM. Since the development of the original RCP scenarios, the climate change research and the land system science community have collaborated to produce a new set of

harmonized socioeconomic scenarios, the so-called Shared Socioeconomic Pathways (SSPs). The SSPs comprise 5 baseline scenarios describing alternative narratives for the 21st century, including sustainable development, regional rivalry, inequality, fossil-fueled development, and middle-of-the-road development, and IAM groups were asked to develop mitigation scenarios consistent with each baseline leading to each of the radiative forcing levels of the RCPs (Riahi et al. 2017). The SSP LUC scenarios should allow for a more systematic assessment of LUC impacts in the different RCPs (Popp et al. 2017), however they are currently available from the SSP database (https://secure.iiasa.ac.at/web-apps/ene/SspDb/, accessed April 28, 2017) only at the spatial disaggregation level of five world regions which makes them unsuitable for an impact assessment such as ours.

To allow for a more robust assessment of the impacts of future LUC, scenarios would need to provide more detailed information. For example, no information on crop irrigation is included in the RCP scenarios. Irrigated crops currently account for 33% of total crop production even though only 16% of global cropland is actually irrigated (Siebert and Döll 2010; Siebert et al. 2010), and irrigation represents the largest human freshwater use accounting for ∼70% of all human water withdrawals and ∼90% of freshwater consumption (e.g. Döll et al. 2012; FAO 2012). We use present-day irrigated areas and scale them linearly with future changes in total cropland to derive future irrigated areas (see section 24.1 of the Methods). Given the required increase in crop productivity, we likely underestimate irrigation requirements especially in the *INDC+* scenario. Although water abstractions already exceed local renewable supplies in some regions, which may hamper future irrigation expansion (e.g. Vörösmarty et al. 2005; Döll et al. 2014), Jägermeyr et al. (2016) estimate a huge potential to increase crop production through integrated crop water management: combining irrigation efficiency improvements and low-tech solutions for small-scale farmers on water-limited croplands they calculate possible increases of global production of more than 40% if these measures were applied globally, all without increasing water withdrawals or expanding total cropland.
The RCP scenarios also lack information on fertilizer use. Intensification has been a major driver of crop production increases during the second half of the 20th century, facilitated among other factors by a 500% increase in fertilizer use (Tilman et al. 2001; Foley et al. 2011; FAO 2016). Low fertilizer use in many developing countries, especially Sub-Saharan Africa, is a chief reason for large yield gaps existing in these regions, providing both opportunities for and challenges to future crop production increases (Bruinsma

2003; Cassman et al. 2005; IAASTD 2009). At the other end of the spectrum, leaching and atmospheric emissions of excess nitrogen cause acidification and eutrophication in aquatic ecosystems, and high nitrogen deposition may induce species composition changes, enhance susceptibility to stress, cause direct foliar damage, and as a whole is linked to reduced plant species richness in many terrestrial ecosystems (Bobbink et al. 2010; Dise et al. 2011; Erisman et al. 2013).

These observations illustrate that the LUC scenarios underlying analysis such as our present study are a source of considerable uncertainty: their dependence on assumptions about global developments regarding increases in population, per capita demand, agricultural technology and management, policy measures influencing land use patterns and their consistency with co-evolving climate policy, interregional trade-offs etc., coupled with considerable model-structural and data-driven uncertainty, is difficult to overcome in a spatially explicit manner for a comprehensive assessment (e.g. Prestele et al. 2016).

27. Conclusions

We show that, together, CC and LUC risk causing major ecosystem change in landscapes covering 38–80% of the global land surface by the end of the 21st century. While LUC is currently the major anthropogenic pressure on the terrestrial biosphere at the global scale, we find that it will likely be outpaced by CC in the second half of this century unless global warming can be limited to well below 2 °C. The large uncertainty range of impacts is caused primarily by the span of climate outcomes analysed here: major CC impacts are projected for 16–27% of the land surface in the most ambitious *Paris success* scenario, but for 48–65% of the land surface in case of a *Paris failure*. In comparison, the best and worst-case scenario in terms of LUC impacts, *INDC+* and *Paris success*, are projected to cause major impacts on 11–13% and 22–25% of the land surface, respectively.

Our analysis is restricted by the limited availability of land use scenarios of sufficient spatial and topical detail. Since the RCPs, research has gone into assessing and ultimately

reducing the sources of uncertainties in future LUC projections (e.g. Verburg et al. 2013; Schmitz et al. 2014; Prestele et al. 2016), but also into a better representation of sustainability aspects (e.g. Godfray and Garnett 2014; Verburg et al. 2015). The new SSP scenarios address some of the limitations of the original RCP scenarios discussed above. A subset of these scenarios will be disaggregated to a harmonized gridded resolution as a contribution of the Land Use Model Intercomparison Project (LUMIP) to CMIP6 (Lawrence et al. 2016). Similar to the RCP LUC scenarios within CMIP5, evaluation of the SSP scenarios with coupled climate-carbon cycle models will then allow for the quantification of biogeophysical impacts of LUC such as albedo changes through afforestation which, in contrast to biogeochemical impacts, are not accounted for by IAMs. For the time being, the RCP scenarios represent the best available set of internally consistent scenarios of future CC and LUC.

Despite large uncertainties, our results emphasize the importance of ambitious climate mitigation in the pursuit of limiting humanity's impact on the terrestrial biosphere. While IAM simulations suggest that low warming scenarios can be achieved following a range of socioeconomic and technology assumptions we show that these very development pathways play an important role in determining future land use and therefore the full impact of humanity on ecosystems. According to our simulations, the focus on preservation and restoration of non-agricultural ecosystems (mostly forests) in the *INDC+* scenario may be able to 'offset' substantial additional warming compared to the more land-intensive *Paris success* scenario, assuming that the large productivity increases required under *INDC+* can be achieved sustainably. To ensure that the Paris Agreement is a full success for the biosphere a co-transformation of the energy system (towards 'clean' sources and efficiency improvements that limit climate change) and the land use system (towards sustainable intensification that avoids and even reverses land expansion) will be required. Strategies proposed to achieve the latter include closing yield gaps in under-performing regions, increasing agricultural resource efficiency, diet shifts and reducing waste (Foley et al. 2011). However, even if a *Paris success* for climate could be combined with an optimistic *INDC+*-like land use scenario this would not be able to fully prevent a substantial expansion of areas with major human interference with the biosphere compared to today.

Supplementary material related to this part is available in Appendix E.

Acknowledgements

S.O. was supported by the German Federal Ministry for the Environment, Nature Conservation and Nuclear Safety (16_II_148_Global_A_IMPACT). L.R.B. was supported by the German Research Foundation's priority program DFG SPP 1689 on 'Climate Engineering – Risks, Challenges and Opportunities?' and specifically the CE-LAND project. S.S. was supported by the German Federal Ministry of Education and Research's (BMBF's) project 'PalMod 2.3 Methankreislauf, Teilprojekt 2 Modellierung der Methanemissionen von Feucht- und Permafrostgebieten mit Hilfe von LPJmL' (Code 01LP1507C). We acknowledge the World Climate Research Programme's Working Group on Coupled Modelling, which is responsible for CMIP, and we thank the climate modelling groups for producing and making available their model output. For CMIP the U.S. Department of Energy's Program for Climate Model Diagnosis and Intercomparison provides coordinating support and led development of software infrastructure in partnership with the Global Organization for Earth System Science Portals. Bias correction of climate model output was kindly provided by Jens Heinke. Other data used are listed in the references, tables and supporting information. Data underlying the analyses will be provided upon request to ostberg@pik-potsdam.de. The authors declare that they have no competing interests.

Part VII.

Summary and outlook

Sebastian Ostberg

28. Summary of key findings

The overarching question of this thesis was to assess the magnitude of human interference with the terrestrial biosphere over the course of the Anthropocene, using a metric that captures changes in basic biospheric properties as modelled by a dynamic global vegetation model (DGVM). In chapter 2 of Part I I broke this down into three main research questions which drove the individual studies presented in Part II to Part VI. The following sections provide a summary of results obtained over the course of the dissertation. They are organised around the main research questions.

28.1. What are the risks of different levels of global warming for ecosystems?

In order to allow for a systematic assessment of climate change (CC) impacts and their likelihood as a function of global mean temperature change Part II introduced a new set of climate scenarios called 'PanClim'. As explained in chapter 5, systematic assessments of CC impacts require that (1) a large range of global mean temperature change can be covered (scenario uncertainty, Hawkins and Sutton 2009), (2) each level of warming is reached at around the same time, and (3) information on local changes in key climate variables considers an ensemble of climate models as large as possible to account for the substantial climate model-structural uncertainty (Hawkins and Sutton 2011). The PanClim dataset is based on existing simulations from 19 general circulation models (GCMs) from the World Climate Research Programme's (WCRP's) Coupled Model Intercomparison Project phase 3 (CMIP3) multi-model ensemble (Meehl et al. 2007). While CMIP3 included simulations for three emissions scenarios from the Intergovernmental Panel on Climate Change's (IPCC's) Special Report on Emissions Scenarios (SRES, Nakićenović et al. 2000) — none of which were specific climate policy scenarios — PanClim greatly expands the scenario range to eight emissions scenarios

designed to reach global warming of 1.5 to 5 K above pre-industrial levels in 0.5 degree steps by 2100. As such, it covers the range from strong mitigation (e.g. distinct 1.5 and 2 K scenarios) to no-climate-policy business-as-usual scenarios (up to 5 K). The four Representative Concentration Pathways (RCPs) providing the basis for the newer CMIP5 multi-model ensemble (Taylor et al. 2012) encompass a similar range of end-of-century warming (Collins et al. 2013) but do not sample climate uncertainty as systematically as the PanClim dataset. Each scenario is generated with the spatial characteristics of 19 GCMs using a pattern scaling approach, resulting in a total of 152 climate projections for the 21st century, compared to 59 combinations available in CMIP3 (Meehl et al. 2007). The pattern scaling method is based on Mitchell (2003) but expands upon the original approach in two important aspects: (1) a bias correction is included in the process of combining time series of climate anomalies (from the GCM) with the reference climate (constructed from historical climate observations) which accounts for biases in the GCM's representation of present-day climate; (2) the approach used here does not only account for changes in precipitation amount, but also changes in the frequency of precipitation-free months. The scaling patterns are demonstrated to retain the properties of the original GCM simulations with sufficient accuracy, supporting the use of pattern scaling as an efficient method to generate climate scenarios that allow for systematic analyses of climate impacts as a function of global mean temperature change.

Using the PanClim dataset as climate forcing to drive the LPJmL model, Part III and Part IV explored the risks of different levels of global warming to ecosystems. An ecosystem is considered '*at risk*' of major ecosystem change if $\Gamma > 0.3$ at the end of the century under at least one GCM. Since there are always 19 GCMs available for each temperature level, the number of simulations agreeing on $\Gamma > 0.3$ is used as a measure of confidence. Values of $0.1 < \Gamma \leq 0.3$ denote a risk of moderate ecosystem change, and all ecosystem changes are computed in comparison to the present-day state. Major ecosystem changes are simulated for all warming levels, but the area found to be *at risk* is less than one-fifth of all ecosystems if warming is limited to 1.5–2 K and increases to more than two-thirds of all ecosystems if global warming reaches 4–5 K (86% at 5 K)(Figure III.1). A large uncertainty due to differences between GCMs is found: for each warming level, there is only low confidence (<4/19 GCM agreement) on 20–40% of the total area *at risk* (dotted black line in Figure III.1). The area *at risk* of major ecosystem considering the full 19-GCM ensemble is between 33 and 67% larger than the largest area simulated by any individual GCM, highlighting the importance of

using a large ensemble of GCMs for this type of risk analysis (Figure III.5). Moderate ecosystem changes are projected with a similar spatial extent as major impacts. However, at global warming levels above 4 K the area affected by moderate CC impacts starts to contract as more ecosystems cross the threshold to major change than go from minor to moderate change. Moderate changes are projected predominantly for the forest biomes whereas CC impacts in tundra or savanna regions tend to be major with smaller surrounding areas experiencing moderate change. Boreal evergreen forests differ from the other forest biomes in that projections show increasing areas of forest decline in the boreal-steppe ecotone with increasing warming (Figure III.2). Changes in tropical forests and savannas have the highest global importance component of the Γ metric among all biomes once global warming exceeds 2 K (Figure III.4 and Figure B.7). This means that they contribute more to global biogeochemical cycles than changes in other biomes that may be stronger on a local level, e.g. very high values of the local change component in the tundra.

In addition to the area-based analysis presented so far, Part IV looked at possible implications of the simulated changes for biodiversity, which is distributed highly unevenly around the world. While the simulations do not contain information at the species level major habitat changes as measured by Γ are considered as a risk indicator for the biodiversity in those areas. Endemism richness of vascular plants across 90 biogeographic regions is used as a biodiversity indicator which combines the number of species (species richness) with the degree to which they are endemic to each region (Kier et al. 2009). At 2 K of global warming, major CC-driven changes are limited mostly to 4–6 (out of 90) distinct biogeographic regions that altogether host 1–1.5% of global endemism richness of vascular plants (Figure IV.4). These values quadruple to 16 biogeographic regions hosting 10% of plant diversity in case of 3.5 K global warming, if at least 50% GCM agreement (medium confidence) is used as an additional criterion. Another 34 biogeographic regions with 39% of global plant endemism richness are simulated to be *at risk* with lower confidence. If emissions cannot be curbed and global warming reaches 5 K, 68 biogeographic regions hosting 74% of plant diversity are estimated to experience major climate change impacts with at least medium confidence, with another 19 biogeographic regions and 24% of plant diversity *at risk* under at least one GCM pattern. As such, the climate change risk to biodiversity, represented here by vascular plant endemism richness, appears to increase much more rapidly with increasing warming than the pure land area experiencing major ecosystem change.

While an analysis of the components of Γ reveals that changes in water fluxes generally play a much smaller role than changes in carbon fluxes and stocks in determining the magnitude of ecosystem change (Figure B.7) changes to the water cycle may still have significant societal consequences. Part IV shows that global warming of 2, 3.5 and 5 K could expose an additional 8%, 11% and 13% of the world population to new or aggravated water scarcity, respectively, with >50% confidence based on GCM agreement (Figure IV.4). Accounting for population growth and changes in water availability, 30–43% of the global population is projected to be exposed to water scarcity in 2100, compared to 21% living under water-scarce conditions in 2000 (following the SRES B1 and A2r demographic projections).

28.2. What has been the magnitude of human interference with the biosphere through land use and climate change over the course of the last three centuries?

There are two main pathways of human interference with the biosphere: (1) indirectly through actions that change the climate which in turn causes ecosystem changes, and (2) directly through human land use. Part III and Part IV assessed the risk to ecosystems from future climate change but did not account for land use change (LUC). Extending the analysis to both CC and LUC impacts, Part V traced the expansion of humanity's dual pressure on the biosphere between 1700 and 2010. While land use generally causes major change when measured directly on the agricultural area landscapes usually contain a mixture of agriculture and natural vegetation. In 1700, almost 60% of landscapes were still virtually free of agriculture, and only 2.5% of landscapes contained more than 25% managed land. Consequently, the impact of land use at the landscape scale was still generally low, with moderate LUC impacts on 2% and major impacts on 0.5% of the global ice-free land surface (Figure D.2). Climate conditions equalled the reference climate so the CC impact was zero by definition. By the beginning of the 20th century, the area used as cropland and pastures had already reached more than half of its present-day extent while anthropogenic climate change was only starting to have an effect on the biosphere through increasing atmospheric CO_2 concentrations and small deviations from the reference climate. LUC alone caused major impacts in landscapes covering 5% of the land surface and moderate impacts in another 10% of

landscapes. Including the effects of early anthropogenic CC on the biosphere, human activities were responsible for major impacts on 6% and moderate impacts on 12% of the land surface (Table V.3). Human interference with the biosphere picked up speed during the 20th century: landscapes with major impacts quadrupled from 6 to 24% while moderate impacts expanded from 12 to 31% of the land surface. In other words, the dual pressure from LUC and CC had already caused at least moderate ecosystem changes in landscapes covering more than half the land surface by the end of the historical period (1981–2010). Comparing both pressures, more landscapes were exposed to major LUC effects than major CC effects (15 and 10% of the land surface, respectively). However, 60% of landscapes worldwide experienced stronger CC effects than LUC effects overall, pointing to the fact that there still are some regions untouched by LUC whereas CC is a truly global phenomenon. There is some uncertainty regarding both historical climate and land use forcing which leads to uncertainty regarding their impacts on the biosphere so far: Using a different historical land use reconstruction and bias-corrected GCM simulations instead of observation-based climate data to drive LPJmL, Part VI estimated slightly higher LUC effects (major impacts on 18–19% of the land surface) and lower CC effects (major impacts on 5–10% of the land surface) for the end of the historical period.

28.3. How do projected land use change and climate change interact in pushing the biosphere further out of its Holocene state?

Extending the historical analysis of Part V and the analysis of future CC impacts presented in Part III and Part IV, Part VI assessed the dual pressure from CC and LUC on the biosphere under the four RCP scenarios. In terms of climate forcing, the RCPs span a similar range as the PanClim scenarios used for Part III and Part IV. Contrary to PanClim, the RCPs are based on socioeconomic scenarios that include assumptions on future population growth, food and bioenergy demand. While all four RCPs assume a growing world population only two RCPs feature a moderate land use expansion whereas the other two scenarios project a reduction of agricultural land compared to today as a result of strong increases in agricultural intensity (Table VI.1). The scenario spread in terms of CC forcing appears to be substantially larger than the

spread of LUC forcing which is reflected in the spread of projected impacts: Individually, major CC impacts are projected for 16–65% of the land surface by the end of the 21st century, while areas subject to major LUC impacts range between 11 and 25% of the land surface. The dual pressure from both CC and LUC is projected to cause major landscape change on 38–80% of the land surface. It is of note that — despite an additional global warming of ≈0.8 K compared to RCP2.6 — the full impact from both CC and LUC is simulated to be slightly lower under the RCP4.5 scenario than under RCP2.6. This is a result of significantly smaller LUC impacts following large-scale cropland abandonment under RCP4.5. The lowest LUC impacts are found in the two intermediate CC scenarios, whereas land use areas as well as the resulting LUC impacts are substantially larger under RCP2.6 and RCP8.5. As discussed in chapter 26, LUC impacts in the intermediate scenarios may be underestimated somewhat in light of the agricultural intensification required to allow for such large-scale land abandonment. Nevertheless, a sizeable trade-off exists between CC and LUC impacts under RCP2.6 and RCP4.5, leading to a similar overall impact on the biosphere under both scenarios despite significant differences in forcing. Low LUC forcing is unable to balance the higher CC forcing under RCP6.0, exposing more landscapes to the risk of major ecosystem change than either RCP2.6 or RCP4.5. Finally, RCP8.5 is characterised by both high CC and high LUC forcing resulting in projected major impacts on 67–80% of the land surface.

28.4. Synthesis of results

Ellis and Ramankutty (2008) argued that more than 75% of the ice-free land showed evidence of human alteration and proposed to map the Earth in terms of anthropogenic biomes or ‘anthromes’ instead of the classical biomes commonly used to describe global patterns of ecosystem processes and structure (Chapin et al. 2011). While they considered nearly half of the terrestrial biosphere to be wild and 45% in a seminatural state with only minor use for agriculture or settlements in 1700, the distribution of anthromes changed profoundly in the last 300 years, with more than 55% now in agricultural or settled anthromes, less than 20% in a seminatural, and 25% in a wild state (Ellis et al. 2010). Anthromes provide a mostly qualitative characterisation of human interference with the biosphere, determined by the presence or absence of land use in an area. In

contrast, the Γ metric used in this dissertation provides a quantitative assessment of the impact land use as well as climate change have on biogeochemical and structural properties of the biosphere. Both indicators show that human interference with the biosphere has expanded exponentially over the course of the last three centuries. Yield increases have slowed down land use expansion during the second half of the 20th century and — according to one estimate — have avoided cropland expansion of 1514 Mha and land use emissions of 161 GtC (Burney et al. 2010). This slowdown is reflected in the simulated Γ metric for the land use change effect which shows a diminishing annual growth rate after 1950 (Figure V.1 and Figure VI.1). However, there has been no matching slowdown of the full impact of human activities on the biosphere because of the growing pressure from anthropogenic climate change. Going into the scenarios, there is a marked shift in the relative importance of CC and LUC: While LUC was the responsible driver for the majority of landscapes with major anthropogenic changes during the last century, CC is projected to take over that role at the global scale by mid-21st century, and by the end of the century major CC effects are projected for more than twice the area that experiences major LUC effects in all scenarios except RCP2.6, the strictest climate mitigation scenario analysed here (Figure VI.1). The latter scenario exposes similar global areas to major CC and LUC impacts.

As discussed in the context of research question 1, the area *at risk* of major CC impacts is substantially larger than the area simulated by any individual GCM because of differences in the spatial patterns of CC between climate models. Results presented in Part VI show the range of affected areas in individual GCMs but they do not account for the fact that the same global aggregate number can result from very different spatial patterns. Figure VII.1 presents a re-analysis of simulation results from Part VI, newly compiled for this synthesis, which assigns a measure of confidence that each grid cell may experience major anthropogenic change based on the number of GCM patterns agreeing on $\Gamma > 0.3$ in said grid cell. Conversely, a low GCM agreement on major impacts in a grid cell can be interpreted as a high chance that impacts will remain of minor or moderate magnitude, at most. Given their different reference conditions — present-day in Part III and pre-industrial in Part VI — the area *at risk* of major CC impacts is larger here than in Figure III.1. The differences are most pronounced in the low warming scenarios whereas results for RCP8.5 are close to the 5 K scenario in Part III. The largest pattern-related uncertainty is found in the lowest warming scenario: 66% of the land surface are projected to be *at risk* of major CC impacts with varying levels of

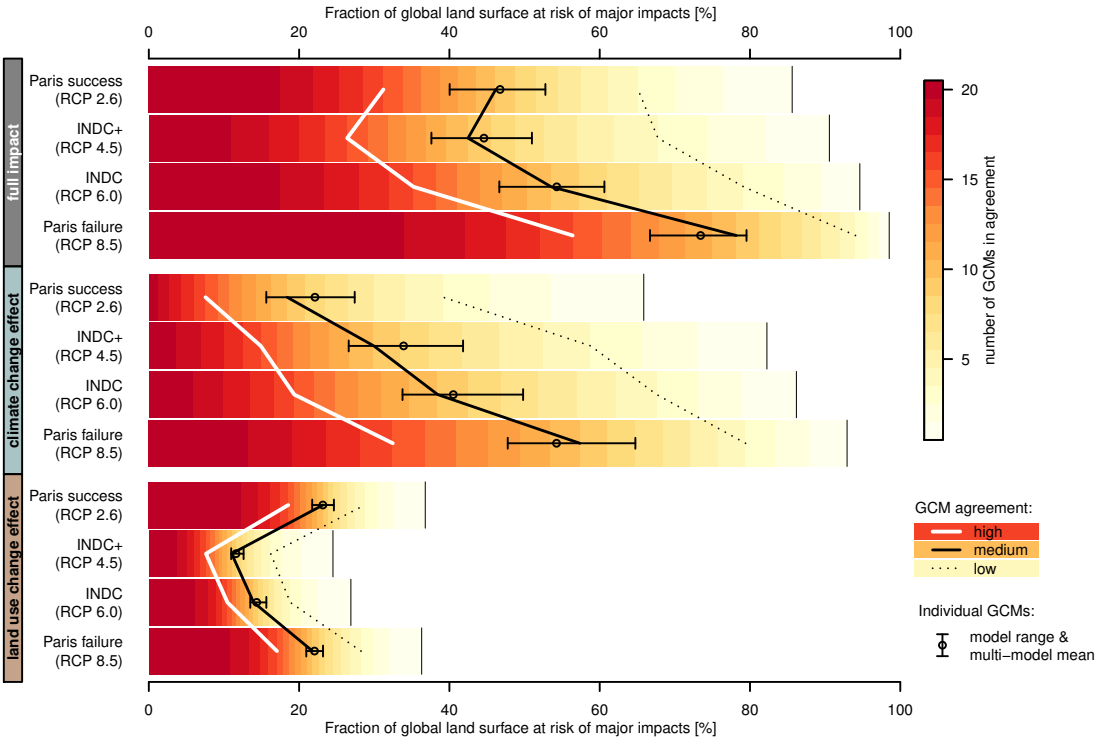

Figure VII.1.: Area at risk of major landscape change from CC, LUC and the combined effect of CC and LUC. Results are based on simulations from Part VI, but presentation corresponds to analysis in Part III. A landscape is considered '*at risk*' of major impacts if $\Gamma > 0.3$ under at least one out of 20 GCM patterns. Textual description of RCP scenarios follows Part VI. Model range und multi-model mean of affected areas in individual GCMs from Figure VI.1 are shown for comparison.

confidence — signified by different colours in Figure VII.1 — while this number amounts to 16–27% of the land surface in individual GCMs. The number of landscapes *at risk* of major CC impacts corresponds to 82 and 86% of the land surface under RCP4.5 and RCP6.0, respectively. Even in the RCP8.5 scenario, the total land area *at risk* of major CC impacts is 44% larger than the maximum single GCM, amounting to 93% of the global land surface.

While only one land use scenario (spatial pattern of cropland, pasture and bioenergy plantation areas) was available per RCP, GCM uncertainty causes some uncertainty regarding the global extent and spatial pattern of major LUC impacts, as well (land use change effect, Figure VII.1). This is because both the landscape state with human land use ($\mathrm{LUC_{CC}}$) and the reference state ($\mathrm{PNV_{CC}}$) are affected by GCM-specific climate

change (Figure I.3). However, the effect of GCM uncertainty on projected LUC impacts is much smaller than its effect on CC impacts.
Finally, almost 99% of the land surface are projected to be *at risk* of major ecosystem change under RCP8.5 when accounting for the combined effect of CC and LUC (full impact, Figure VII.1). The total area *at risk* of major full impacts is not much smaller in the other scenarios, amounting to 95, 91 and 86% of the global land surface under RCP6.0, RCP4.5 and RCP2.6, respectively. However, there are significant differences between the four RCPs which can best be illustrated using the inverse interpretation of the level of confidence: Based on the GCM ensemble and land use scenario, only 8% of the global land surface have a high chance ($\geq 80\%$) that human interference with the biosphere will remain minor or moderate, at most, in the RCP8.5 scenario. 25% of the land surface have a medium chance ($\geq 50\%$) of staying below the threshold for major impacts. This number increases to 26% of the land surface with a high chance and 50% with a medium chance under RCP6.0. Based on individual GCMs, the full impact of CC and LUC is slightly lower under RCP4.5 than RCP2.6. Accordingly, the global area with a medium chance of staying below $\Gamma > 0.3$ is higher under RCP4.5. However, because of the larger uncertainty associated with CC impacts than LUC impacts, the global area with a low GCM agreement on major change and the total area *at risk* of major change are slightly higher under RCP4.5 than RCP2.6.

29. Conclusions

29.1. Outcomes

As summarised above, this dissertation has provided a quantitative assessment of human interference with the terrestrial biosphere throughout the Anthropocene, focussing on climate change and land use change as the main drivers of ecosystem change at the global scale. The work complements and partly integrates a long tradition of using dynamic global vegetation models (DGVMs), hydrological and similar models to assess impacts of CC and LUC on individual aspects of the carbon and water cycle (e.g. Cramer

et al. 2001; Friedlingstein et al. 2006; Piao et al. 2007; Gerten et al. 2008; Sitch et al. 2008; Gosling et al. 2010; Haddeland et al. 2011; Schaphoff et al. 2013; Schewe et al. 2014; Nishina et al. 2015; Veldkamp et al. 2017). The ability of the LPJmL DGVM to simulate not only the dynamics and functioning of natural vegetation but also crops, managed grasslands and bioenergy plantations provided the unique opportunity to study the effects of both CC and LUC consistently within one modelling framework using the same indicator. Only a small number of previous CC impact studies have attempted to provide a comprehensive sampling of climate uncertainty, and future land use change was usually not considered at all. For example, Schaphoff et al. (2013) used an extended version of the PanClim dataset from Part II to study the long-term fate of permafrost soil carbon stocks and their contribution to the global carbon budget under different levels of warming. Similarly, Gosling et al. (2010) used another large ensemble of pattern-scaled climate scenarios to assess regional runoff changes. Recognising that CC and LUC affect more than one or a few isolated ecosystem processes, a comprehensive risk assessment should encompass several aspects of ecosystem functioning (e.g. Scholze et al. 2006; Heyder et al. 2011). That is why this dissertation combined a large ensemble of climate simulations with an aggregated metric of changes in biogeochemical and vegetation-structural properties — the Γ metric — acting as a proxy for the risk of critical changes or even collapse of more complex ecosystem features. The use of this macro-level indicator based on parameters that can be simulated using LPJmL allowed for a consistent, transient quantification of biospheric change over a long period of time — from 1700 to 2100 — rather than attempting to synthesise a large number of individual, often smaller-scale, ecological studies into a coherent global picture (e.g. Parmesan and Yohe 2003; Warren et al. 2011; Peñuelas et al. 2013, and references therein). The results have illustrated how human interference with the terrestrial biosphere has already caused at least moderate or even major ecosystem change on more than half the global land surface. Given the range of future land use scenarios and the large climate uncertainty — both in terms of the level of radiative forcing (RF) and the spatial patterns of CC — there is a risk for 86–99% of the biosphere to experience a major transformation compared to its state at the beginning of the Anthropocene by the end of the 21st century. CC is likely to become the main driver of major ecosystem change during the 21st century, and limiting global warming is crucial not only for the biosphere, but to prevent a number of tipping elements in the Earth system from changing irreversibly (Schellnhuber et al. 2016). However, results from this dissertation also highlight the

importance of different land use strategies in determining the full impact of human activities on the terrestrial biosphere, as evidenced by the similar full impact under RCP2.6 and RCP4.5.

The PanClim climate scenarios from Part II have been made publicly available through http://www.panclim.org to allow for their use in other studies of CC impacts.

29.2. Limitations

While the Γ metric allows for a consistent, quantitative assessment of the *magnitude* of CC and LUC impacts its integrated value by itself gives little indication of the *type* of ecosystem change without a detailed analysis of its components. On a related note, the metric does not distinguish between positive and negative ecosystem change. If anything, Γ takes a conservative approach in which any external pressure is considered a challenge pushing species and communities to adapt, migrate to more favourable conditions or go extinct (Mooney et al. 2009). Since each species reacts differently to this pressure, CC and LUC alter community composition and have the potential to disrupt long-standing biotic interactions such as predator-prey and host-parasite relations (Parmesan 2006), complementarity and competition regarding resource use (Hooper et al. 2005), or mutual interactions like pollination (Mooney et al. 2009). From a food production perspective, converting natural vegetation into agricultural land has certainly been a positive ecosystem modification because it has allowed food supply to generally keep pace with the growing world population, but this modification has caused changes of moderate or even major magnitude in landscapes covering almost a third of the land surface today. From a carbon budget perspective, the terrestrial biosphere has been a carbon sink for at least the last six decades and has offset almost 1/3 of anthropogenic CO_2 emissions during that period (Le Quéré et al. 2016), but increases in vegetation productivity and carbon stocks have been responsible for at least part of the moderate or major CC impacts found today. So while some CC and LUC-driven ecosystem changes may be considered desirable from a human perspective they do contribute to pushing the terrestrial biosphere out of its Holocene state, and the Γ metric treats them no differently from other ecosystem changes generally perceived as negative.

Because of the limited availability of global, spatially resolved land use scenarios, this dissertation could not study the uncertainty of future LUC impacts as systematically as it did for climate uncertainty. Each RCP climate scenario was developed with only one associated LUC scenario. The RCP LUC scenarios cover a wide range of assumptions regarding future land use (Hurtt et al. 2011; van Vuuren et al. 2011a), but other land use patterns may well be compatible with the different RF levels of the RCPs. This means that LUC impacts associated with each RCP in this dissertation represent one possible — but not necessarily the most likely — option out of many. Complicating the matter, land use is closely linked to regional and global climate through a number of feedbacks such as (1) greenhouse gas emissions from deforestation or fertilizer use and CO_2 uptake by biomass plantations or afforestation which affect atmospheric composition, and (2) biogeophysical effects such as changes in albedo, moisture fluxes or surface roughness which directly affect temperature, precipitation and atmospheric transport (Feddema et al. 2005; Popp et al. 2010; Pitman et al. 2011; de Noblet-Ducoudré et al. 2012; Humpenöder et al. 2014). As illustrated by Figure VII.1, the magnitude of LUC impacts also depends on the underlying climate pattern, which in turn is affected by land use, meaning that land use scenarios cannot simply be interchanged without creating inconsistencies. To fully resolve these issues and still account for climate uncertainty would require running each land use scenario with each climate model.

Finally, while this dissertation accounted for scenario uncertainty in terms climate uncertainty and — to a limited extent — land use uncertainty there is also response uncertainty resulting from the choice of LPJmL as the only impact model used. DGVMs differ regarding the ecosystem processes that they include and, even for common ecophysiological processes such as photosynthesis, allocation, tissue turnover or mortality, how these processes are formulated (e.g. Friend et al. 2014; Thurner et al. 2017). Model intercomparisons such as the ongoing Inter-Sectoral Impact Model Intercomparison Project (ISIMIP, `http://www.isimip.org`) attempt to quantify this response uncertainty by running different impact models with harmonised settings and forcing data (e.g. Cramer et al. 2001; Sitch et al. 2008; Warszawski et al. 2014). Within ISIMIP, the Γ metric was applied to simulations from 7 DGVMs to assess CC impacts under the RCP scenarios in a setting without any land use (Warszawski et al. 2013; Piontek et al. 2014). Results show considerable response uncertainty across DGVMs although some of this is to be expected because of important differences in the included processes (e.g. dynamic vegetation composition: 4 out of 7 models; fire disturbance: 3 models;

permafrost: 3 models; nitrogen cycling: 2 models) (Warszawski et al. 2013). In a separate study ISIMIP showed that model agreement about CC impacts on agriculture varied from crop to crop (Rosenzweig et al. 2014). In both cases LPJmL results fell well within the range spanned by the other impact models, suggesting that overall the model does not represent a high or low outlier at the global scale.

LPJmL was selected for this dissertation because of its capability to simulate both natural vegetation and agricultural vegetation dynamics (including bioenergy plantations) with a relatively high process detail. In theory, a few other DGVMs offer similar functionality, although some of it was only implemented quite recently (e.g. Lindeskog et al. 2013; Osborne et al. 2015; Wu et al. 2016). From a practical standpoint, code availability and user support played just as important a role in model selection as model capabilities. Working with any DGVM is not a trivial task, and direct access to the principal LPJmL developers was invaluable in understanding the model, implementing some model changes required for the analyses conducted for this dissertation, and fixing bugs. Besides preparation time, the large number of simulations carried out also required substantial computing resources. Because of these points, using several DGVMs instead of just one would have been infeasible, especially in the confines of a dissertation project. Model intercomparison projects such as ISIMIP address this problem by relying on individual modelling groups to carry out the simulations — often on a voluntary basis — but also by reducing the number of requested simulations. In other words, extending the analysis to more than one DGVM would likely have meant that fewer GCMs and fewer scenarios could have been covered.

29.3. Outlook

The main source of uncertainty regarding the future extent of human transformation of the terrestrial biosphere appears to be the level of global warming. Reducing that uncertainty is foremost a climate policy problem: A global climate target has been set in the Paris Agreement with the stated goal of 'holding the increase in the global average temperature to well below 2 °C above pre-industrial levels and pursuing efforts to limit the temperature increase to 1.5 °C above pre-industrial levels' (UNFCCC 2016). However, national policies proposed so far appear insufficient to achieve that goal (Rogelj et al. 2016). Assuming that emissions reductions will be stepped up and warming will

be held below 2 °C future land use is a second large source of uncertainty in determining the fate of the biosphere. Recently developed new land use scenarios for the Shared Socioeconomic Pathways (SSPs, Riahi et al. 2017) suggest that the range of LUC scenarios compatible with a low warming target is not much smaller than the scenario range studied in this dissertation (Popp et al. 2017). The large scenario spread is caused by different assumptions regarding food and bioenergy demand, but also the level of agricultural intensification. While historically the focus of agricultural intensification has solely been on increasing crop production, this focus is shifting towards sustainable intensification which aims to increase production while reducing its negative side-effects (e.g. Godfray et al. 2010; Foley et al. 2011; Godfray and Garnett 2014; Clark and Tilman 2017; Rockström et al. 2017). LPJmL-based research is already contributing to the question of sustainable water use for agriculture (e.g. Jägermeyr et al. 2017). To account for nutrient limitation and leaching of excess nutrients, another major factor in agricultural intensification, LPJmL is currently being extended by a terrestrial nitrogen cycle. In addition to improving model skill in simulating crop productivity, the inclusion of nitrogen limitation is also expected to better constrain future productivity increases in natural ecosystems due to climate change and CO_2 fertilisation (Wieder et al. 2015; Kolby Smith et al. 2016). For the moment, LUC impacts in this dissertation are determined primarily by the fraction of land used, with only a small effect of agricultural management (see section D.2 for a sensitivity experiment). However, since the Γ metric is flexible in terms of the parameters describing ecosystem states it could be extended fairly easily to account for anthropogenic changes to the nitrogen cycle. Similar to its treatment of carbon cycle changes Γ could account for changes in nitrogen pools and fluxes. Such an extended setup would allow for a more systematic trade-off analysis between extensification and intensification of agriculture (Burney et al. 2010; Tilman et al. 2011; Johnson et al. 2014), carbon sequestration opportunities and environmental costs of bioenergy plantations and afforestation (Boysen et al. 2016; Smith et al. 2016), and provide a better estimate of the residual 'unavoidable' impacts of human interference with the biosphere.

Appendix

Appendix A.

Supporting information for A new climate dataset for systematic assessments of climate change impacts as a function of global warming[1]

Jens Heinke, Sebastian Ostberg, Sibyll Schaphoff, Katja Frieler, Christoph Müller, Dieter Gerten, Malte Meinshausen, and Wolfgang Lucht

[1] An edited version of this appendix has been published under the Creative Commons Attribution 3.0 License as Supplement to J. Heinke et al. 2013. 'A new climate dataset for systematic assessments of climate change impacts as a function of global warming.' *Geoscientific Model Development* 6 (5): 1689–1703. doi:10.5194/gmd-6-1689-2013

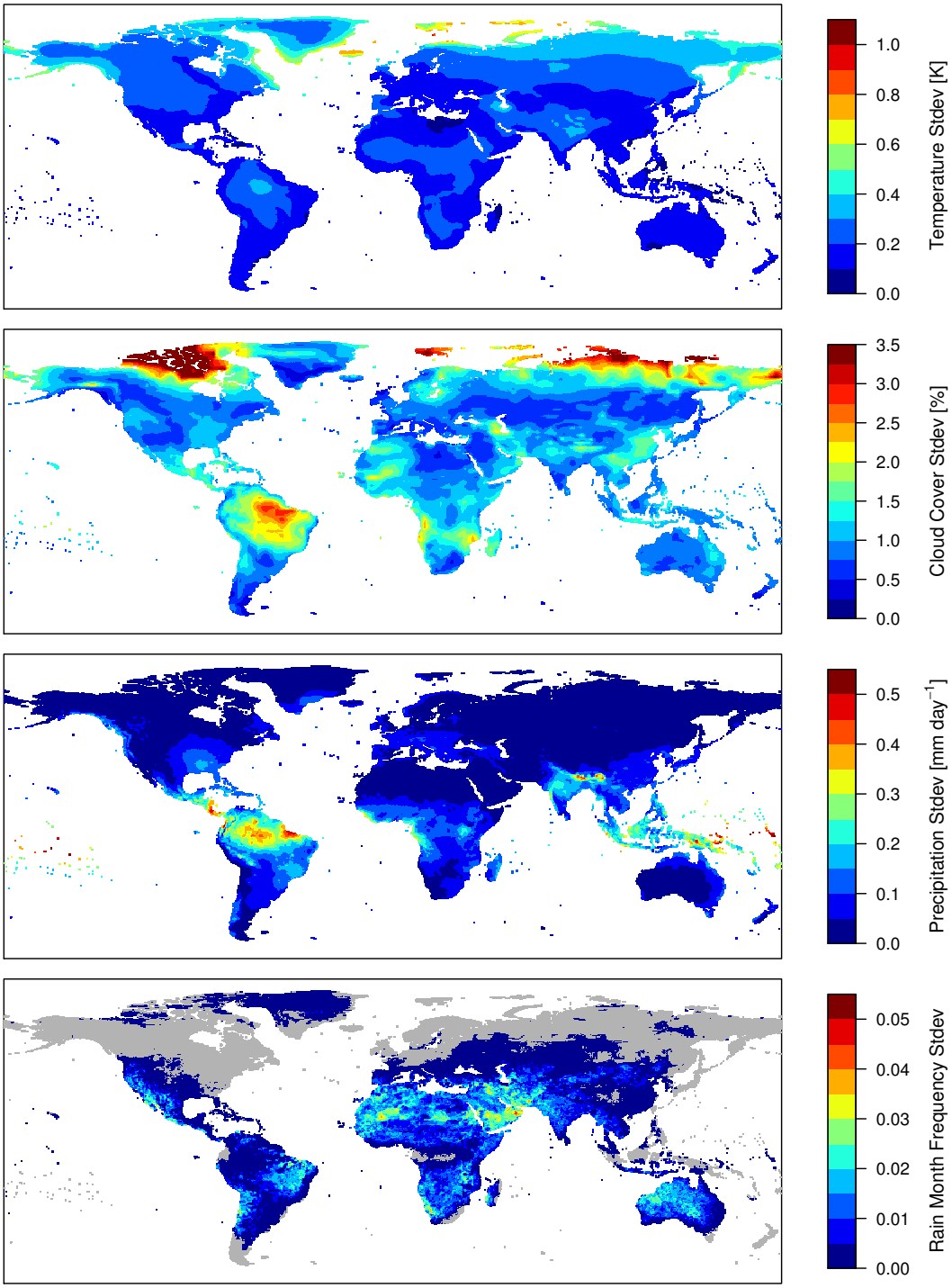

Figure A.1.: Inter-model standard deviation of mean annual change for a 1-degree increase in global mean temperature over all AOGCMs

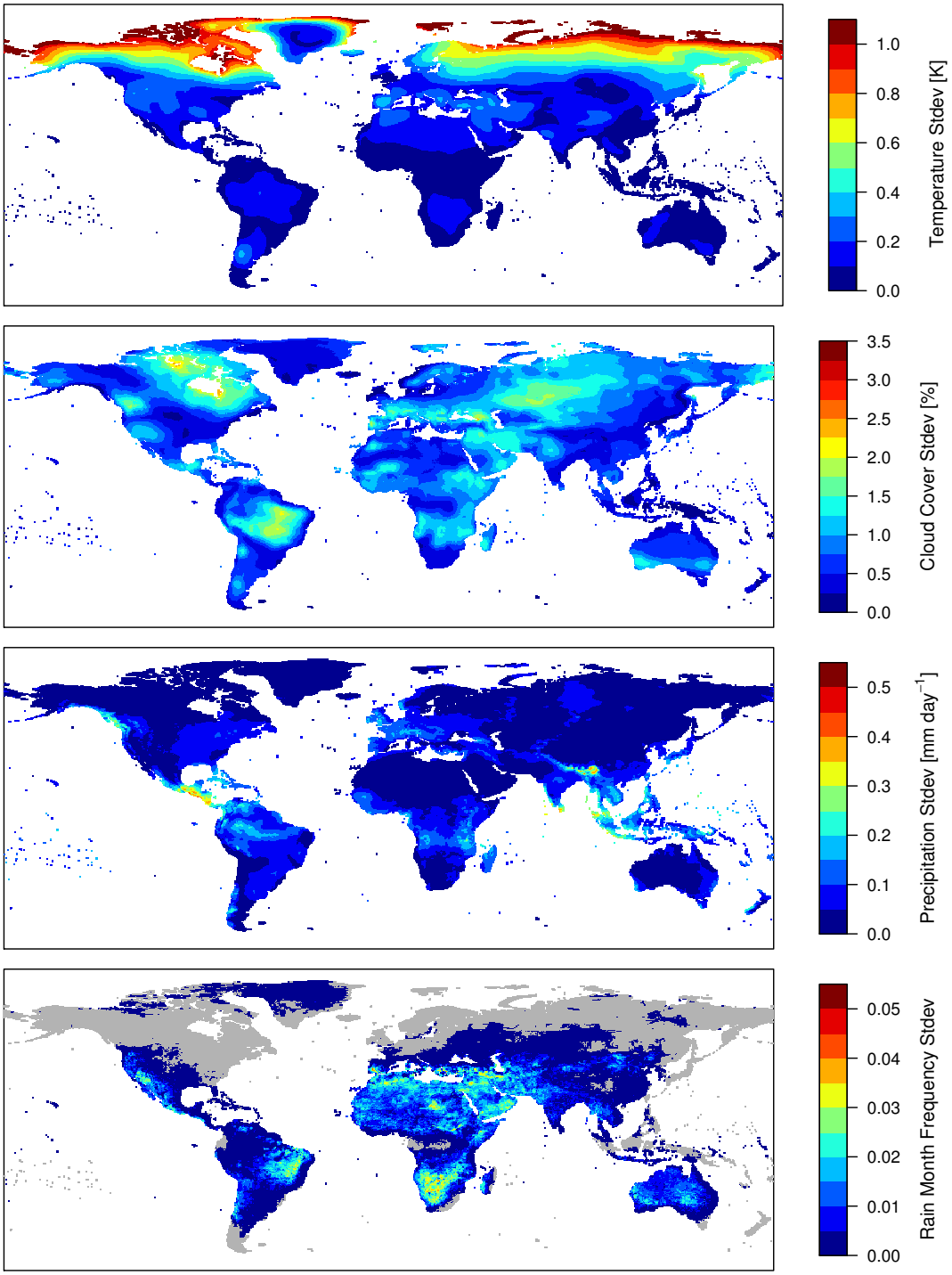

Figure A.2.: Seasonality of change for a 1-degree increase in global mean temperature expressed by the standard deviation of monthly mean anomalies (averaged over all AOGCMs)

Appendix B.

Supporting information for Critical impacts of global warming on land ecosystems[1]

Sebastian Ostberg, Wolfgang Lucht, Sibyll Schaphoff, and Dieter Gerten

B.1. Model settings and simulation protocol

All vegetation simulations are computed on a 0.5° by 0.5° spatial grid using monthly climate data to force LPJmL. Since the focus of this study is on natural vegetation, the modules for agriculture, represented by 12 crop-functional types (CFTs) (Bondeau et al. 2007), and biomass plantations, represented by three types of biomass production for bioenergy (Beringer et al. 2011), are switched off. Potential natural vegetation is simulated, represented by the nine plant-functional types (PFT) listed in Table B.1. The fire module has been modified to include fire carbon fluxes for the grass PFTs which in the standard version of the model are limited to tree PFTs. Fire resistance of grass is set to 0.5 meaning that leaf biomass may be reduced by up to 50% in a given year if conditions for fire (soil moisture and litter availability) are met. The change is made primarily to avoid infinite relative increases in fire carbon emissions in grasslands that are projected to experience woody encroachment in the future.

Table B.1.: Plant-functional types in LPJmL

Name	Abbreviation
Tropical broadleaved evergreen tree	TrBE
Tropical broadleaved raingreen tree	TrBR
Temperate needleleaved evergreen tree	TeNE
Temperate broadleaved evergreen tree	TeBE
Temperate broadleaved summergreen tree	TeBS
Boreal needleleaved evergreen tree	BoNE
Boreal summergreen tree (primarily broadleaved, but including larch)	BoS
C3 grass	C3
C4 grass	C4

The model is spun up for 10 020 years using pre-industrial atmospheric CO_2 concentrations (280 ppmv) and cycling the first 30 years of the historical climatological data (CRU/GPCC, see chapter 11 *Climate uncertainty* in Part III) repeatedly to allow vegetation structure and carbon pools to reach equilibrium. The spin-up is followed by a transient run from 1901 to the end of 2009 using the full CRU/GPCC climate time series and observed atmospheric CO_2 concentrations. The last 30 years of the historical run (1980–2009) provide the reference state from which ecosystems diverge under projected climate change. All 152 climate scenario runs are started from the same reference state and forced by the climate scenario data, running from 2010 to 2115. A specific atmospheric CO_2 concentration trajectory, provided by the MAGICC6 model, is used for each of the 8 GMT trajectories. The last 30 years of the scenario period provide the future state that is compared to the reference state.

Vegetation simulations cover a total of 133 million km^2 or about 90% of the Earth's land surface, excluding areas permanently covered in ice like Antarctica and most of Greenland. About 41.7 million km^2 or 31% of the simulated area are classified as agricultural areas (cropland, pasture and managed grassland, Figure B.1) and not considered in the analysis. Agricultural areas are based on MIRCA2000 (Portmann et al. 2010), as modified by Fader et al. (2010). This leaves a total base area of 91.6 million km^2. Almost 86% of this base area is covered with natural to semi-natural vegetation during the reference period, while the rest is classified as non-vegetated (primarily desert and

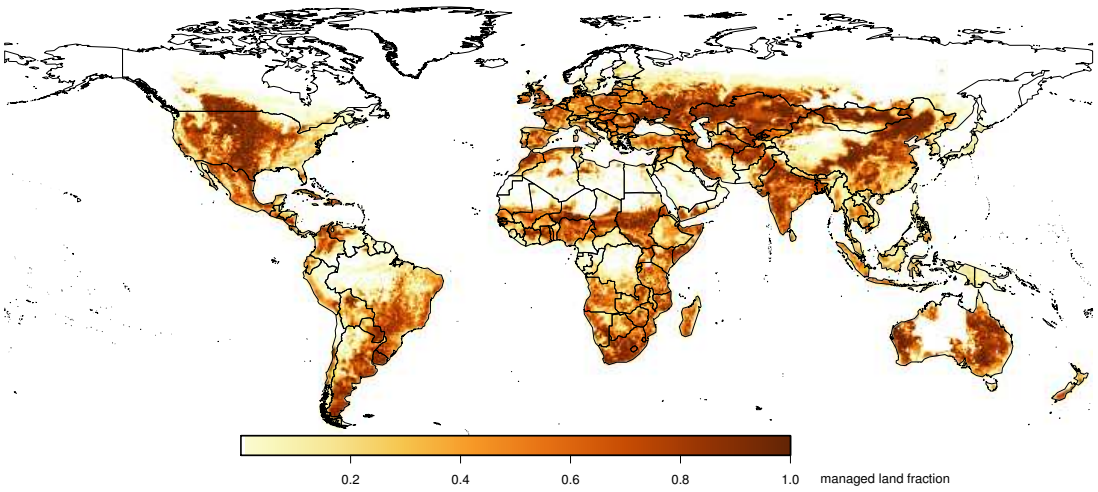

Figure B.1.: Fraction of each grid cell used as crop land or managed grassland.

some tundra regions in Figure B.3).

The Γ metric is computed for each grid cell for all 152 scenario runs based on the model parameters in Table III.1 in Part III. In summing up affected areas across grid cells each grid cell area is reduced by its agricultural area fraction. Global mean values of the model parameters, used to compute the global importance component in Γ, are derived as area-weighted means, using only the non-agricultural area of each cell. Since our study investigates climate change effects, not land use change effects, land use patterns are kept constant in the future assuming no further anthropogenic conversion of natural ecosystems.

B.2. Vegetation-structural changes

Changes in vegetation structure ΔV are one component of the change metric Γ. To compare vegetation structure between a future ecosystem state and present-day conditions we use a modified version of the ΔV metric developed by Sykes et al. (1999), adapted to the PFTs simulated by LPJmL (Table B.1). The metric measures the difference in vegetation structure in terms of the importance of broad life form types (grass, trees, bare ground), further characterised by their assigned attributes.

$$\Delta V(i,j) = 1 - \sum_k \left\{ \min(V_{ik}, V_{jk}) * \left[1 - \sum_l (\omega_{kl} * |a_{ikl} - a_{jkl}|) \right] \right\}$$

V_{ik} and V_{jk} describe the area fractions covered by life form k in ecosystem i and j, a_{ikl} and a_{jkl} are the attributes l of lifeform k in ecosystem i and j, respectively. Attributes are weighted for each life form by ω_{kl}. Attributes can be climatic (tropical, temperate, boreal), or phenologic (evergreen, deciduous) or describe leaf types (needleleaved, broadleaved).

Table B.2 lists modelled PFTs categorised into life forms tree and grass, together with their assigned attributes. The remaining area fraction not covered by any PFT is considered bare ground, without any further attributes.

Table B.2.: Plant-functional types with their assigned attributes. For PFT abbreviations see Table B.1

Lifeform	**Attributes**			
Tree:	**Evergreenness**	**Needleleavedness**	**Tropicalness**	**Borealness**
TrBE	1	0	1	0
TrBR	0	0	1	0
TeNE	1	1	0	0
TeBE	1	0	0	0
TeBS	0	0	0	0
BoNE	1	1	0	1
BoS	0	0.25*	0	1
(attribute weights:	0.2	0.2	0.3	0.3)

Grass:	**Tropicalness**
C3 grass	0
C4 grass	1
(attribute weights:	0.3)

* BoS primarily represents broadleaved trees, but includes larchs.

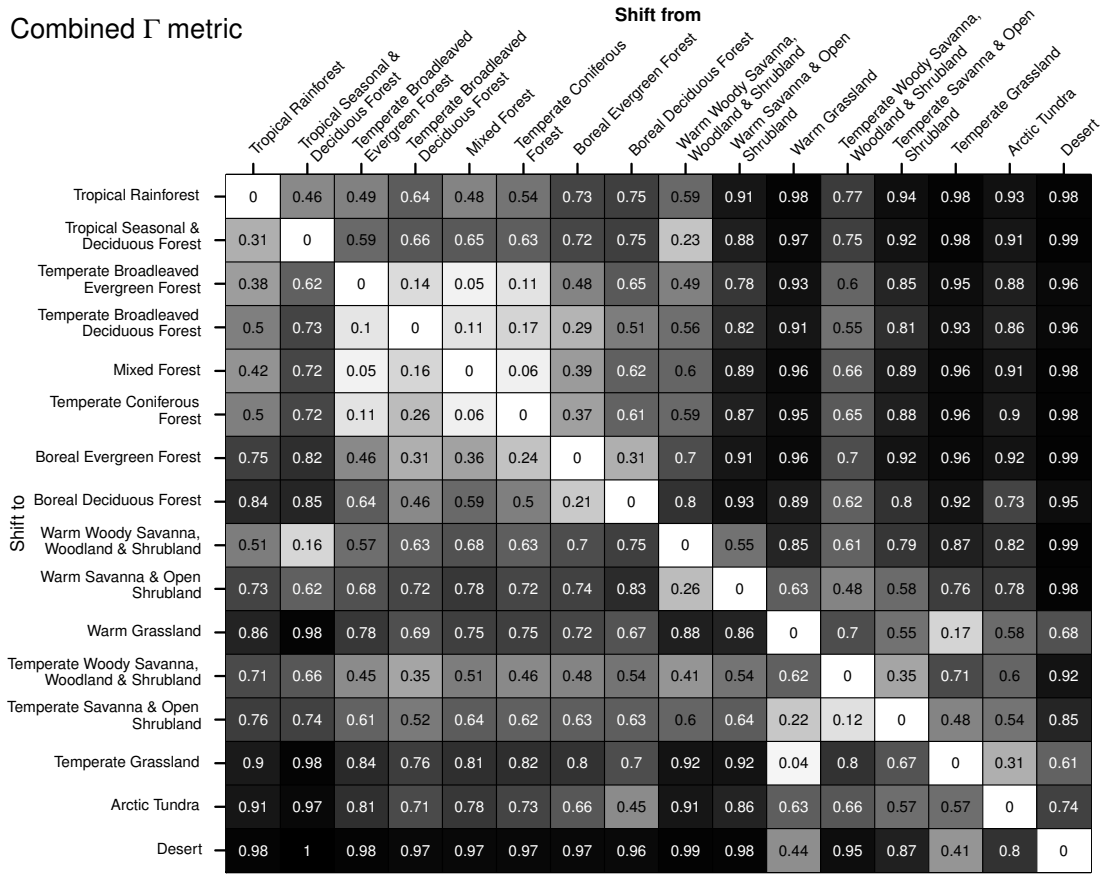

Figure B.2.: Illustrative Γ values for a complete transformation between present-day biomes

B.3. Illustrative examples of the change metric

We compute Γ values for hypothetical transformations between present-day biomes, using the biome classification below. To compare biomes, all LPJmL outputs used to compute the metric (Table III.1 in Part III) are averaged over all grid cells of each biome. Biome means of all parameters are then used to describe two different biomes as hypothetical states of the same biome. Interannual variability during the reference period (required for the change to variability ratio S in Equation III.1 in Part III) is computed for each grid cell and then averaged over all biome cells instead of estimating it from averaged LPJ outputs. The table in Figure B.2 is not symmetric because for the local change component c and ecosystem balance b changes are normalised to the reference state (which is different depending on whether biome i shifts into biome j or

Table B.3.: Example of Γ components in biome transformation. For definitions of the components see Part III.

Biome transformation	Γ	**ΔV**	c	$S(c,\sigma_c)$	g	$S(g,\sigma_g)$	b	$S(b,\sigma_b)$
Tropical Rainforest ⇒ Tropical Seasonal & Deciduous Forest	0.31	0.04	0.31	1	0.72	1	0.16	0.97
Tropical Seasonal & Deciduous Forest ⇒ Tropical Rainforest	0.46	0.04	0.93	1	0.72	0.86	0.25	1
Arctic Tundra ⇒ Boreal Deciduous Forest	0.73	0.81	1	1	0.34	1	0.80	1
Boreal Deciduous Forest ⇒ Arctic Tundra	0.45	0.81	0.45	1	0.34	1	0.20	0.98

biome j shifts into biome i). In addition, c, g and b are scaled by a factor S representing the natural state variability of the original biome. $S(g,\sigma_g)$ may differ even though g is identical. The correct reading direction for Figure B.2 is that biomes listed on the horizontal axis shift into biomes listed on the vertical axis. For quick visual reference, the table background is shaded based on Γ values (from white, $\Gamma = 0$, to black, $\Gamma = 1$).

Table B.3 uses the example of a change between the two tropical forest biomes and between a boreal forest and a tundra to illuminate why Γ depends on the direction of change.

B.3.1. Biome classification scheme

The biome classification used in this study is based primarily on the composition of PFTs modelled in LPJmL, except for the tundra biome which is based on a temperature limit. The classification uses a sequence of simple rules such as total vegetation cover to delineate deserts, and increasing tree cover to differentiate between grasslands, savannas, woody savannas and forests. Forests are categorised further based on the dominant tree PFT. For tropical forests, the classification includes an additional biomass limit. Figure B.3a shows a map of present-day biomes derived from LPJmL output for the reference period 1980–2009. Figure B.4 illustrates the classification rules.

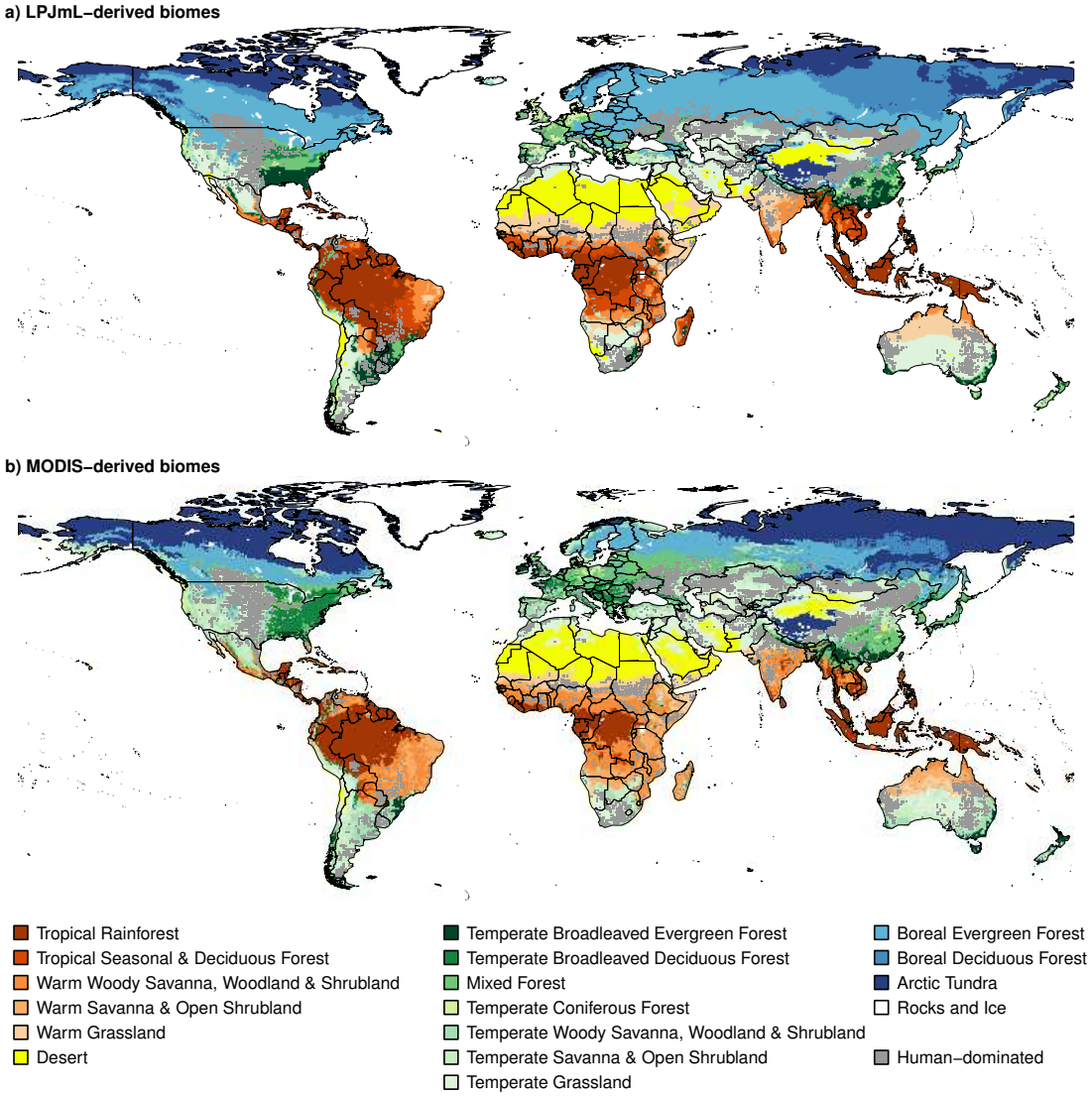

Figure B.3.: Present-day biome classification derived from a) LPJmL results and b) MODIS land cover data. Grid cells with more than 80% cropland and pasture are marked as human-dominated.

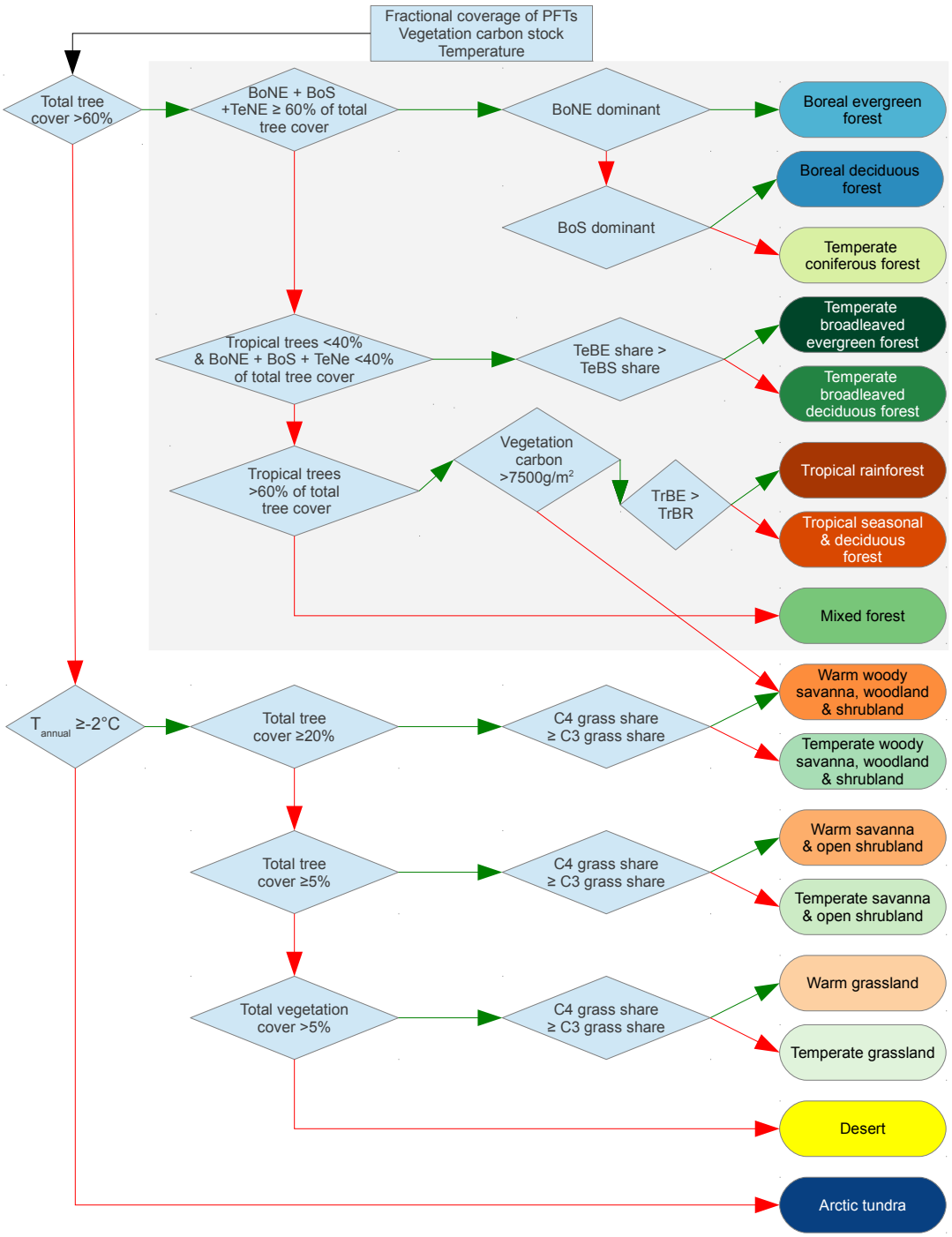

Figure B.4.: Biome classification scheme. Each rhombus represents a classification rule. Classification starts in the upper left corner and proceeds through the rule chain based on whether a rule is fulfilled (green arrow) or not (red arrow). For PFT abbreviations see Table B.1

B.4. Discussion of modelled vegetation dynamics

The biome distribution in Figure B.3a is a result of bioclimatic limits and modelled vegetation dynamics as PFTs in LPJmL compete for space and resources. While the processes controlling competition among PFTs are difficult to validate, it is possible to compare the resulting vegetation composition to observations. We use MODIS land cover data and apply the biome classification scheme described above. The Land Cover Type Yearly Climate Modelling Grid Version 5 (short name: MCD12C1)[2] distinguishes 17 land cover classes defined by the International Geosphere Biosphere Programme (IGBP), which includes 11 natural vegetation classes, 3 developed and mosaicked land classes, and 3 non-vegetated land classes (Table B.4). In order to compare actual land cover as derived from MODIS satellite imagery with potential natural vegetation as simulated by LPJmL, some modifications are necessary to remove human land use from the MODIS data. Since there is no distinction between natural and anthropogenic grasslands, MODIS grassland fractions are reduced by the managed grassland fraction used to mask grid cell areas in LPJmL (see *Model settings and simulation protocol* above). In addition, the 3 developed and mosaicked land classes as well as the water and the snow and ice class are discarded and fractional cover of the remaining classes is scaled up accordingly. Bioclimatic limits as implemented in LPJmL are used to map MODIS forest classes to LPJmL tree PFTs and to distinguish between C3 and C4 grass. Without further information on tree composition in the MODIS mixed forest, shrubland and savanna classes, tree cover from these classes is distributed equally to the 2 dominant tree PFTs.

Overall, there is good agreement between the biomes derived from LPJmL and MODIS (Figure B.3). LPJmL simulates more forest and less savanna in tropical Africa and South America. There is continuing debate on the mechanisms controlling the persistence of grass-tree mixtures in savannas, including resource competition, fire, herbivory and rainfall variability (Sankaran et al. 2004). Some of these processes, such as herbivory, cannot be reproduced in the model. Others like rainfall variability depend heavily on the quality of the climate data used, with limited availability of station data especially in central Africa possibly affecting accuracy (Rudolf et al. 2010). On the other hand, the

[2]NASA Land Processes Distributed Active Archive Center (LP DAAC). MODIS MCD12C1. USGS/Earth Resources Observation and Science (EROS) Center, Sioux Falls, South Dakota. 2008.

Table B.4.: MODIS land cover classes. To derive biomes, classes are redistributed as percentage tree and grass cover and mapped to LPJmL PFTs. For PFT abbreviations see Table B.1

MODIS class	**Re-mapped to**		
	% tree	**% grass**	**PFTs**
Water	0	0	discarded
Evergreen Needleleaf Forest	95	5	trees: TeNE, BoNE, grass: C3, C4
Evergreen Broadleaf Forest	95	5	trees: TrBE, TeBE, grass: C3, C4
Deciduous Needleleaf Forest	95	5	trees: BoS, TrBR[(1)], TeNE[(1)], grass: C3, C4
Deciduous Broadleaf Forest	95	5	trees: TrBR, TeBS, grass: C3, C4
Mixed Forests	95	5	trees: dominant tree PFTs, grass: C3, C4
Closed Shrublands	80	20	trees: dominant tree PFTs, grass: C3, C4
Open Shrublands	5	95	trees: dominant tree PFTs, grass: C3, C4
Woody Savannas	50	50	trees: dominant tree PFTs, grass: C3, C4
Savannas	10	90	trees: dominant tree PFTs, grass: C3, C4
Grasslands[(2)]	0	100	C3, C4
Permanent Wetlands	0	100	C3, C4
Croplands	0	0	discarded
Urban and Built-Up	0	0	discarded
Cropland/Natural Vegetation Mosaic	20	0	discarded
Snow and Ice	0	0	discarded
Barren or Sparsely Vegetated	0	2.5	C3, C4

[(1)] There are no direct equivalents of deciduous needleleaved PFTs for tropical and temperate climates, so the closest match is used.

[(2)] MODIS grassland fraction reduced by managed grassland fraction

discrepancies between MODIS and LPJmL are mostly found in regions with considerable human land use (compare Figure B.1), where there is also greater uncertainty regarding the MODIS-derived biome class.

The transition zone between boreal forest and tundra is another region of disagreement between MODIS and LPJmL. Boreal trees extend farther north in LPJmL because the model version used in this study does not include permafrost. A new development version including permafrost dynamics shows better results for this region.

There are also differences regarding the dominant tree types in some forests. MODIS data suggest a higher fractional coverage of temperate broadleaved deciduous trees than

simulated by LPJmL. It is unclear how much of this disagreement is an artefact of the re-classification algorithm.

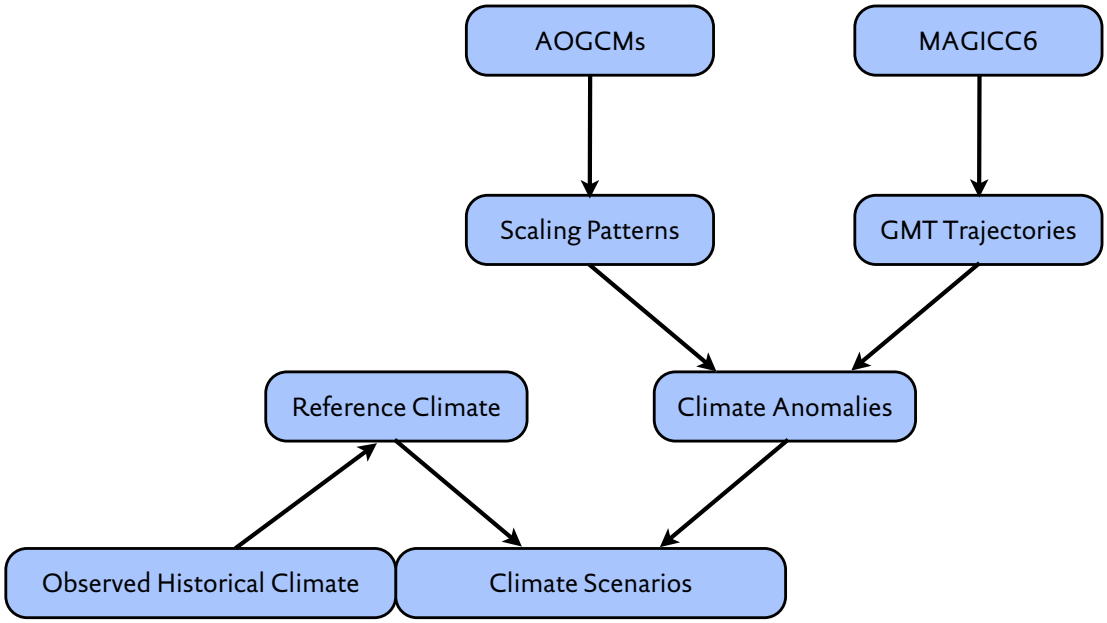

Figure B.5.: Flow chart of data processing for the generation of the 'PanClim' climate scenarios. Source: Heinke et al. (2013)

B.5. Projected risk of ecosystem changes across biomes

In addition to the globally affected areas from Figure III.1 in Part III, Figure B.6 presents results differentiated by biomes. Areas are classified based on present-day vegetation (Figure B.3a). Areas of ecosystems projected to shift to a different biome type under climate change are still grouped according to their present-day biome classes.

For the sake of readability, Figure III.3 in Part III uses a reduced number of biome classes. The biomes 'Warm Woody Savanna, Woodland & Shrubland' and 'Warm Savanna & Open Shrubland' are grouped as 'Warm Savanna & Shrubland', 'Temperate Woody Savanna, Woodland & Shrubland' and 'Temperate Savanna & Open Shrubland' are grouped as 'Temperate Savanna & Shrubland', and 'Temperate Broadleaved Deciduous Forest' and 'Mixed Forest' are grouped as 'Temperate Summergreen & Mixed Forest'.

Figure B.7 shows the dimensions of change for all 16 biome classes. It is the full version of Figure III.4 in Part III.

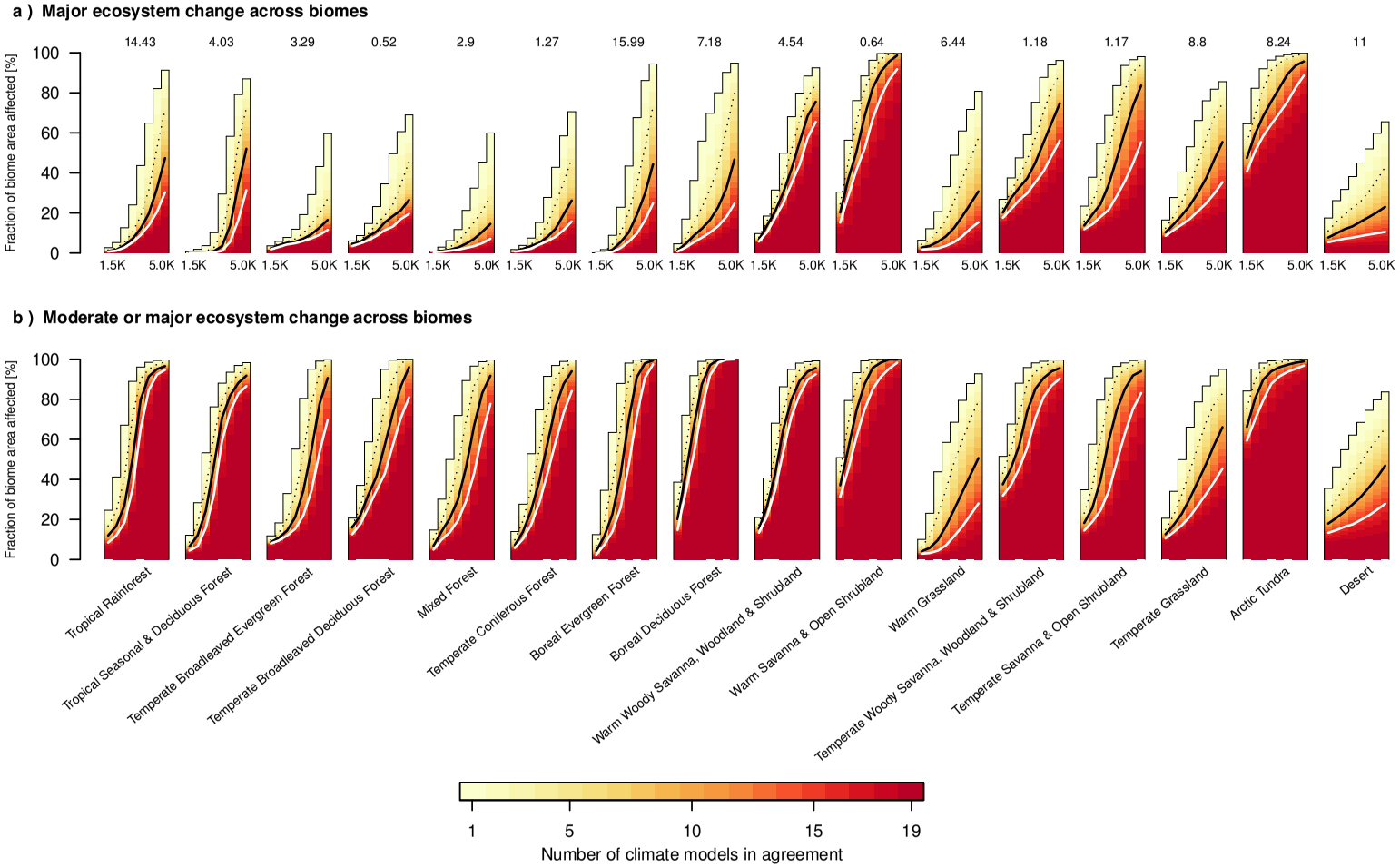

Figure B.6.: Climate uncertainty of areas at risk by biome. 8 Bars per biome refer to the 8 warming levels (1.5 K to 5 K left to right). Solid white, black and dotted black lines mark areas affected with high, medium and low confidence, respectively. Numbers above each biome list total biome area in 10^6 km^2 during the reference period.

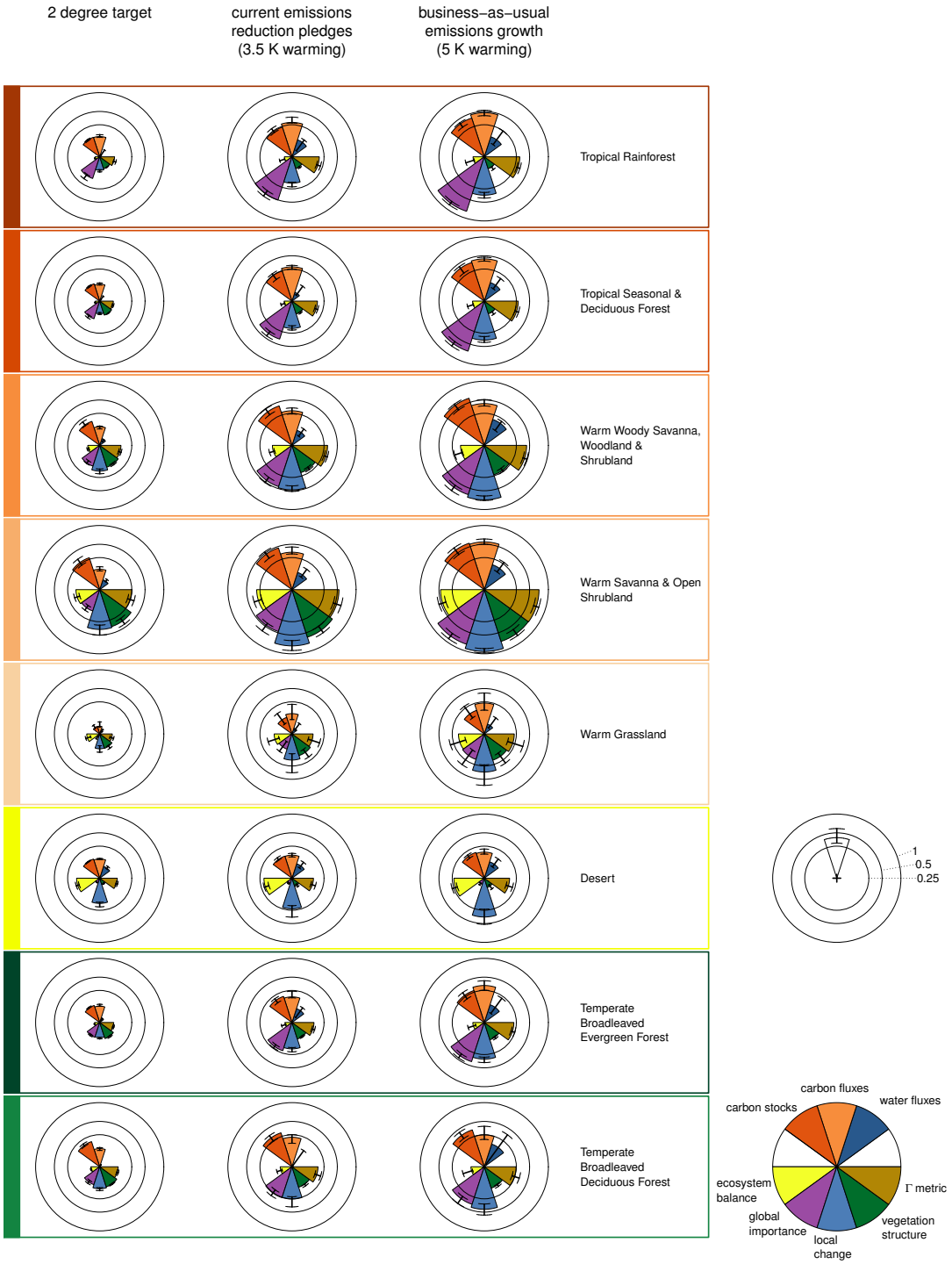

Figure B.7.: Dimensions of ecosystem change for biomes. For definitions of the variables see Figure III.4 in Part III. Biome colours correspond to maps in Figure B.3

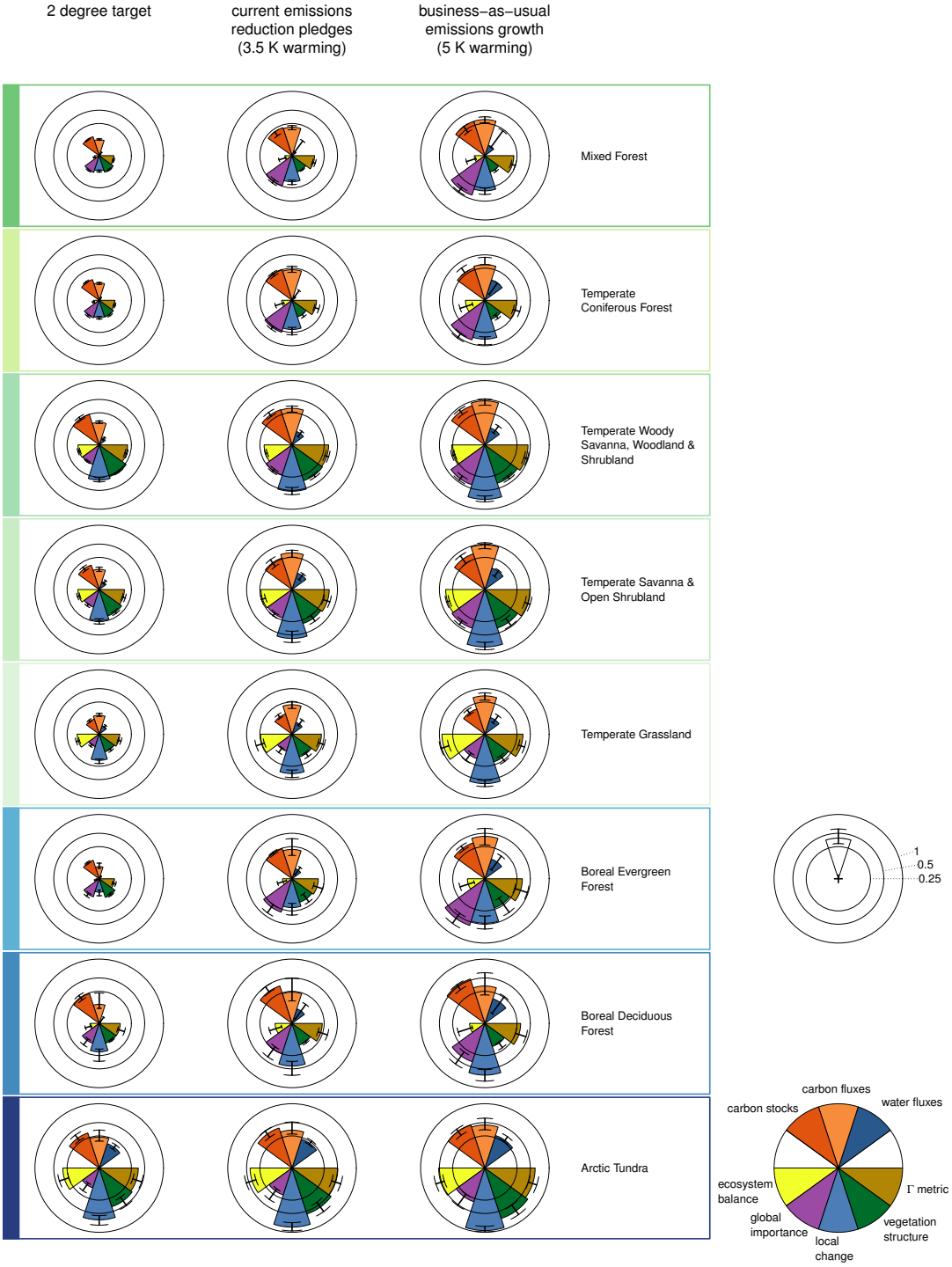

Figure B.7.: Dimensions of ecosystem change for biomes (continued).

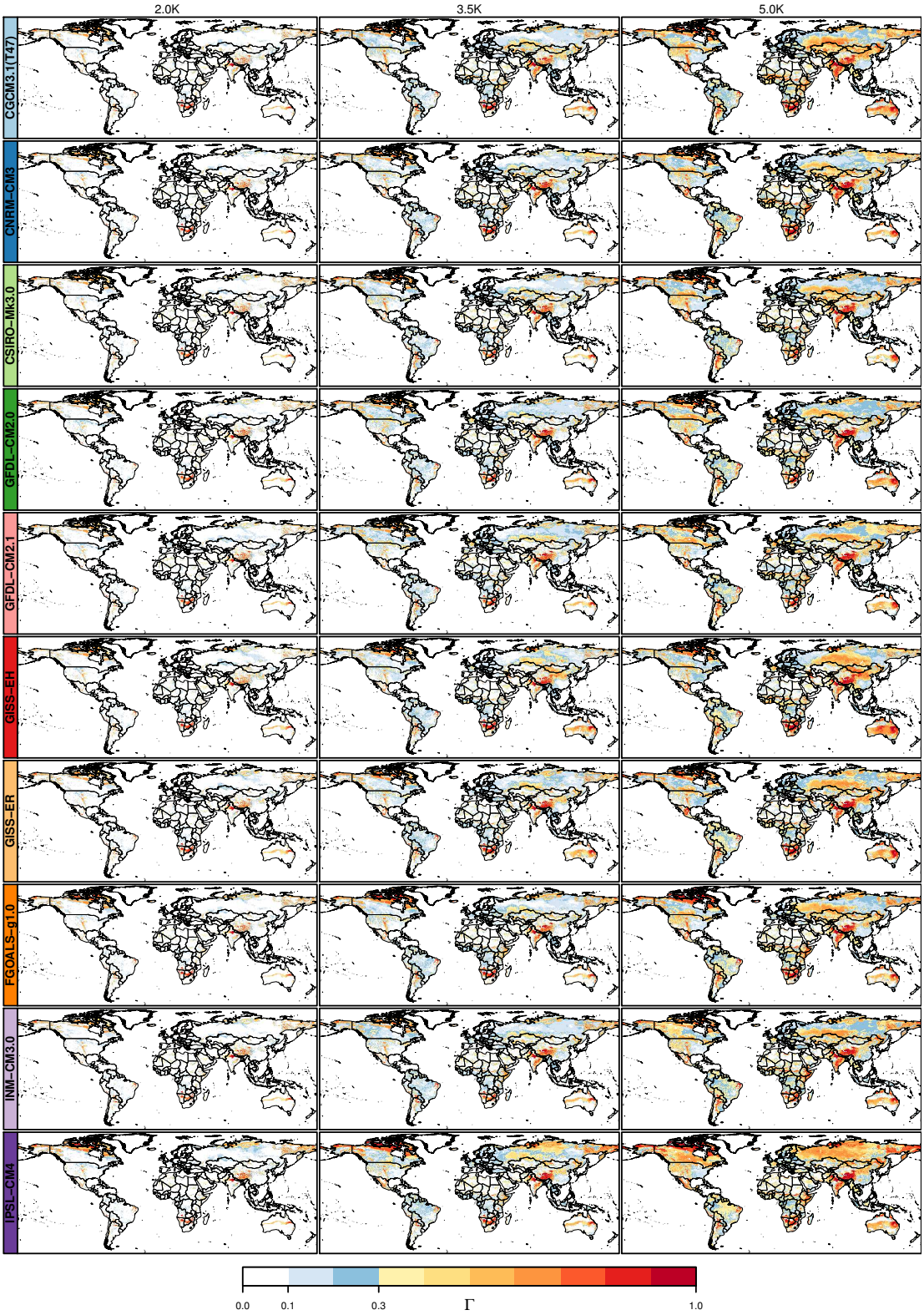

Figure B.8.: Maps of Γ values from individual simulation runs, grouped by AOGCM (rows) and warming level (columns). Colour coding of models corresponds to Figure III.5 in Part III.

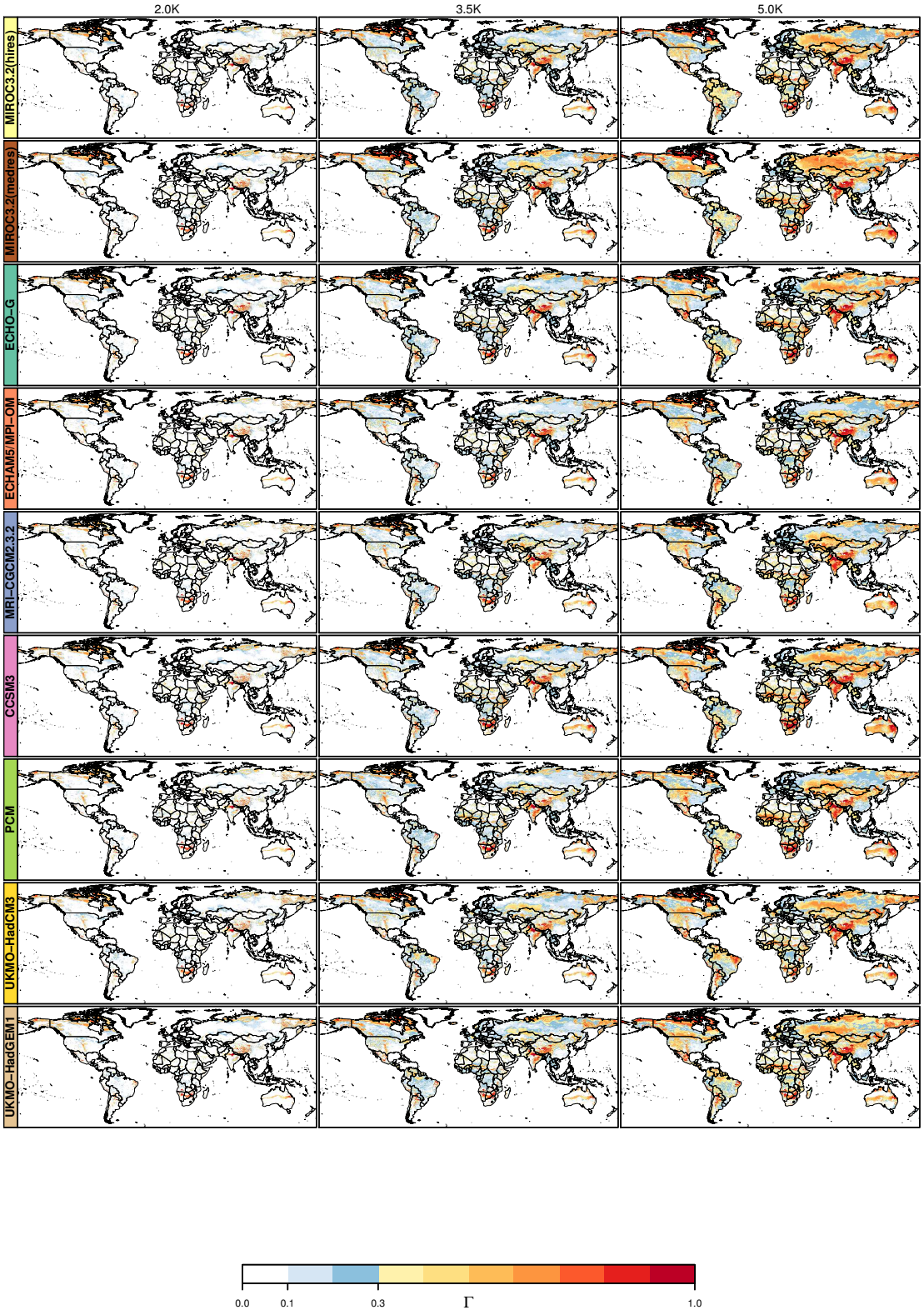

Figure B.8.: Maps of Γ values from individual simulation runs (continued).

Appendix C.

Supporting information for Asynchronous exposure to global warming: freshwater resources and terrestrial ecosystems[1]

Dieter Gerten, Wolfgang Lucht, Sebastian Ostberg, Jens Heinke, Martin Kowarsch, Holger Kreft, Zbigniew W. Kundzewicz, Johann Rastgooy, Rachel Warren, and Hans Joachim Schellnhuber

[1]An edited version of this appendix has been published under the Creative Commons Attribution 3.0 License as Supplementary data to D. Gerten et al. 2013. 'Asynchronous exposure to global warming: freshwater resources and terrestrial ecosystems.' *Environmental Research Letters* 8 (3): 034032. doi:10.1088/1748-9326/8/3/034032

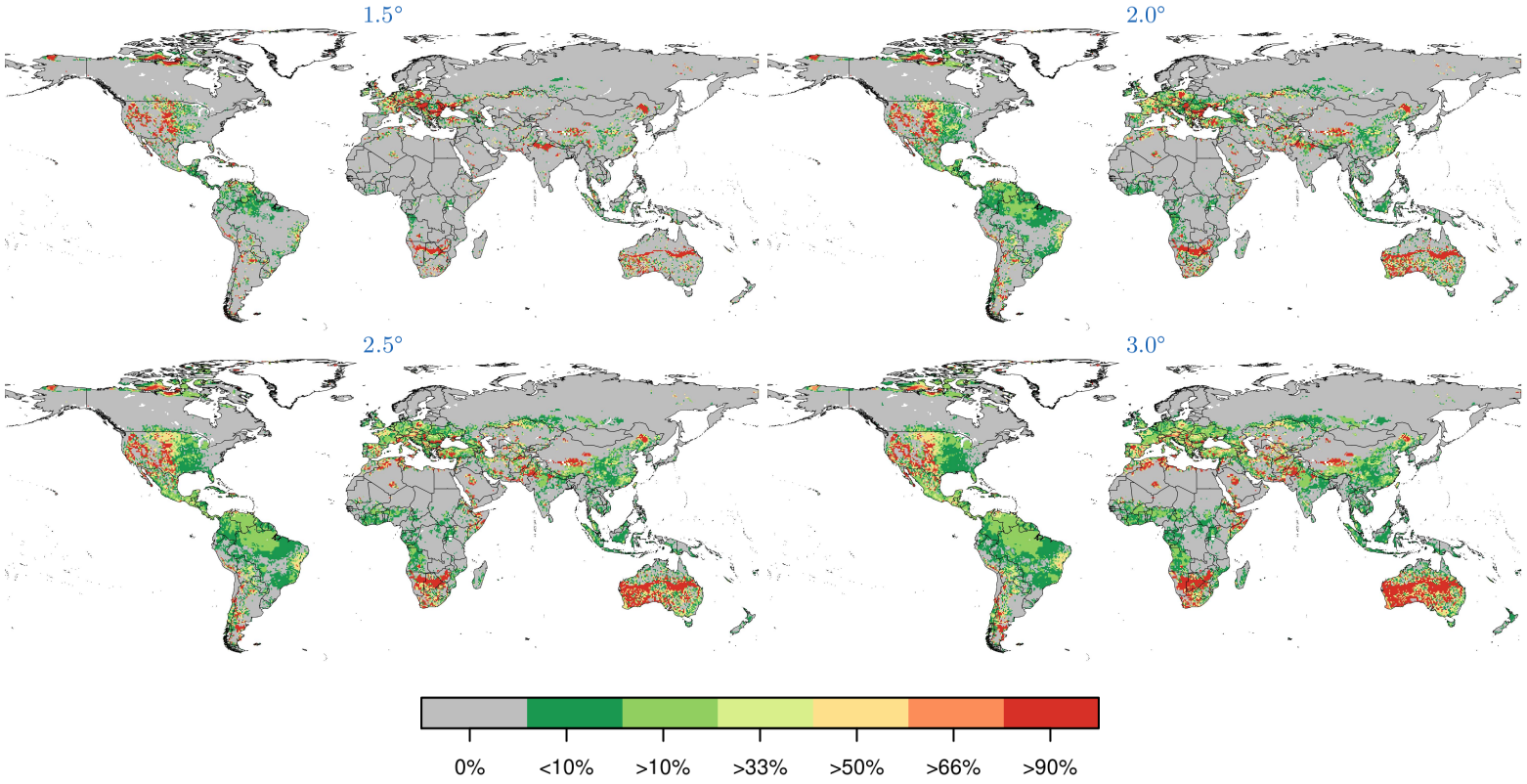

Figure C.1.: Likelihood (derived from the 19 GCM patterns) of a decrease in water resources for each of the eight ΔT_g levels. Shown is whether the decrease in average annual runoff exceeds its present standard deviation, or whether monthly runoff will >10% more frequently fall below its present median.

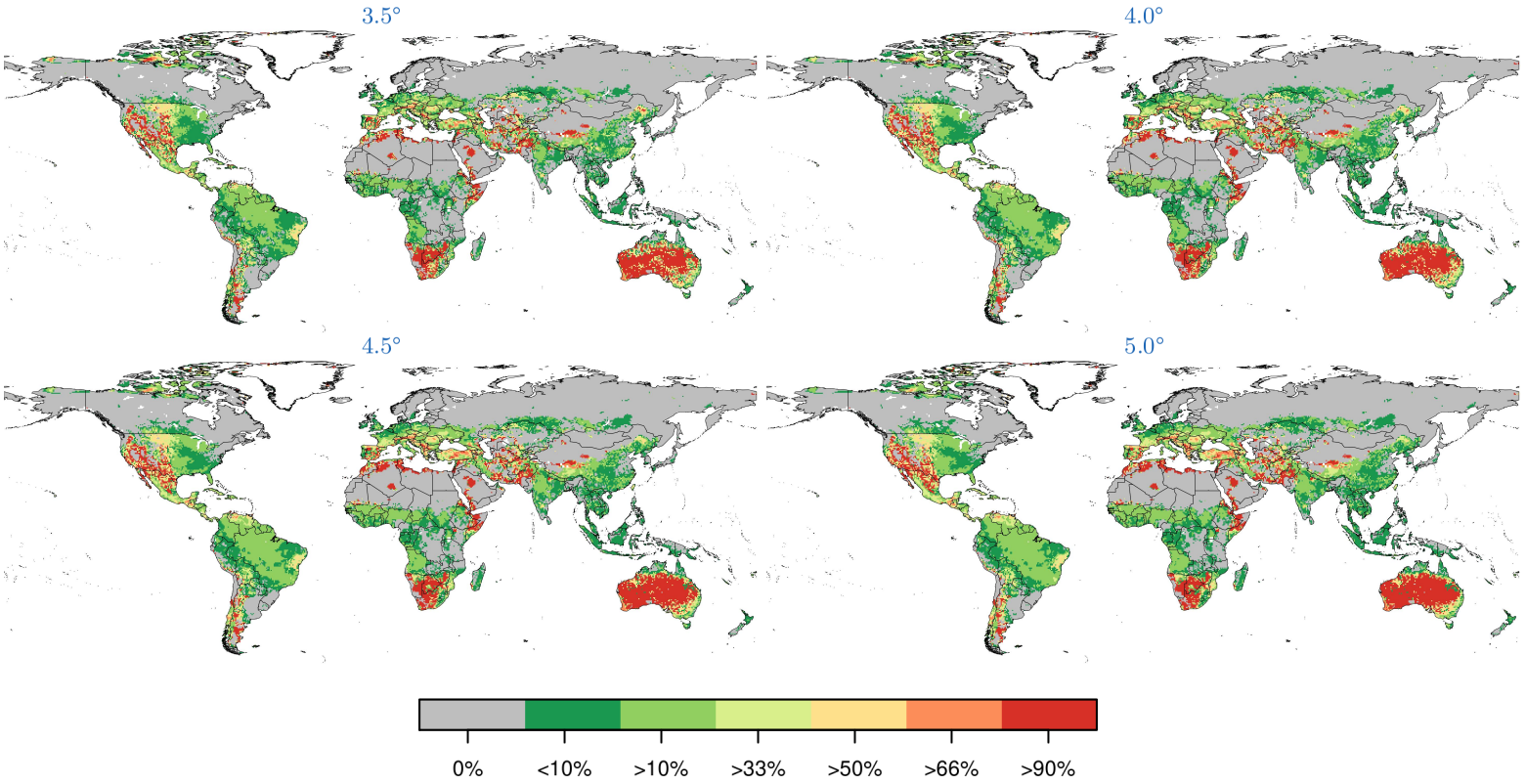

Figure C.1.: Likelihood of a decrease in water resources for each of the eight ΔT_g levels (continued).

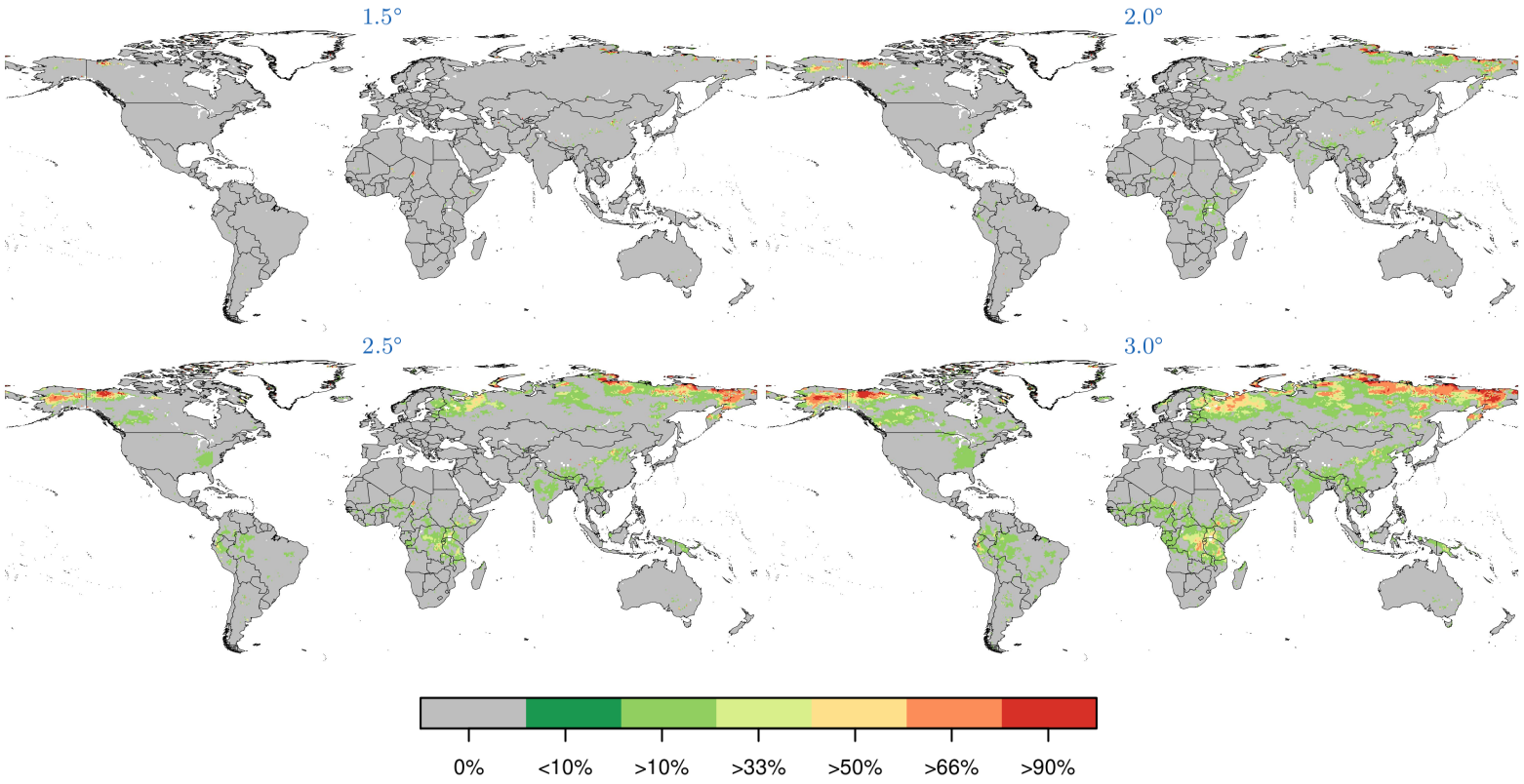

Figure C.2.: Likelihood (derived from the 19 GCM patterns) of an increase in water resources for each of the eight ΔT_g levels. Shown is whether the increase in average annual runoff exceeds its present standard deviation, or whether monthly runoff will >10% more frequently exceed its present median value.

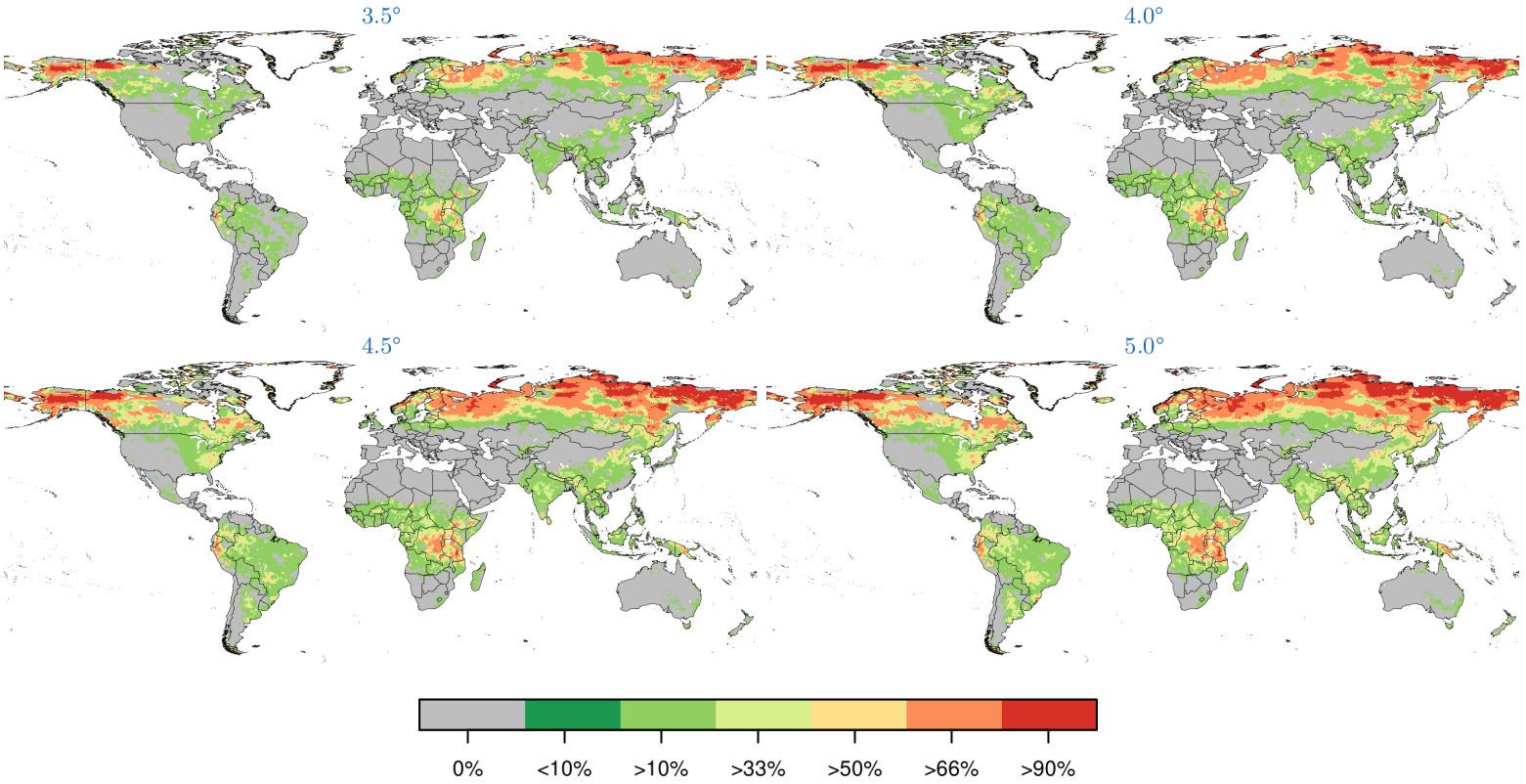

Figure C.2.: Likelihood of an increase in water resources for each of the eight ΔT_g levels (continued).

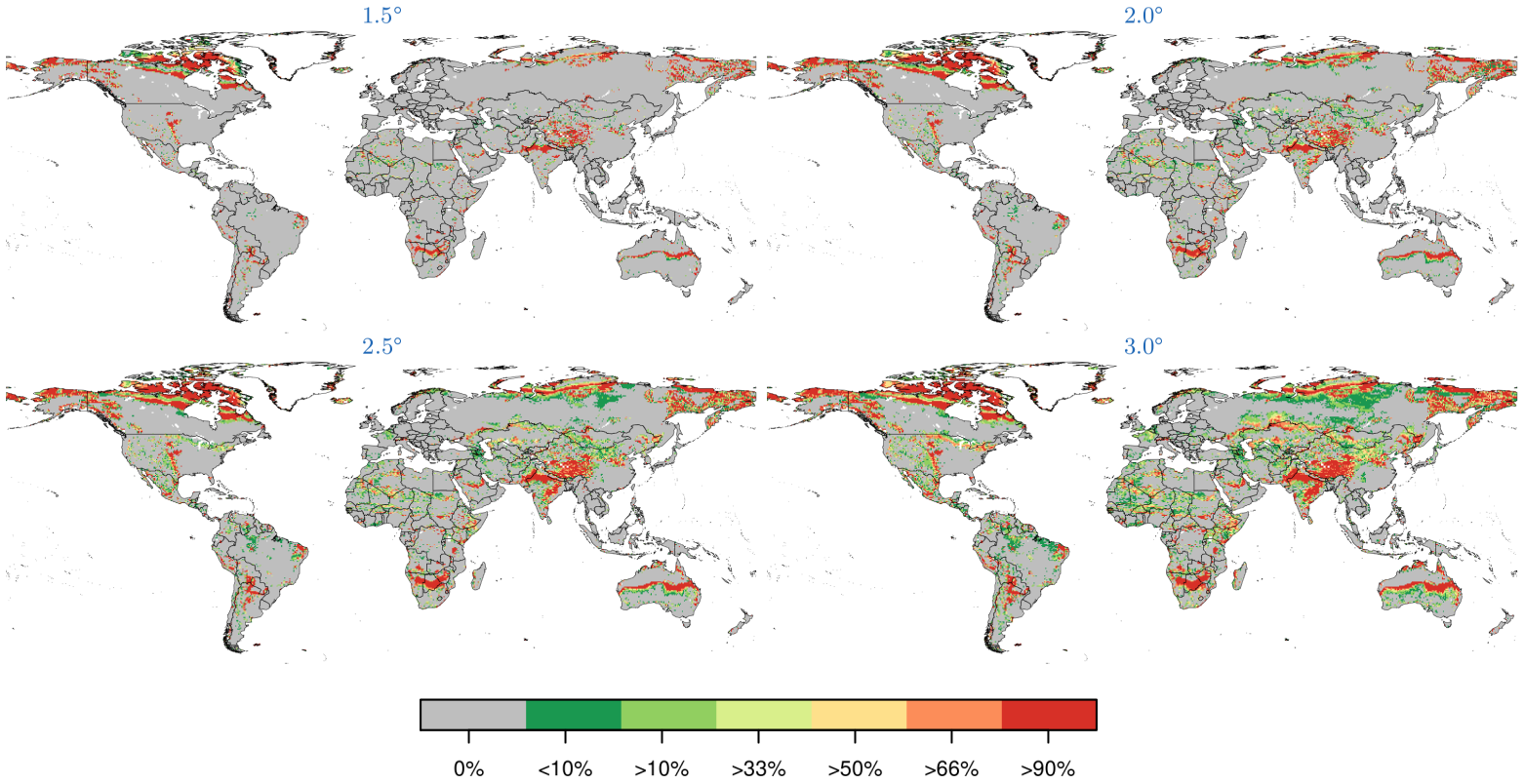

Figure C.3.: Likelihood (derived from the 19 GCM patterns) of severe ecosystem change ($\Gamma > 0.3$) for each of the eight ΔT_g levels. See Figure C.4 for a variant of this figure, aggregated for the biogeographic zones.

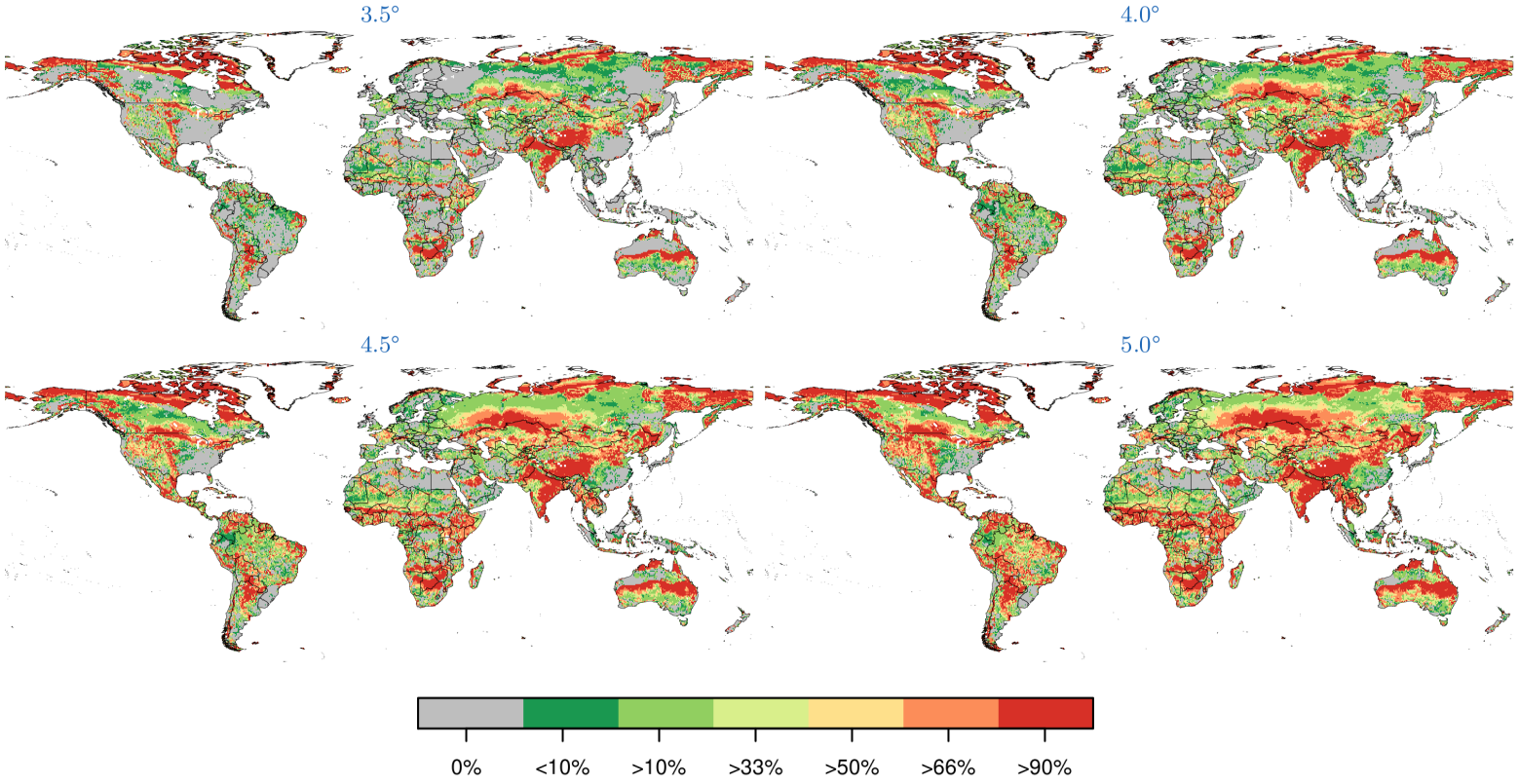

Figure C.3.: Likelihood of severe ecosystem change ($\Gamma > 0.3$) for each of the eight ΔT_g levels (continued).

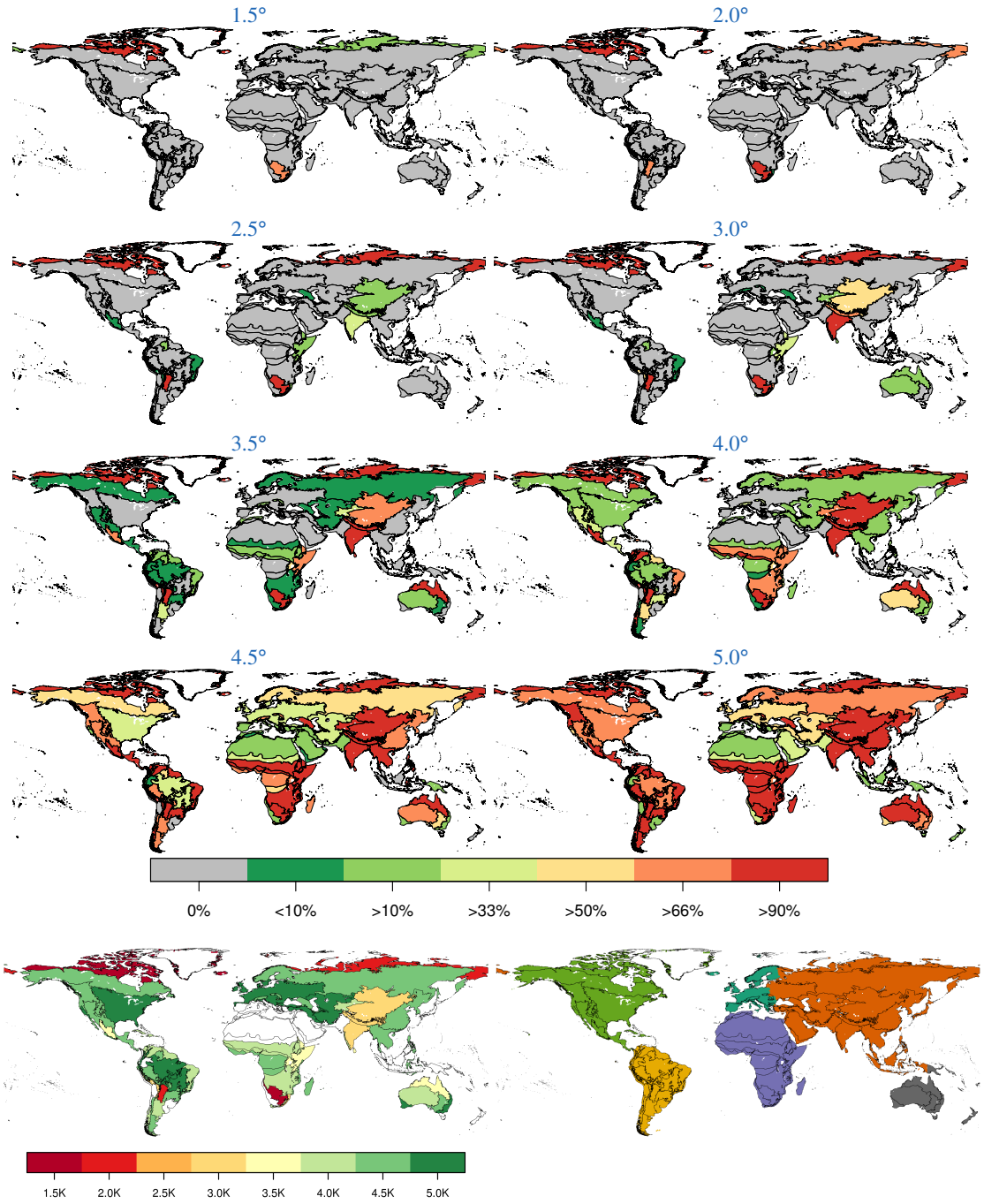

Figure C.4.: Likelihood that $> 33\%$ of the areas of biogeographic regions are subjected to severe ecosystem transformation ($\Gamma > 0.3$), for each ΔT_g level. The two maps at the bottom show the corresponding ΔT_g level at which this change first occurs with $> 50\%$ confidence (left), and the distribution of the 90 biogegeographic regions across the continents (right) as used for Figures IV.1(b) and C.6(b) and (d). As in the other figures, likelihoods are derived from the 19 GCM patterns.

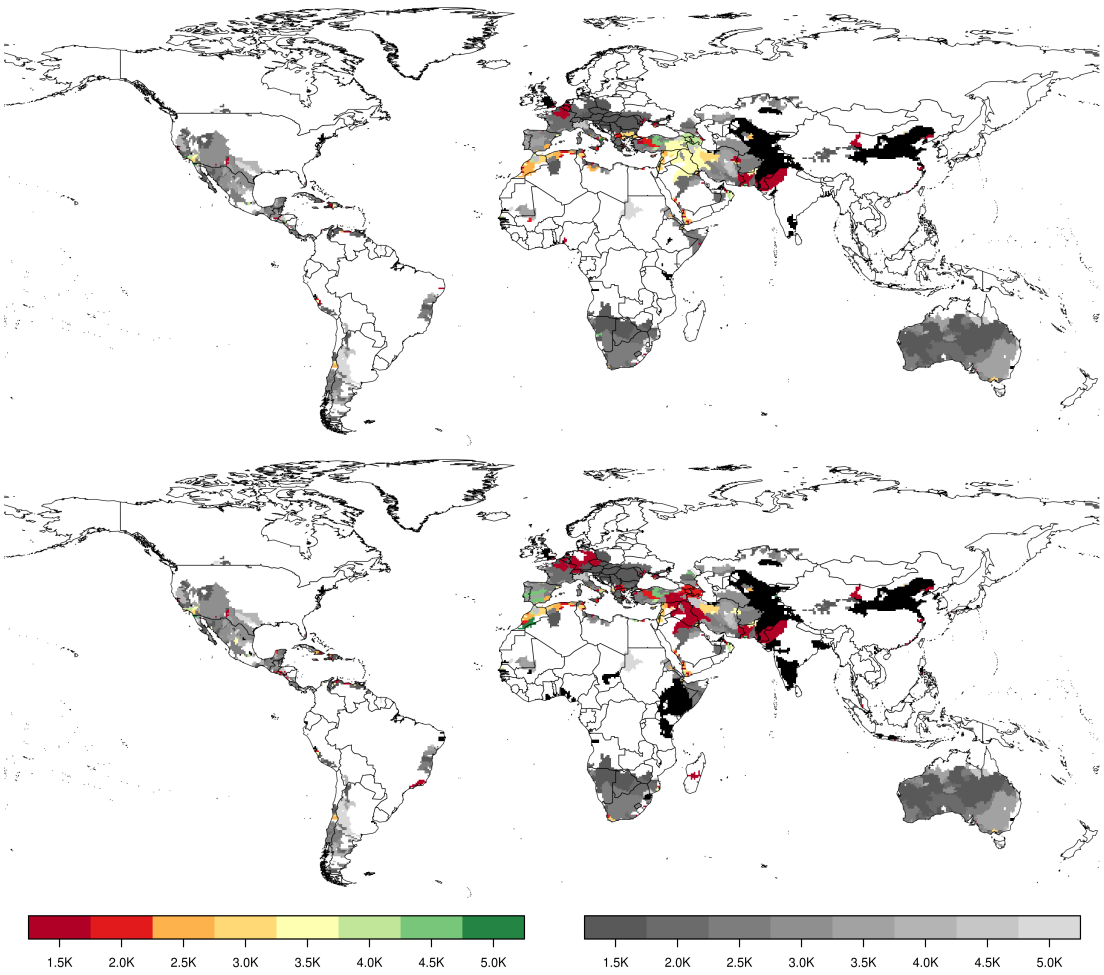

Figure C.5.: Threshold ΔT_g level associated with higher water scarcity given different future population scenarios (basins with presently $<10\,\mathrm{mm\,yr^{-1}}$ masked out). Results are shown for basins where $>50\%$ of the climate simulations agree, assuming future (year 2100) population according to the B1 (top) and the A2r scenario (bottom), respectively. Shown is the ΔT_g for a future world affected by climate change relative to that future world in the absence of climate change. Coloured areas: higher water scarcity in basins that are already chronically water-scarce or basins moving to a water-scarce status; grey areas: basins not water-scarce but experiencing decreases in water resources. Black areas: basins that are water-scarce given the respective population scenario but without an increase in scarcity due to climate change — these areas and the affected population (cf. Table IV.1 in Part IV) are substantially larger than those in the corresponding Figure IV.1(a) in Part IV, which is based on population around year 2000.

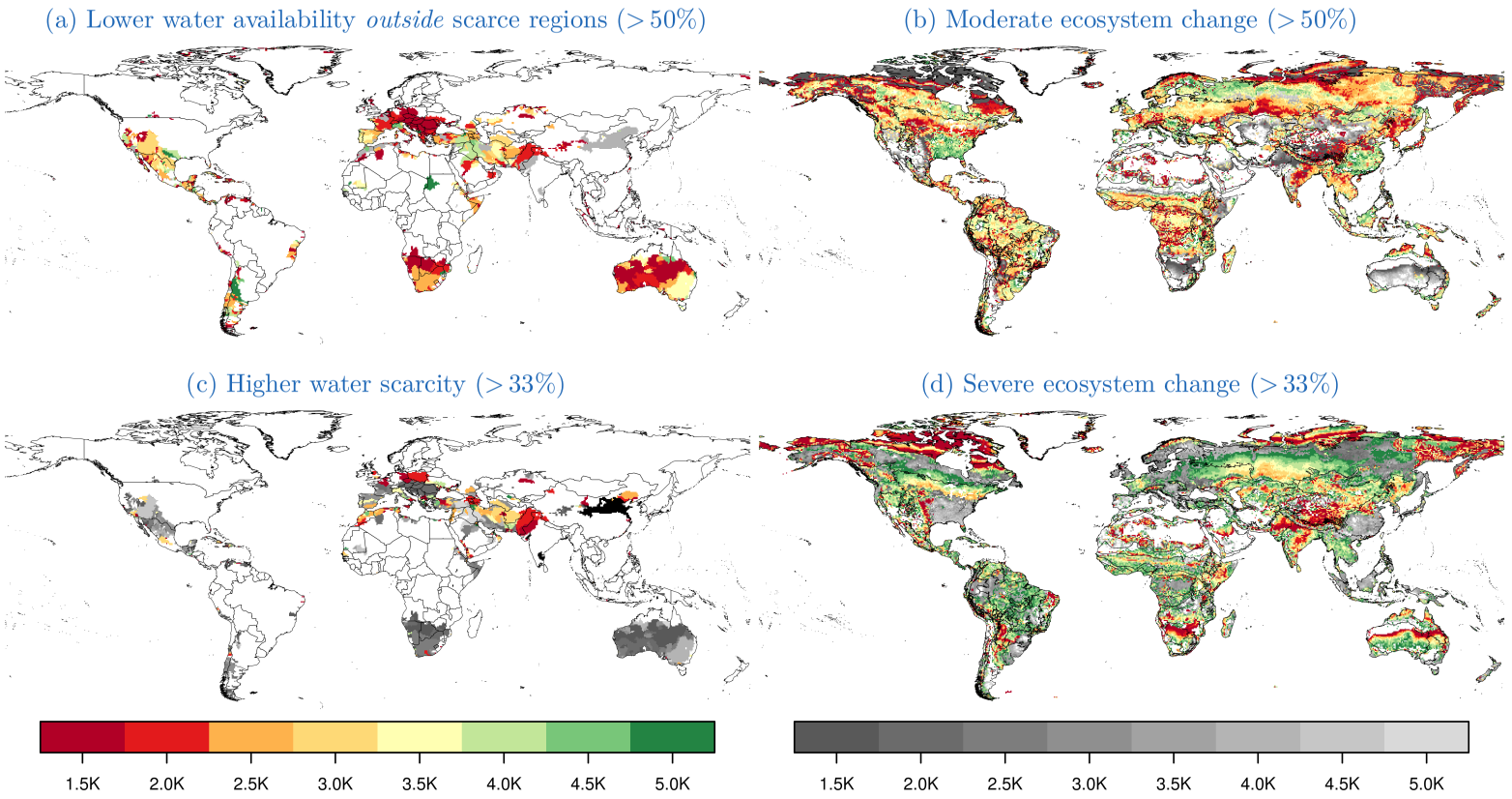

Figure C.6.: Level of ΔT_g associated with local changes less severe or less likely than in the main analysis. (a) $>50\%$ of scenarios show lower water availability (annual runoff decreasing by >1 standard deviation or median monthly runoff falling ≥ 0.1 times more frequently below its present value) outside of chronically water-scarce river basins (grey). (b) colours, $>50\%$ of scenarios show moderate ecosystem change ($0.1 < \Gamma \leq 0.3$); grey, areas where severe change ($\Gamma > 0.3$) but no moderate change is simulated under $>50\%$ of scenarios. (c) $>33\%$ of scenarios show new water scarcity or stronger water scarcity within scarce basins (colour scale) or, respectively, lower water availability outside of scarce basins (grey scale); black areas, basins already water-scarce but not experiencing aggravated scarcity. (d) $>33\%$ of scenarios show severe (colours) or moderate (grey) ecosystem change. No population change assumed in (a) and (c).

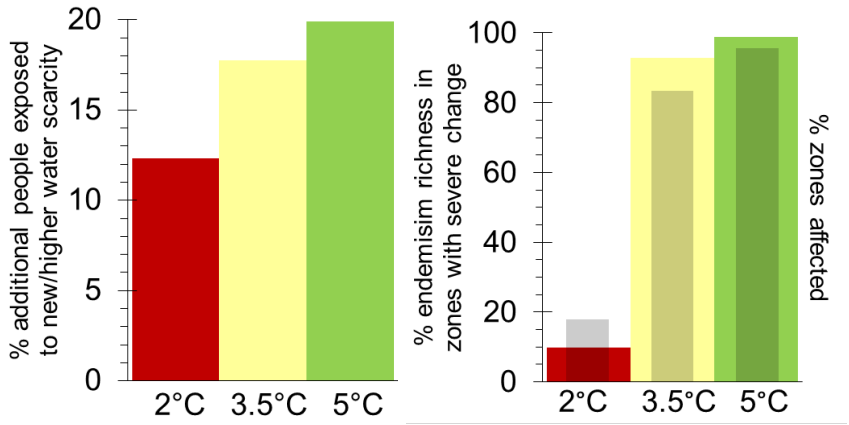

Figure C.7.: Globally aggregated changes given 2 °C, 3.5 °C and 5 °C warming under > 50% of the climate change patterns, considering less strict metrics than in the main analysis. Left: additional percentage of world population living in non-water scarce river basins but experiencing lower annual or monthly water availability. Right: percentage of global vascular plant endemism richness residing in biogeographic regions that are exposed to moderate or severe biogeochemical/vegetation structural shifts (> 33% of the area affected by $\Gamma > 0.1$ in > 50% of the simulations). Grey-shaded bars show the corresponding percentage of affected biogeographic regions (out of 90), plotted on the same axis.

Appendix D.

Supporting information for Three centuries of dual pressure from land use and climate change on the biosphere[1]

Sebastian Ostberg, Sibyll Schaphoff, Wolfgang Lucht, and Dieter Gerten

D.1. ΔV metric

The ΔV metric measures the difference in vegetation structure in terms of the importance of broad life form types (grass, trees, bare ground), further characterized by their assigned attributes (Sykes et al. 1999).

$$\Delta V(i,j) = 1 - \sum_k \left\{ min(V_{ik}, V_{jk}) * \left[1 - \sum_l (\omega_{kl} * |a_{ikl} - a_{jkl}|) \right] \right\} \tag{D.1}$$

V_{ik} and V_{jk} describe the area fractions covered by life form k in ecosystem i and j, a_{ikl} and a_{jkl} are the attributes l of lifeform k in ecosystem i and j, respectively. Attributes are weighted for each life form by ω_{kl}. Attributes can be climatic (tropical, temperate, boreal), or phenologic (evergreen, deciduous) or describe leaf types (needleleaved, broadleaved). A new attribute 'naturalness' is added to distinguish between natural vegetation and croplands and pastures.

[1] An edited version of this appendix has been published under the Creative Commons Attribution 3.0 License as Supplementary data to S. Ostberg et al. 2015. 'Three centuries of dual pressure from land use and climate change on the biosphere.' *Environmental Research Letters* 10 (4): 044011. doi:10.1088/1748-9326/10/4/044011

Table D.1.: Plant-functional types and *crop-functional types* with their assigned attributes.

Lifeform	**Attributes**				
Tree:	**Evergreenness**	**Needleleavedness**	**Tropicalness**	**Borealness**	**Naturalness**
TrBE	1	0	1	0	1
TrBR	0	0	1	0	1
TeNE	1	1	0	0	1
TeBE	1	0	0	0	1
TeBS	0	0	0	0	1
BoNE	1	1	0	1	1
BoS	0	0.25*	0	1	1
(attribute weights:	0.2	0.2	0.3	0.3	0.3)

Grass:	**Tropicalness**	**Naturalness**
C3 grass	0	1
C4 grass	1	1
Temperate Cereals	0	0
Rice	1	0
Maize	1	0
Tropical Cereals	1	0
Pulses	0.5	0
Temperate Roots	0	0
Tropical Roots	1	0
Sunflower	0.5	0
Soybean	1	0
Groundnut	1	0
Rapeseed	0.5	0
Sugarcane	1	0
Others	0.5	0
Managed grass	**	0
(attribute weights:	0.3	0.3)

* BoS primarily represents broadleaved trees, but includes larchs.

** Derived from relative share of C4 grasses as determined dynamically by LPJmL

Table D.1 lists plant-functional types (PFT) and crop-functional types (CFT) simulated by LPJmL with their associated lifeforms and attributes.

PFT abbreviations used: TrBE, tropical broadleaf evergreen tree; TrBR, tropical broadlead raingreen tree, TeNE, temperate needleleaf evergreen tree; TeBE, temperate broadleaf evergreen tree; TeBS, temperate broadleaf summergreen tree; BoNE, boreal needleleaf evergreen tree; BoS, boreal summergreen tree.

D.2. Crop management in LPJmL

Different forms of crop management are not explicitly modelled in LPJmL. In order to calibrate simulated yields to match production statistics, e.g. by the United Nations Food and Agriculture Organization (FAO), LAI_{max}, the maximum leaf area index of crops, can be scaled between 1 and 7, acting as a proxy for planting density and fertiliser application. When calibrated, developed countries have mostly high LAI_{max} values, fast developing countries have middle LAI_{max} values and developing countries have low LAI_{max} values (Fader et al. 2010). We use a fixed setting of LAI_{max}=5 for the whole period and all crops in all our simulations because historical management intensities are not well-documented. Figure D.1 tests the sensitivity of the Γ metric to different values of LAI_{max}. It shows that the effect of different management intensities on Γ is at least one order of magnitude smaller than the measured land use change effect. Differences are largest for the lowest LAI_{max} setting of 1, which increases the global mean land use change effect for the period 1981–2010 from 0.11 to 0.117. The area exposed to major LULCC impacts increases from 15.5 to 16.6%. Differences for the middle and high LAI_{max} settings are even smaller. Looking at the combined full impact of LULCC and CC, the uncertainty from management intensities is well within the range of uncertainty caused by the 20 climate realizations.

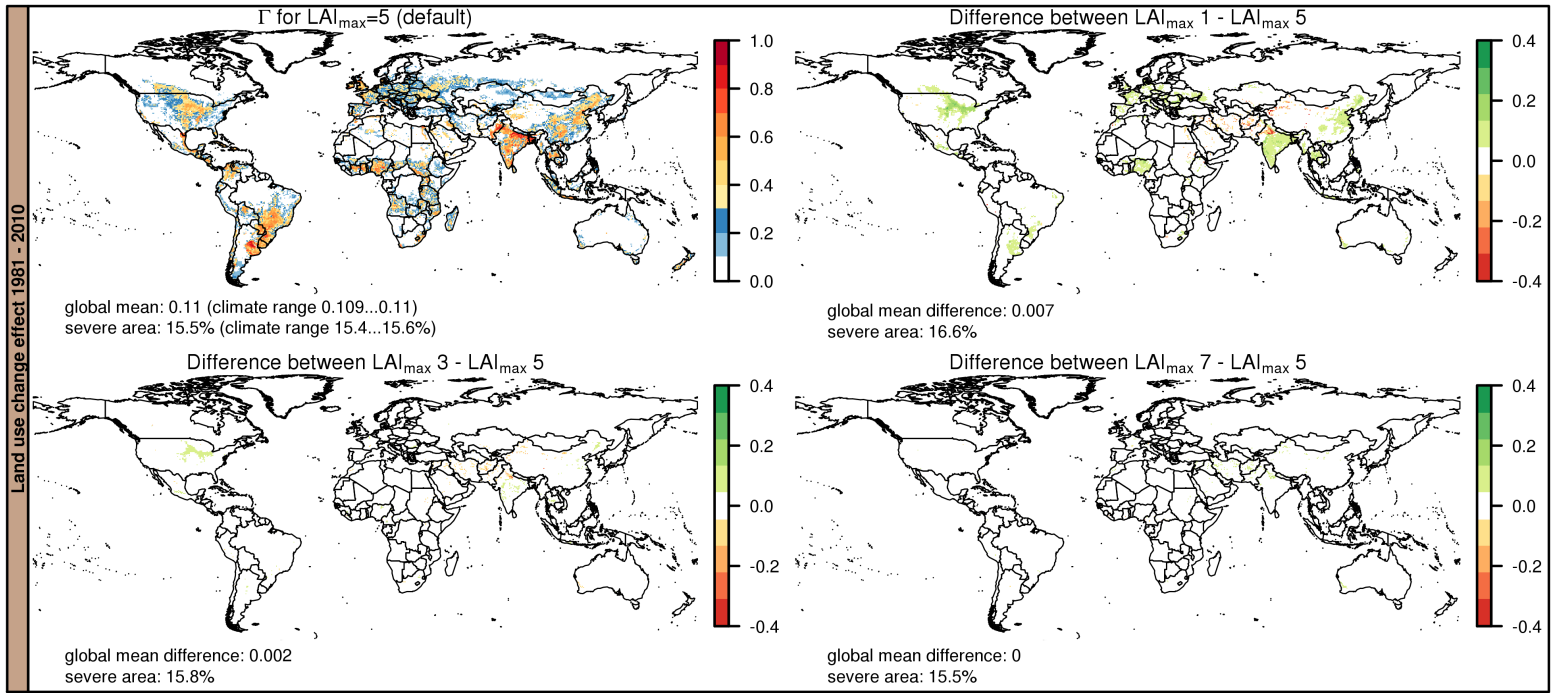

Figure D.1.: Impact of management settings in LPJmL on Γ. Default LAI_{max}=5 used for the analysis in this study. Difference in Γ values for LAI_{max} settings of 1, 3 and 7 plotted for the end (1981–2010) of the simulation period. Values in brackets denote range across 20 different climate realizations. Analysis of management impacts done for one of the 20 climate realizations.

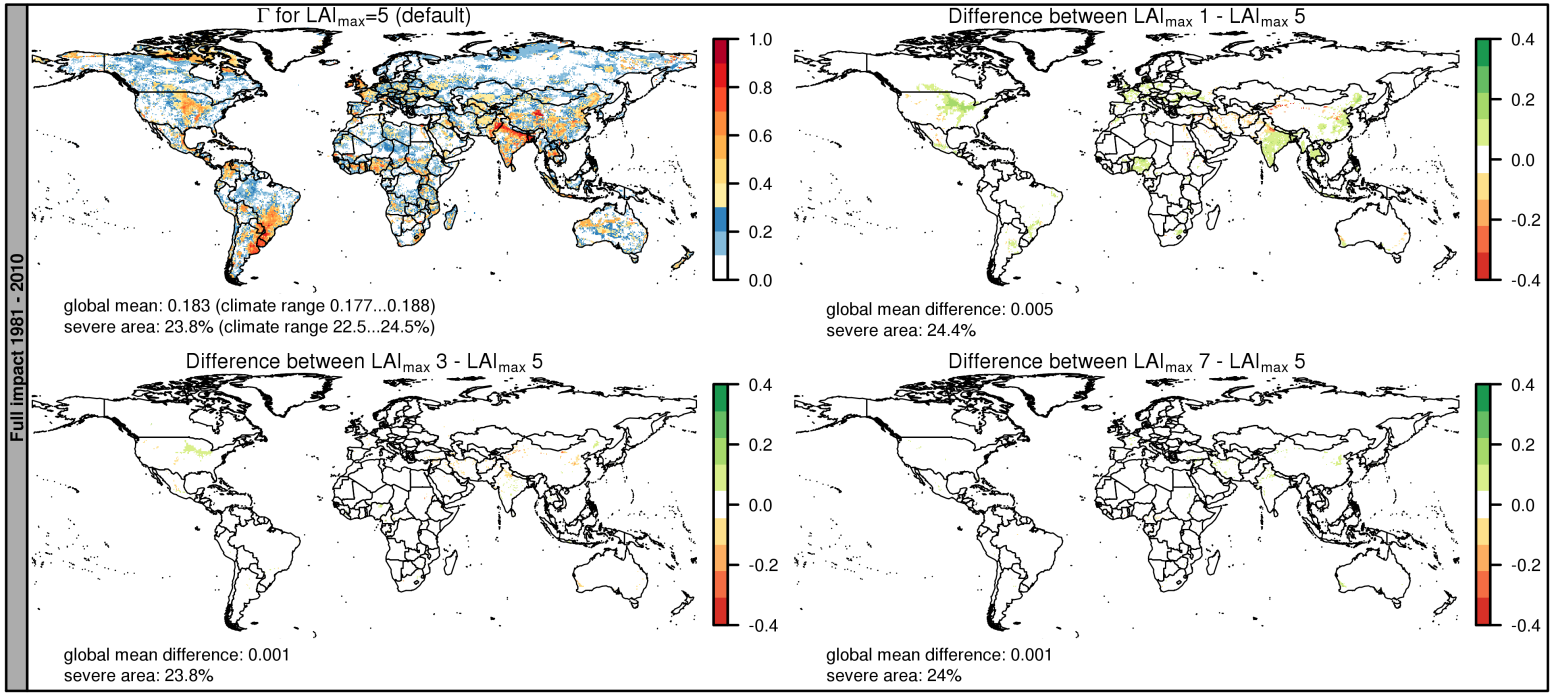

Figure D.1.: Impact of management settings in LPJmL on Γ (continued).

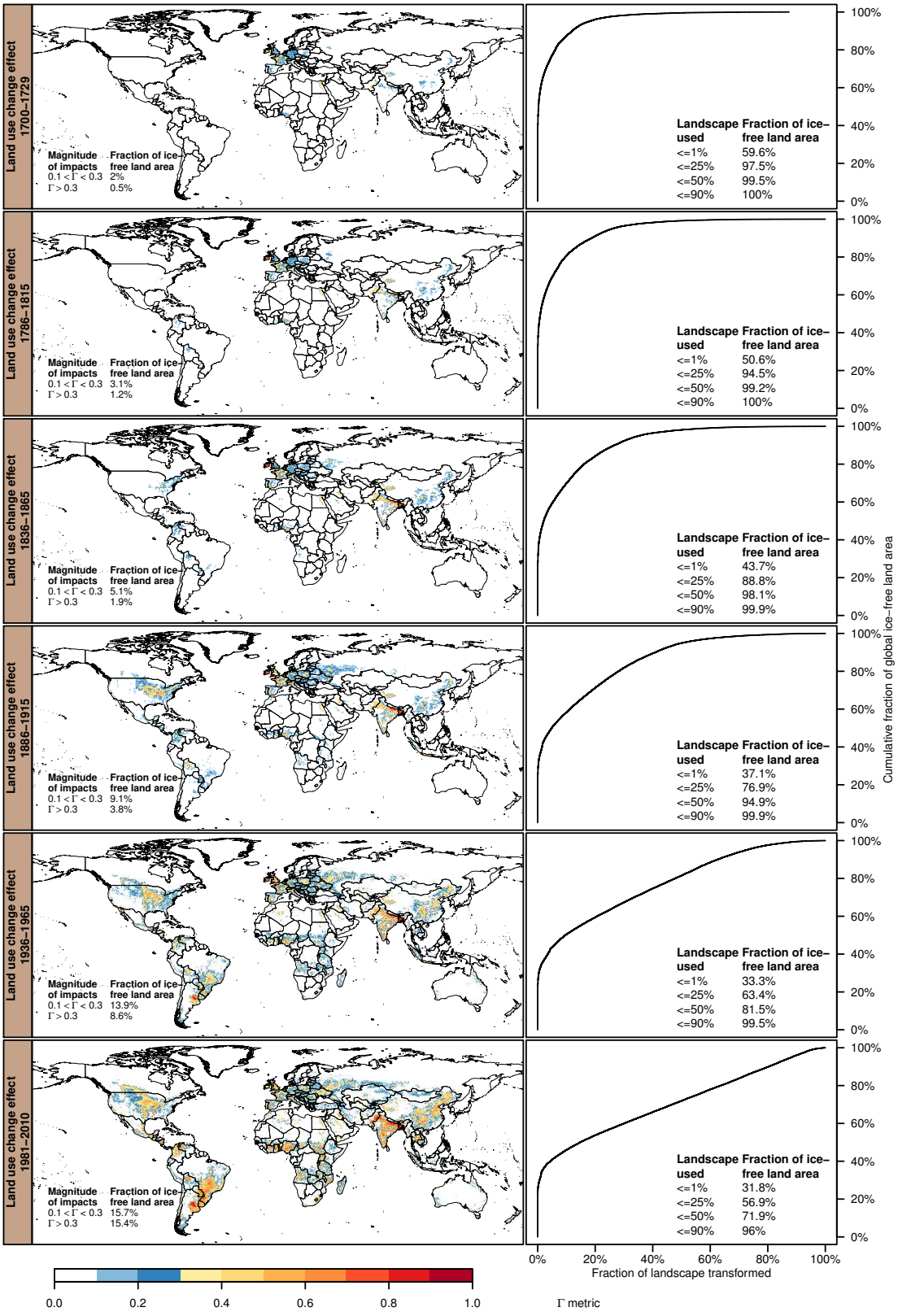

Figure D.2.: Historical expansion and intensification of land use. Left panels show *land use change effect* at the landscape scale (ensemble mean across 20 climate realizations) while right panels show cumulative land use density for the corresponding time frame.

D.3. Decomposition into metric components

The full Γ metric measures the magnitude of change, but provides little insight into the type of change taking place in response to climate or land use. Figure D.3 shows how the four components ecosystem balance $b \cdot S(b, \sigma_b)$, global importance $g \cdot S(g, \sigma_g)$, local change $c \cdot S(c, \sigma_c)$ and vegetation structure $\Delta V \cdot S(\Delta V, \sigma_{\Delta V})$ from Equation V.1 in Part V add up to Γ in each biome. To illustrate the relative contributions of different processes, we also provide the combination of ecosystem balance, local change and global importance computed for the variable subsets 'carbon stocks', 'carbon exchange fluxes' and 'water exchange fluxes' from Table V.1 in Part V. We provide results for the full impact as well as the land use change effect and climate change effect. For example, LULCC has a far larger impact on water fluxes than climate change in most biomes. This is because LULCC causes a strong shift from productive (transpiration) to unproductive water use (evaporation from bare soils). The shifts in vegetation structure caused by LULCC are also larger than those caused by climate change, with a few exceptions: there is a climate and CO_2-driven expansion of tropical forests and woody savanna into some warm (open) savannas and grasslands, which causes strong compositional shifts. Infilling of sparse tree populations in the tundra also results in changes of vegetation structure at a magnitude that is otherwise only achieved by LULCC.

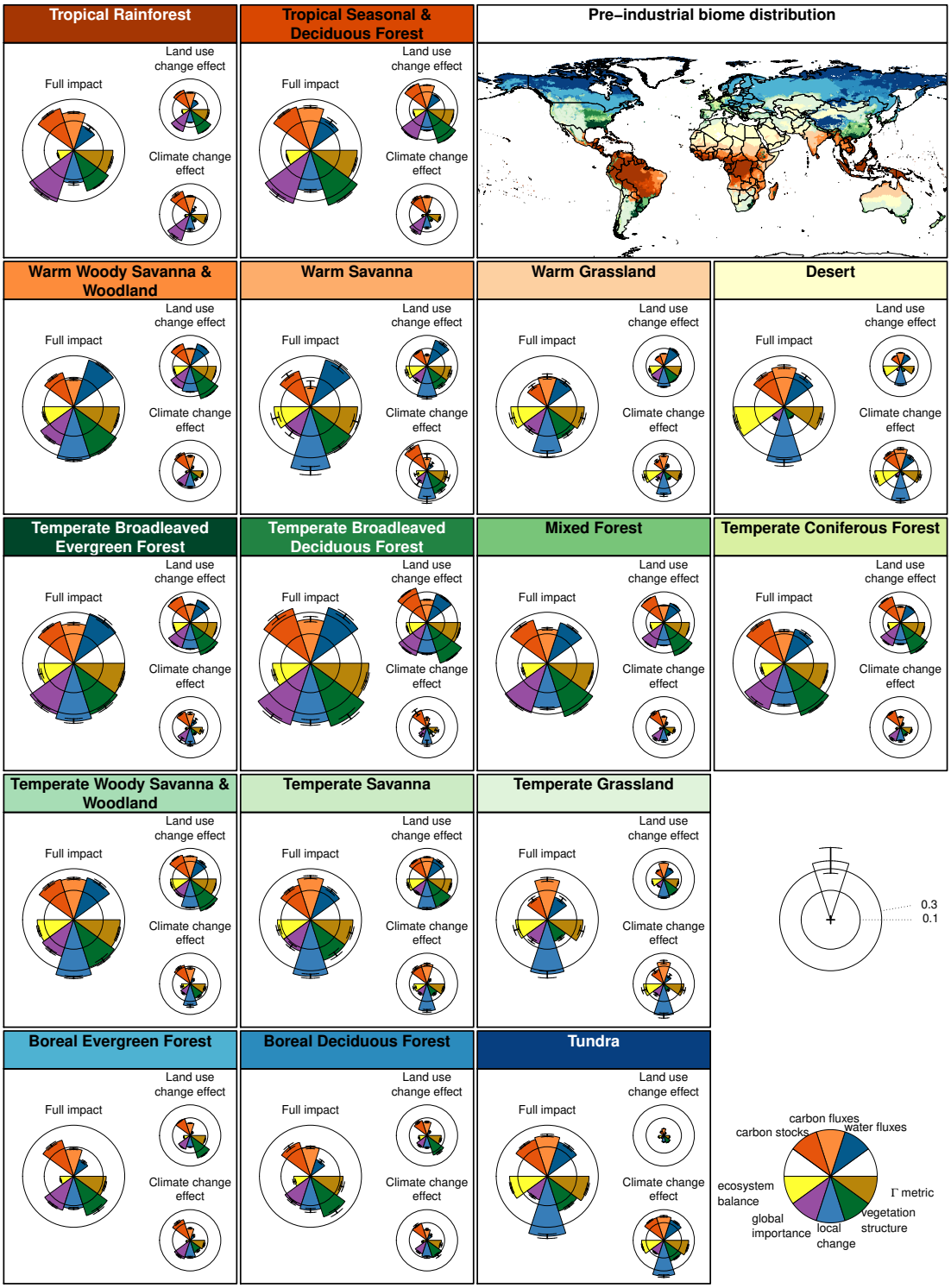

Figure D.3.: Decomposition of Γ values per biome. Components ecosystem balance $b \cdot S(b, \sigma_b)$, global importance $g \cdot S(g, \sigma_g)$, local change $c \cdot S(c, \sigma_c)$ and vegetation structure $\Delta V \cdot S(\Delta V, \sigma_{\Delta V})$ are combined into the full Γ metric. Values for carbon stocks, carbon fluxes and water fluxes illustrate the relative contribution of different processes to the full metric. Results shown for the period 1981–2010. Colours used in biome titles correspond to colours in the map.

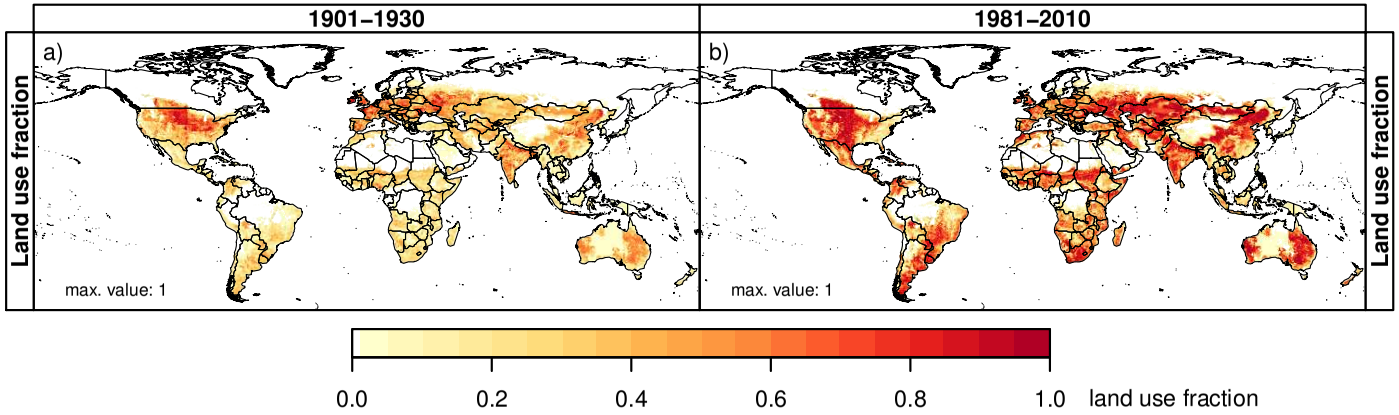

Figure D.4.: Total land use fraction. Maps show land use fraction (sum of croplands and managed grasslands/pastures) corresponding to impacts shown in Figure V.2 in Part V.

D.4. Biome classification scheme

Biome classification in this study is based on a modified version of the scheme presented in Ostberg et al. (2013a)(section B.3.1). It is based primarily on the composition of PFTs modelled in LPJmL. Compared to our earlier work, tree cover limits for the different savanna types (warm woody savanna & woodland, temperate woody savanna & woodland, warm savanna and temperate savanna) have been aligned with the IGBP classification scheme (Friedl et al. 2002). Also, Ostberg et al. (2013a)(section B.3.1) used an additional vegetation carbon limit to distinguish between tropical forests and warm woody savannas, which has been replaced by a tree leaf area index (LAI) limit to achieve better results under pre-industrial conditions (Figure D.5).

Figure D.5.: Biome classification scheme. For PFT abbreviations see section D.1. Modified after Ostberg et al. (2013a)(Figure B.4 in section B.3.1).

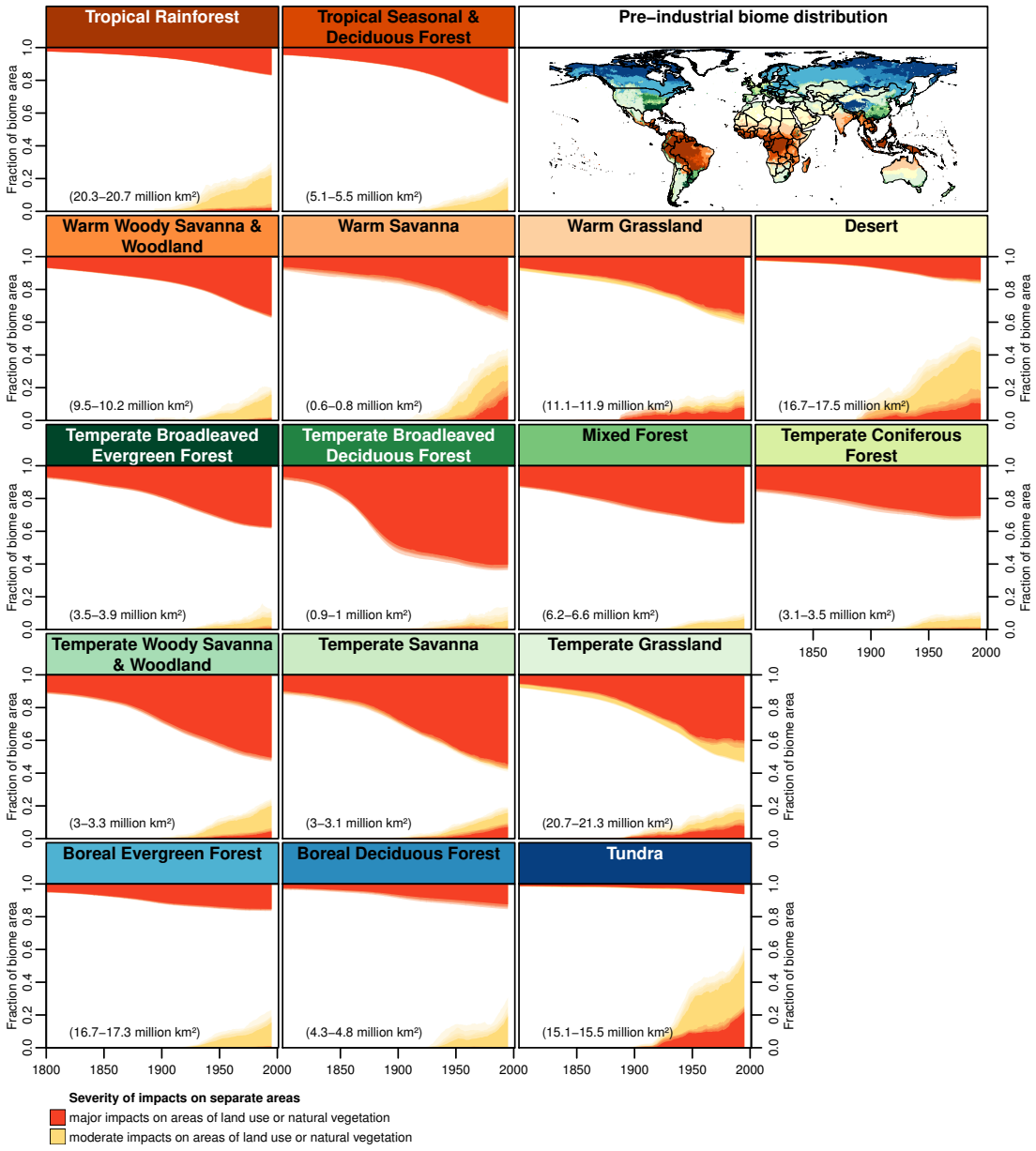

Figure D.6.: Human transformation of natural ecosystems across biomes. Impacts on land use areas shown from above. Analogous to Figure V.1a) in Part V these are calculated just for the cultivated fraction, not at the landscape level. Impacts of climate change on remaining natural ecosystems shown from below.

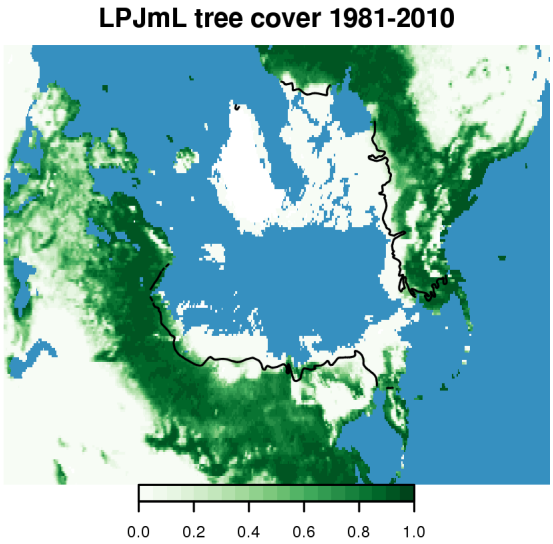

Figure D.7.: Simulated tree cover in the high latitudes. Black line denotes tree line according to Brown et al. (1998).

Appendix E.

Supporting information for The biosphere under potential Paris outcomes[1]

Sebastian Ostberg, Lena R. Boysen, Sibyll Schaphoff, Wolfgang Lucht, and Dieter Gerten

Contents of this file

1. Text E.1 to E.6
2. Figure E.1 to E.9
3. Table E.1 & E.2

Introduction

This Supporting Information provides further methodological details regarding the Γ metric (Texts E.1 and E.2, Tables E.1 and E.2), land use input data (Text E.3, Figures E.1 and E.2) and the biome classification used in this study to aggregate grid-cell results (Text E.4, Figures E.3 and E.4). Figures E.5 and E.6 show additional results discussed in the main paper. Text E.5 and Figure E.7 present a decomposition of the full Γ metric into its components. Text E.6, Figures E.8 and E.9 present a sensitivity analysis.

[1] A revised version of this appendix has been published under the Creative Commons Attribution-NonCommercial-NoDerivatives 4.0 License as Supporting Information to S. Ostberg et al. 2018. 'The Biosphere Under Potential Paris Outcomes.' *Earth's Future* 6 (1): 23–39. doi:10.1002/2017EF000628

Table E.1.: Parameters describing landscape states in the Γ metric (modified after Ostberg et al. 2015). BFT, biomass-functional type; CFT, crop-functional type; PFT, plant-functional type.

Parameter group	Individual parameters
Carbon exchange fluxes	Net primary production, sum of heterotrophic respiration and harvest (from croplands, managed grasslands and bioenergy plantations), fire carbon emissions
Carbon stocks	Carbon contained in vegetation, sum of litter and soils
Water exchange fluxes	Transpiration, sum of soil evaporation and interception loss from vegetation canopies, runoff
Other system-internal processes	Fire frequency, soil water content (upper 1 m)
Vegetation structure	Composition of BFTs, CFTs and PFTs

E.1. ΔV metric description

Originally developed by Sykes et al. (1999) and extended by Ostberg et al. (2015), ΔV measures the difference in vegetation structure in terms of the importance of broad life form types (grass, trees, bare ground), further characterized by a series of life-form specific attributes a.

$$\Delta V(i,j) = 1 - \sum_{k} \left\{ min(V_{ik}, V_{jk}) * \left[1 - \sum_{l} (\omega_{kl} * |a_{ikl} - a_{jkl}|) \right] \right\} \tag{E.1}$$

V_{ik} and V_{jk} represent the area fractions covered by life form k in landscapes i and j, a_{ikl} and a_{jkl} represent attribute l of life form k in i and j, respectively. Attributes are weighted for each life form by ω_{kl}. Plant-functional types (PFTs), crop-functional types (CFTs) and biomass-functional types (BFTs) from LPJmL are each grouped by life form k and assigned attributes according to Table E.2. Attributes evergreenness, needleleavedness, tropicalness and borealness are taken over from the original implementation by Sykes et al. (1999), while naturalness was added by Ostberg et al. (2015) to distinguish crops (and now also bioenergy plantations) from natural vegetation.

Table E.2.: Plant-functional types, *crop-functional types* and biomass-functional types and their assigned attributes (modified after Ostberg et al. 2015). PFT abbreviations: TrBE, tropical broadleaf evergreen tree; TrBR, tropical broadlead raingreen tree, TeNE, temperate needleleaf evergreen tree; TeBE, temperate broadleaf evergreen tree; TeBS, temperate broadleaf summergreen tree; BoNE, boreal needleleaf evergreen tree; BoS, boreal summergreen tree; TrBi, tropical bioenergy tree; TeBi, temperate bioenergy tree.

Lifeform	**Attributes**				
Tree:	**Evergreenness**	**Needleleavedness**	**Tropicalness**	**Borealness**	**Naturalness**
TrBE	1	0	1	0	1
TrBR	0	0	1	0	1
TeNE	1	1	0	0	1
TeBE	1	0	0	0	1
TeBS	0	0	0	0	1
BoNE	1	1	0	1	1
BoS	0	0.25*	0	1	1
TrBi	1	0	1	0	0
TeBi	0	0	0	0	0
(attribute weights:	0.2	0.2	0.3	0.3	0.3)

Grass:	**Tropicalness**	**Naturalness**
C3 grass	0	1
C4 grass	1	1
Temperate Cereals	0	0
Rice	1	0
Maize	1	0
Tropical Cereals	1	0
Pulses	0.5	0
Temperate Roots	0	0
Tropical Roots	1	0
Sunflower	0.5	0
Soybean	1	0
Groundnut	1	0
Rapeseed	0.5	0
Sugarcane	1	0
Others	0.5	0
Managed grass	**	0
Bioenergy grass	1	0
Grass under bioenergy trees***	**	0
(attribute weights:	0.3	0.3)

* BoS primarily represents broadleaved trees, but includes larchs.

** Derived from relative share of C4 grasses as determined dynamically by LPJmL.

*** Grass under bioenergy trees is not harvested.

E.2. Vector geometry and scaling of Γ metric

The calculation of the Γ metric follows Heyder et al. (2011). Two ecosystem states are expressed by state vectors $\vec{s_1}$ and $\vec{s_2}$ for variables $v_i, i = [1, \ldots, n]$:

$$\vec{s_1} = \begin{pmatrix} v_{1,1} \\ \vdots \\ v_{n,1} \end{pmatrix}, \vec{s_2} = \begin{pmatrix} v_{1,2} \\ \vdots \\ v_{n,2} \end{pmatrix}, \tag{E.2}$$

where $\vec{s_1}$ represents the reference state and $\vec{s_2}$ the changed state under climate change and/or land use change, with v_i given by the parameters in Table E.1 except those for vegetation structure. Since the values of state parameters v_i can differ by several orders of magnitude they are normalized. For local change c state parameters are normalized to the local value of v_i under reference conditions, leading to:

$$\vec{s_{l_1}} = \begin{pmatrix} 1 \\ \vdots \\ 1 \end{pmatrix}, \vec{s_{l_2}} = \begin{pmatrix} v_{1,l} \\ \vdots \\ v_{n,l} \end{pmatrix} \tag{E.3}$$

where

$$v_{i,l} = \frac{v_{i,2}}{v_{i,1}}, \quad \text{for } v_{i,1} \neq 0. \tag{E.4}$$

For global importance g state vectors are normalized to the global, spatially averaged mean value of v_i under reference conditions, resulting in:

$$\vec{s_{g_1}} = \begin{pmatrix} v_{1,g,1} \\ \vdots \\ v_{n,g,1} \end{pmatrix}, \vec{s_{g_2}} = \begin{pmatrix} v_{1,g,2} \\ \vdots \\ v_{n,g,2} \end{pmatrix} \tag{E.5}$$

where

$$v_{i,g,t} = \frac{v_{i,t}}{\overline{v_{i,\text{refg}}}}, \quad \text{for } \overline{v_{i,\text{refg}}} \neq 0 \tag{E.6}$$

and

$$\overline{v_{i,\text{refg}}} = \frac{1}{\sum a_p} \sum_{p=1}^{z} a_p v_{i,p} \tag{E.7}$$

for cells $p = 1, \ldots, z$ with cell area a_p.

The difference d between two states is calculated as the magnitude of the difference vector $\vec{d}$. For local change c

$$d_c = |\vec{d_c}| = |\vec{s_{l_2}} - \vec{s_{l_1}}| \tag{E.8}$$

while for global importance g

$$d_g = |\vec{d_g}| = |\vec{s_{g2}} - \vec{s_{g1}}|. \tag{E.9}$$

Shifts in the balance b' of ecosystem processes are calculated as the angle α between two state vectors with local normalization:

$$b' = 1 - \cos\alpha = 1 - \frac{\vec{s_{l1}} \cdot \vec{s_{l2}}}{|\vec{s_{l1}}||\vec{s_{l2}}|}. \tag{E.10}$$

If the relative contributions of all parameters v_i are constant the direction of $\vec{s_{l1}}$ and $\vec{s_{l2}}$ is identical and $\cos\alpha = 1$. For orthogonal state vectors $\cos\alpha = 0$, whereas $\cos\alpha = -1$ if both state vectors are opposed. b' is scaled to a range between 0 and 1 assigning a value of 1 if the angle between state vectors is larger than 60°:

$$b = \begin{cases} b' \cdot 2 & \text{for } \alpha \leq 60° \\ 1 & \text{for } \alpha > 60° \end{cases} \tag{E.11}$$

Values for metric components c and g are derived by scaling d_c and d_g to a range between 0 and 1 using the following sigmoid transformation function T:

$$c = T(d_c), \quad g = T(d_g), \tag{E.12}$$

with

$$T(x) = A + \frac{1 - A}{1 + \mathrm{e}^{-6(x-0.5)}} \tag{E.13}$$

where $A = -\frac{1}{\mathrm{e}^3}$. The transformation function assigns a value of 0 in case of 'no change' and $T(x) \geq 0.95$ if the change is larger than one mean value.
The change-to-variability ratio $S(x, \sigma_x)$ for components $x(d_c, d_g, b'$ and $\Delta V)$ is calculated as

$$S(x, \sigma_x) = \frac{1}{1 + \mathrm{e}^{-4(\frac{x}{\sigma_x} - 2)}} \tag{E.14}$$

with σ_x the interannual standard deviation of x under reference conditions. This transformation function assigns values of $S \leq 0.018$ to changes within one standard deviation, $S = 0.5$ to changes of two standard deviations and $S \geq 0.982$ to changes larger than three standard deviations. For full details see Heyder et al. (2011). Section E.5 and Figure E.7 illustrate the contribution of the different components to the full metric value in major biomes.

E.3. Filtering of unproductive bioenergy tree plantations

Figure E.1 shows the fraction of each grid cell covered by 3 major land use types (cropland, pasture, bioenergy plantations) for the end of the historical period (1976–2005) as well as the end of all four scenarios (2070–2099). Bioenergy fractions under RCP2.6 and RCP6.0 are assumed to be covered with 50% bioenergy grass and 50% bioenergy tree plantations. However, climate conditions in some of the grid cells with bioenergy fractions do not support tree growth, causing planted bioenergy trees to die. If this happens repeatedly dead biomass will accumulate in the modelled litter and soil carbon pools. Since carbon contained in the sapling is subtracted from harvest it can also lead to negative harvest values. To avoid this, all $\mathrm{LUC}_{\mathrm{noCC}}$ and $\mathrm{LUC}_{\mathrm{CC}}$ simulations for RCP2.6 and RCP6.0 are run twice. After the first run, all grid cells where either mean harvest averaged over all climate models is below $100\,\mathrm{g/m^2}$ of carbon or harvest is negative in at least one simulation are marked as unproductive. This means that the bioenergy tree fraction in the land use input is reassigned to bioenergy grass in all years following the first unproductive harvest. In case a grid cell returns to productive conditions at a later year of the test simulations, bioenergy tree plantations can be restored. The updated land use patterns are then applied to all climate models during the second iteration of $\mathrm{LUC}_{\mathrm{noCC}}$ and $\mathrm{LUC}_{\mathrm{CC}}$ simulations. Results from this second iteration are used in the calculation of the Γ metric. Figure E.2 shows bioenergy tree and bioenergy grass areas after filtering. Up to 23% and 13% of global bioenergy tree area is reassigned to bioenergy grass under RCP2.6 and RCP6.0, respectively.

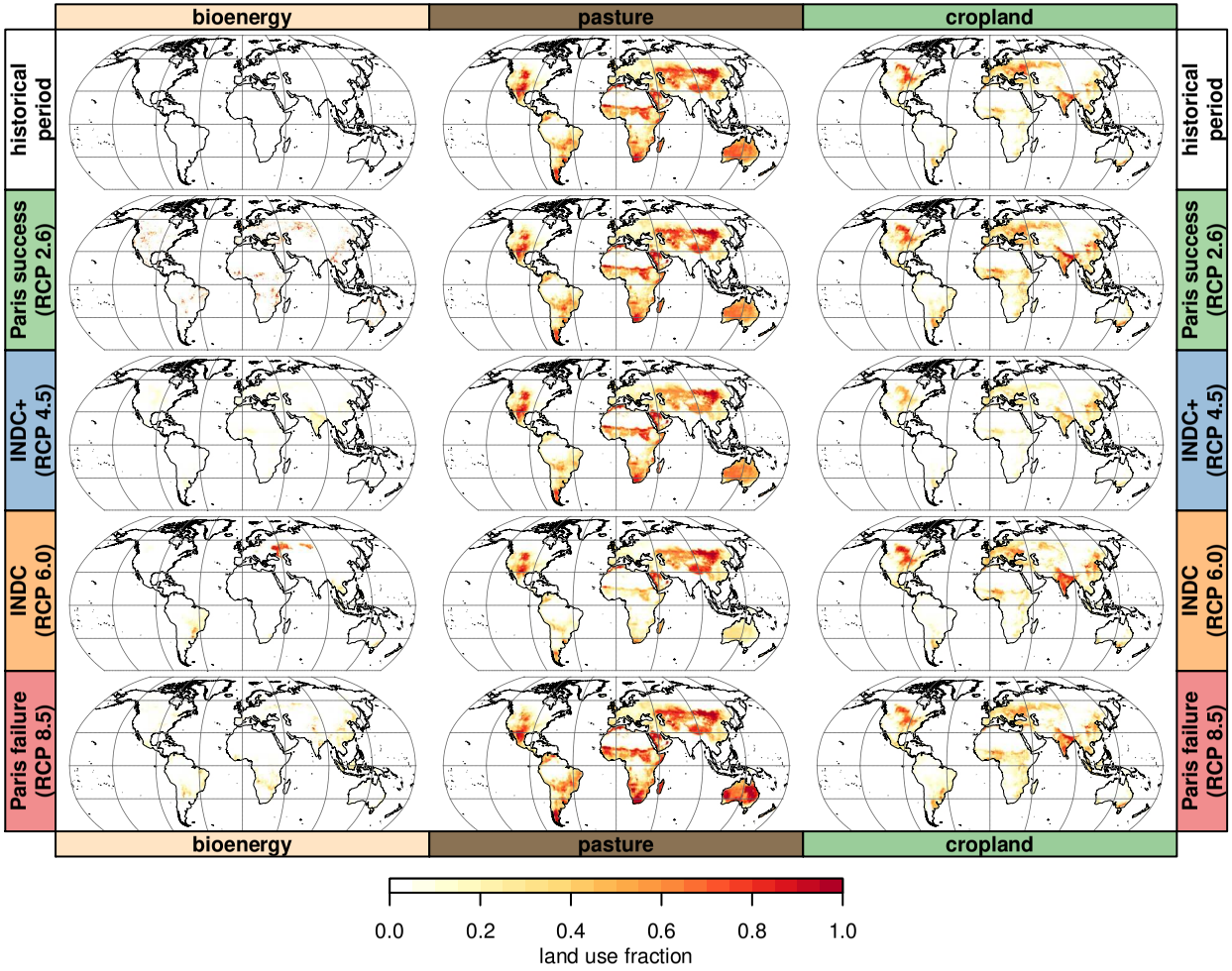

Figure E.1.: Land use maps. Fraction of each grid cell covered by major types of land use at the end of the historical period (1976–2005) and the end of the four studied scenarios (2070–2099).

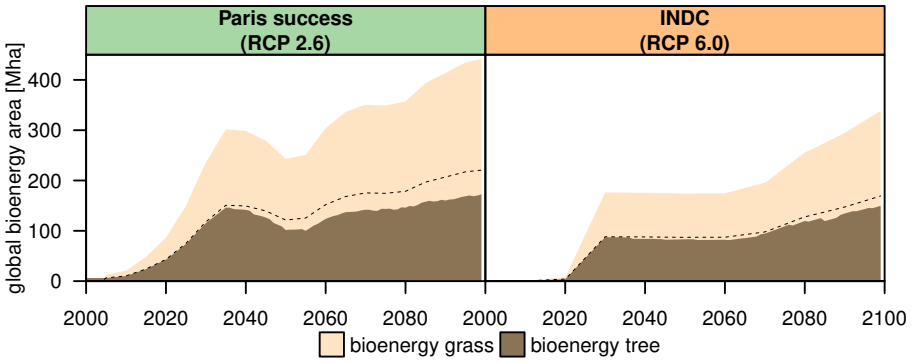

Figure E.2.: Bioenergy areas by plantation type after filtering. Dashed line marks 50% share.

E.4. Biome classification

The biome classification follows Ostberg et al. (2015). It is based on the composition of PFTs modeled in LPJmL. An additional tree leaf area index (LAI) limit is used to distinguish between tropical forests and warm woody savannas. A temperature limit is used to classify tundra. The classification scheme is illustrated in Figure D.5 in Appendix D. Figure E.3 below shows modelled biome distributions for the end of the historical period (1976–2005) as well as the end of all four scenarios (2070–2099). In cases where LPJmL simulations driven by different climate models do not agree on the biome class in a grid cell the dominant (most frequent) value is shown. Figures E.4–E.6 as well as Figure VI.3 in Part VI use an aggregated version of this biome classification which distinguishes only one forest type per climate region and combines 'woody savanna & woodland', 'savanna' and 'grassland' biomes into 'non-forest'.

Figure E.4 aggregates the three land use categories from Figure E.1 per major biome class and presents the temporal evolution during the 20th and 21st century. While Figure VI.3 in Part VI shows the fraction of biomes projected to experience major full impacts (the combination of climate change and land use change), Figures E.5 & E.6 present results for the individual effects of climate change and land use change.

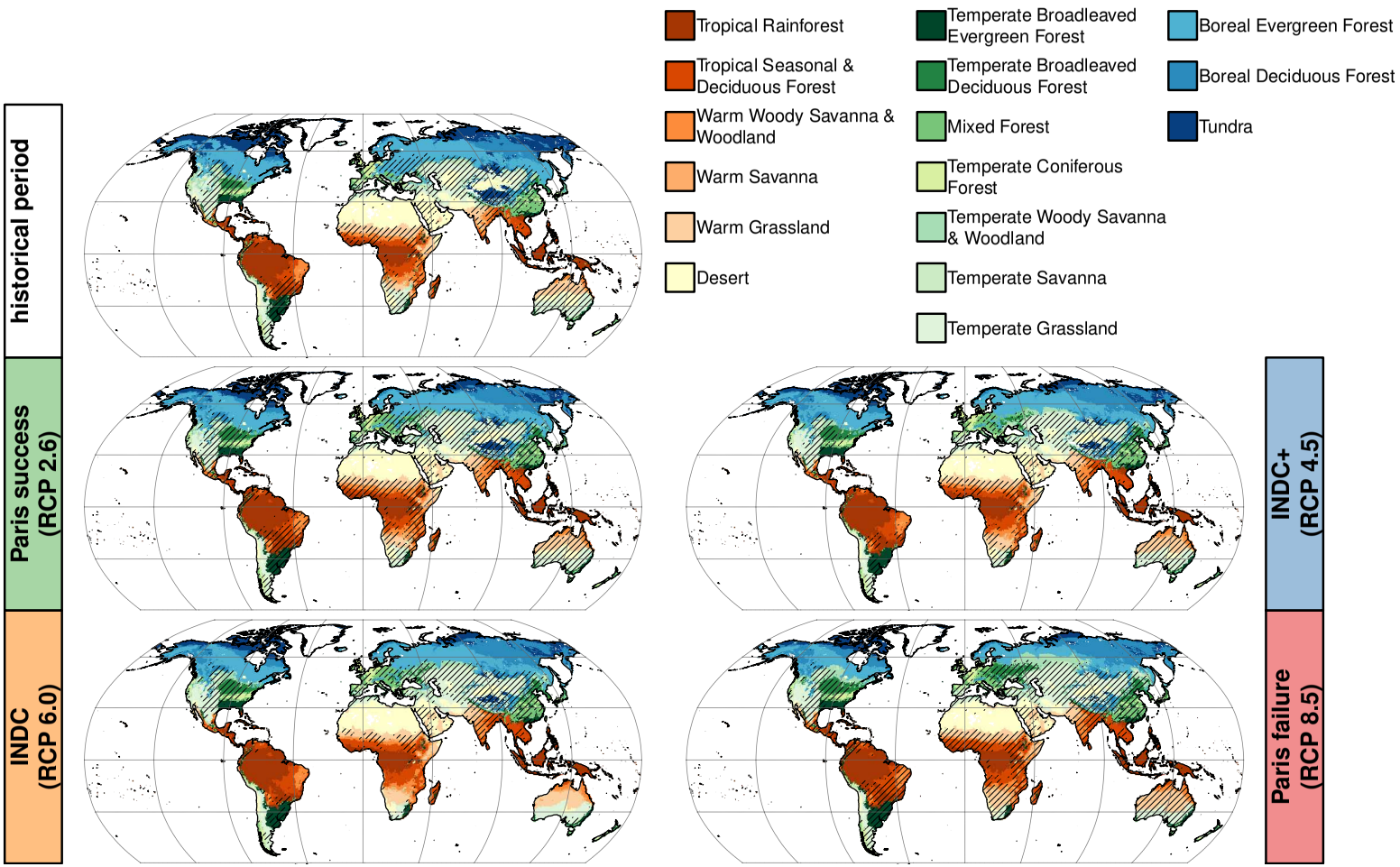

Figure E.3.: Modelled biome distribution. Historical period refers to 1976–2005, all scenarios refer to 2070–2099. Hatching marks grid cells with at least 50% land use.

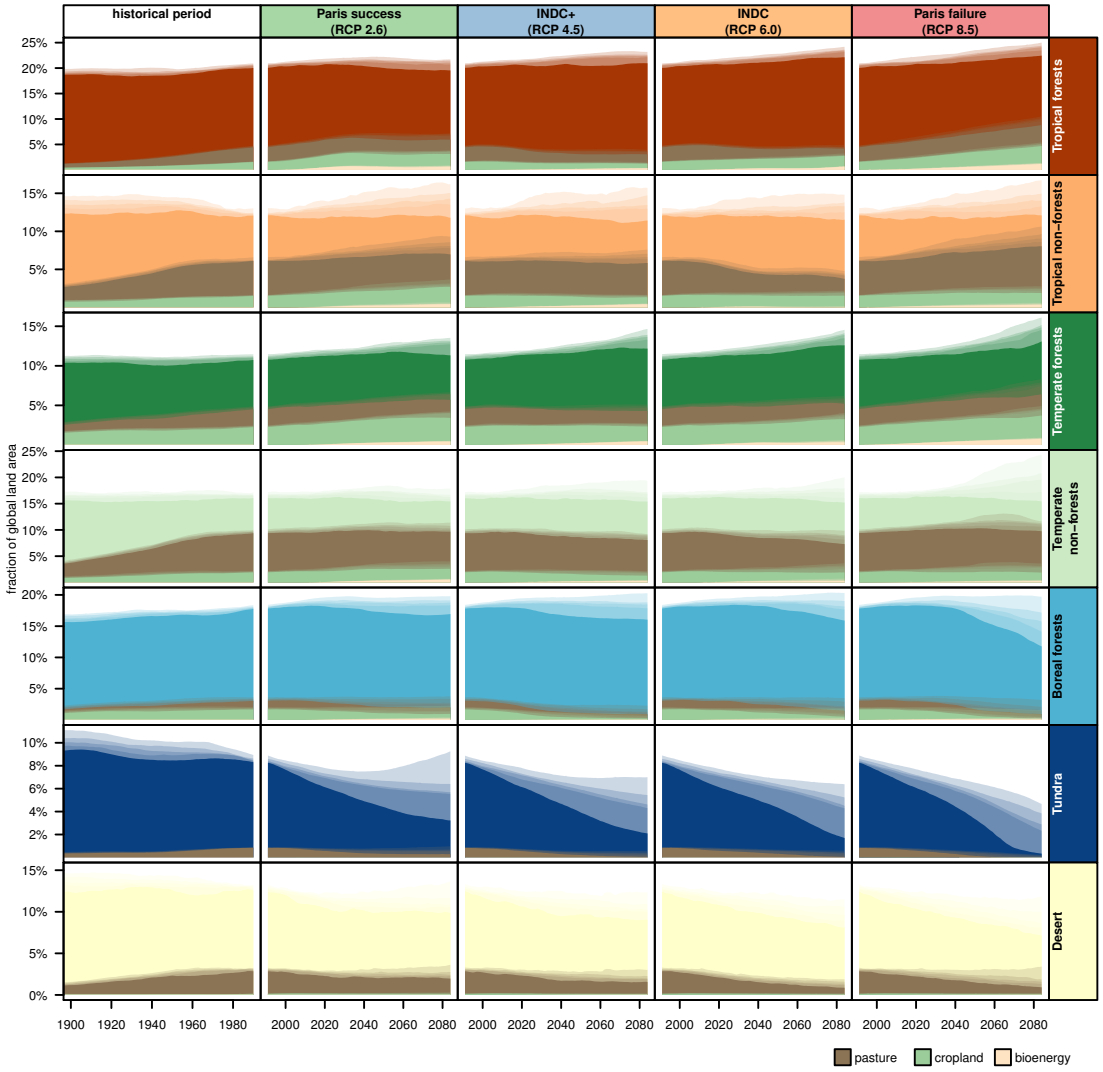

Figure E.4.: Land use in major biomes over time. Each plot shows the total area covered by the respective biome as well as the fraction of the biome covered by the major types of land use shown in Figure E.1. Landscapes (grid cells) are classified into biomes based on their potential natural vegetation even if land has been converted to agriculture. As in Figure VI.3 in Part VI, semitransparent shading denotes the uncertainty arising out of using 20 climate models to drive vegetation simulations (maximum, 75%, 50% and 25% quantile and minimum extent).

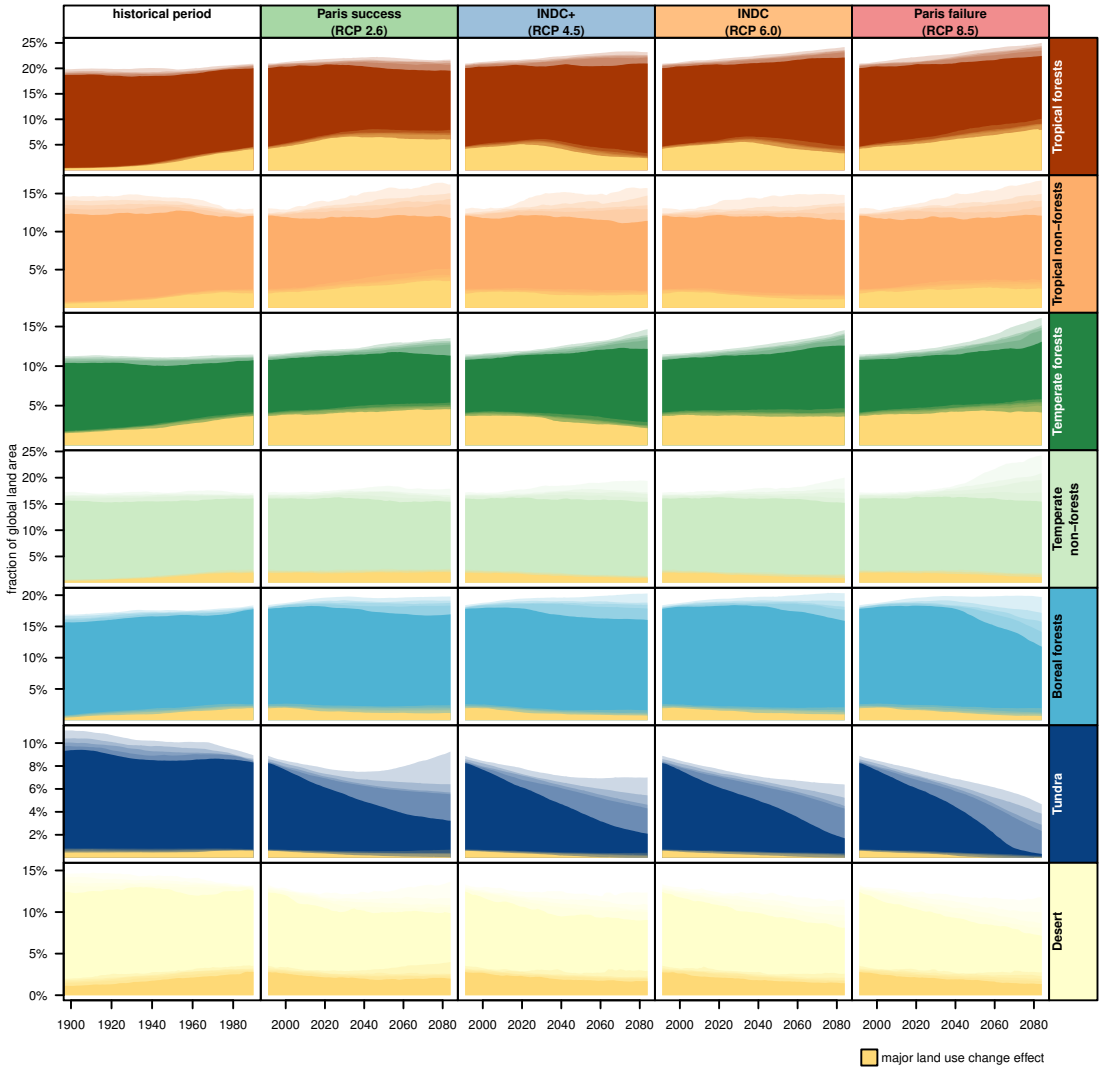

Figure E.5.: Impacts of land use change in major biomes over time. Each plot shows the total area covered by the respective biome as well as the fraction of the biome projected to experience major change (yellow overlay). As in Figure VI.3 in Part VI, semitransparent shading denotes the uncertainty arising out of using 20 climate models to drive vegetation simulations (maximum, 75%, 50% and 25% quantile and minimum extent).

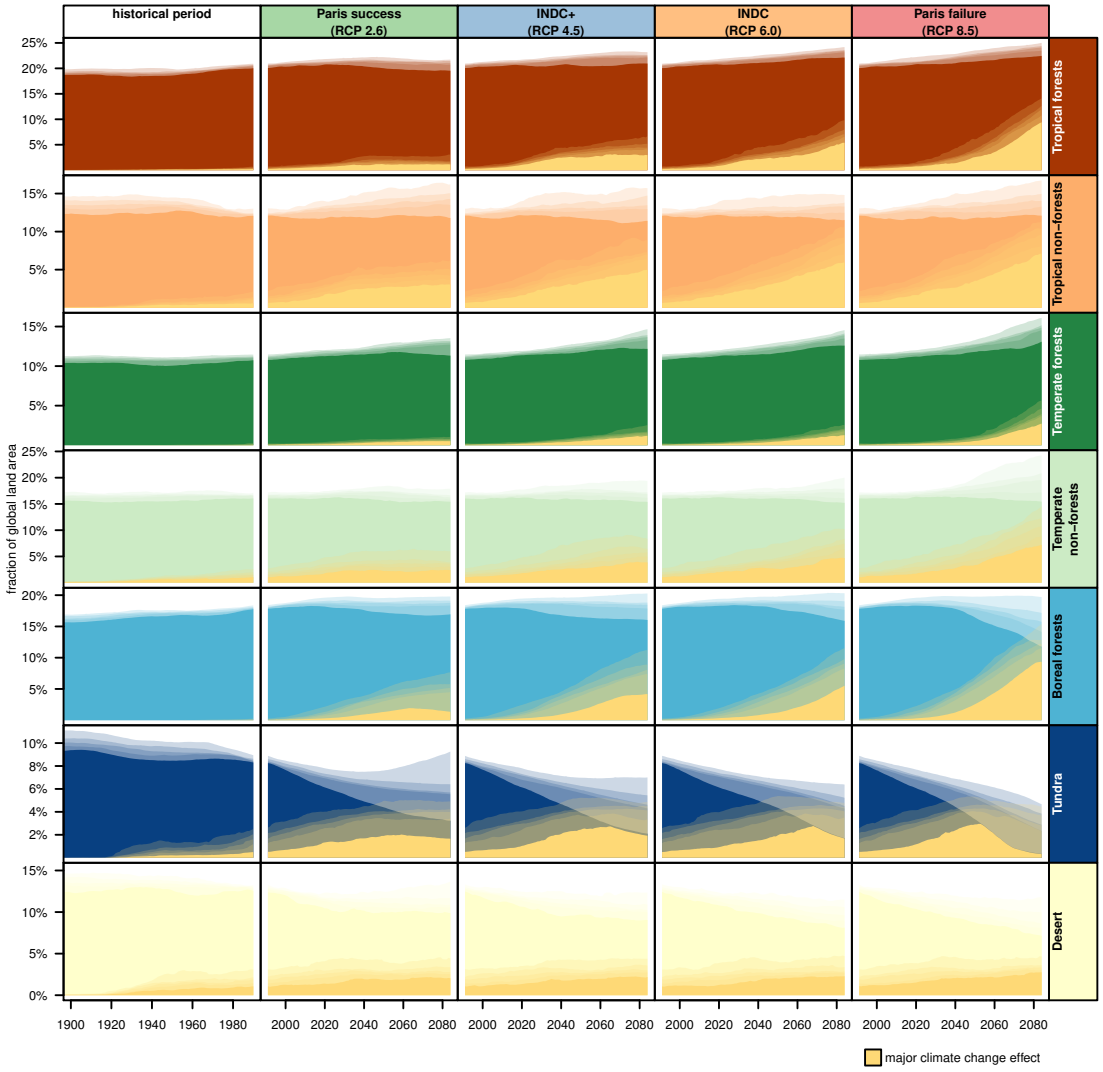

Figure E.6.: Impacts of climate change in major biomes over time. Each plot shows the total area covered by the respective biome as well as the fraction of the biome projected to experience major change (yellow overlay). As in Figure VI.3 in Part VI, semitransparent shading denotes the uncertainty arising out of using 20 climate models to drive vegetation simulations (maximum, 75%, 50% and 25% quantile and minimum extent).

E.5. Metric components

Figure E.7 presents a decomposition of the full Γ metric into its components for major biomes and for the climate change effect, land use change effect and full impact. Values for all grid cells belonging to each major biome (see section E.4) are spatially averaged using a cell-area based weighting. Whiskers denote the range across simulations driven by 20 different climate models. Ecosystem balance $b \cdot S(b, \sigma_b)$, global importance $g \cdot S(g, \sigma_g)$, local change $c \cdot S(c, \sigma_c)$ and vegetation structure $\Delta V \cdot S(\Delta V, \sigma_{\Delta V})$ are combined into the full Γ metric (see Equation VI.1 in Part VI). We also provide the combination of ecosystem balance, local change and global importance for the subsets of parameters from Table E.1 'carbon exchange fluxes', 'carbon stocks' and 'water exchange fluxes'. On average, changes in tropical forests have the highest global importance g of all biomes across all four scenarios. This means that changes in tropical forests contribute more to global biogeochemical cycles in absolute terms than changes in the other biomes. In contrast, changes in deserts have a low global importance even though local change c and ecosystem balance b may adopt high values. This is because ecosystem state parameters generally have very low values in deserts. Small changes in weather can lead to large relative changes in these parameters — which are captured by b and c — but changes are small in absolute terms (g). Changes to vegetation structure (ΔV) are also generally small in deserts. In tropical and temperate biomes land use usually has a higher impact on vegetation structure (ΔV) than climate change. This is especially true for tropical and temperate forests. Climate-driven changes in vegetation structure are more common in tropical and temperate savanna ecosystems which are often in the transition zone between forests and grasslands. Both boreal forests and tundra regions have low land use change impacts but high climate-driven ΔV values because of woody encroachment into the tundra and drought and heat-related tree mortality along the warm edge of the boreal zone. The metric values for carbon exchange fluxes are often larger than the values for carbon stocks. This is because carbon stocks change only if the balance between inputs and outputs is shifted, not if the relative contribution of fluxes into and out of the biosphere stays constant. Land use change (deforestation) has a strong impact on carbon stocks in forests which is larger than carbon stock changes driven by changes in carbon fluxes. In most biomes changes in water fluxes are smaller than changes in carbon fluxes, although this difference between carbon flux changes and water flux changes is usually more pronounced for the climate change effect than the

land use change effect.

E.6. Alternative measures of human interference with the biosphere

A threshold of $\Gamma > 0.3$ is used for the main analysis to distinguish landscapes with major impacts of human interference with the biosphere. Figure E.8 presents global results using the globally area-weighted mean value of Γ instead of a threshold. While absolute values are not comparable, the relative ranking of scenarios and the relative strength of climate change effects compared to land use change effects stays the same as in the main results: (1) average CC impacts increase with increasing CC forcing from lowest in the *Paris success* case to highest in the *Paris failure* scenario; (2) average land use change effects are lowest in the *INDC+* and highest in the *Paris success* scenario; (3) average impacts of CC far surpass average LUC impacts by the end of the 21st century in all scenarios except *Paris success*; (4) the average full impact is slightly lower under *INDC+* than *Paris success*. Figure E.9 explores different thresholds of the Γ metric. For a very low threshold of $\Gamma > 0.1$, CC impacts may surpass LUC impacts in terms of the affected global area even in the *Paris success* scenario — which means that CC will expose more landscapes globally to at least moderate change than LUC under all four scenarios according to our simulations. On the other hand, the global land area projected to experience at least moderate full impacts — from the combination of CC and LUC — is lowest in the *Paris success* scenario instead of the *INDC+* scenario found in the main results. If higher thresholds than $\Gamma > 0.3$ are used to mark landscapes with major human interference with the biosphere the full impact in the *Paris success* scenario comes progressively closer to the full impact in the *INDC* scenario, suggesting that *INDC+* is more successful than *Paris success* in avoiding increasingly strong human impacts on the biosphere.

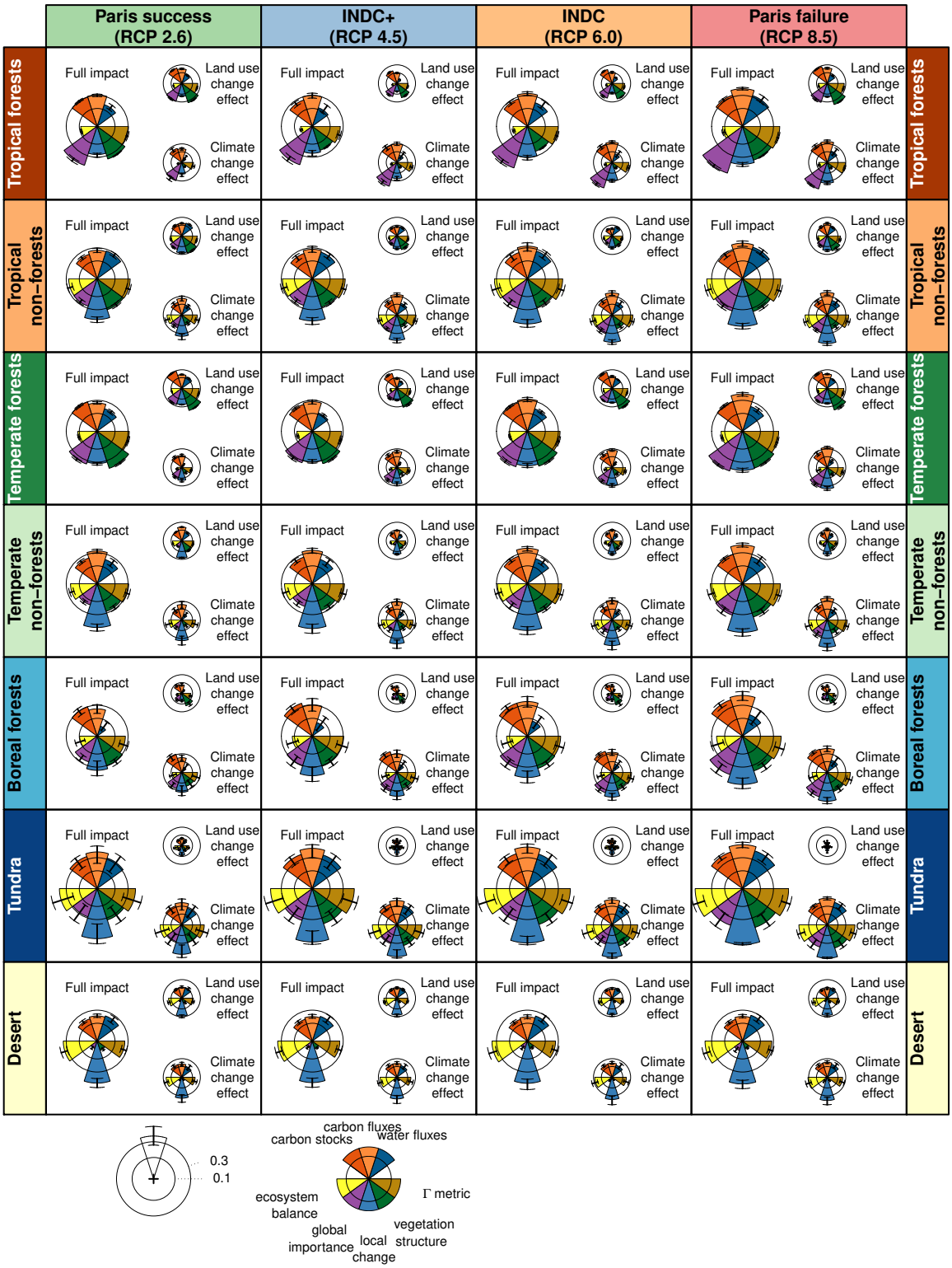

Figure E.7.: Decomposition of Γ values for major biomes. Components ecosystem balance $b \cdot S(b, \sigma_b)$, global importance $g \cdot S(g, \sigma_g)$, local change $c \cdot S(c, \sigma_c)$ and vegetation structure $\Delta V \cdot S(\Delta V, \sigma_{\Delta V})$ are combined into the full Γ metric. Values for carbon stocks, carbon fluxes and water fluxes illustrate the relative contribution of different processes to the full metric. Pies denote ensemble mean while whiskers show range across 20 climate models.

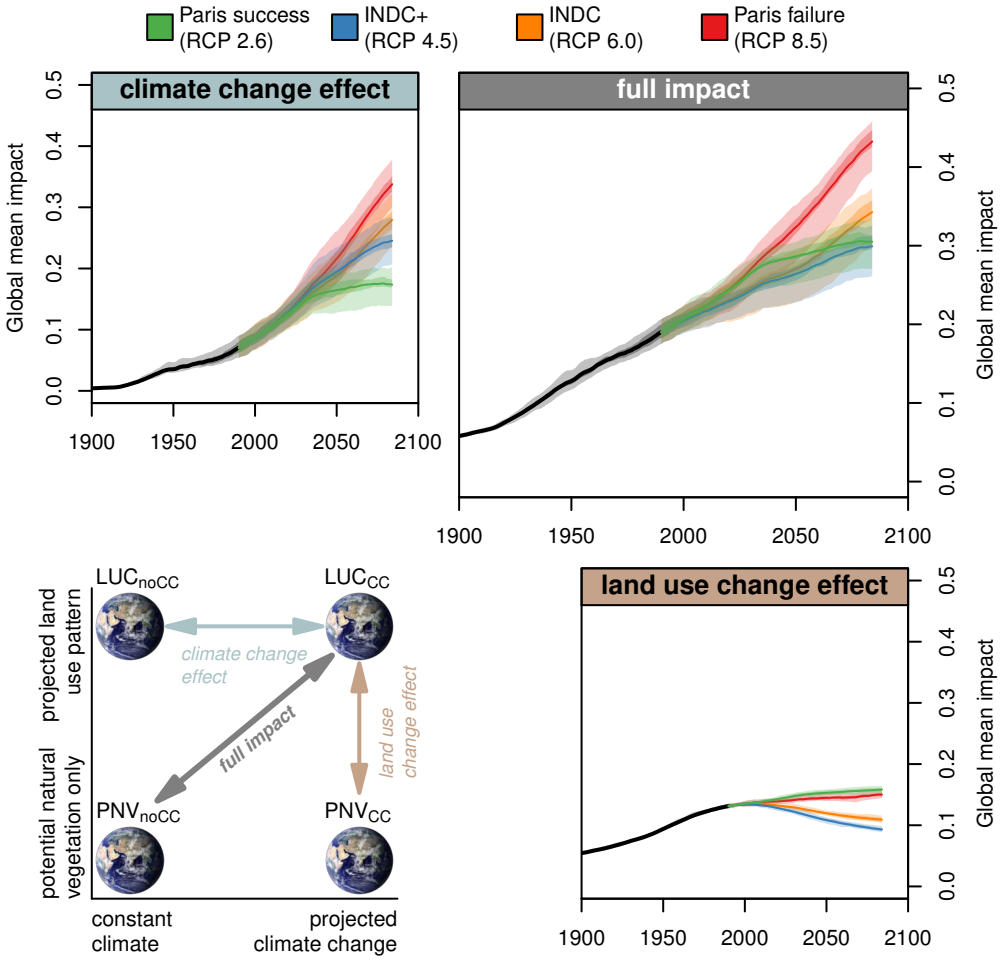

Figure E.8.: Global mean impact of climate change and land use change on the biosphere. Analogous to Figure VI.1 in Part VI, climate change effect and land use change effect describe the individual impacts of CC and LUC while the full impact measures the combined effect of both drivers. Instead of using a threshold to distinguish areas with major impacts, Γ values in each landscape (grid cell) are averaged using an area-weighted mean. Earth image by NASA Goddard Space Flight Center.

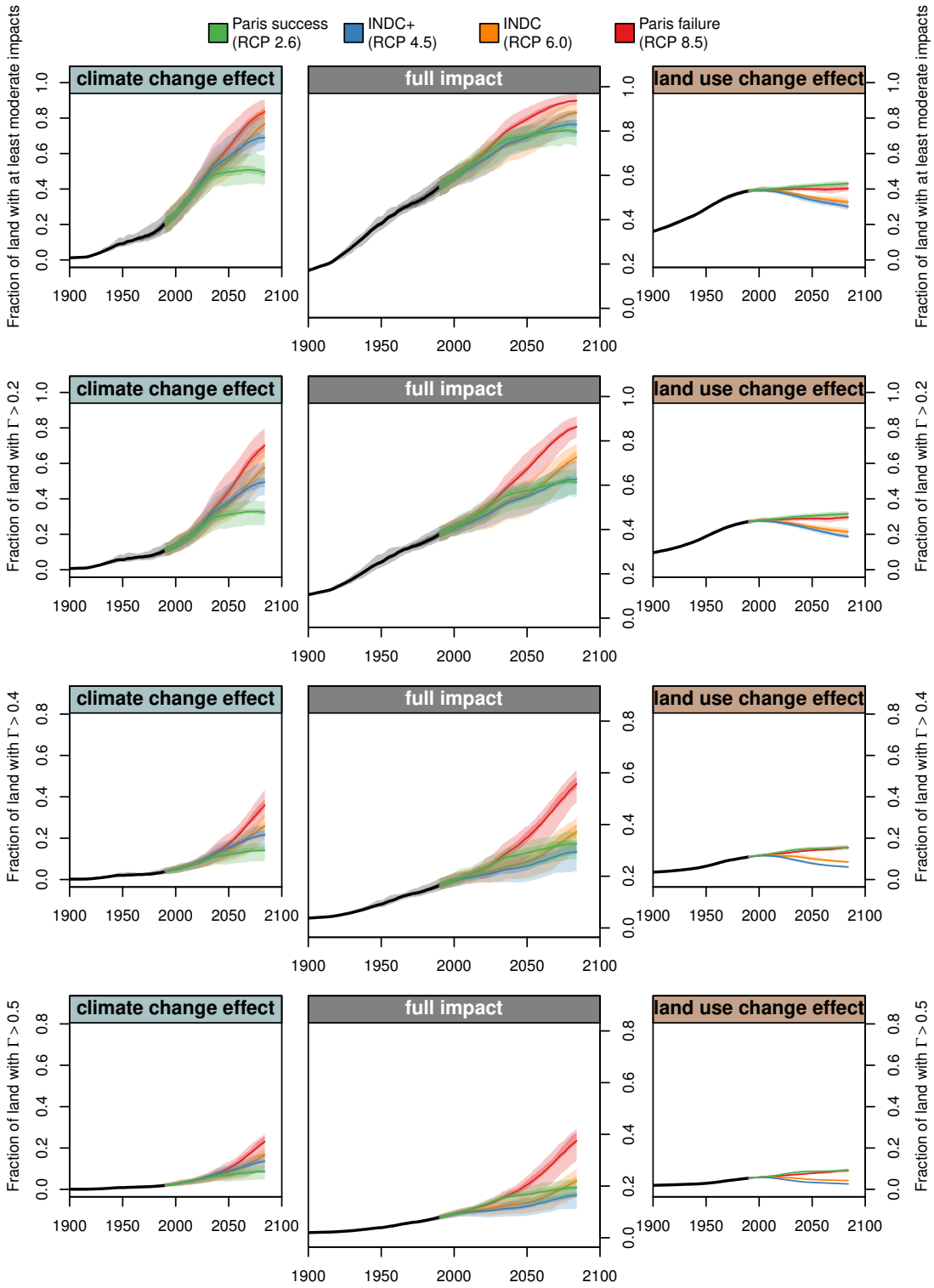

Figure E.9.: Sensitivity of the area with projected major impacts to the threshold used. Presentation as in Figure E.8 and Figure VI.1 in Part VI.

Bibliography

Abram, N. J., H. V. McGregor, J. E. Tierney, M. N. Evans, N. P. McKay, D. S. Kaufman, K. Thirumalai, B. Martrat, H. Goosse, S. J. Phipps, E. J. Steig, K. H. Kilbourne, C. P. Saenger, J. Zinke, G. Leduc, J. A. Addison, P. G. Mortyn, M.-S. Seidenkrantz, M.-A. Sicre, K. Selvaraj, H. L. Filipsson, R. Neukom, J. Gergis, M. A. J. Curran, and L. von Gunten. 2016. 'Early onset of industrial-era warming across the oceans and continents.' *Nature* 536 (7617): 411–418. doi:10.1038/nature19082. (Cited on page 20).

Ainsworth, E. A., C. Beier, C. Calfapietra, R. Ceulemans, M. Durand-Tardif, G. D. Farquhar, D. L. Godbold, G. R. Hendrey, T. Hickler, J. Kaduk, D. F. Karnosky, B. A. Kimball, C. Körner, M. Koornneef, T. Lafarge, A. D. B. Leakey, K. F. Lewin, S. P. Long, R. Manderscheid, D. L. McNeil, T. A. Mies, F. Miglietta, J. A. Morgan, J. Nagy, R. J. Norby, R. M. Norton, K. E. Percy, A. Rogers, J.-F. Soussana, M. Stitt, H.-J. Weigel, and J. W. White. 2008. 'Next generation of elevated [CO2] experiments with crops: a critical investment for feeding the future world.' *Plant, Cell & Environment* 31 (9): 1317–1324. doi:10.1111/j.1365-3040.2008.01841.x. (Cited on page 12).

Allen, C. D., A. K. Macalady, H. Chenchouni, D. Bachelet, N. McDowell, M. Vennetier, T. Kitzberger, A. Rigling, D. D. Breshears, E. (Hogg, P. Gonzalez, R. Fensham, Z. Zhang, J. Castro, N. Demidova, J.-h. Lim, G. Allard, S. W. Running, A. Semerci, and N. Cobb. 2010. 'A global overview of drought and heat-induced tree mortality reveals emerging climate change risks for forests.' *Forest Ecology and Management* 259 (4): 660–684. doi:10.1016/j.foreco.2009.09.001. (Cited on page 98).

Alton, P., R. Fisher, S. Los, and M. Williams. 2009. 'Simulations of global evapotranspiration using semiempirical and mechanistic schemes of plant hydrology.' *Global Biogeochemical Cycles* 23 (4): GB4023. doi:10.1029/2009GB003540. (Cited on page 5).

Anderson, R. C., J. S. Fralish, and J. M. Baskin. 1999. 'Introduction.' In *Savanna, Barrens, and Rock Outcrop Plant Communities of North America,* edited by R. C. Anderson, J. S. Fralish, and J. M. Baskin, 1–6. Cambridge University Press. (Cited on page 65).

Arnell, N. W., J. A. Lowe, S. Brown, S. N. Gosling, P. Gottschalk, J. Hinkel, B. Lloyd-Hughes, R. J. Nicholls, T. J. Osborn, T. M. Osborne, G. A. Rose, P. Smith, and R. F. Warren. 2013. 'A global assessment of the effects of climate policy on the impacts of climate change.' *Nature Climate Change* 3 (5): 512–519. doi:10.1038/nclimate1793. (Cited on page 101).

Arnell, N. W., D. P. van Vuuren, and M. Isaac. 2011. 'The implications of climate policy for the impacts of climate change on global water resources.' *Global Environmental Change* 21 (2): 592–603. doi:10.1016/j.gloenvcha.2011.01.015. (Cited on pages 26, 84, 88).

Balvanera, P., S. Quijas, D. S. Karp, N. Ash, E. M. Bennett, R. Boumans, C. Brown, K. M. A. Chan, R. Chaplin-Kramer, B. S. Halpern, J. Honey-Rosés, C.-K. Kim, W. Cramer, M. J. Martínez-Harms, H. Mooney, T. Mwampamba, J. Nel, S. Polasky, B. Reyers, J. Roman, W. Turner, R. J. Scholes, H. Tallis, K. Thonicke, F. Villa, M. Walpole, and A. Walz. 2017. 'Ecosystem Services.' Chap. 3 in *The GEO Handbook on Biodiversity Observation Networks,* edited by M. Walters and R. J. Scholes, 39–78. Cham: Springer International Publishing. doi:10.1007/978-3-319-27288-7_3. (Cited on page 6).

Bates, B. C., Z. W. Kundzewicz, S. Wu, and J. P. Palutikof, eds. 2008. *Climate Change and Water. Technical Paper of the Intergovernmental Panel on Climate Change.* 210 pp. Geneva: IPCC Secretariat. (Cited on page 91).

Beck, P. S. A., and S. J. Goetz. 2011. 'Satellite observations of high northern latitude vegetation productivity changes between 1982 and 2008: ecological variability and regional differences.' *Environmental Research Letters* 6 (4): 045501. doi:10.1088/1748-9326/6/4/045501. (Cited on pages 13, 147).

Becker, A., P. Finger, A. Meyer-Christoffer, B. Rudolf, K. Schamm, U. Schneider, and M. Ziese. 2013. 'A description of the global land-surface precipitation data products of the Global Precipitation Climatology Centre with sample applications including centennial (trend) analysis from 1901–present.' *Earth System Science Data* 5 (1): 71–99. doi:10.5194/essd-5-71-2013. (Cited on pages 18, 112, 136).

Beer, C., M. Reichstein, E. Tomelleri, P. Ciais, M. Jung, N. Carvalhais, C. Rodenbeck, M. A. Arain, D. Baldocchi, G. B. Bonan, A. Bondeau, A. Cescatti, G. Lasslop, A. Lindroth, M. Lomas, S. Luyssaert, H. Margolis, K. W. Oleson, O. Roupsard, E. Veenendaal, N. Viovy, C. Williams, F. I. Woodward, and D. Papale. 2010. 'Terrestrial Gross Carbon Dioxide Uptake: Global Distribution and Covariation with Climate.' *Science* 329 (5993): 834–838. doi:10.1126/science.1184984. (Cited on page 4).

Belda, M., E. Holtanová, T. Halenka, and J. Kalvová. 2014. 'Climate classification revisited: from Köppen to Trewartha.' *Climate Research* 59 (1): 1–13. doi:10.3354/cr01204. (Cited on page 6).

Benton, M. J. 2001. 'Biodiversity on land and in the sea.' *Geological Journal* 36 (3-4): 211–230. doi:10.1002/gj.877. (Cited on page 4).

Beringer, T., W. Lucht, and S. Schaphoff. 2011. 'Bioenergy production potential of global biomass plantations under environmental and agricultural constraints.' *GCB Bioenergy* 3 (4): 299–312. doi:10.1111/j.1757-1707.2010.01088.x. (Cited on pages 17, 18, 134, 177).

Biemans, H., I. Haddeland, P. Kabat, F. Ludwig, R. W. A. Hutjes, J. Heinke, W. von Bloh, and D. Gerten. 2011. 'Impact of reservoirs on river discharge and irrigation water supply during the 20th century.' *Water Resources Research* 47 (3): W03509. doi:10.1029/2009WR008929. (Cited on page 138).

Bindoff, N. L., P. A. Stott, K. M. AchutaRao, M. R. Allen, N. Gillett, D. Gutzler, K. Hansingo, G. Hegerl, Y. Hu, S. Jain, I. I. Mokhov, J. Overland, J. Perlwitz, R. Sebbari, and X. Zhang. 2013. 'Detection and Attribution of Climate Change: from Global to Regional.' Chap. 10 in *Climate Change 2013: The Physical Science Basis. Contribution of Working Group I to the Fifth Assessment Report of the Intergovernmental Panel on Climate Change,* edited by T. Stocker, D. Qin, G.-K. Plattner, M. Tignor, S. Allen, J. Boschung, A. Nauels, Y. Xia, V. Bex, and P. Midgley, 867–952. Cambridge, UK and New York, NY, USA: Cambridge University Press. doi:10.1017/CBO9781107415324.022. (Cited on page 20).

Blois, J. L., J. W. Williams, M. C. Fitzpatrick, S. T. Jackson, and S. Ferrier. 2013. 'Space can substitute for time in predicting climate-change effects on biodiversity.' *Proceedings of the National Academy of Sciences* 110 (23): 9374–9. doi:10.1073/pnas.1220228110. (Cited on page 65).

Bobbink, R., K. Hicks, J. Galloway, T. Spranger, R. Alkemade, M. Ashmore, M. Bustamante, S. Cinderby, E. Davidson, F. Dentener, B. Emmett, J.-W. Erisman, M. Fenn, F. Gilliam, A. Nordin, L. Pardo, and W. De Vries. 2010. 'Global assessment of nitrogen deposition effects on terrestrial plant diversity: a synthesis.' *Ecological Applications* 20 (1): 30–59. doi:10.1890/08-1140.1. (Cited on pages 9, 151).

Boit, A., B. Sakschewski, L. Boysen, A. Cano-Crespo, J. Clement, N. Garcia-Alaniz, K. Kok, M. Kolb, F. Langerwisch, A. Rammig, R. Sachse, M. van Eupen, W. von Bloh, D. Clara Zemp, and K. Thonicke. 2016. 'Large-scale impact of climate change vs. land-use change on future biome shifts in Latin America.' *Global Change Biology* 22 (11): 3689–3701. doi:10.1111/gcb.13355. (Cited on pages 131, 148).

Bondeau, A., P. C. Smith, S. Zaehle, S. Schaphoff, W. Lucht, W. Cramer, D. Gerten, H. Lotze-Campen, C. Müller, M. Reichstein, and B. Smith. 2007. 'Modelling the role of agriculture for the 20th century global terrestrial carbon balance.' *Global Change Biology* 13 (3): 679–706. doi:10.1111/j.1365-2486.2006.01305.x. (Cited on pages 9, 17, 18, 85–87, 110, 111, 134, 135, 177).

Boucher, O., D. Randall, P. Artaxo, C. Bretherton, G. Feingold, P. Forster, V.-M. Kerminen, Y. Kondo, H. Liao, U. Lohmann, P. Rasch, S. K. Satheesh, S. Sherwood, B. Stevens, and X. Y. Zhang. 2013. 'Clouds and Aerosols.' Chap. 7 in *Climate Change 2013: The Physical Science Basis. Contribution of Working Group I to the Fifth Assessment Report of the Intergovernmental Panel on Climate Change,* edited by T. Stocker, D. Qin, G.-K. Plattner, M. Tignor, S. Allen, J. Boschung, A. Nauels, Y. Xia, V. Bex, and P. Midgley, 571–658. Cambridge, UK and New York, NY, USA: Cambridge University Press. doi:10.1017/CBO9781107415324.016. (Cited on page 11).

Boysen, L. R., W. Lucht, D. Gerten, and V. Heck. 2016. 'Impacts devalue the potential of large-scale terrestrial CO 2 removal through biomass plantations.' *Environmental Research Letters* 11 (9): 095010. doi:10.1088/1748-9326/11/9/095010. (Cited on page 170).

Brando, P. M., J. K. Balch, D. C. Nepstad, D. C. Morton, F. E. Putz, M. T. Coe, D. Silvério, M. N. Macedo, E. A. Davidson, C. C. Nobrega, A. Alencar, and B. S. Soares-Filho. 2014. 'Abrupt increases in Amazonian tree mortality due to drought-fire interactions.' *Proceedings of the National Academy of Sciences* 111 (17): 6347–6352. doi:10.1073/pnas.1305499111. (Cited on page 13).

Brook, B. W., and D. M. J. S. Bowman. 2006. 'Postcards from the past: charting the landscape-scale conversion of tropical Australian savanna to closed forest during the 20th century.' *Landscape Ecology* 21 (8): 1253–1266. doi:10.1007/s10980-006-0018-7. (Cited on page 123).

Brown, J., O. J. Ferrians Jr., J. A. Heginbottom, and E. S. Melnikow. 1998. *Circum-arctic map of permafrost and ground ice conditions.* Bolder, Co: National Snow and Ice Data Center, Available online at http://nsidc.org/data/ggd318.html. (Cited on page 219).

Bruinsma, J., ed. 2003. *World agriculture : towards 2015 / 2030 – an FAO perspective.* 444 pp. London, UK: Earthscan Publications Ltd. (Cited on page 150).

Burney, J. a., S. J. Davis, and D. B. Lobell. 2010. 'Greenhouse gas mitigation by agricultural intensification.' *Proceedings of the National Academy of Sciences* 107 (26): 12052–12057. doi:10.1073/pnas.0914216107. (Cited on pages 7, 163, 170).

Carter, T., M. Parry, H. Harasawa, and S. Nishioka. 1994. *IPCC Technical Guidelines for Assessing Climate Change Impacts and Adaptations,* 72 pp. Department of Geography, University College London, UK / the Center for Global Environmental Research, National Institute for Environmental Studies, Japan. (Cited on pages 19, 38).

Cassman, K. G., S. Wood, P. S. Choo, H. D. Cooper, C. Devendra, J. Dixon, J. Gaskell, S. Khan, R. Lal, L. Lipper, J. Pretty, J. Primavera, N. Ramankutty, E. Viglizzo, K. Wiebe, S. Kadungure, N. Kanbar, Z. Khan, R. Leakey, S. Porter, K. Sebastian, and R. Tharme. 2005. 'Cultivated Systems.' Chap. 26 in *Ecosystems and Human Well-being: Current State & Trends, Volume 1,* edited by A. Balisacan and P. Gardiner, 745–794. Island Press, Washington, DC. (Cited on pages 7, 8, 151).

Chapin, F. S., P. A. Matson, and P. M. Vitousek. 2011. *Principles of Terrestrial Ecosystem Ecology.* 2nd edition. 546 pp. New York, NY: Springer New York. doi:10.1007/978-1-4419-9504-9. (Cited on pages 3–5, 61, 162).

Chen, I.-C., J. K. Hill, R. Ohlemüller, D. B. Roy, and C. D. Thomas. 2011. 'Rapid Range Shifts of Species Associated with High Levels of Climate Warming.' *Science* 333 (6045): 1024–1026. doi:10.1126/science.1206432. (Cited on page 12).

Ciais, P., C. Sabine, G. Bala, L. Bopp, V. Brovkin, J. Canadell, A. Chhabra, R. DeFries, J. Galloway, M. Heimann, C. Jones, C. Le Quéré, R. Myneni, S. Piao, and P. Thornton. 2013. 'Carbon and Other Biogeochemical Cycles.' Chap. 6 in *Climate Change 2013: The Physical Science Basis. Contribution of Working Group I to the Fifth Assessment Report of the Intergovernmental Panel on Climate Change,* edited by T. Stocker, D. Qin, G.-K. Plattner, M. Tignor, S. Allen, J. Boschung, A. Nauels, Y. Xia, V. Bex, and P. Midgley, 465–570. Cambridge, UK and New York, NY, USA: Cambridge University Press. doi:10.1017/CBO9781107415324.015. (Cited on pages 4, 9).

Clark, M., and D. Tilman. 2017. 'Comparative analysis of environmental impacts of agricultural production systems, agricultural input efficiency, and food choice.' *Environmental Research Letters* 12 (6): 064016. doi:10.1088/1748-9326/aa6cd5. (Cited on page 170).

Clarke, L. E., K. Jiang, K. Akimoto, M. Babiker, G. Blanford, K. Fisher-Vanden, J.-C. Hourcade, V. Krey, E. Kriegler, A. Löschel, D. McCollum, S. Paltsev, S. K. Rose, P. R. Shukla, M. Tavoni, B. C. C. van der Zwaan, and D. P. van Vuuren. 2014. 'Assessing Transformation Pathways.' Chap. 6 in *Climate Change 2014: Mitigation of Climate Change. Contribution of Working Group III to the Fifth Assessment Report of the Intergovernmental Panel on Climate Change,* edited by O. Edenhofer, R. Pichs-Madruga, Y. Sokona, E. Farahani, S. Kadner, K. Seyboth, A. Adler, I. Baum, S. Brunner, P. Eickemeier, B. Kriemann, J. Savolainen, S. Schlömer, C. von Stechow, T. Zwickel, and J. C. Minx, 413–510. Cambridge, UK and New York, NY, USA: Cambridge University Press. (Cited on page 14).

Collatz, G. J., M. Ribas-Carbo, and J. A. Berry. 1992. 'Coupled Photosynthesis-Stomatal Conductance Model for Leaves of C 4 Plants.' *Australian Journal of Plant Physiology* 19 (5): 519–538. doi:10.1071/PP9920519. (Cited on page 64).

Collins, M., R. Knutti, J. Arblaster, J.-L. Dufresne, T. Fichefet, P. Friedlingstein, X. Gao, W. J. Gutowski, T. Johns, G. Krinner, M. Shongwe, C. Tebaldi, A. J. Weaver, and M. Wehner. 2013. 'Long-term Climate Change: Projections, Commitments and Irreversibility.' Chap. 12 in *Climate Change 2013: The Physical Science Basis. Contribution of Working Group I to the Fifth Assessment Report of the Intergovernmental Panel on Climate Change,* edited by T. Stocker, D. Qin, G.-K. Plattner, M. Tignor, S. Allen, J. Boschung, A. Nauels, Y. Xia, V. Bex, and P. Midgley, 1029–1136. Cambridge: Cambridge University Press. doi:10.1017/CBO9781107415324.024. (Cited on pages 132, 139, 158).

Costello, M. J., R. M. May, and N. E. Stork. 2013. 'Can We Name Earth's Species Before They Go Extinct?' *Science* 339 (6118): 413–416. doi:10.1126/science.1230318. (Cited on page 4).

Cramer, W., A. Bondeau, F. I. Woodward, I. C. Prentice, R. A. Betts, V. Brovkin, P. M. Cox, V. Fisher, J. A. Foley, A. D. Friend, C. Kucharik, M. R. Lomas, N. Ramankutty, S. Sitch, B. Smith, A. White, and C. Young-Molling. 2001. 'Global response of terrestrial ecosystem structure and function to CO2 and climate change: results from six dynamic global vegetation models.' *Global Change Biology* 7 (4): 357–373. doi:10.1046/j.1365-2486.2001.00383.x. (Cited on pages 77, 165, 168).

Cramer, W., G. W. Yohe, M. Auffhammer, C. Huggel, U. Molau, M. A. F. da Silva Dias, A. Solow, D. A. Stone, and L. Tibig. 2014. 'Detection and Attribution of Observed Impacts.' Chap. 18 in *Climate Change 2014: Impacts, Adaptation, and Vulnerability. Part A: Global and Sectoral Aspects. Contribution of Working Group II to the Fifth Assessment Report of the Intergovernmental Panel on Climate Change,* edited by C. B. Field, V. R. Barros, D. J. Dokken, K. J. Mach, M. D. Mastrandrea, and L. L. White, 979–1038. Cambridge, UK and New York, NY, USA: Cambridge University Press. doi:10.1017/CBO9781107415379.023. (Cited on page 5).

Crutzen, P. J. 2002. 'Geology of mankind.' *Nature* 415 (6867): 23–23. doi:10.1038/415023a. (Cited on page 3).

Davies-Barnard, T., P. J. Valdes, J. S. Singarayer, A. J. Wiltshire, and C. D. Jones. 2015. 'Quantifying the relative importance of land cover change from climate and land use in the representative concentration pathways.' *Global Biogeochemical Cycles* 29 (6): 842–853. doi:10.1002/2014GB004949. (Cited on pages 131, 148).

De Noblet-Ducoudré, N., J.-P. Boisier, A. Pitman, G. B. Bonan, V. Brovkin, F. Cruz, C. Delire, V. Gayler, B. J. J. M. van den Hurk, P. J. Lawrence, M. K. van der Molen, C. Müller, C. H. Reick, B. J. Strengers, and A. Voldoire. 2012. 'Determining Robust Impacts of Land-Use-Induced Land Cover Changes on Surface Climate over North America and Eurasia: Results from the First Set of LUCID Experiments.' *Journal of Climate* 25 (9): 3261–3281. doi:10.1175/JCLI-D-11-00338.1. (Cited on page 168).

Deser, C., A. Phillips, V. Bourdette, and H. Teng. 2010. 'Uncertainty in climate change projections: the role of internal variability.' *Climate Dynamics* 38 (3-4): 527–546. doi:10.1007/s00382-010-0977-x. (Cited on page 66).

Diffenbaugh, N. S., and C. B. Field. 2013. 'Changes in Ecologically Critical Terrestrial Climate Conditions.' *Science* 341 (6145): 486–492. doi:10.1126/science.1237123. arXiv: 9605103 [cs]. (Cited on page 99).

Dise, N. B., M. Ashmore, S. Belyazid, A. Bleeker, R. Bobbink, W. de Vries, J. W. Erisman, T. Spranger, C. J. Stevens, and L. van den Berg. 2011. 'Nitrogen as a threat to European terrestrial biodiversity.' Chap. 20 in *The European Nitrogen Assessment,* edited by M. A. Sutton, C. M. Howard, J. W. Erisman, G. Billen, A. Bleeker, P. Grennfelt, and H. van Grinsven, 463–494. Cambridge University Press, Cambridge, United Kingdom / New York, NY, USA. (Cited on pages 9, 151).

Dlugokencky, E., and P. Tans. 2017. 'Trends in Atmospheric Carbon Dioxide.' National Oceanic & Atmospheric Administration, Earth System Research Laboratory (NOAA/ESRL). Accessed May 17, 2017. http://www.esrl.noaa.gov/gmd/ccgg/trends/global.html. (Cited on pages 10, 130).

Döll, P., K. Fiedler, and J. Zhang. 2009. 'Global-scale analysis of river flow alterations due to water withdrawals and reservoirs.' *Hydrology and Earth System Sciences* 13 (12): 2413–2432. doi:10.5194/hess-13-2413-2009. (Cited on page 9).

Döll, P., H. Hoffmann-Dobrev, F. T. Portmann, S. Siebert, A. Eicker, M. Rodell, G. Strassberg, and B. R. Scanlon. 2012. 'Impact of water withdrawals from groundwater and surface water on continental water storage variations.' *Journal of Geodynamics* 59-60:143–156. doi:10.1016/j.jog.2011.05.001. (Cited on pages 9, 150).

Döll, P., H. Müller Schmied, C. Schuh, F. T. Portmann, and A. Eicker. 2014. 'Global-scale assessment of groundwater depletion and related groundwater abstractions: Combining hydrological modeling with information from well observations and GRACE satellites.' *Water Resources Research* 50 (7): 5698–5720. doi:10.1002/2014WR015595. (Cited on pages 9, 150).

Donohue, R. J., M. L. Roderick, and T. R. McVicar. 2007. 'On the importance of including vegetation dynamics in Budyko's hydrological model.' *Hydrology and Earth System Sciences* 11 (2): 983–995. doi:10.5194/hess-11-983-2007. (Cited on page 5).

Donohue, R. J., M. L. Roderick, T. R. McVicar, and G. D. Farquhar. 2013. 'Impact of CO 2 fertilization on maximum foliage cover across the globe's warm, arid environments.' *Geophysical Research Letters* 40 (12): 3031–3035. doi:10.1002/grl.50563. (Cited on pages 12, 107).

Ellis, E. C. 2011. 'Anthropogenic transformation of the terrestrial biosphere.' *Philosophical transactions. Series A, Mathematical, physical, and engineering sciences* 369 (1938): 1010–35. doi:10.1098/rsta.2010.0331. (Cited on page 3).

Ellis, E. C., J. O. Kaplan, D. Q. Fuller, S. Vavrus, K. Klein Goldewijk, and P. H. Verburg. 2013. 'Used planet: a global history.' *Proceedings of the National Academy of Sciences* 110 (20): 7978–85. doi:10.1073/pnas.1217241110. (Cited on pages 119, 125).

Ellis, E. C., K. Klein Goldewijk, S. Siebert, D. Lightman, and N. Ramankutty. 2010. 'Anthropogenic transformation of the biomes, 1700 to 2000.' *Global Ecology and Biogeography* 19 (5): 589–606. doi:10.1111/j.1466-8238.2010.00540.x. (Cited on pages 130, 141, 162).

Ellis, E. C., and N. Ramankutty. 2008. 'Putting people in the map: anthropogenic biomes of the world.' *Frontiers in Ecology and the Environment* 6 (8): 439–447. doi:10.1890/070062. (Cited on pages 106, 131, 162).

Erisman, J. W., J. N. Galloway, S. Seitzinger, A. Bleeker, N. B. Dise, A. M. R. Petrescu, A. M. Leach, and W. de Vries. 2013. 'Consequences of human modification of the global nitrogen cycle.' *Philosophical transactions of the Royal Society of London. Series B, Biological sciences* 368 (1621): 20130116. doi:10.1098/rstb.2013.0116. (Cited on pages 5, 9, 151).

Fader, M., D. Gerten, M. Thammer, J. Heinke, H. Lotze-Campen, W. Lucht, and W. Cramer. 2011. 'Internal and external green-blue agricultural water footprints of nations, and related water and land savings through trade.' *Hydrology and Earth System Sciences* 15 (5): 1641–1660. doi:10.5194/hess-15-1641-2011. (Cited on page 88).

Fader, M., S. Rost, C. Müller, A. Bondeau, and D. Gerten. 2010. 'Virtual water content of temperate cereals and maize: Present and potential future patterns.' *Journal of Hydrology* 384 (3-4): 218–231. doi:10.1016/j.jhydrol.2009.12.011. (Cited on pages 87, 111, 135, 136, 178, 209).

Falkenmark, M., and C. Widstrand. 1992. 'Population and Water Resources: A Delicate Balance.' *Population Bulletin* 47 (3). (Cited on page 88).

FAO. 2012. *Coping with water scarcity – An action framework for agriculture and food security.* 79 pp. Rome: Food and Agriculture Organization of the United Nations. (Cited on page 150).

FAO. 2014. 'AQUASTAT database.' Food and Agriculture Organization of the United Nations, Rome. Accessed October 18, 2014. http://www.fao.org/nr/water/aquastat/data/query/index.html?lang=en. (Cited on page 137).

FAO. 2016. 'FAOSTAT.' Food and Agriculture Organization of the United Nations, Rome. Accessed December 29, 2016. http://www.fao.org/faostat/en/. (Cited on pages 7, 8, 130, 139, 150).

FAO, IFAD, and WFP. 2015. *The State of Food Insecurity in the World: Meeting the 2015 international hunger targets: taking stock of uneven progress.* 62 pp. Rome: Food and Agriculture Organization of the United Nations. (Cited on page 8).

FAO, IIASA, ISRIC, ISSCAS, and JRC. 2012. *Harmonized World Soil Database (version 1.2).* Available online at http://webarchive.iiasa.ac.at/Research/LUC/External-World-soil-database/HTML/. FAO, Rome, Italy and IIASA, Laxenburg, Austria. (Cited on page 138).

Farquhar, G. D., S. Caemmerer, and J. A. Berry. 1980. 'A biochemical model of photosynthetic CO2 assimilation in leaves of C3 species.' *Planta* 149 (1): 78–90. doi:10.1007/BF00386231. (Cited on page 64).

Fawcett, A. A., G. C. Iyer, L. E. Clarke, J. A. Edmonds, N. E. Hultman, H. C. McJeon, J. Rogelj, R. Schuler, J. Alsalam, G. R. Asrar, J. Creason, M. Jeong, J. McFarland, A. Mundra, and W. Shi. 2015. 'Can Paris pledges avert severe climate change?' *Science* 350 (6265): 1168–1169. doi:10.1126/science.aad5761. (Cited on page 131).

Feddema, J. J., K. W. Oleson, G. B. Bonan, L. O. Mearns, L. E. Buja, G. A. Meehl, and W. M. Washington. 2005. 'The Importance of Land-Cover Change in Simulating Future Climates.' *Science* 310 (5754): 1674–1678. doi:10.1126/science.1118160. (Cited on page 168).

Fensham, R. J., R. J. Fairfax, and S. R. Archer. 2005. 'Rainfall, land use and woody vegetation cover change in semi-arid Australian savanna.' *Journal of Ecology* 93 (3): 596–606. doi:10.1111/j.1365-2745.2005.00998.x. (Cited on page 124).

Foley, J. A., R. Defries, G. P. Asner, C. Barford, G. Bonan, S. R. Carpenter, F. S. Chapin, M. T. Coe, G. C. Daily, H. K. Gibbs, J. H. Helkowski, T. Holloway, E. a. Howard, C. J. Kucharik, C. Monfreda, J. a. Patz, I. C. Prentice, N. Ramankutty, and P. K. Snyder. 2005. 'Global consequences of land use.' *Science* 309 (5734): 570–4. doi:10.1126/science.1111772. (Cited on page 7).

Foley, J. A., N. Ramankutty, K. A. Brauman, E. S. Cassidy, J. S. Gerber, M. Johnston, N. D. Mueller, C. O'Connell, D. K. Ray, P. C. West, C. Balzer, E. M. Bennett, S. R. Carpenter, J. Hill, C. Monfreda, S. Polasky, J. Rockström, J. Sheehan, S. Siebert, D. Tilman, and D. P. M. Zaks. 2011. 'Solutions for a cultivated planet.' *Nature* 478 (7369): 337–42. doi:10.1038/nature10452. (Cited on pages 7, 125, 150, 152, 170).

Frenken, K., and V. Gillet. 2012. *Irrigation water requirement and water withdrawal by country.* Technical report. Rome: Food and Agriculture Organization of the United Nations. (Cited on page 9).

Friedl, M. A., D. McIver, J. C. Hodges, X. Zhang, D. Muchoney, A. Strahler, C. Woodcock, S. Gopal, A. Schneider, A. Cooper, A. Baccini, F. Gao, and C. Schaaf. 2002. 'Global land cover mapping from MODIS: algorithms and early results.' *Remote Sensing of Environment* 83 (1-2): 287–302. doi:10.1016/S0034-4257(02)00078-0. (Cited on page 216).

Friedlingstein, P., P. Cox, R. Betts, L. Bopp, W. von Bloh, V. Brovkin, P. Cadule, S. Doney, M. Eby, I. Fung, G. Bala, J. John, C. Jones, F. Joos, T. Kato, M. Kawamiya, W. Knorr, K. Lindsay, H. D. Matthews, T. Raddatz, P. Rayner, C. Reick, E. Roeckner, K.-G. Schnitzler, R. Schnur, K. Strassmann, A. J. Weaver, C. Yoshikawa, and N. Zeng. 2006. 'Climate-Carbon Cycle Feedback Analysis: Results from the C 4 MIP Model Intercomparison.' *Journal of Climate* 19 (14): 3337–3353. doi:10.1175/JCLI3800.1. (Cited on page 166).

Friedlingstein, P., R. A. Houghton, G. Marland, J. Hackler, T. A. Boden, T. J. Conway, J. G. Canadell, M. R. Raupach, P. Ciais, and C. Le Quéré. 2010. 'Update on CO2 emissions.' *Nature Geoscience* 3 (12): 811–812. doi:10.1038/ngeo1022. (Cited on page 107).

Friend, A. D., W. Lucht, T. T. Rademacher, R. Keribin, R. Betts, P. Cadule, P. Ciais, D. B. Clark, R. Dankers, P. D. Falloon, A. Ito, R. Kahana, A. Kleidon, M. R. Lomas, K. Nishina, S. Ostberg, R. Pavlick, P. Peylin, S. Schaphoff, N. Vuichard, L. Warszawski, A. Wiltshire, and F. I. Woodward. 2014. 'Carbon residence time dominates uncertainty in terrestrial vegetation responses to future climate and atmospheric CO2.' *Proceedings of the National Academy of Sciences* 111 (9): 3280–3285. doi:10.1073/pnas.1222477110. (Cited on page 168).

Fung, F., A. Lopez, and M. New. 2011. 'Water availability in +2 C and +4 C worlds.' *Philosophical Transactions of the Royal Society A: Mathematical, Physical and Engineering Sciences* 369 (1934): 99–116. doi:10.1098/rsta.2010.0293. (Cited on page 84).

Füssel, H.-M. 2003. 'Impacts analysis for inverse integrated assessments of climate change.' PhD diss., Potsdam University, Potsdam, Germany. (Cited on page 38).

Füssel, H.-M. 2010. 'How inequitable is the global distribution of responsibility, capability, and vulnerability to climate change: A comprehensive indicator-based assessment.' *Global Environmental Change* 20 (4): 597–611. doi:10.1016/j.gloenvcha.2010.07.009. (Cited on page 85).

Galloway, J. N., A. R. Townsend, J. W. Erisman, M. Bekunda, Z. Cai, J. R. Freney, L. a. Martinelli, S. P. Seitzinger, and M. a. Sutton. 2008. 'Transformation of the nitrogen cycle: recent trends, questions, and potential solutions.' *Science* 320 (5878): 889–92. doi:10.1126/science.1136674. (Cited on page 9).

Gerber, S., F. Joos, and I. C. Prentice. 2004. 'Sensitivity of a dynamic global vegetation model to climate and atmospheric CO2.' *Global Change Biology* 10 (8): 1223–1239. doi:10.1111/j.1529-8817.2003.00807.x. (Cited on pages 26, 89).

Gerten, D., J. Heinke, H. Hoff, H. Biemans, M. Fader, and K. Waha. 2011. 'Global Water Availability and Requirements for Future Food Production.' *Journal of Hydrometeorology* 12 (5): 885–899. doi:10.1175/2011JHM1328.1. (Cited on pages 38, 88).

Gerten, D., W. Lucht, S. Ostberg, J. Heinke, M. Kowarsch, H. Kreft, Z. W. Kundzewicz, J. Rastgooy, R. Warren, and H. J. Schellnhuber. 2013. 'Asynchronous exposure to global warming: freshwater resources and terrestrial ecosystems.' *Environmental Research Letters* 8 (3): 034032. doi:10.1088/1748-9326/8/3/034032. (Cited on pages 74, 77, 81, 195).

Gerten, D., S. Rost, W. von Bloh, and W. Lucht. 2008. 'Causes of change in 20th century global river discharge.' *Geophysical Research Letters* 35 (20): L20405. doi:10.1029/2008GL035258. (Cited on pages 107, 166).

Gerten, D., S. Schaphoff, U. Haberlandt, W. Lucht, and S. Sitch. 2004. 'Terrestrial vegetation and water balance—hydrological evaluation of a dynamic global vegetation model.' *Journal of Hydrology* 286 (1-4): 249–270. doi:10.1016/j.jhydrol.2003.09.029. (Cited on pages 5, 64, 85–87, 111, 135).

Gibbs, H. K., A. S. Ruesch, F. Achard, M. K. Clayton, P. Holmgren, N. Ramankutty, and J. A. Foley. 2010. 'Tropical forests were the primary sources of new agricultural land in the 1980s and 1990s.' *Proceedings of the National Academy of Sciences* 107 (38): 16732–16737. doi:10.1073/pnas.0910275107. (Cited on page 8).

GISTEMP Team. 2017. 'GISS Surface Temperature Analysis (GISTEMP).' NASA Goddard Institute for Space Studies. Accessed March 13, 2017. https://data.giss.nasa.gov/gistemp/. (Cited on page 130).

Godfray, H. C. J., J. R. Beddington, I. R. Crute, L. Haddad, D. Lawrence, J. F. Muir, J. Pretty, S. Robinson, S. M. Thomas, and C. Toulmin. 2010. 'Food Security: The Challenge of Feeding 9 Billion People.' *Science* 327 (5967): 812–818. doi:10.1126/science.1185383. (Cited on page 170).

Godfray, H. C. J., and T. Garnett. 2014. 'Food security and sustainable intensification.' *Philosophical Transactions of the Royal Society B: Biological Sciences* 369 (1639): 20120273–20120273. doi:10.1098/rstb.2012.0273. (Cited on pages 152, 170).

Goetz, S. J., M. C. Mack, K. R. Gurney, J. T. Randerson, and R. A. Houghton. 2007. 'Ecosystem responses to recent climate change and fire disturbance at northern high latitudes: observations and model results contrasting northern Eurasia and North America.' *Environmental Research Letters* 2 (4): 045031. doi:10.1088/1748-9326/2/4/045031. (Cited on page 13).

Gonzalez, P., R. P. Neilson, J. M. Lenihan, and R. J. Drapek. 2010. 'Global patterns in the vulnerability of ecosystems to vegetation shifts due to climate change.' *Global Ecology and Biogeography* 19 (6): 755–768. doi:10.1111/j.1466-8238.2010.00558.x. (Cited on page 147).

Gosling, S. N., D. Bretherton, K. Haines, and N. W. Arnell. 2010. 'Global hydrology modelling and uncertainty: running multiple ensembles with a campus grid.' *Philosophical Transactions of the Royal Society A: Mathematical, Physical and Engineering Sciences* 368 (1926): 4005–4021. doi:10.1098/rsta.2010.0164. (Cited on pages 26, 27, 88, 91, 166).

Grübler, A., B. O'Neill, K. Riahi, V. Chirkov, A. Goujon, P. Kolp, I. Prommer, S. Scherbov, and E. Slentoe. 2007. 'Regional, national, and spatially explicit scenarios of demographic and economic change based on SRES.' *Technological Forecasting and Social Change* 74 (7): 980–1029. doi:10.1016/j.techfore.2006.05.023. (Cited on page 89).

Haberl, H., K. H. Erb, F. Krausmann, V. Gaube, A. Bondeau, C. Plutzar, S. Gingrich, W. Lucht, and M. Fischer-Kowalski. 2007. 'Quantifying and mapping the human appropriation of net primary production in earth's terrestrial ecosystems.' *Proceedings of the National Academy of Sciences* 104 (31): 12942–7. doi:10.1073/pnas.0704243104. (Cited on pages 8, 106).

Haddeland, I., D. B. Clark, W. Franssen, F. Ludwig, F. Voß, N. W. Arnell, N. Bertrand, M. Best, S. Folwell, D. Gerten, S. Gomes, S. N. Gosling, S. Hagemann, N. Hanasaki, R. Harding, J. Heinke, P. Kabat, S. Koirala, T. Oki, J. Polcher, T. Stacke, P. Viterbo, G. P. Weedon, and P. Yeh. 2011. 'Multimodel Estimate of the Global Terrestrial Water Balance: Setup and First Results.' *Journal of Hydrometeorology* 12 (5): 869–884. doi:10.1175/2011JHM1324.1. (Cited on pages 88, 166).

Hansen, J., R. Ruedy, M. Sato, and K. Lo. 2010. 'Global Surface Temperature Change.' *Reviews of Geophysics* 48 (4): RG4004. doi:10.1029/2010RG000345. (Cited on page 130).

Hare, W. L., W. Cramer, M. Schaeffer, A. Battaglini, and C. C. Jaeger. 2011. 'Climate hotspots: key vulnerable regions, climate change and limits to warming.' *Regional Environmental Change* 11 (S1): 1–13. doi:10.1007/s10113-010-0195-4. (Cited on page 93).

Harris, I., P. Jones, T. Osborn, and D. Lister. 2014. 'Updated high-resolution grids of monthly climatic observations - the CRU TS3.10 Dataset.' *International Journal of Climatology* 34 (3): 623–642. doi:10.1002/joc.3711. (Cited on pages 18, 35, 40, 68, 112, 136).

Hartmann, D. J., A. M. G. Klein Tank, M. Rusticucci, L. V. Alexander, S. Brönnimann, Y. A. R. Charabi, F. J. Dentener, E. J. Dlugokencky, D. R. Easterling, A. Kaplan, B. J. Soden, P. W. Thorne, M. Wild, and P. M. Zhai. 2013. 'Observations: Atmosphere and Surface.' Chap. 2 in *Climate Change 2013: The Physical Science Basis. Contribution of Working Group I to the Fifth Assessment Report of the Intergovernmental Panel on Climate Change,* edited by T. Stocker, D. Qin, G.-K. Plattner, M. Tignor, S. Allen, J. Boschung, A. Nauels, Y. Xia, V. Bex, and P. Midgley, 159–254. Cambridge, UK and New York, NY, USA: Cambridge University Press. doi:10.1017/CBO9781107415324.008. (Cited on pages 10, 11).

Hawkins, E., and R. Sutton. 2009. 'The Potential to Narrow Uncertainty in Regional Climate Predictions.' *Bulletin of the American Meteorological Society* 90 (8): 1095–1107. doi:10.1175/2009BAMS2607.1. (Cited on pages 14, 27, 157).

Hawkins, E., and R. Sutton. 2011. 'The potential to narrow uncertainty in projections of regional precipitation change.' *Climate Dynamics* 37 (1-2): 407–418. doi:10.1007/s00382-010-0810-6. (Cited on pages 14, 27, 60, 86, 157).

Haynes, G. 2012. 'Elephants (and extinct relatives) as earth-movers and ecosystem engineers.' *Geomorphology* 157-158:99–107. doi:10.1016/j.geomorph.2011.04.045. (Cited on page 3).

Heck, V., D. Gerten, W. Lucht, and L. R. Boysen. 2016. 'Is extensive terrestrial carbon dioxide removal a 'green' form of geoengineering? A global modelling study.' *Global and Planetary Change* 137:123–130. doi:10.1016/j.gloplacha.2015.12.008. (Cited on page 135).

Heinke, J., S. Ostberg, S. Schaphoff, K. Frieler, C. Müller, D. Gerten, M. Meinshausen, and W. Lucht. 2012. 'A new dataset for systematic assessments of climate change impacts as a function of global warming.' *Geoscientific Model Development Discussions* 5 (4): 3533–3572. doi:10.5194/gmdd-5-3533-2012. (Cited on pages 66–68, 84–87).

Heinke, J., S. Ostberg, S. Schaphoff, K. Frieler, C. Müller, D. Gerten, M. Meinshausen, and W. Lucht. 2013. 'A new climate dataset for systematic assessments of climate change impacts as a function of global warming.' *Geoscientific Model Development* 6 (5): 1689–1703. doi:10.5194/gmd-6-1689-2013. (Cited on pages 23, 112, 136, 173, 187).

Heyder, U., S. Schaphoff, D. Gerten, and W. Lucht. 2011. 'Risk of severe climate change impact on the terrestrial biosphere.' *Environmental Research Letters* 6 (3): 034036. doi:10.1088/1748-9326/6/3/034036. (Cited on pages 17, 26, 62, 64, 68, 89, 93, 108, 109, 131–134, 166, 224, 225).

Hickler, T., I. C. Prentice, B. Smith, M. T. Sykes, and S. Zaehle. 2006. 'Implementing plant hydraulic architecture within the LPJ Dynamic Global Vegetation Model.' *Global Ecology and Biogeography* 15 (6): 567–577. doi:10.1111/j.1466-8238.2006.00254.x. (Cited on page 87).

Hickler, T., B. Smith, I. C. Prentice, K. Mjöfors, P. Miller, A. Arneth, and M. T. Sykes. 2008. 'CO2 fertilization in temperate FACE experiments not representative of boreal and tropical forests.' *Global Change Biology* 14 (7): 1531–1542. doi:10.1111/j.1365-2486.2008.01598.x. (Cited on pages 12, 78).

Higgins, S. I., and S. Scheiter. 2012. 'Atmospheric CO2 forces abrupt vegetation shifts locally, but not globally.' *Nature* 488 (7410): 209–212. doi:10.1038/nature11238. (Cited on page 98).

Hockey, P. A. R., C. Sirami, A. R. Ridley, G. F. Midgley, and H. A. Babiker. 2011. 'Interrogating recent range changes in South African birds: confounding signals from land use and climate change present a challenge for attribution.' *Diversity and Distributions* 17 (2): 254–261. doi:10.1111/j.1472-4642.2010.00741.x. (Cited on pages 5, 12).

Hoekstra, A. 1998. *Perspectives on Water: An Integrated Model-Based Exploration of the Future.* 1st edition. Edited by A. Weitsel. 356 pp. International Books, Utrecht, the Netherlands. (Cited on pages 111, 136).

Holling, C. S. 2001. 'Understanding the Complexity of Economic, Ecological, and Social Systems.' *Ecosystems* 4 (5): 390–405. doi:10.1007/s10021-001-0101-5. (Cited on page 60).

Hoogeveen, J., J.-M. Faurès, L. Peiser, J. Burke, and N. van de Giesen. 2015. 'GlobWat – a global water balance model to assess water use in irrigated agriculture.' *Hydrology and Earth System Sciences* 19 (9): 3829–3844. doi:10.5194/hess-19-3829-2015. (Cited on page 9).

Hooper, D. U., F. S. I. Chapin, J. J. Ewel, A. Hector, P. Inchausti, S. Lavorel, J. H. Lawton, D. M. Lodge, M. Loreau, S. Naeem, B. Schmid, H. Setälä, A. J. Symstad, J. Vandermeer, and D. A. Wardle. 2005. 'Effects of Biodiversity on Ecosystem Functioning: A Consensus of Current Knowledge.' *Ecological Monographs* 75 (1): 3–35. doi:10.1890/04-0922. (Cited on pages 62, 106, 167).

Houghton, R. A. 2003. 'Revised estimates of the annual net flux of carbon to the atmosphere from changes in land use and land management 1850-2000.' *Tellus B* 55 (2): 378–390. doi:10.1034/j.1600-0889.2003.01450.x. (Cited on page 106).

Hulme, M., T. Jiang, and T. Wigley. 1995. *SCENGEN: A Climate Change SCENario GENerator. Software User Manual, Version 1.0.* Norwich, UK: Climatic Research Unit, University of East Anglia. (Cited on page 38).

Humpenöder, F., A. Popp, J. P. Dietrich, D. Klein, H. Lotze-Campen, M. Bonsch, B. L. Bodirsky, I. Weindl, M. Stevanovic, and C. Müller. 2014. 'Investigating afforestation and bioenergy CCS as climate change mitigation strategies.' *Environmental Research Letters* 9 (6): 064029. doi:10.1088/1748-9326/9/6/064029. (Cited on page 168).

Huntingford, C., and P. M. Cox. 2000. 'An analogue model to derive additional climate change scenarios from existing GCM simulations.' *Climate Dynamics* 16 (8): 575–586. doi:10.1007/s003820000067. (Cited on pages 27, 30, 67).

Huntingford, C., P. Zelazowski, D. Galbraith, L. M. Mercado, S. Sitch, R. Fisher, M. Lomas, A. P. Walker, C. D. Jones, B. B. B. Booth, Y. Malhi, D. Hemming, G. Kay, P. Good, S. L. Lewis, O. L. Phillips, O. K. Atkin, J. Lloyd, E. Gloor, J. Zaragoza-Castells, P. Meir, R. Betts, P. P. Harris, C. Nobre, J. Marengo, and P. M. Cox. 2013. 'Simulated resilience of tropical rainforests to CO2-induced climate change.' *Nature Geoscience* 6 (4): 268–273. doi:10.1038/ngeo1741. (Cited on page 98).

Hurtt, G. C., L. P. Chini, S. Frolking, R. A. Betts, J. Feddema, G. Fischer, J. P. Fisk, K. Hibbard, R. a. Houghton, A. Janetos, C. D. Jones, G. Kindermann, T. Kinoshita, K. Klein Goldewijk, K. Riahi, E. Shevliakova, S. Smith, E. Stehfest, A. Thomson, P. Thornton, D. P. Vuuren, and Y. P. Wang. 2011. 'Harmonization of land-use scenarios for the period 1500–2100: 600 years of global gridded annual land-use transitions, wood harvest, and resulting secondary lands.' *Climatic Change* 109 (1-2): 117–161. doi:10.1007/s10584-011-0153-2. (Cited on pages 14, 19, 132, 136, 168).

IAASTD. 2009. *Agriculture at a Crossroads: Global Report.* Edited by B. D. McIntyre, H. R. Herren, J. Wakhungu, and R. T. Watson. 606 pp. Washington, DC, USA: Island Press. (Cited on page 151).

Imhoff, M. L., L. Bounoua, T. Ricketts, C. Loucks, R. Harriss, and W. T. Lawrence. 2004. 'Global patterns in human consumption of net primary production.' *Nature* 429 (6994): 870–3. doi:10.1038/nature02619. (Cited on page 8).

IPCC. 2007a. *Climate Change 2007: Impacts, Adaptation and Vulnerability. Contribution of Working Group II to the Fourth Assessment Report of the IPCC.* Edited by M. L. Parry, O. F. Canziani, J. P. Palutikof, P. J. van der Linden, and C. E. Hanson. 976 pp. Cambridge, UK: Cambridge University Press. (Cited on page 26).

IPCC. 2007b. *Climate Change 2007: The Physical Science Basis. Contribution of Working Group I to the Fourth Assessment Report of the Intergovernmental Panel on Climate Change.* Edited by S. Solomon, D. Qin, M. Manning, Z. Chen, M. Marquis, K. Averyt, M. M. Tignor, and H. L. Miller. 996 pp. Cambridge, UK and New York, NY, USA: Cambridge University Press. (Cited on pages 50, 51, 55, 60, 66, 68).

IPCC. 2013a. 'Annex III: Glossary.' In *Climate Change 2013: The Physical Science Basis. Contribution of Working Group I to the Fifth Assessment Report of the Intergovernmental Panel on Climate Change,* edited by S. Planton, 1447–1466. Cambridge, UK and New York, NY, USA: Cambridge University Press. doi:10.1017/CBO9781107415324.031. (Cited on pages 4, 11, 13).

IPCC. 2013b. *Climate Change 2013: The Physical Science Basis. Contribution of Working Group I to the Fifth Assessment Report of the Intergovernmental Panel on Climate Change.* Edited by T. Stocker, D. Qin, G.-K. Plattner, M. Tignor, S. Allen, J. Boschung, A. Nauels, Y. Xia, V. Bex, and P. Midgley. 1552 pp. Cambridge, UK and New York, NY, USA: Cambridge University Press. doi:10.1017/CBO9781107415324. (Cited on pages 6, 112, 124).

IPCC. 2014a. *Climate Change 2014: Impacts, Adaptation, and Vulnerability. Part A: Global and Sectoral Aspects. Contribution of Working Group II to the Fifth Assessment Report of the Intergovernmental Panel on Climate Change.* Edited by C. Field, V. Barros, D. Dokken, K. Mach, M. Mastrandrea, T. Bilir, M. Chatterjee, K. Ebi, Y. Estrada, R. Genova, B. Girma, E. Kissel, A. Levy, S. MacCracken, P. Mastrandrea, and L. White. 1132 pp. Cambridge, UK and New York, NY, USA: Cambridge University Press. doi:10.1017/CBO9781107415379. (Cited on pages 6, 106).

IPCC. 2014b. *Climate Change 2014: Impacts, Adaptation, and Vulnerability. Part B: Regional Aspects. Contribution of Working Group II to the Fifth Assessment Report of the Intergovernmental Panel on Climate Change.* Edited by V. R. Barros, C. B. Field, D. J. Dokken, M. D. Mastrandrea, K. J. Mach, T. E. Bilir, M. Chatterjee, K. L. Ebi, Y. O. Estrada, R. C. Genova, B. Girma, E. S. Kissel, A. N. Levy, S. MacCracken, P. R. Mastrandrea, and L. L. White. 688 pp. Cambridge, UK and New York, NY, USA: Cambridge University Press. doi:10.1017/CBO9781107415386. (Cited on pages 6, 106).

IPCC. 2014c. 'Summary for Policymakers.' In *Climate Change 2014: Impacts, Adaptation, and Vulnerability. Part A: Global and Sectoral Aspects. Contribution of Working Group II to the Fifth Assessment Report of the Intergovernmental Panel on Climate Change,* edited by C. B. Field, V. R. Barros, D. J. Dokken, K. J. Mach, M. D. Mastrandrea, and L. L. White, 1–32. Cambridge, UK and New York, NY, USA: Cambridge University Press. doi:10.1017/CBO9781107415379.003. (Cited on page 12).

IPCC. 2014d. 'Summary for Policymakers.' In *Climate Change 2014: Mitigation of Climate Change. Contribution of Working Group III to the Fifth Assessment Report of the Intergovernmental Panel on Climate Change,* edited by O. Edenhofer, R. Pichs-Madruga, Y. Sokona, E. Farahani, S. Kadner, K. Seyboth, A. Adler, I. Baum, S. Brunner, P. Eickemeier, B. Kriemann, J. Savolainen, S. Schlömer, C. von Stechow, T. Zwickel, and J. C. Minx, 1–32. Cambridge, UK and New York, NY, USA: Cambridge University Press. (Cited on pages 14, 130).

Jägermeyr, J., D. Gerten, J. Heinke, S. Schaphoff, M. Kummu, and W. Lucht. 2015. 'Water savings potentials of irrigation systems: global simulation of processes and linkages.' *Hydrology and Earth System Sciences* 19 (7): 3073–3091. doi:10.5194/hess-19-3073-2015. (Cited on pages 9, 135, 137).

Jägermeyr, J., D. Gerten, S. Schaphoff, J. Heinke, W. Lucht, and J. Rockström. 2016. 'Integrated crop water management might sustainably halve the global food gap.' *Environmental Research Letters* 11 (2): 025002. doi:10.1088/1748-9326/11/2/025002. (Cited on page 150).

Jägermeyr, J., A. Pastor, H. Biemans, and D. Gerten. 2017. 'Reconciling irrigated food production with environmental flows for Sustainable Development Goals implementation.' *Nature Communications* 8:15900. doi:10.1038/ncomms15900. (Cited on page 170).

Jasechko, S., Z. D. Sharp, J. J. Gibson, S. J. Birks, Y. Yi, and P. J. Fawcett. 2013. 'Terrestrial water fluxes dominated by transpiration.' *Nature* 496 (7445): 347–350. doi:10.1038/nature11983. (Cited on page 5).

Johnson, J. A., C. F. Runge, B. Senauer, J. Foley, and S. Polasky. 2014. 'Global agriculture and carbon trade-offs.' *Proceedings of the National Academy of Sciences* 111 (34): 12342–7. doi:10.1073/pnas.1412835111. (Cited on pages 14, 125, 170).

Jones, C., J. Lowe, S. Liddicoat, and R. Betts. 2009a. 'Committed terrestrial ecosystem changes due to climate change.' *Nature Geoscience* 2 (7): 484–487. doi:10.1038/ngeo555. (Cited on page 12).

Jones, C. G., J. H. Lawton, and M. Shachak. 1994. 'Organisms as Ecosystem Engineers.' *Oikos* 69 (3): 373–386. doi:10.2307/3545850. (Cited on page 3).

Jones, D. A., W. Wang, and R. Fawcett. 2009b. 'High-quality spatial climate data-sets for Australia.' *Australian Meteorological and Oceanographic Journal* 58:233–248. (Cited on page 122).

Joos, F., and R. Spahni. 2008. 'Rates of change in natural and anthropogenic radiative forcing over the past 20,000 years.' *Proceedings of the National Academy of Sciences* 105 (5): 1425–1430. doi:10.1073/pnas.0707386105. (Cited on pages 10, 130).

Joshi, M., E. Hawkins, R. Sutton, J. Lowe, and D. Frame. 2011. 'Projections of when temperature change will exceed 2 °C above pre-industrial levels.' *Nature Climate Change* 1 (8): 407–412. doi:10.1038/nclimate1261. (Cited on pages 84, 85).

Kaplan, J. O., K. M. Krumhardt, E. C. Ellis, W. F. Ruddiman, C. Lemmen, and K. K. Goldewijk. 2010. 'Holocene carbon emissions as a result of anthropogenic land cover change.' *The Holocene* 21 (5): 775–791. doi:10.1177/0959683610386983. (Cited on pages 106, 119).

KC, S., and W. Lutz. 2017. 'The human core of the shared socioeconomic pathways: Population scenarios by age, sex and level of education for all countries to 2100.' *Global Environmental Change* 42:181–192. doi:10.1016/j.gloenvcha.2014.06.004. (Cited on page 13).

Keeling, C. D., S. C. Piper, R. B. Bacastow, M. Wahlen, T. P. Whorf, M. Heimann, and H. A. Meijer. 2001. *Exchanges of Atmospheric CO2 and 13CO2 with the Terrestrial Biosphere and Oceans from 1978 to 2000. I. Global Aspects.* Technical report, SIO Reference. San Diego: Scripps Institution of Oceanography. (Cited on pages 18, 112).

Kier, G., H. Kreft, T. M. Lee, W. Jetz, P. L. Ibisch, C. Nowicki, J. Mutke, and W. Barthlott. 2009. 'A global assessment of endemism and species richness across island and mainland regions.' *Proceedings of the National Academy of Sciences* 106 (23): 9322–7. doi:10.1073/pnas.0810306106. (Cited on pages 90, 159).

Kirch, P. V. 2005. 'Archaeology and Global Change: The Holocene Record.' *Annual Review of Environment and Resources* 30 (1): 409–440. doi:10.1146/annurev.energy.29.102403.140700. (Cited on pages 3, 117).

Klein Goldewijk, K., A. Beusen, and P. Janssen. 2010. 'Long-term dynamic modeling of global population and built-up area in a spatially explicit way: HYDE 3.1.' *The Holocene* 20 (4): 565–573. doi:10.1177/0959683609356587. (Cited on pages 6, 7, 15).

Klein Goldewijk, K., A. Beusen, G. Van Drecht, and M. De Vos. 2011. 'The HYDE 3.1 spatially explicit database of human-induced global land-use change over the past 12,000 years.' *Global Ecology and Biogeography* 20 (1): 73–86. doi:10.1111/j.1466-8238.2010.00587.x. (Cited on pages 7, 106).

Klein Goldewijk, K., and G. van Drecht. 2006. 'HYDE 3. Current and Historical Population and Land Cover.' In *Integrated Modelling of Global Environmental Change. An Overview of IMAGE 2.4,* edited by A. F. Bouwman, T. Kram, and K. Klein Goldewijk. Bilthoven, The Netherlands: Netherlands Environmental Assessment Agency (MNP). (Cited on pages 18, 111, 136).

Klein Goldewijk, K., and P. H. Verburg. 2013. 'Uncertainties in global-scale reconstructions of historical land use: an illustration using the HYDE data set.' *Landscape Ecology* 28 (5): 861–877. doi:10.1007/s10980-013-9877-x. (Cited on page 119).

Knopf, B., M. Kowarsch, C. Flachsland, and O. Edenhofer. 2012. 'The 2°C Target Reconsidered.' In *Climate Change, Justice and Sustainability,* edited by O. Edenhofer, J. Wallacher, H. Lotze-Campen, M. Reder, B. Knopf, and J. Müller, 121–137. Dordrecht: Springer Netherlands. doi:10.1007/978-94-007-4540-7_12. (Cited on page 84).

Knutti, R., R. Furrer, C. Tebaldi, J. Cermak, and G. A. Meehl. 2010. 'Challenges in Combining Projections from Multiple Climate Models.' *Journal of Climate* 23 (10): 2739–2758. doi:10.1175/2009JCLI3361.1. (Cited on page 86).

Knutti, R., and J. Sedláček. 2012. 'Robustness and uncertainties in the new CMIP5 climate model projections.' *Nature Climate Change* 3 (4): 369–373. doi:10.1038/nclimate1716. (Cited on page 84).

Kolby Smith, W., S. C. Reed, C. C. Cleveland, A. P. Ballantyne, W. R. L. Anderegg, W. R. Wieder, Y. Y. Liu, and S. W. Running. 2016. 'Large divergence of satellite and Earth system model estimates of global terrestrial CO2 fertilization.' *Nature Climate Change* 6 (3): 306–310. doi:10.1038/nclimate2879. (Cited on page 170).

Köppen, W. 1936. *Das geographische System der Klimate,* edited by W. Köppen and R. Geiger, vol. I, part C, 43 pp. Berlin: Gebr. Borntraeger. (Cited on page 6).

Krausmann, F., K.-H. Erb, S. Gingrich, H. Haberl, A. Bondeau, V. Gaube, C. Lauk, C. Plutzar, and T. D. Searchinger. 2013. 'Global human appropriation of net primary production doubled in the 20th century.' *Proceedings of the National Academy of Sciences* 110 (25): 10324–9. doi:10.1073/pnas.1211349110. (Cited on pages 8, 106).

Kueppers, L. M., M. A. Snyder, and L. C. Sloan. 2007. 'Irrigation cooling effect: Regional climate forcing by land-use change.' *Geophysical Research Letters* 34 (3): L03703. doi:10.1029/2006GL028679. (Cited on page 11).

Kundzewicz, Z. W., L. J. Mata, N. W. Arnell, P. Döll, B. Jimenez, K. Miller, T. Oki, Z. Şen, and I. Shiklomanov. 2008. 'The implications of projected climate change for freshwater resources and their management.' *Hydrological Sciences Journal* 53 (1): 3–10. doi:10.1623/hysj.53.1.3. (Cited on page 91).

Kurz, W. A., G. Stinson, G. J. Rampley, C. C. Dymond, and E. T. Neilson. 2008. 'Risk of natural disturbances makes future contribution of Canada's forests to the global carbon cycle highly uncertain.' *Proceedings of the National Academy of Sciences* 105 (5): 1551–1555. doi:10.1073/pnas.0708133105. (Cited on page 13).

Lambert, F. H., and J. C. H. Chiang. 2007. 'Control of land-ocean temperature contrast by ocean heat uptake.' *Geophysical Research Letters* 34 (13): L13704. doi:10.1029/2007GL029755. (Cited on page 44).

Lawrence, D. M., G. C. Hurtt, A. Arneth, V. Brovkin, K. V. Calvin, A. D. Jones, C. D. Jones, P. J. Lawrence, N. de Noblet-Ducoudré, J. Pongratz, S. I. Seneviratne, and E. Shevliakova. 2016. 'The Land Use Model Intercomparison Project (LUMIP) contribution to CMIP6: rationale and experimental design.' *Geoscientific Model Development* 9 (9): 2973–2998. doi:10.5194/gmd-9-2973-2016. (Cited on page 152).

Le Quéré, C., R. M. Andrew, J. G. Canadell, S. Sitch, J. I. Korsbakken, G. P. Peters, A. C. Manning, T. A. Boden, P. P. Tans, R. A. Houghton, R. F. Keeling, S. Alin, O. D. Andrews, P. Anthoni, L. Barbero, L. Bopp, F. Chevallier, L. P. Chini, P. Ciais, K. Currie, C. Delire, S. C. Doney, P. Friedlingstein, T. Gkritzalis, I. Harris, J. Hauck, V. Haverd, M. Hoppema, K. Klein Goldewijk, A. K. Jain, E. Kato, A. Körtzinger, P. Landschützer, N. Lefèvre, A. Lenton, S. Lienert, D. Lombardozzi, J. R. Melton, N. Metzl, F. Millero, P. M. S. Monteiro, D. R. Munro, J. E. M. S. Nabel, S.-i. Nakaoka, K. O'Brien, A. Olsen, A. M. Omar, T. Ono, D. Pierrot, B. Poulter, C. Rödenbeck, J. Salisbury, U. Schuster, J. Schwinger, R. Séférian, I. Skjelvan, B. D. Stocker, A. J. Sutton, T. Takahashi, H. Tian, B. Tilbrook, I. T. van der Laan-Luijkx, G. R. van der Werf, N. Viovy, A. P. Walker, A. J. Wiltshire, and S. Zaehle. 2016. 'Global Carbon Budget 2016.' *Earth System Science Data* 8 (2): 605–649. doi:10.5194/essd-8-605-2016. (Cited on pages 4, 9, 130, 167).

Leemans, R., and B. Eickhout. 2004. 'Another reason for concern: regional and global impacts on ecosystems for different levels of climate change.' *Global Environmental Change* 14 (3): 219–228. doi:10.1016/j.gloenvcha.2004.04.009. (Cited on pages 76, 77, 89).

Lehner, B., and P. Döll. 2004. 'Development and validation of a global database of lakes, reservoirs and wetlands.' *Journal of Hydrology* 296 (1-4): 1–22. doi:10.1016/j.jhydrol.2004.03.028. (Cited on page 138).

Lehner, B., P. Döll, J. Alcamo, T. Henrichs, and F. Kaspar. 2006. 'Estimating the Impact of Global Change on Flood and Drought Risks in Europe: A Continental, Integrated Analysis.' *Climatic Change* 75 (3): 273–299. doi:10.1007/s10584-006-6338-4. (Cited on page 88).

Lehner, B., C. R. Liermann, C. Revenga, C. Vörösmarty, B. Fekete, P. Crouzet, P. Döll, M. Endejan, K. Frenken, J. Magome, C. Nilsson, J. C. Robertson, R. Rödel, N. Sindorf, and D. Wisser. 2011. 'High-resolution mapping of the world's reservoirs and dams for sustainable river-flow management.' *Frontiers in Ecology and the Environment* 9 (9): 494–502. doi:10.1890/100125. (Cited on page 138).

Leipprand, A., and D. Gerten. 2006. 'Global effects of doubled atmospheric CO2 content on evapotranspiration, soil moisture and runoff under potential natural vegetation.' *Hydrological Sciences Journal* 51 (1): 171–185. doi:10.1623/hysj.51.1.171. (Cited on page 99).

Lenton, T. M. 2011. 'Beyond 2°C: redefining dangerous climate change for physical systems.' *Wiley Interdisciplinary Reviews: Climate Change* 2 (3): 451–461. doi:10.1002/wcc.107. (Cited on page 84).

Lenton, T. M., H. Held, E. Kriegler, J. W. Hall, W. Lucht, S. Rahmstorf, and H. J. Schellnhuber. 2008. 'Tipping elements in the Earth's climate system.' *Proceedings of the National Academy of Sciences* 105 (6): 1786–93. doi:10.1073/pnas.0705414105. (Cited on page 98).

Levermann, A., J. L. Bamber, S. Drijfhout, A. Ganopolski, W. Haeberli, N. R. P. Harris, M. Huss, K. Krüger, T. M. Lenton, R. W. Lindsay, D. Notz, P. Wadhams, and S. Weber. 2012. 'Potential climatic transitions with profound impact on Europe.' *Climatic Change* 110 (3-4): 845–878. doi:10.1007/s10584-011-0126-5. (Cited on page 98).

Li, F., X. D. Zeng, and S. Levis. 2012. 'A process-based fire parameterization of intermediate complexity in a Dynamic Global Vegetation Model.' *Biogeosciences* 9 (7): 2761–2780. doi:10.5194/bg-9-2761-2012. (Cited on page 87).

Lindeskog, M., A. Arneth, A. Bondeau, K. Waha, J. Seaquist, S. Olin, and B. Smith. 2013. 'Implications of accounting for land use in simulations of ecosystem carbon cycling in Africa.' *Earth System Dynamics* 4 (2): 385–407. doi:10.5194/esd-4-385-2013. (Cited on page 169).

Lloyd, A. H. 2005. 'Ecological histories from Alaskan tree lines provide insight into future change.' *Ecology* 86 (7): 1687–1695. doi:10.1890/03-0786. (Cited on pages 70, 122).

Loarie, S. R., P. B. Duffy, H. Hamilton, G. P. Asner, C. B. Field, and D. D. Ackerly. 2009. 'The velocity of climate change.' *Nature* 462 (7276): 1052–1055. doi:10.1038/nature08649. (Cited on page 99).

Lobell, D., G. Bala, A. Mirin, T. Phillips, R. Maxwell, and D. Rotman. 2009. 'Regional Differences in the Influence of Irrigation on Climate.' *Journal of Climate* 22 (8): 2248–2255. doi:10.1175/2008JCLI2703.1. (Cited on page 11).

Long, S. P., E. A. Ainsworth, A. D. B. Leakey, J. Nösberger, and D. R. Ort. 2006. 'Food for Thought: Lower-Than-Expected Crop Yield Stimulation with Rising CO2 Concentrations.' *Science* 312 (5782): 1918–1921. doi:10.1126/science.1114722. (Cited on page 12).

Lotze-Campen, H., A. Popp, T. Beringer, C. Müller, A. Bondeau, S. Rost, and W. Lucht. 2010. 'Scenarios of global bioenergy production: The trade-offs between agricultural expansion, intensification and trade.' *Ecological Modelling* 221 (18): 2188–2196. doi:10.1016/j.ecolmodel.2009.10.002. (Cited on page 78).

Lucht, W., I. C. Prentice, R. B. Myneni, S. Sitch, P. Friedlingstein, W. Cramer, P. Bousquet, W. Buermann, and B. Smith. 2002. 'Climatic Control of the High-Latitude Vegetation Greening Trend and Pinatubo Effect.' *Science* 296 (5573): 1687–1689. doi:10.1126/science.1071828. (Cited on page 87).

MacDonald, G. M., K. V. Kremenetski, and D. W. Beilman. 2008. 'Climate change and the northern Russian treeline zone.' *Philosophical transactions of the Royal Society of London. Series B, Biological sciences* 363 (1501): 2285–99. doi:10.1098/rstb.2007.2200. (Cited on page 122).

MacFarling Meure, C., D. Etheridge, C. Trudinger, P. Steele, R. Langenfelds, T. van Ommen, A. Smith, and J. Elkins. 2006. 'Law Dome CO2 , CH4 and N2O ice core records extended to 2000 years BP.' *Geophysical Research Letters* 33 (14): L14810. doi:10.1029/2006GL026152. (Cited on page 10).

Mahlstein, I., R. Knutti, S. Solomon, and R. W. Portmann. 2011. 'Early onset of significant local warming in low latitude countries.' *Environmental Research Letters* 6 (3): 034009. doi:10.1088/1748-9326/6/3/034009. (Cited on page 85).

Mahlstein, I., J. S. Daniel, and S. Solomon. 2013. 'Pace of shifts in climate regions increases with global temperature.' *Nature Climate Change* 3 (8): 739–743. doi:10.1038/nclimate1876. (Cited on page 84).

Mann, M. E. 2009. 'Defining dangerous anthropogenic interference.' *Proceedings of the National Academy of Sciences* 106 (11): 4065–4066. doi:10.1073/pnas.0901303106. (Cited on page 26).

Masson, D., and R. Knutti. 2011. 'Climate model genealogy.' *Geophysical Research Letters* 38 (8): L08703. doi:10.1029/2011GL046864. (Cited on page 87).

Mastrandrea, M. D., C. B. Field, T. F. Stocker, O. Edenhofer, K. L. Ebi, D. J. Frame, H. Held, E. Kriegler, K. J. Mach, P. R. Matschoss, G.-K. Plattner, G. W. Yohe, and F. W. Zwiers. 2010. *Guidance Note for Lead Authors of the IPCC Fifth Assessment Report on Consistent Treatment of Uncertainties*. 7 pp. Intergovernmental Panel on Climate Change (IPCC). (Cited on page 87).

Masui, T., K. Matsumoto, Y. Hijioka, T. Kinoshita, T. Nozawa, S. Ishiwatari, E. Kato, P. R. Shukla, Y. Yamagata, and M. Kainuma. 2011. 'An emission pathway for stabilization at 6 Wm-2 radiative forcing.' *Climatic Change* 109 (1-2): 59–76. doi:10.1007/s10584-011-0150-5. (Cited on pages 140, 149).

May, R. M. 2010. 'Tropical Arthropod Species, More or Less?' *Science* 329 (5987): 41–42. doi:10.1126/science.1191058. (Cited on page 4).

Meehl, G. A., C. Covey, K. E. Taylor, T. Delworth, R. J. Stouffer, M. Latif, B. McAvaney, and J. F. B. Mitchell. 2007. 'The WCRP CMIP3 Multimodel Dataset: A New Era in Climate Change Research.' *Bulletin of the American Meteorological Society* 88 (9): 1383–1394. doi:10.1175/BAMS-88-9-1383. (Cited on pages 27, 66, 86, 157, 158).

Meinshausen, M., S. C. B. Raper, and T. M. L. Wigley. 2011a. 'Emulating coupled atmosphere-ocean and carbon cycle models with a simpler model, MAGICC6 – Part 1: Model description and calibration.' *Atmospheric Chemistry and Physics* 11 (4): 1417–1456. doi:10.5194/acp-11-1417-2011. (Cited on pages 28, 31, 67, 86).

Meinshausen, M., B. Hare, T. M. L. Wigley, D. Van Vuuren, M. G. J. Den Elzen, and R. Swart. 2006. 'Multi-gas Emissions Pathways to Meet Climate Targets.' *Climatic Change* 75 (1-2): 151–194. doi:10.1007/s10584-005-9013-2. (Cited on page 32).

Meinshausen, M., N. Meinshausen, W. Hare, S. C. B. Raper, K. Frieler, R. Knutti, D. J. Frame, and M. R. Allen. 2009. 'Greenhouse-gas emission targets for limiting global warming to 2 degrees C.' *Nature* 458 (7242): 1158–62. doi:10.1038/nature08017. (Cited on page 32).

Meinshausen, M., S. J. Smith, K. Calvin, J. S. Daniel, M. L. T. Kainuma, J.-F. Lamarque, K. Matsumoto, S. A. Montzka, S. C. B. Raper, K. Riahi, A. Thomson, G. J. M. Velders, and D. P. P. van Vuuren. 2011b. 'The RCP greenhouse gas concentrations and their extensions from 1765 to 2300.' *Climatic Change* 109 (1-2): 213–241. doi:10.1007/s10584-011-0156-z. (Cited on page 32).

Millar, C. I., N. L. Stephenson, and S. L. Stephens. 2007. 'Climate change and forests of the future: Managing in the face of uncertainty.' *Ecological Applications* 17 (8): 2145–2151. doi:10.1890/06-1715.1. (Cited on page 100).

Millennium Ecosystem Assessment (MEA). 2005. *Ecosystems and Human Well-being: Synthesis.* Island Press, Washington, DC. (Cited on pages 5, 6, 8, 60, 130).

Milly, P. C. D., J. Betancourt, M. Falkenmark, R. M. Hirsch, Z. W. Kundzewicz, D. P. Lettenmaier, and R. J. Stouffer. 2008. 'Stationarity Is Dead: Whither Water Management?' *Science* 319 (5863): 573–574. doi:10.1126/science.1151915. (Cited on page 100).

Mitchell, T. D. 2003. 'Pattern scaling: an examination of the accuracy of the technique for describing future climates.' *Climatic Change* 60 (3): 217–242. doi:10.1023/A:1026035305597. (Cited on pages 27, 29, 30, 45, 85, 158).

Mitchell, T. D., and P. D. Jones. 2005. 'An improved method of constructing a database of monthly climate observations and associated high-resolution grids.' *International Journal of Climatology* 25 (6): 693–712. doi:10.1002/joc.1181. (Cited on page 86).

Mooney, H., A. Larigauderie, M. Cesario, T. Elmquist, O. Hoegh-Guldberg, S. Lavorel, G. M. Mace, M. Palmer, R. Scholes, and T. Yahara. 2009. 'Biodiversity, climate change, and ecosystem services.' *Current Opinion in Environmental Sustainability* 1 (1): 46–54. doi:10.1016/j.cosust.2009.07.006. (Cited on pages 61, 62, 77, 106, 167).

Mora, C., D. P. Tittensor, S. Adl, A. G. B. Simpson, and B. Worm. 2011. 'How Many Species Are There on Earth and in the Ocean?' Edited by G. M. Mace. *PLoS Biology* 9 (8): e1001127. doi:10.1371/journal.pbio.1001127. (Cited on page 4).

Morice, C. P., J. J. Kennedy, N. A. Rayner, and P. D. Jones. 2012. 'Quantifying uncertainties in global and regional temperature change using an ensemble of observational estimates: The HadCRUT4 data set.' *Journal of Geophysical Research: Atmospheres* 117 (D8): D08101. doi:10.1029/2011JD017187. (Cited on page 10).

Müller, C., W. Cramer, W. L. Hare, and H. Lotze-Campen. 2011. 'Climate change risks for African agriculture.' *Proceedings of the National Academy of Sciences* 108 (11): 4313–4315. doi:10.1073/pnas.1015078108. (Cited on page 26).

Murray, S. J., P. N. Foster, and I. C. Prentice. 2012. 'Future global water resources with respect to climate change and water withdrawals as estimated by a dynamic global vegetation model.' *Journal of Hydrology* 448-449:14–29. doi:10.1016/j.jhydrol.2012.02.044. (Cited on pages 26, 27).

Murray, S. J., I. M. Watson, and I. C. Prentice. 2013. 'The use of dynamic global vegetation models for simulating hydrology and the potential integration of satellite observations.' *Progress in Physical Geography* 37 (1): 63–97. doi:10.1177/0309133312460072. (Cited on pages 62, 87).

Myhre, G., D. Shindell, F.-M. Bréon, W. Collins, J. Fuglestvedt, J. Huang, D. Koch, J.-F. Lamarque, D. Lee, B. Mendoza, T. Nakajima, A. Robock, G. Stephens, T. Takemura, and H. Zhang. 2013. 'Anthropogenic and Natural Radiative Forcing.' Chap. 8 in *Climate Change 2013: The Physical Science Basis. Contribution of Working Group I to the Fifth Assessment Report of the Intergovernmental Panel on Climate Change,* edited by T. Stocker, D. Qin, G.-K. Plattner, M. Tignor, S. Allen, J. Boschung, A. Nauels, Y. Xia, V. Bex, and P. Midgley, 659–740. Cambridge, UK and New York, NY, USA: Cambridge University Press. doi:10.1017/CBO9781107415324.018. (Cited on pages 6, 10, 11).

Nakićenović, N., J. Alcamo, G. Davis, B. de Vries, J. Fenhann, S. Gaffin, K. Gregory, A. Grübler, T. Y. Jung, T. Kram, E. L. La Rovere, L. Michaelis, S. Mori, T. Morita, W. Pepper, H. Pitcher, L. Price, K. Riahi, A. Roehrl, H.-H. Rogner, A. Sankovski, M. Schlesinger, P. Shukla, S. Smith, R. Swart, S. van Rooijen, N. Victor, and Z. Dadi. 2000. *Special Report on Emissions Scenarios : a special report of Working Group III of the Intergovernmental Panel on Climate Change.* Edited by N. Nakićenović and R. Swart. 608 pp. Cambridge, UK and New York, NY, USA: Cambridge University Press. (Cited on page 157).

New, M., M. Hulme, and P. Jones. 2000. 'Representing Twentieth-Century Space-Time Climate Variability. Part II: Development of 1901–96 Monthly Grids of Terrestrial Surface Climate.' *Journal of Climate* 13 (13): 2217–2238. doi:10.1175/1520-0442(2000)013<2217:RTCSTC>2.0.CO;2. (Cited on pages 35, 40, 68, 112).

New, M., D. Liverman, H. Schroder, and K. Anderson. 2011. 'Four degrees and beyond: the potential for a global temperature increase of four degrees and its implications.' *Philosophical Transactions of the Royal Society A: Mathematical, Physical and Engineering Sciences* 369 (1934): 6–19. doi:10.1098/rsta.2010.0303. (Cited on page 26).

Nishina, K., A. Ito, P. Falloon, A. D. Friend, D. J. Beerling, P. Ciais, D. B. Clark, R. Kahana, E. Kato, W. Lucht, M. Lomas, R. Pavlick, S. Schaphoff, L. Warszawaski, and T. Yokohata. 2015. 'Decomposing uncertainties in the future terrestrial carbon budget associated with emission scenarios, climate projections, and ecosystem simulations using the ISI-MIP results.' *Earth System Dynamics* 6 (2): 435–445. doi:10.5194/esd-6-435-2015. (Cited on page 166).

NRC. 2000. *Watershed Management for Potable Water Supply: Assessing the New York City Strategy.* 564 pp. Washington, DC, USA: National Academy Press. (Cited on page 5).

Oki, T., and S. Kanae. 2006. 'Global Hydrological Cycles and World Water Resources.' *Science* 313 (5790): 1068–1072. doi:10.1126/science.1128845. (Cited on page 5).

Osborne, T., J. Gornall, J. Hooker, K. Williams, A. Wiltshire, R. Betts, and T. Wheeler. 2015. 'JULES-crop: a parametrisation of crops in the Joint UK Land Environment Simulator.' *Geoscientific Model Development* 8 (4): 1139–1155. doi:10.5194/gmd-8-1139-2015. (Cited on page 169).

Ostberg, S., L. R. Boysen, S. Schaphoff, W. Lucht, and D. Gerten. 2018. 'The Biosphere Under Potential Paris Outcomes.' *Earth's Future* 6 (1): 23–39. doi:10.1002/2017EF000628. (Cited on pages 127, 221).

Ostberg, S., W. Lucht, S. Schaphoff, and D. Gerten. 2013a. 'Critical impacts of global warming on land ecosystems.' *Earth System Dynamics* 4 (2): 347–357. doi:10.5194/esd-4-347-2013. (Cited on pages 57, 106, 109, 125, 132, 133, 177, 216, 217).

Ostberg, S., W. Lucht, S. Schaphoff, and D. Gerten. 2013b. 'Critical impacts of global warming on land ecosystems.' *Earth System Dynamics Discussions* 4 (1): 541–565. doi:10.5194/esdd-4-541-2013. (Cited on pages 89, 90, 93).

Ostberg, S., S. Schaphoff, W. Lucht, and D. Gerten. 2015. 'Three centuries of dual pressure from land use and climate change on the biosphere.' *Environmental Research Letters* 10 (4): 044011. doi:10.1088/1748-9326/10/4/044011. (Cited on pages 103, 131–133, 139, 207, 222, 223, 228).

Pan, Y., R. A. Birdsey, J. Fang, R. Houghton, P. E. Kauppi, W. A. Kurz, O. L. Phillips, A. Shvidenko, S. L. Lewis, J. G. Canadell, P. Ciais, R. B. Jackson, S. W. Pacala, A. D. McGuire, S. Piao, A. Rautiainen, S. Sitch, and D. Hayes. 2011. 'A Large and Persistent Carbon Sink in the World's Forests.' *Science* 333 (6045): 988–993. doi:10.1126/science.1201609. (Cited on page 13).

Parmesan, C. 2006. 'Ecological and Evolutionary Responses to Recent Climate Change.' *Annual Review of Ecology, Evolution, and Systematics* 37 (1): 637–669. doi:10.1146/annurev.ecolsys.37.091305.110100. (Cited on pages 12, 62, 106, 167).

Parmesan, C. 2007. 'Influences of species, latitudes and methodologies on estimates of phenological response to global warming.' *Global Change Biology* 13 (9): 1860–1872. doi:10.1111/j.1365-2486.2007.01404.x. (Cited on pages 12, 107).

Parmesan, C., and G. Yohe. 2003. 'A globally coherent fingerprint of climate change impacts across natural systems.' *Nature* 421 (6918): 37–42. doi:10.1038/nature01286. (Cited on pages 12, 107, 166).

Parry, M., N. Arnell, T. McMichael, R. Nicholls, P. Martens, S. Kovats, M. Livermore, C. Rosenzweig, A. Iglesias, and G. Fischer. 2001. 'Millions at risk: defining critical climate change threats and targets.' *Global Environmental Change* 11 (3): 181–183. doi:10.1016/S0959-3780(01)00011-5. (Cited on page 100).

Pennell, C., and T. Reichler. 2011. 'On the Effective Number of Climate Models.' *Journal of Climate* 24 (9): 2358–2367. doi:10.1175/2010JCLI3814.1. (Cited on page 87).

Peñuelas, J., J. Sardans, M. Estiarte, R. Ogaya, J. Carnicer, M. Coll, A. Barbeta, A. Rivas-Ubach, J. Llusià, M. Garbulsky, I. Filella, and A. S. Jump. 2013. 'Evidence of current impact of climate change on life: a walk from genes to the biosphere.' *Global Change Biology* 19 (8): 2303–2338. doi:10.1111/gcb.12143. (Cited on pages 12, 166).

Phillips, O. L., L. E. O. C. Aragão, S. L. Lewis, J. B. Fisher, J. Lloyd, G. López-González, Y. Malhi, A. Monteagudo, J. Peacock, C. A. Quesada, G. van der Heijden, S. Almeida, I. Amaral, L. Arroyo, G. Aymard, T. R. Baker, O. Bánki, L. Blanc, D. Bonal, P. Brando, J. Chave, A. C. A. de Oliveira, N. D. Cardozo, C. I. Czimczik, T. R. Feldpausch, M. A. Freitas, E. Gloor, N. Higuchi, E. Jiménez, G. Lloyd, P. Meir, C. Mendoza, A. Morel, D. A. Neill, D. Nepstad, S. Patiño, M. C. Peñuela, A. Prieto, F. Ramírez, M. Schwarz, J. Silva, M. Silveira, A. S. Thomas, H. ter Steege, J. Stropp, R. Vásquez, P. Zelazowski, E. Alvarez Dávila, S. Andelman, A. Andrade, K.-J. Chao, T. Erwin, A. Di Fiore, E. Honorio C, H. Keeling, T. J. Killeen, W. F. Laurance, A. Peña Cruz, N. C. A. Pitman, P. Núñez Vargas, H. Ramírez-Angulo, A. Rudas, R. Salamão, N. Silva, J. Terborgh, and A. Torres-Lezama. 2009. 'Drought sensitivity of the Amazon rainforest.' *Science* 323 (5919): 1344–7. doi:10.1126/science.1164033. (Cited on page 13).

Piao, S., P. Friedlingstein, P. Ciais, N. de Noblet-Ducoudré, D. Labat, and S. Zaehle. 2007. 'Changes in climate and land use have a larger direct impact than rising CO2 on global river runoff trends.' *Proceedings of the National Academy of Sciences* 104 (39): 15242–7. doi:10.1073/pnas.0707213104. (Cited on page 166).

Piao, S., S. Sitch, P. Ciais, P. Friedlingstein, P. Peylin, X. Wang, A. Ahlström, A. Anav, J. G. Canadell, N. Cong, C. Huntingford, M. Jung, S. Levis, P. E. Levy, J. Li, X. Lin, M. R. Lomas, M. Lu, Y. Luo, Y. Ma, R. B. Myneni, B. Poulter, Z. Sun, T. Wang, N. Viovy, S. Zaehle, and N. Zeng. 2013. 'Evaluation of terrestrial carbon cycle models for their response to climate variability and to CO2 trends.' *Global Change Biology* 19 (7): 2117–2132. doi:10.1111/gcb.12187. (Cited on page 87).

Pincus, R., C. P. Batstone, R. J. P. Hofmann, K. E. Taylor, and P. J. Glecker. 2008. 'Evaluating the present-day simulation of clouds, precipitation, and radiation in climate models.' *Journal of Geophysical Research* 113:D14209. doi:10.1029/2007JD009334. (Cited on page 86).

Piontek, F., C. Müller, T. A. M. Pugh, D. B. Clark, D. Deryng, J. Elliott, F. D. J. Colón González, M. Flörke, C. Folberth, W. Franssen, K. Frieler, A. D. Friend, S. N. Gosling, D. Hemming, N. Khabarov, H. Kim, M. R. Lomas, Y. Masaki, M. Mengel, A. Morse, K. Neumann, K. Nishina, S. Ostberg, R. Pavlick, A. C. Ruane, J. Schewe, E. Schmid, T. Stacke, Q. Tang, Z. D. Tessler, A. M. Tompkins, L. Warszawski, D. Wisser, and H. J. Schellnhuber. 2014. 'Multisectoral climate impact hotspots in a warming world.' *Proceedings of the National Academy of Sciences* 111 (9): 3233–8. doi:10.1073/pnas.1222471110. (Cited on pages 77, 99, 101, 168).

Pitman, A. J., F. B. Avila, G. Abramowitz, Y. P. Wang, S. J. Phipps, and N. de Noblet-Ducoudré. 2011. 'Importance of background climate in determining impact of land-cover change on regional climate.' *Nature Climate Change* 1 (9): 472–475. doi:10.1038/nclimate1294. (Cited on page 168).

Pongratz, J., C. Reick, T. Raddatz, and M. Claussen. 2008. 'A reconstruction of global agricultural areas and land cover for the last millennium.' *Global Biogeochemical Cycles* 22 (3): GB3018. doi:10.1029/2007GB003153. (Cited on pages 8, 106).

Popp, A., K. Calvin, S. Fujimori, P. Havlik, F. Humpenöder, E. Stehfest, B. L. Bodirsky, J. P. Dietrich, J. C. Doelmann, M. Gusti, T. Hasegawa, P. Kyle, M. Obersteiner, A. Tabeau, K. Takahashi, H. Valin, S. Waldhoff, I. Weindl, M. Wise, E. Kriegler, H. Lotze-Campen, O. Fricko, K. Riahi, and D. P. van Vuuren. 2017. 'Land-use futures in the shared socio-economic pathways.' *Global Environmental Change* 42:331–345. doi:10.1016/j.gloenvcha.2016.10.002. (Cited on pages 150, 170).

Popp, A., H. Lotze-Campen, and B. Bodirsky. 2010. 'Food consumption, diet shifts and associated non-CO2 greenhouse gases from agricultural production.' *Global Environmental Change* 20 (3): 451–462. doi:10.1016/j.gloenvcha.2010.02.001. (Cited on page 168).

Portmann, F. T., S. Siebert, and P. Döll. 2010. 'MIRCA2000-Global monthly irrigated and rainfed crop areas around the year 2000: A new high-resolution data set for agricultural and hydrological modeling.' *Global Biogeochemical Cycles* 24 (1): GB1011. doi:10.1029/2008GB003435. (Cited on pages 18, 106, 111, 136, 178).

Prentice, I., G. Farquhar, M. Fasham, M. Goulden, M. Heimann, V. Jaramillo, H. Kheshgi, C. Le Quéré, R. Scholes, and D. Wallace. 2001. 'The Carbon Cycle and Atmospheric Carbon Dioxide.' Chap. 3 in *Climate Change 2001: The Scientific Basis. Contribution of Working Group I to the Third Assessment Report of the Intergovernmental Panel on Climate Change,* edited by J. Houghton, Y. Ding, D. Griggs, M. Noguer, P. van der Linden, X. Dai, K. Maskell, and C. Johnson, 183–237. Cambridge, UK and New York, NY, USA: Cambridge University Press. (Cited on page 4).

Prestele, R., P. Alexander, M. D. A. Rounsevell, A. Arneth, K. Calvin, J. Doelman, D. A. Eitelberg, K. Engström, S. Fujimori, T. Hasegawa, P. Havlik, F. Humpenöder, A. K. Jain, T. Krisztin, P. Kyle, P. Meiyappan, A. Popp, R. D. Sands, R. Schaldach, J. Schüngel, E. Stehfest, A. Tabeau, H. Van Meijl, J. Van Vliet, and P. H. Verburg. 2016. 'Hotspots of uncertainty in land-use and land-cover change projections: a global-scale model comparison.' *Global Change Biology* 22 (12): 3967–3983. doi:10.1111/gcb.13337. (Cited on pages 151, 152).

R Development Core Team. 2011. *R: A Language and Environment for Statistical Computing.* Vienna, Austria: R Foundation for Statistical Computing. (Cited on page 31).

Ramanathan, V., and Y. Feng. 2008. 'On avoiding dangerous anthropogenic interference with the climate system: Formidable challenges ahead.' *Proceedings of the National Academy of Sciences* 105 (38): 14245–14250. doi:10.1073/pnas.0803838105. (Cited on page 32).

Rammig, A., T. Jupp, K. Thonicke, B. Tietjen, J. Heinke, S. Ostberg, W. Lucht, W. Cramer, and P. Cox. 2010. 'Estimating the risk of Amazonian forest dieback.' *New Phytologist* 187 (3): 694–706. doi:10.1111/j.1469-8137.2010.03318.x. (Cited on page 98).

Riahi, K., S. Rao, V. Krey, C. Cho, V. Chirkov, G. Fischer, G. Kindermann, N. Nakicenovic, and P. Rafaj. 2011. 'RCP 8.5—A scenario of comparatively high greenhouse gas emissions.' *Climatic Change* 109 (1-2): 33–57. doi:10.1007/s10584-011-0149-y. (Cited on page 149).

Riahi, K., D. P. van Vuuren, E. Kriegler, J. Edmonds, B. C. O'Neill, S. Fujimori, N. Bauer, K. Calvin, R. Dellink, O. Fricko, W. Lutz, A. Popp, J. C. Cuaresma, S. KC, M. Leimbach, L. Jiang, T. Kram, S. Rao, J. Emmerling, K. Ebi, T. Hasegawa, P. Havlik, F. Humpenöder, L. A. Da Silva, S. Smith, E. Stehfest, V. Bosetti, J. Eom, D. Gernaat, T. Masui, J. Rogelj, J. Strefler, L. Drouet, V. Krey, G. Luderer, M. Harmsen, K. Takahashi, L. Baumstark, J. C. Doelman, M. Kainuma, Z. Klimont, G. Marangoni, H. Lotze-Campen, M. Obersteiner, A. Tabeau, and M. Tavoni. 2017. 'The Shared Socioeconomic Pathways and their energy, land use, and greenhouse gas emissions implications: An overview.' *Global Environmental Change* 42:153–168. doi:10.1016/j.gloenvcha.2016.05.009. (Cited on pages 150, 170).

Ripl, W. 2003. 'Water: the bloodstream of the biosphere.' *Philosophical transactions of the Royal Society of London. Series B, Biological sciences* 358 (1440): 1921–1934. doi:10.1098/rstb.2003.1378. (Cited on page 61).

Rockström, J., H. J. Schellnhuber, B. Hoskins, V. Ramanathan, P. Schlosser, G. P. Brasseur, O. Gaffney, C. Nobre, M. Meinshausen, J. Rogelj, and W. Lucht. 2016. 'The world's biggest gamble.' *Earth's Future* 4 (10): 465–470. doi:10.1002/2016EF000392. (Cited on page 130).

Rockström, J., J. Williams, G. Daily, A. Noble, N. Matthews, L. Gordon, H. Wetterstrand, F. DeClerck, M. Shah, P. Steduto, C. de Fraiture, N. Hatibu, O. Unver, J. Bird, L. Sibanda, and J. Smith. 2017. 'Sustainable intensification of agriculture for human prosperity and global sustainability.' *Ambio* 46 (1): 4–17. doi:10.1007/s13280-016-0793-6. (Cited on page 170).

Rogelj, J., M. den Elzen, N. Höhne, T. Fransen, H. Fekete, H. Winkler, R. Schaeffer, F. Sha, K. Riahi, and M. Meinshausen. 2016. 'Paris Agreement climate proposals need a boost to keep warming well below 2 °C.' *Nature* 534 (7609): 631–639. doi:10.1038/nature18307. (Cited on pages 131, 169).

Rogelj, J., M. Meinshausen, and R. Knutti. 2012. 'Global warming under old and new scenarios using IPCC climate sensitivity range estimates.' *Nature Climate Change* 2 (4): 248–253. doi:10.1038/nclimate1385. (Cited on pages 61, 69, 84, 87, 99, 125).

Rogelj, J., J. Nabel, C. Chen, W. Hare, K. Markmann, M. Meinshausen, M. Schaeffer, K. Macey, and N. Höhne. 2010. 'Copenhagen Accord pledges are paltry.' *Nature* 464 (7292): 1126–1128. doi:10.1038/4641126a. (Cited on pages 60, 83).

Rohwer, J., D. Gerten, and W. Lucht. 2007. *Development of Functional Irrigation Types for Improved Global Crop Modelling.* Technical report 104. Potsdam, Germany: Potsdam Institute for Climate Impact Research. (Cited on page 111).

Rojstaczer, S., S. M. Sterling, and N. J. Moore. 2001. 'Human Appropriation of Photosynthesis Products.' *Science* 294 (5551): 2549–2552. doi:10.1126/science.1064375. (Cited on page 8).

Rose, S. K., E. Kriegler, R. Bibas, K. Calvin, A. Popp, D. P. van Vuuren, and J. Weyant. 2013. 'Bioenergy in energy transformation and climate management.' *Climatic Change* 123 (3-4): 477–493. doi:10.1007/s10584-013-0965-3. (Cited on page 125).

Rosenzweig, C., J. Elliott, D. Deryng, A. C. Ruane, C. Müller, A. Arneth, K. J. Boote, C. Folberth, M. Glotter, N. Khabarov, K. Neumann, F. Piontek, T. A. M. Pugh, E. Schmid, E. Stehfest, H. Yang, and J. W. Jones. 2014. 'Assessing agricultural risks of climate change in the 21st century in a global gridded crop model intercomparison.' *Proceedings of the National Academy of Sciences* 111 (9): 3268–3273. doi:10.1073/pnas.1222463110. (Cited on page 169).

Roskov, Y., L. Abucay, T. Orrell, D. Nicolson, C. Flann, N. Bailly, P. Kirk, T. Bourgoin, R. DeWalt, W. Decock, and A. De Wever, eds. 2016. 'Species 2000 & ITIS Catalogue of Life, 2016 Annual Checklist.' Species 2000: Naturalis Biodiversity Center, Leiden, Netherlands. Accessed December 20, 2016. http://www.catalogueoflife.org/annual-checklist/2016/. (Cited on page 4).

Rost, S., D. Gerten, A. Bondeau, W. Lucht, J. Rohwer, and S. Schaphoff. 2008a. 'Agricultural green and blue water consumption and its influence on the global water system.' *Water Resources Research* 44 (9): W09405. doi:10.1029/2007WR006331. (Cited on pages 5, 86, 87).

Rost, S., D. Gerten, and U. Heyder. 2008b. 'Human alterations of the terrestrial water cycle through land management.' *Advances in Geosciences* 18:43–50. doi:10.5194/adgeo-18-43-2008. (Cited on pages 106, 110, 111, 134, 138).

Rost, S., D. Gerten, H. Hoff, W. Lucht, M. Falkenmark, and J. Rockström. 2009. 'Global potential to increase crop production through water management in rainfed agriculture.' *Environmental Research Letters* 4 (4): 044002. doi:10.1088/1748-9326/4/4/044002. (Cited on page 100).

Rowlands, D. J., D. J. Frame, D. Ackerley, T. Aina, B. B. B. Booth, C. Christensen, M. Collins, N. Faull, C. E. Forest, B. S. Grandey, E. Gryspeerdt, E. J. Highwood, W. J. Ingram, S. Knight, A. Lopez, N. Massey, F. McNamara, N. Meinshausen, C. Piani, S. M. Rosier, B. M. Sanderson, L. A. Smith, D. A. Stone, M. Thurston, K. Yamazaki, Y. Hiro Yamazaki, and M. R. Allen. 2012. 'Broad range of 2050 warming from an observationally constrained large climate model ensemble.' *Nature Geoscience* 5 (4): 256–260. doi:10.1038/ngeo1430. (Cited on page 87).

Rudolf, B., A. Becker, U. Schneider, A. Meyer-Christoffer, and M. Ziese. 2010. *GPCC Status Report December 2010 (On the most recent gridded global data set issued in fall 2010 by the Global Precipitation Climatology Centre (GPCC)).* Technical report. Global Precipitation Climatology Centre. (Cited on pages 35, 40, 68, 86, 185).

Sandel, B., L. Arge, B. Dalsgaard, R. G. Davies, K. J. Gaston, W. J. Sutherland, and J.-. C. Svenning. 2011. 'The Influence of Late Quaternary Climate-Change Velocity on Species Endemism.' *Science* 334 (6056): 660–664. doi:10.1126/science.1210173. (Cited on page 99).

Sankaran, M., J. Ratnam, and N. P. Hanan. 2004. 'Tree-grass coexistence in savannas revisited - insights from an examination of assumptions and mechanisms invoked in existing models.' *Ecology Letters* 7 (6): 480–490. doi:10.1111/j.1461-0248.2004.00596.x. (Cited on page 185).

Schaphoff, S., U. Heyder, S. Ostberg, D. Gerten, J. Heinke, and W. Lucht. 2013. 'Contribution of permafrost soils to the global carbon budget.' *Environmental Research Letters* 8 (1): 014026. doi:10.1088/1748-9326/8/1/014026. (Cited on pages 98, 110, 111, 134, 166).

Schellnhuber, H. J., S. Rahmstorf, and R. Winkelmann. 2016. 'Why the right climate target was agreed in Paris.' *Nature Climate Change* 6 (7): 649–653. doi:10.1038/nclimate3013. (Cited on page 166).

Schellnhuber, H. J., R. Warren, A. Haxeltine, and L. Naylor. 2004. 'Integrated Assessment of Benefits of Climate Policy.' Chap. 3 in *The Benefits of Climate Change Policies,* edited by J. Corfee-Morlot and S. Agrawala, 83–110. Paris, France: OECD Publishing. doi:10.1787/9789264108325-en. (Cited on page 100).

Schewe, J., J. Heinke, D. Gerten, I. Haddeland, N. W. Arnell, D. B. Clark, R. Dankers, S. Eisner, B. M. Fekete, F. J. Colón-González, S. N. Gosling, H. Kim, X. Liu, Y. Masaki, F. T. Portmann, Y. Satoh, T. Stacke, Q. Tang, Y. Wada, D. Wisser, T. Albrecht, K. Frieler, F. Piontek, L. Warszawski, and P. Kabat. 2014. 'Multimodel assessment of water scarcity under climate change.' *Proceedings of the National Academy of Sciences* 111 (9): 3245–3250. doi:10.1073/pnas.1222460110. (Cited on pages 99, 100, 166).

Schmitz, C., H. van Meijl, P. Kyle, G. C. Nelson, S. Fujimori, A. Gurgel, P. Havlik, E. Heyhoe, D. M. D'Croz, A. Popp, R. Sands, A. Tabeau, D. van der Mensbrugghe, M. von Lampe, M. Wise, E. Blanc, T. Hasegawa, A. Kavallari, and H. Valin. 2014. 'Land-use change trajectories up to 2050: insights from a global agro-economic model comparison.' *Agricultural Economics* 45 (1): 69–84. doi:10.1111/agec.12090. (Cited on page 152).

Schneider von Deimling, T., M. Meinshausen, A. Levermann, V. Huber, K. Frieler, D. M. Lawrence, and V. Brovkin. 2012. 'Estimating the near-surface permafrost-carbon feedback on global warming.' *Biogeosciences* 9 (2): 649–665. doi:10.5194/bg-9-649-2012. (Cited on page 98).

Schneider, S. H., and M. D. Mastrandrea. 2005. 'Probabilistic assessment of "dangerous" climate change and emissions pathways.' *Proceedings of the National Academy of Sciences* 102 (44): 15728–15735. doi:10.1073/pnas.0506356102. (Cited on page 84).

Schneider, U., A. Becker, P. Finger, A. Meyer-Christoffer, B. Rudolf, and M. Ziese. 2011. *GPCC Full Data Reanalysis Version 6.0 at 0.5°: Monthly Land-Surface Precipitation from Rain-Gauges built on GTS-based and Historic Data.* [Internet] Global Precipitation Climatology Centre (GPCC, http://gpcc.dwd.de/) at Deutscher Wetterdienst. doi:10.5676/DWD_GPCC/FD_M_V6_050. (Cited on pages 18, 112, 136).

Scholze, M., W. Knorr, N. W. Arnell, and I. C. Prentice. 2006. 'A climate-change risk analysis for world ecosystems.' *Proceedings of the National Academy of Sciences* 103 (35): 13116–13120. doi:10.1073/pnas.0601816103. (Cited on pages 26, 27, 68, 84, 89, 147, 166).

Settele, J., R. J. Scholes, R. A. Betts, S. Bunn, P. Leadley, D. Nepstad, J. T. Overpeck, and M. A. Toboada. 2014. 'Terrestrial and Inland Water Systems.' Chap. 4 in *Climate Change 2014: Impacts, Adaptation, and Vulnerability. Part A: Global and Sectoral Aspects. Contribution of Working Group II to the Fifth Assessment Report of the Intergovernmental Panel on Climate Change,* edited by C. B. Field, V. R. Barros, D. J. Dokken, K. J. Mach, M. D. Mastrandrea, and L. L. White, 271–359. Cambridge, UK and New York, NY, USA: Cambridge University Press. doi:10.1017/CBO9781107415379.009. (Cited on pages 12, 13).

Siebert, S., J. Burke, J. M. Faures, K. Frenken, J. Hoogeveen, P. Döll, and F. T. Portmann. 2010. 'Groundwater use for irrigation – a global inventory.' *Hydrology and Earth System Sciences* 14 (10): 1863–1880. doi:10.5194/hess-14-1863-2010. (Cited on page 150).

Siebert, S., M. Kummu, M. Porkka, P. Döll, N. Ramankutty, and B. R. Scanlon. 2015. 'A global data set of the extent of irrigated land from 1900 to 2005.' *Hydrology and Earth System Sciences* 19 (3): 1521–1545. doi:10.5194/hess-19-1521-2015. (Cited on page 7).

Siebert, S., and P. Döll. 2010. 'Quantifying blue and green virtual water contents in global crop production as well as potential production losses without irrigation.' *Journal of Hydrology* 384 (3-4): 198–217. doi:10.1016/j.jhydrol.2009.07.031. (Cited on pages 8, 150).

Sitch, S., C. Huntingford, N. Gedney, P. E. Levy, M. R. Lomas, S. L. Piao, R. A. Betts, P. Ciais, P. M. Cox, P. Friedlingstein, C. D. Jones, I. C. Prentice, and F. I. Woodward. 2008. 'Evaluation of the terrestrial carbon cycle, future plant geography and climate-carbon cycle feedbacks using five Dynamic Global Vegetation Models (DGVMs).' *Global Change Biology* 14 (9): 2015–2039. doi:10.1111/j.1365-2486.2008.01626.x. (Cited on pages 26, 77, 87, 89, 107, 111, 147, 166, 168).

Sitch, S., B. Smith, I. C. Prentice, A. Arneth, A. Bondeau, W. Cramer, J. O. Kaplan, S. Levis, W. Lucht, M. T. Sykes, K. Thonicke, and S. Venevsky. 2003. 'Evaluation of ecosystem dynamics, plant geography and terrestrial carbon cycling in the LPJ dynamic global vegetation model.' *Global Change Biology* 9 (2): 161–185. doi:10.1046/j.1365-2486.2003.00569.x. (Cited on pages 17, 18, 64, 85–87, 110, 111, 134).

Smith, B. D. 2007. 'The Ultimate Ecosystem Engineers.' *Science* 315 (5820): 1797–1798. doi:10.1126/science.1137740. (Cited on page 3).

Smith, J. B., S. H. Schneider, M. Oppenheimer, G. W. Yohe, W. Hare, M. D. Mastrandrea, A. Patwardhan, I. Burton, J. Corfee-Morlot, C. H. D. Magadza, H.-M. Fussel, A. B. Pittock, A. Rahman, A. Suarez, and J.-P. van Ypersele. 2009. 'Assessing dangerous climate change through an update of the Intergovernmental Panel on Climate Change (IPCC) "reasons for concern".' *Proceedings of the National Academy of Sciences* 106 (11): 4133–4137. doi:10.1073/pnas.0812355106. (Cited on pages 26, 84).

Smith, P., S. J. Davis, F. Creutzig, S. Fuss, J. Minx, B. Gabrielle, E. Kato, R. B. Jackson, A. Cowie, E. Kriegler, D. P. van Vuuren, J. Rogelj, P. Ciais, J. Milne, J. G. Canadell, D. McCollum, G. Peters, R. Andrew, V. Krey, G. Shrestha, P. Friedlingstein, T. Gasser, A. Grübler, W. K. Heidug, M. Jonas, C. D. Jones, F. Kraxner, E. Littleton, J. Lowe, J. R. Moreira, N. Nakicenovic, M. Obersteiner, A. Patwardhan, M. Rogner, E. Rubin, A. Sharifi, A. Torvanger, Y. Yamagata, J. Edmonds, and C. Yongsung. 2016. 'Biophysical and economic limits to negative CO2 emissions.' *Nature Climate Change* 6 (1): 42–50. doi:10.1038/nclimate2870. (Cited on page 170).

Solomon, S., G.-K. Plattner, R. Knutti, and P. Friedlingstein. 2009. 'Irreversible climate change due to carbon dioxide emissions.' *Proceedings of the National Academy of Sciences* 106 (6): 1704–1709. doi:10.1073/pnas.0812721106. (Cited on page 27).

Sommer, J. H., H. Kreft, G. Kier, W. Jetz, J. Mutke, and W. Barthlott. 2010. 'Projected impacts of climate change on regional capacities for global plant species richness.' *Proceedings of the Royal Society B: Biological Sciences* 277 (1692): 2271–2280. doi:10.1098/rspb.2010.0120. (Cited on page 90).

Srinivasan, U. T., S. P. Carey, E. Hallstein, P. A. T. Higgins, A. C. Kerr, L. E. Koteen, A. B. Smith, R. Watson, J. Harte, and R. B. Norgaard. 2008. 'The debt of nations and the distribution of ecological impacts from human activities.' *Proceedings of the National Academy of Sciences* 105 (5): 1768–1773. doi:10.1073/pnas.0709562104. (Cited on page 100).

Steffen, W., P. J. Crutzen, and J. R. McNeill. 2007. 'The Anthropocene: Are Humans Now Overwhelming the Great Forces of Nature.' *AMBIO: A Journal of the Human Environment* 36 (8): 614–621. doi:10.1579/0044-7447(2007)36[614:TAAHNO]2.0.CO;2. (Cited on pages 3, 105, 130).

Steffen, W., J. Grinevald, P. J. Crutzen, and J. R. McNeill. 2011. 'The Anthropocene: conceptual and historical perspectives.' *Philosophical Transactions of the Royal Society A: Mathematical, Physical and Engineering Sciences* 369 (1938): 842–867. doi:10.1098/rsta.2010.0327. (Cited on page 3).

Stinson, G., W. A. Kurz, C. E. Smyth, E. T. Neilson, C. C. Dymond, J. M. Metsaranta, C. Boisvenue, G. J. Rampley, Q. Li, T. M. White, and D. Blain. 2011. 'An inventory-based analysis of Canada's managed forest carbon dynamics, 1990 to 2008.' *Global Change Biology* 17 (6): 2227–2244. doi:10.1111/j.1365-2486.2010.02369.x. (Cited on page 13).

Stone, D., M. Auffhammer, M. Carey, G. Hansen, C. Huggel, W. Cramer, D. Lobell, U. Molau, A. Solow, L. Tibig, and G. Yohe. 2013. 'The challenge to detect and attribute effects of climate change on human and natural systems.' *Climatic Change* 121 (2): 381–395. doi:10.1007/s10584-013-0873-6. (Cited on pages 5, 107).

Sykes, M. T., I. C. Prentice, and F. Laarif. 1999. 'Quantifying the Impact of Global Climate Change on Potential Natural Vegetation.' *Climatic Change* 41 (1): 37–52. doi:10.1023/A:1005435831549. (Cited on pages 63, 89, 109, 133, 179, 207, 222).

Syvitski, J. P. M., and A. Kettner. 2011. 'Sediment flux and the Anthropocene.' *Philosophical Transactions of the Royal Society A: Mathematical, Physical and Engineering Sciences* 369 (1938): 957–975. doi:10.1098/rsta.2010.0329. (Cited on page 3).

Tang, Q., and D. P. Lettenmaier. 2012. '21st century runoff sensitivities of major global river basins.' *Geophysical Research Letters* 39 (6): L06403. doi:10.1029/2011GL050834. (Cited on page 84).

Taylor, K. E., R. J. Stouffer, and G. A. Meehl. 2012. 'An overview of CMIP5 and the experiment design.' *Bulletin of the American Meteorological Society* 93 (4): 485–498. doi:10.1175/BAMS-D-11-00094.1. (Cited on pages 18, 131, 158).

Thomson, A. M., K. V. Calvin, L. P. Chini, G. Hurtt, J. A. Edmonds, B. Bond-Lamberty, S. Frolking, M. a. Wise, and A. C. Janetos. 2010. 'Climate mitigation and the future of tropical landscapes.' *Proceedings of the National Academy of Sciences* 107 (46): 19633–19638. doi:10.1073/pnas.0910467107. (Cited on page 149).

Thomson, A. M., K. V. Calvin, S. J. Smith, G. P. Kyle, A. Volke, P. Patel, S. Delgado-Arias, B. Bond-Lamberty, M. A. Wise, L. E. Clarke, and J. A. Edmonds. 2011. 'RCP4.5: a pathway for stabilization of radiative forcing by 2100.' *Climatic Change* 109 (1-2): 77–94. doi:10.1007/s10584-011-0151-4. (Cited on pages 140, 144, 149).

Thonicke, K., S. Venevsky, S. Sitch, and W. Cramer. 2001. 'The role of fire disturbance for global vegetation dynamics: Coupling fire into a dynamic global vegetation model.' *Global Ecology and Biogeography* 10 (6): 661–677. doi:10.1046/j.1466-822X.2001.00175.x. (Cited on pages 18, 87, 110, 134).

Thurner, M., C. Beer, P. Ciais, A. D. Friend, A. Ito, A. Kleidon, M. R. Lomas, S. Quegan, T. T. Rademacher, S. Schaphoff, M. Tum, A. Wiltshire, and N. Carvalhais. 2017. 'Evaluation of climate-related carbon turnover processes in global vegetation models for boreal and temperate forests.' *Global Change Biology* 23 (8): 3076–3091. doi:10.1111/gcb.13660. (Cited on page 168).

Tilman, D., C. Balzer, J. Hill, and B. L. Befort. 2011. 'Global food demand and the sustainable intensification of agriculture.' *Proceedings of the National Academy of Sciences* 108 (50): 20260–4. doi:10.1073/pnas.1116437108. (Cited on pages 14, 125, 170).

Tilman, D., J. Fargione, B. Wolff, C. D'Antonio, A. Dobson, R. Howarth, D. Schindler, W. H. Schlesinger, D. Simberloff, and D. Swackhamer. 2001. 'Forecasting Agriculturally Driven Global Environmental Change.' *Science* 292 (5515): 281–284. doi:10.1126/science.1057544. (Cited on pages 7, 150).

Trenberth, K. E. 1999. 'Atmospheric Moisture Recycling: Role of Advection and Local Evaporation.' *Journal of Climate* 12 (5): 1368–1381. doi:10.1175/1520-0442(1999)012<1368:AMRROA>2.0.CO;2. (Cited on page 5).

Tyrrell, T. 2011. 'Anthropogenic modification of the oceans.' *Philosophical Transactions of the Royal Society A: Mathematical, Physical and Engineering Sciences* 369 (1938): 887–908. doi:10.1098/rsta.2010.0334. (Cited on page 3).

UNFCCC. 1992. *United Nations Framework Convention on Climate Change.* United Nations, New York. (Cited on page 70).

UNFCCC. 2011. *Report of the Conference of the Parties on its sixteenth session, held in Cancun from 29 November to 10 December 2010. Addendum. Part Two: Action taken by the Conference of the Parties at its sixteenth session.* Report FCCC /CP/2010/7/Add.1. Bonn, Germany: UNFCCC Secretariat. (Cited on pages 60, 84).

UNFCCC. 2015. *Synthesis report on the aggregate effect of the intended nationally determined contributions.* Report FCCC/CP/2015/7. Bonn, Germany: UNFCCC Secretariat. (Cited on page 131).

UNFCCC. 2016. *Adoption of the Paris Agreement.* Report FCCC/CP/2015/10/Add.1. Bonn, Germany: UNFCCC Secretariat. (Cited on pages 130, 169).

Unger, N. 2014. 'Human land-use-driven reduction of forest volatiles cools global climate.' *Nature Climate Change* 4 (10): 907–910. doi:10.1038/nclimate2347. (Cited on page 124).

United Nations, Department of Economic and Social Affairs, Population Division (UNPD). 2015. *World population prospects: The 2015 Revision.* United Nations, New York. (Cited on pages 6, 7, 13, 130).

University of East Anglia Climatic Research Unit (CRU), P. D. Jones, and I. C. Harris. 2013. *CRU TS3.21: Climatic Research Unit (CRU) Time-Series (TS) Version 3.21 of High Resolution Gridded Data of Month-by-month Variation in Climate (Jan. 1901 - Dec. 2012),* NCAS British Atmospheric Data Centre. doi:10.5285/D0E1585D-3417-485F-87AE-4FCECF10A992. (Cited on pages 18, 112, 136).

Van Vuuren, D. P., J. Edmonds, M. Kainuma, K. Riahi, A. Thomson, K. Hibbard, G. C. Hurtt, T. Kram, V. Krey, J.-F. Lamarque, T. Masui, M. Meinshausen, N. Nakicenovic, S. J. Smith, and S. K. Rose. 2011a. 'The representative concentration pathways: an overview.' *Climatic Change* 109 (1-2): 5–31. doi:10.1007/s10584-011-0148-z. (Cited on pages 13, 14, 18, 125, 131, 139, 140, 149, 168).

Van Vuuren, D. P., M. Isaac, M. G. den Elzen, E. Stehfest, and J. van Vliet. 2010. 'Low Stabilization Scenarios and Implications for Major World Regions from an Integrated Assessment Perspective.' *The Energy Journal* 31 (01): 165–191. doi:10.5547/ISSN0195-6574-EJ-Vol31-NoSI-7. (Cited on page 78).

Van Vuuren, D. P., E. Stehfest, M. G. J. den Elzen, T. Kram, J. van Vliet, S. Deetman, M. Isaac, K. Klein Goldewijk, A. Hof, A. Mendoza Beltran, R. Oostenrijk, and B. van Ruijven. 2011b. 'RCP2.6: exploring the possibility to keep global mean temperature increase below 2°C.' *Climatic Change* 109 (1-2): 95–116. doi:10.1007/s10584-011-0152-3. (Cited on page 149).

Veldkamp, T., Y. Wada, J. Aerts, P. Döll, S. N. Gosling, J. Liu, Y. Masaki, T. Oki, S. Ostberg, Y. Pokhrel, Y. Satoh, H. Kim, and P. J. Ward. 2017. 'Water scarcity hotspots travel downstream due to human interventions in the 20th and 21st century.' *Nature Communications* 8:15697. doi:10.1038/ncomms15697. (Cited on page 166).

Verburg, P. H., N. Crossman, E. C. Ellis, A. Heinimann, P. Hostert, O. Mertz, H. Nagendra, T. Sikor, K.-H. Erb, N. Golubiewski, R. Grau, M. Grove, S. Konaté, P. Meyfroidt, D. C. Parker, R. R. Chowdhury, H. Shibata, A. Thomson, and L. Zhen. 2015. 'Land system science and sustainable development of the earth system: A global land project perspective.' *Anthropocene* 12:29–41. doi:10.1016/j.ancene.2015.09.004. (Cited on page 152).

Verburg, P. H., A. Tabeau, and E. Hatna. 2013. 'Assessing spatial uncertainties of land allocation using a scenario approach and sensitivity analysis: A study for land use in Europe.' *Journal of Environmental Management* 127:S132–S144. doi:10.1016/j.jenvman.2012.08.038. (Cited on page 152).

Vitousek, P. M., J. D. Aber, R. W. Howarth, G. E. Likens, P. A. Matson, D. W. Schindler, W. H. Schlesinger, and D. G. Tilman. 1997. 'Human Alteration of the Global Nitrogen Cycle: Sources and Consequences.' *Ecological Applications* 7 (3): 737. doi:10.2307/2269431. (Cited on page 5).

Vitousek, P. M., P. R. Ehrlich, A. H. Ehrlich, and P. A. Matson. 1986. 'Human Appropriation of the Products of Photosynthesis.' *BioScience* 36 (6): 368–373. doi:10.2307/1310258. (Cited on pages 4, 8).

Vörösmarty, C. J., B. M. Fekete, M. Meybeck, and R. B. Lammers. 2000. 'Global system of rivers: Its role in organizing continental land mass and defining land-to-ocean linkages.' *Global Biogeochemical Cycles* 14 (2): 599–621. doi:10.1029/1999GB900092. (Cited on page 137).

Vörösmarty, C. J., C. Lévêque, C. Revenga, R. Bos, C. Caudill, J. Chilton, E. M. Douglas, M. Meybeck, D. Prager, P. Balvanera, S. Barker, M. Maas, C. Nilsson, T. Oki, and C. A. Reidy. 2005. 'Fresh Water.' Chap. 7 in *Ecosystems and Human Well-being: Current State & Trends, Volume 1,* edited by F. Rijsberman, R. Costanza, and P. Jacobi, 165–207. Island Press, Washington, DC. (Cited on pages 9, 150).

Wada, Y., D. Wisser, and M. F. P. Bierkens. 2014. 'Global modeling of withdrawal, allocation and consumptive use of surface water and groundwater resources.' *Earth System Dynamics* 5 (1): 15–40. doi:10.5194/esd-5-15-2014. (Cited on page 9).

Waha, K., L. G. J. van Bussel, C. Müller, and A. Bondeau. 2012. 'Climate-driven simulation of global crop sowing dates.' *Global Ecology and Biogeography* 21 (2): 247–259. doi:10.1111/j.1466-8238.2011.00678.x. (Cited on pages 110, 135).

Walker, D. A., H. E. Epstein, M. K. Raynolds, P. Kuss, M. A. Kopecky, G. V. Frost, F. J. A. Daniëls, M. O. Leibman, N. G. Moskalenko, G. V. Matyshak, O. V. Khitun, A. V. Khomutov, B. C. Forbes, U. S. Bhatt, A. N. Kade, C. M. Vonlanthen, and L. Tichý. 2012. 'Environment, vegetation and greenness (NDVI) along the North America and Eurasia Arctic transects.' *Environmental Research Letters* 7 (1): 015504. doi:10.1088/1748-9326/7/1/015504. (Cited on pages 70, 122).

Walker, M., S. Johnsen, S. O. Rasmussen, T. Popp, J.-P. Steffensen, P. Gibbard, W. Hoek, J. Lowe, J. Andrews, S. Björck, L. C. Cwynar, K. Hughen, P. Kershaw, B. Kromer, T. Litt, D. J. Lowe, T. Nakagawa, R. Newnham, and J. Schwander. 2009. 'Formal definition and dating of the GSSP (Global Stratotype Section and Point) for the base of the Holocene using the Greenland NGRIP ice core, and selected auxiliary records.' *Journal of Quaternary Science* 24 (1): 3–17. doi:10.1002/jqs.1227. (Cited on page 3).

Warren, R., J. Price, A. Fischlin, S. de la Nava Santos, and G. Midgley. 2011. 'Increasing impacts of climate change upon ecosystems with increasing global mean temperature rise.' *Climatic Change* 106 (2): 141–177. doi:10.1007/s10584-010-9923-5. (Cited on pages 84, 166).

Warszawski, L., K. Frieler, V. Huber, F. Piontek, O. Serdeczny, and J. Schewe. 2014. 'The Inter-Sectoral Impact Model Intercomparison Project (ISI–MIP): Project framework.' *Proceedings of the National Academy of Sciences* 111 (9): 3228–3232. doi:10.1073/pnas.1312330110. (Cited on page 168).

Warszawski, L., A. Friend, S. Ostberg, K. Frieler, W. Lucht, S. Schaphoff, D. Beerling, P. Cadule, P. Ciais, D. B. Clark, R. Kahana, A. Ito, R. Keribin, A. Kleidon, M. Lomas, K. Nishina, R. Pavlick, T. T. Rademacher, M. Buechner, F. Piontek, J. Schewe, O. Serdeczny, and H. J. Schellnhuber. 2013. 'A multi-model analysis of risk of ecosystem shifts under climate change.' *Environmental Research Letters* 8 (4): 044018. doi:10.1088/1748-9326/8/4/044018. (Cited on pages 77, 109, 125, 147, 168, 169).

Watanabe, S., S. Kanae, S. Seto, P. J.-F. Yeh, Y. Hirabayashi, and T. Oki. 2012. 'Intercomparison of bias-correction methods for monthly temperature and precipitation simulated by multiple climate models.' *Journal of Geophysical Research: Atmospheres* 117:D23114. doi:10.1029/2012JD018192. (Cited on page 135).

Watterson, I. G. 2008. 'Calculation of probability density functions for temperature and precipitation change under global warming.' *Journal of Geophysical Research* 113:D12106. doi:10.1029/2007JD009254. (Cited on page 34).

Wieder, W. R., C. C. Cleveland, W. K. Smith, and K. Todd-Brown. 2015. 'Future productivity and carbon storage limited by terrestrial nutrient availability.' *Nature Geoscience* 8 (6): 441–444. doi:10.1038/ngeo2413. (Cited on page 170).

Williams, J. W., and S. T. Jackson. 2007. 'Novel climates, no-analog communities, and ecological surprises.' *Frontiers in Ecology and the Environment* 5 (9): 475–482. doi:10.1890/070037. (Cited on pages 6, 62, 77).

Wise, M. A., K. V. Calvin, A. M. Thomson, L. E. Clarke, B. Bond-Lamberty, R. D. Sands, S. J. Smith, A. C. Janetos, and J. A. Edmonds. 2009a. *The Implications of Limiting CO2 Concentrations for Agriculture, Land Use, Land-use Change Emissions and Bioenergy.* Technical report PNNL-17943. Richmond, Washington: Pacific Northwest National Laboratory. (Cited on page 149).

Wise, M., K. Calvin, A. Thomson, L. Clarke, B. Bond-Lamberty, R. Sands, S. J. Smith, A. Janetos, and J. Edmonds. 2009b. 'Implications of Limiting CO2 Concentrations for Land Use and Energy.' *Science* 324 (5931): 1183–1186. doi:10.1126/science.1168475. (Cited on page 149).

Wood, S., S. Ehui, J. Alder, S. Benin, K. G. Cassman, H. D. Cooper, T. Johns, J. Gaskell, R. Grainger, S. Kadungure, J. Otte, A. Rola, R. Watson, U. Wijkstrom, C. Devendra, N. Kanbar, Z. Khan, W. Masters, S. Porter, S. Vannuccini, and U. Wood-Sichra. 2005. 'Food.' Chap. 8 in *Ecosystems and Human Well-being: Current State & Trends, Volume 1,* edited by A. M. Balisacan and P. Gardiner, 209–241. Island Press, Washington, DC. (Cited on pages 6, 9).

Woodward, F. I., M. R. Lomas, and C. K. Kelly. 2004. 'Global climate and the distribution of plant biomes.' *Philosophical transactions of the Royal Society of London. Series B, Biological sciences* 359 (1450): 1465–1476. doi:10.1098/rstb.2004.1525. (Cited on pages 6, 60).

Woodward, F. I., and B. G. Williams. 1987. 'Climate and plant distribution at global and local scales.' *Vegetatio* 69 (1-3): 189–197. doi:10.1007/BF00038700. (Cited on page 6).

Wu, X., N. Vuichard, P. Ciais, N. Viovy, N. de Noblet-Ducoudré, X. Wang, V. Magliulo, M. Wattenbach, L. Vitale, P. Di Tommasi, E. J. Moors, W. Jans, J. Elbers, E. Ceschia, T. Tallec, C. Bernhofer, T. Grünwald, C. Moureaux, T. Manise, A. Ligne, P. Cellier, B. Loubet, E. Larmanou, and D. Ripoche. 2016. 'ORCHIDEE-CROP (v0), a new process-based agro-land surface model: model description and evaluation over Europe.' *Geoscientific Model Development* 9 (2): 857–873. doi:10.5194/gmd-9-857-2016. (Cited on page 169).

Zalasiewicz, J., M. Williams, R. Fortey, A. Smith, T. L. Barry, A. L. Coe, P. R. Bown, P. F. Rawson, A. Gale, P. Gibbard, F. J. Gregory, M. W. Hounslow, A. C. Kerr, P. Pearson, R. Knox, J. Powell, C. Waters, J. Marshall, M. Oates, and P. Stone. 2011. 'Stratigraphy of the Anthropocene.' *Philosophical Transactions of the Royal Society A: Mathematical, Physical and Engineering Sciences* 369 (1938): 1036–1055. doi:10.1098/rsta.2010.0315. (Cited on page 3).

Zelazowski, P., Y. Malhi, C. Huntingford, S. Sitch, and J. B. Fisher. 2011. 'Changes in the potential distribution of humid tropical forests on a warmer planet.' *Philosophical transactions. Series A, Mathematical, physical, and engineering sciences* 369 (1934): 137–60. doi:10.1098/rsta.2010.0238. (Cited on page 84).

Zhu, Z., S. Piao, R. B. Myneni, M. Huang, Z. Zeng, J. G. Canadell, P. Ciais, S. Sitch, P. Friedlingstein, A. Arneth, C. Cao, L. Cheng, E. Kato, C. Koven, Y. Li, X. Lian, Y. Liu, R. Liu, J. Mao, Y. Pan, S. Peng, J. Peñuelas, B. Poulter, T. A. M. Pugh, B. D. Stocker, N. Viovy, X. Wang, Y. Wang, Z. Xiao, H. Yang, S. Zaehle, and N. Zeng. 2016. 'Greening of the Earth and its drivers.' *Nature Climate Change* 6 (8): 791–795. doi:10.1038/nclimate3004. (Cited on page 12).

Selbständigkeitserklärung

Ich erkläre, dass ich die Dissertation selbständig und nur unter Verwendung der von mir gemäß § 7 Abs. 3 der Promotionsordnung der Mathematisch-Naturwissenschaftlichen Fakultät, veröffentlicht im Amtlichen Mitteilungsblatt der Humboldt-Universität zu Berlin Nr. 126/2014 am 18.11.2014, angegebenen Hilfsmittel angefertigt habe.

Ich habe mich nicht anderwärts um einen Doktorgrad im Promotionsfach Geographie beworben und besitze keinen Doktorgrad im Promotionsfach Geographie.

Die Promotionsordnung der Mathematisch-Naturwissenschaftlichen Fakultät, veröffentlicht im Amtlichen Mitteilungsblatt der Humboldt-Universität zu Berlin Nr. 126/2014 am 18.11.2014, habe ich zur Kenntnis genommen.

Berlin, den _____ _____

Datum Unterschrift